

Synthesis and biological evaluation of novel antibacterial agents

DISSERTATION

Zur Erlangung des Grades
des Doktors der Naturwissenschaften
Der Naturwissenschaftlich-Technischen Fakultät
Der Universität des Saarlandes

von

Reem Khaled Fathy Fathalla, M.Sc.

Saarbrücken

2022

Tag des Kolloquiums: 12. Dezember 2022

Dekan: Prof. Dr. Ludger Santen

Berichterstatter: Prof. Dr. Christian Ducho
Prof. Dr. Anna K.H. Hirsch

Vorsitz: Prof. Dr. Thorsten Lehr

Akademischer Mitarbeiter: Dr. Britta Diesel

Die vorliegende Arbeit wurde an der Universität des Saarlandes an der Naturwissenschaftlich - Technischen Fakultät in der Fachrichtung Pharmazie im Zeitraum von Juli 2018 bis April 2022 angefertigt.

Erstgutachter: Prof. Dr. Christian Ducho

Zweitgutachter: Prof. Dr. Anna Hirsch

*Written with God's grace and dedicated to
my family!*

"All that is gold does not glitter,
Not all those who wander are lost;
The old that is strong does not wither,
Deep roots are not reached by the frost."

Bilbo Baggins

Abstract

The early steps of bacterial cell wall synthesis are underutilized as antibacterial drug targets with only fosfomycin being clinically used. They represent an opportunity to escape the rising problem of bacterial resistance. Fosfomycin targets MurA, the first member of the Mur family of enzymes. MurA was the main target for the development of inhibitors in this work. Pyrazolidinones were discovered as dual inhibitors of MurA/MurB enzymes, possessing a broad-spectrum antibacterial action (chapter 3.2). Screenings of an available compound library led to the discovery of pyrrolidinedione derivatives as MurA inhibitors, active on both wild-type (WT) and fosfomycin-resistant C115D mutant MurA (chapter 3.3). The second group of discovered MurA inhibitors were 8-anilinonaphthalene-1-sulfonic acid (ANS) derivatives. These ANS analogues acted on various subtypes of MurA, WT and C115D *E. coli* MurA, in addition to *E. cloacae* MurA (chapter 3.4). The final project involved optimization of the entry of an established MurB inhibitor into resistant bacterial cells, without increasing the mammalian cell toxicity, through the use of liposomes loaded with nanoparticles (chapter 3.5).

Zusammenfassung in deutscher Sprache

Die frühen Schritte der bakteriellen Zellwandsynthese sind ein selten verwendetes antibakterielles Wirkstoff-Target, wobei lediglich Fosfomycin klinisch angewendet wird. Insofern bietet eine Hemmung dieser Schritte eine Möglichkeit, bakteriellen Resistenzen entgegenzuwirken. Das Target-Protein von Fosfomycin ist MurA, welches das erste Mitglied der Mur-Enzym-Familie darstellt. MurA war das Haupttarget für die Entwicklung neuer Inhibitoren in der hier vorliegenden Arbeit. Hierfür wurden Pyrazolidinone, welche ein breites antibakterielles Wirkungsspektrum aufwiesen, als duale Inhibitoren der Enzyme MurA und MurB entdeckt (Kapitel 3.2). Das Screening einer verfügbaren Substanzbibliothek resultierte in der Entdeckung von Pyrrolidindion-Derivaten als MurA-Inhibitoren. Diese wiesen sowohl gegen Wildtyp-(WT)-MurA als auch gegen die Fosfomycin-resistente C115D-Mutante von MurA inhibitorische Aktivität auf (Kapitel 3.3). Als eine weitere Gruppe von MurA-Inhibitoren wurden außerdem Derivate von 8-Anilidonaphthalin-1-sulfonsäure (ANS) identifiziert. Diese zeigten inhibitorische Aktivität gegenüber verschiedenen Subtypen von MurA: WT- und C115D-MurA aus *E. coli* sowie MurA aus *E. cloacae* (Kapitel 3.4). Als letztes Projekt wurde die Optimierung der Aufnahme eines etablierten MurB-Inhibitors in resistente Bakterienzellen angestrebt. Hierbei sollte die Toxizität gegenüber Säugerzellen nicht erhöht werden, was durch die Verwendung von Nanopartikel-beladenen Liposomen erfolgte (Kapitel 3.5).

Publications

Synthesis of Novel 1,2-Diarylpyrazolidin-3-one-based Compounds and their Evaluation as Broad spectrum Antibacterial Agents

Salma A. Mokbel, Reem K. Fathalla, Lina Y. El-Sharkawy, Ashraf H. Abadi, Matthias Engel and Mohammad Abdel-Halim

Bioorg. Chem. **2020**, *99*, 103759, DOI: 10.1016/j.bioorg.2020.103759.

Identification and Biochemical Characterization of Pyrrolidinediones as Novel Inhibitors of the Bacterial Enzyme MurA

Reem K. Fathalla, Wolfgang Fröhner, Chantal D. Bader, Patrick D. Fischer, Charlotte Dahlem, Deep Chatterjee, Sebastian Mathea, Alexandra K. Kiemer, Haribabu Arthanari, Rolf Müller, Mohammad Abdel-Halim, Christian Ducho and Matthias Engel

Published in Journal of Medicinal chemistry on October 21st, 2022.

J. Med. Chem. **2022**, DOI: 10.1021/acs.jmedchem.2c01275.

Targeting the Binding Pocket of the Fluorescent dye 8-Anilinonaphthalene 1-sulfonic acid (ANS) in MurA Holds Potential for the Development of Novel Broad-spectrum Antibiotic Agents

Reem K. Fathalla, Christian Ducho and Matthias Engel

Manuscript prepared and will be submitted to *Eur. J. Med. Chem.*

Nanoparticle Fraught Liposomes: A Platform for Increased Antibiotic Selectivity in Multidrug Resistant Bacteria

Suzan Fangary, Mohammad Abdel-Halim, Reem K. Fathalla, Raghda Hassan, Noha Farrag, Matthias Engel, Samar Mansour and Salma N. Tammam

Mol. Pharmaceutics **2022**, *19*, 3163-3177, DOI: <https://doi.org/10.1021/acs.molpharmaceut.2c00258>.

Acknowledgement

This work would not have been possible without the help of many remarkable individuals who aided and supported me both professionally and personally throughout the different stages of my PhD journey.

First of all, I would like to express my deep gratitude to my main supervisor, Prof. Dr. Christian Ducho for giving me the chance to join his research group, and for his continuous support and encouragement, as well as all his professional help throughout my PhD journey. He has helped me become a better scientist and opened a lot of previously closed doors.

Next comes Dr. Matthias Engel, who was a tremendous help both on a professional and personal level. He has been an integral part of this work and was always there to give a sound opinion, and offer lots of troubleshooting advice whenever needed.

I also thank Prof. Dr. Anna Hirsch for taking on the role of a second PhD advisor.

For their tremendous help in taking on various assays and measurements throughout my work, I want to thank Dr. Stefan Boettcher, Martina Jankowski and Nathalie Kagerah. Many thanks also go to Dr. Mohammad Abdel-Halim who helped me kickstart my PhD work and did all the UPLCMS measurements and was always an inspirational teacher throughout my scientific career.

I also extend my gratitude to Dr. Patrick Fischer and Dr. Chantal Bader for helping me with the protein NMR and native MS parts of my thesis.

For the fun times we had both inside and outside the lab, I would like to thank my friends Tobias Betzholz, Manuel Hawner, Sven Lauterbach, Christian Rohrbacher, Laura Thilmont, and my EAB partner in crime, Pierre Junghanns. I would also like to

thank all my coworkers in our AK for their personal and professional help throughout the years of my PhD.

A massive thank you goes to my amazing ladies, Dr. Verena Böttner-Schäfer, Dr. Giuliana Niro, the soon to be Dr. Stefanie Weck, and Dr. Melissa Wojtyniak. You were always there whenever I needed you and you have kept me sane when everything around was driving me crazy.

My friends in Egypt Basma, Dalia, Menna, and Randa also get many thanks for their encouragement. You have been with me every step of the way and I am extremely grateful for your presence in my life.

My family gets the lion's share of my thanks for always helping and supporting without question and for giving me every kind of tool to be the woman I am today. I thank my mum, dad, sister, grandparents who have left this world and who are still here, and my uncle and aunt. You are the light of my life and the reason I carried on whenever I wanted to stop. And last but not least, I want to thank my lovely husband Mohamed who has been extremely supportive from the start. You are the love of my life and without you I wouldn't have been as strong, thank you for helping me, supporting me and loving me.

Abbreviations and Symbols

Ac	Acetyl
Ac-CoA	Acetyl coenzyme A
ADP	Adenosine diphosphate
Ala	Alanine
Alr	Alanine racemase
ANS	8-Anilinonaphthalene-1-sulfonic acid
Arg	Arginine
Asn	Asparagine
Asp	Aspartic acid
ATP	Adenosine triphosphate
BSA	Bovine serum albumin
Cys	Cysteine
δ	Chemical shift [ppm] (NMR)
d	Doublet (NMR)
Ddl	D-Ala-D-Ala ligase
ddH ₂ O	Double deionized water
DCM	Dichloromethane
DMSO	Dimethylsulfoxide
DNA	Deoxyribonucleic acid
DTT	Dithiothreitol
EDTA	Ethylenediaminetetraacetic acid
EP	Enol pyruvate
EPSP	5-Enolpyruvylshikimate-3-phosphate
ESI	Electrospray ionization
<i>et al.</i>	And others
GlcN-1-P	Glucosamine-1-phosphate
GlcN-6-P	Glucosamine-6-phosphate
GlcNAc	<i>N</i> -acetylglucosamine
GlmS	Glucosamine-6-phosphate synthase
GlmM	Phosphoglucosamine-mutase

GlmU	<i>N</i> -Acetylglucosamine-1-phosphate uridyltransferase
GlpT	Glycerol-3-phosphate transporter
Gln	Glutamine
Glu	Glutamic acid
Gly	Glycine
GSH	Glutathione
GT	Glycosyl transferase
HGT	Horizontal gene transfer
HSQC	Heteronuclear Single-Quantum Correlation Spectroscopy
IC ₅₀	Half maximal inhibitory concentration
<i>J</i>	Coupling constant [Hz] (NMR)
kDa	Kilo Dalton
LC	Liquid chromatography
LD ₅₀	Lethal dose 50%
LPS	Lipopolysaccharide
Lys	Lysine
mDAP	<i>meso</i> -diaminopimelic acid
M	Molar
m	multiplet (NMR)
MDR	Multiple drug-resisant
MG	Malachite green
MRSA	Methicillin-resistant <i>Staphylococcus aureus</i>
MS	Mass spectrometry
MTT	3-(4,5-dimethylthiazol-2-yl)-2,5-diphenyltetrazolium bromide
MurNAc	<i>N</i> -acetylmuramic acid
NADPH	Reduced nicotinamide adenine dinucleotide phosphate
NMR	Nuclear magnetic resonance
NO	Nitric oxide
NPs	Nanoparticles
OD	Optical density
PAINs	Pan-assay interference compounds
PBPs	Penicillin-binding proteins
PCR	Polymerase chain reaction

PEP	Phosphoenolpyruvate
PG	Peptidoglycan
P _i	Inorganic phosphate
PP _i	Pyrophosphate
Pro	Proline
PMBN	Polymyxin B nonapeptide
q	quartet (NMR)
RNA	Ribonucleic acid
rt	Room temperature
s	singlet (NMR)
SAR	Structure-activity relationship
SBVS	Structure-based virtual screening
t	triplet (NMR)
<i>t</i> -Bu	<i>tert</i> -butyl
TB	Tuberculosis
THI	Tetrahedral intermediate
TP	Transpeptidase
UDP	Uridine diphosphate
UhpT	Hexose phosphate transporter
UNAG	UDP- <i>N</i> -acetylglucosamine
UPLC-MS	Ultra performance liquid chromatography-mass spectrometry
UTI	Urinary tract infection
UTP	Uridine triphosphate
VISA	Vancomycin-intermediate <i>Staphylococcus aureus</i>
VRSA	Vancomycin-resistant <i>Staphylococcus aureus</i>
WT	Wild type
XDR-TB	Extensively drug-resistant tuberculosis

Comments on the citation style:

References are given as superscripted numbers and refer to the numbers inside brackets (number) listed in Chapter 6 'References'. If a reference refers to the informational content of a whole sentence, it is placed immediately after the punctuation finishing the sentence. If one sentence contains more than one information, the reference is placed immediately posterior to the information it refers to.

Content

1.	Introduction.....	1
1.1	Antibacterial Drug Discovery and Development of Resistance.....	1
1.2	Antibacterial Drug Classes and their Mechanisms of Action.....	3
1.3	Bacterial Cell Wall Structure.....	7
1.4	Peptidoglycan Biosynthesis.....	8
1.4.1	UDP-GlcNAc Synthesis Pathway.....	8
1.4.2	Synthesis of UDP-MurNAc Pentapeptide.....	9
1.4.3	Membrane-associated Steps of PG Biosynthesis.....	10
1.4.4	Extracellular Steps of PG Biosynthesis.....	11
1.5	Mur Enzymes.....	13
1.5.1	Inhibitors of Mur Enzymes.....	15
1.6	MurA.....	21
1.6.1	MurA Structure and Catalysis.....	22
1.6.2	MurA Inhibitors.....	28
1.6.2.1	Fosfomycin.....	28
1.6.2.2	Other MurA Inhibitors.....	29
1.7	ANS.....	34
2.	Objectives.....	38
3.	Results.....	41
3.1	General Comments.....	41
3.2	Synthesis of Novel 1,2-Diarylpyrazolidin-3-one-based Compounds and their Evaluation as Broad spectrum Antibacterial Agents.....	42
3.2.1	Abstract.....	43
3.2.2	Introduction.....	43
3.2.3	Results and Discussion.....	45
3.2.3.1	Compound Design.....	45
3.2.3.2	Chemistry.....	48
3.2.3.3	Biological Evaluation.....	52
3.2.4	Conclusion.....	59
3.2.5	Experimental Section.....	60
3.2.5.1	Chemistry.....	60
3.2.5.2	Biology.....	75
3.2.6	References.....	78
3.3	Identification and Biochemical Characterization of Pyrrolidinediones as Novel Inhibitors of the Bacterial Enzyme MurA.....	81
3.3.1	Abstract.....	83

3.3.2	Introduction.....	83
3.3.3	Results and Discussion.....	87
3.3.3.1	Chemistry.....	87
3.3.3.2	Biological Evaluation.....	91
3.3.4	Conclusions.....	115
3.3.5	Supporting Information.....	116
3.3.6	Abbreviations Used.....	116
3.3.7	References.....	117
3.4	Targeting the Binding Pocket of the Fluorescent dye 8-Anilinonaphthalene-1-sulfonic acid (ANS) in MurA Holds Potential for the Development of Novel Broad-spectrum Antibiotic Agents.....	125
3.4.1	Abstract.....	126
3.4.2	Introduction.....	127
3.4.3	Results and Discussion.....	130
3.4.3.1	Biological Evaluation.....	131
3.4.3.2	Binding Model of the ANS Derivative Compound 26	141
3.4.4	Conclusions.....	143
3.4.5	References.....	144
3.5	Nanoparticle Fraught Liposomes: A Platform for Increased Antibiotic Selectivity in Multidrug Resistant Bacteria.....	151
3.5.1	Abstract.....	153
3.5.2	Introduction.....	154
3.5.3	Methods.....	156
3.5.3.1	Assessing the Effectiveness of 3c against <i>E. coli</i> DH5 α and <i>E. coli tolC</i> with the Aid of Polymyxin B nonapeptide (PMBN).....	156
3.5.3.2	Preparation and Characterization of Unloaded Polymeric Nanoparticles-(NPs) and Liposomes-(Lip).....	157
3.5.3.3	Encapsulation of NPs in Liposomes.....	158
3.5.3.4	<i>In vitro</i> Cell Viability Assessment.....	161
3.5.3.5	<i>In vitro</i> Antimicrobial Susceptibility Testing towards Gram-negative Bacteria.....	162
3.5.3.6	<i>In vitro</i> Antimicrobial Susceptibility of <i>P. aeruginosa</i>	163
3.5.3.7	Statistical Analysis.....	165
3.5.4	Results and Discussion.....	165
3.5.4.1	Introduction Assessing the Effectiveness of 3c against <i>E. coli</i> DH5 α and <i>E. coli tolC</i> with the Aid of Polymyxin B (PMBN).....	165
3.5.4.2	Preparation and Characterization of NP, Lip and NP-Lip.....	166
3.5.4.3	<i>In vitro</i> Cell Viability Assessment.....	172
3.5.4.4	<i>In vitro</i> Antimicrobial Susceptibility Testing towards Gram-negative Bacteria.....	175
3.5.4.5	<i>In vivo</i> Antimicrobial Susceptibility of <i>P. aeruginosa</i>	180
3.5.5	Conclusion.....	185

3.5.6	References.....	186
4.	Conclusions and Outlook.....	197
4.1	Synthesis of Novel 1,2-Diarylpyrazolidin-3-one-based Compounds and their Evaluation as Broad Spectrum Antibacterial Agents.....	198
4.2	Identification and Biochemical Characterization of Pyrrolidinediones as Novel Inhibitors of the Bacterial Enzyme MurA.....	200
4.3	Targeting the Binding Pocket of the Fluorescent Dye 8-Anilino-naphthalene 1-sulfonic acid (ANS) in MurA Holds Potential for the Development of Novel Broad-spectrum Antibiotic Agents.....	202
4.4	Nanoparticle Fraught Liposomes: A Platform for Increased Antibiotic Selectivity in Multidrug Resistant Bacteria.....	204
5.	Experimental Section.....	207
5.1	Experimental Methodology of Chapter 3.3.....	207
5.1.1	General Chemical and Analytical Methods.....	207
5.1.2	General Procedure for Synthesis of the Compounds.....	208
5.1.3	Analysis Results for the Compounds.....	209
5.1.4	Biological Evaluation.....	229
5.1.4.1	Protein Expression.....	229
5.1.4.2	MurA Assay.....	230
5.1.4.3	MurB Expression and Assay.....	231
5.1.4.4	Evaluation of the Reversibility of Inhibition.....	231
5.1.4.5	Examination of the Synergism between Compound 46 and Fosfomycin.....	232
5.1.4.6	Enzyme Kinetics Properties.....	232
5.1.4.7	Native MS.....	232
5.1.4.8	Protein X-ray Co-crystallography.....	233
5.1.4.9	Expression and Purification of U- ¹⁵ N MurA and U- ¹⁵ N C115D MurA.....	234
5.1.4.10	Protein NMR Experiments.....	235
5.1.4.11	Cytotoxicity Evaluation.....	236
5.1.4.12	Antibacterial Testing and IC ₉₀ Determination.....	236
5.1.4.13	Stability in Biological Media.....	237
5.2	Experimental Methodology of Chapter 3.4.....	238
5.2.1	Chemistry.....	238
5.2.2	Biological Evaluation.....	238
5.2.2.1	Cloning of the <i>E. cloacae murA</i> Insert into an Expression Plasmid.....	238
5.2.2.2	Transformation for Overexpression of MurA.....	239
5.2.2.3	Protein Expression and Purification.....	240
5.2.2.4	Antibacterial Activities.....	241
5.2.2.5	Fluorescence Binding Assay.....	241
5.2.3	Molecular Modelling and Docking.....	242
6.	References.....	243

7.	Appendix.....	271
7.1	Fluorescence Binding Assays.....	271
7.1.1	Compound 46 Binding to MurA in the Fluorescence Binding Assay.....	271
7.2	Design and Expression of MurA Mutants.....	273
7.2.1	Expression of the MurA Mutants.....	275
7.2.1.1	Preparations for Site-directed Mutagenesis.....	275
7.2.1.2	Site-directed Mutagenesis	277
7.2.1.3	Transformation of XL10-Gold Ultracompetent Cells.....	279
7.2.1.4	Expression of the Mutant Proteins.....	281
7.2.2	Activity and Inhibition of the Mutant Proteins.....	282
7.2.3	Native MS Analysis of the Mutant Proteins	283
7.3	Studies on 2-Phosphonopropionic acid, a PEP Analogue	285
7.4	Enzymatic Synthesis of UDP-MurNAc	286
7.4.1	Steps of the Enzymatic Synthesis of UDP-MurNAc.....	287
7.5	Expression of MurC with a His-tag.....	289
7.5.1	Strategy for His-tag Insertion into MurC.....	289
7.5.2	Procedure of the His-tagged MurC Subcloning.....	290
7.5.3	Expression of His-tagged MurC.....	292
7.6	Supplementary Information for Chapter 3.3 : Identification and Biochemical Characterization of Pyrrolidinediones as Novel Inhibitors of the Bacterial Enzyme MurA.....	293
7.7	Supplementary Information for Chapter 3.4 : Targeting the Binding Pocket of the Fluorescent Dye 8-Anilino-naphthalene-1-sulfonic acid (ANS) in MurA Holds Potential for the Development of Novel Antibacterial Agents.....	307
7.8	Supplementary information for Chapter 3.5 : Nanoparticle Fraught Liposomes: A Platform for Increased Antibiotic Selectivity in Multidrug Resistant Bacteria.....	314

1. Introduction

1.1 Antibacterial Drug Discovery and Development of Resistance

The introduction of antibiotics in the first half of the 20th century has been a key event in history and human development, helping save millions of lives world-wide. While the term antibiotic has been coined by American microbiologist Selman Waksman to describe microorganism-produced chemicals that inhibit the growth of other microorganisms, the management of bacterial infections has been recorded since ancient times in Greece, Serbia, China, and Egypt, where poultices of moldy bread were used to treat open wounds.¹⁻⁴

The discovery of the first antibacterial drug salvarsan in 1910 was followed by the subsequent discovery of several classes of antibacterial agents which led to a revolution in drug discovery, and a 23-year increase in the average human lifespan.^{2,3}

The discovery of penicillin in 1928 by Alexander Fleming heralded the start of the golden age of antibiotic discovery, peaking in the 1950s and 1960s (*Figure 1.1*).⁵⁻⁷ At first, new classes of antibiotics were discovered via low throughput screening of fermentation products, and whole cell screenings.^{8,9} After that, the development of antibiotics focused on creating synthetic derivatives of the discovered natural scaffolds, which improved their spectrum, pharmacokinetic properties, and lowered their dosing.^{7,10,11} The modern era ushered in innovative drug discovery approaches with advancing technology in high-throughput screenings and synthesis, combined with emergent genomic technologies and protein structure determination.^{7,12} Yet, these modern innovations were not translated into discovery of new antibacterial scaffolds, and the period from 1962-2000 saw what is called a discovery void.^{3,9,12} In

this discovery void period, no new major classes of antibiotics were introduced, and at the same time the incidence of bacterial resistance was on a constant rise, starting with the resistance to penicillin, all the way up to the discovery of multiple drug resistant (MDR) strains of bacteria which are unconquerable by most, if not all the antibacterial drug classes present (*Figure 1.1*).^{8,13,14} Indeed misuse, overprescribing, and the extensive use of antibiotics in agriculture, combined with the innate bacterial tendency for mutation and horizontal gene transfer (HGT) of antibiotic resistance genes, have led to the current bacterial resistance crisis, which costs governments billions of dollars worldwide.^{3,13,14} The main mechanisms by which the bacteria escape the known antibacterial agents are target alteration, enzymatic modification or destruction of the drug, enhanced efflux pump expression, in addition to alteration of membrane permeability.¹⁵⁻¹⁷

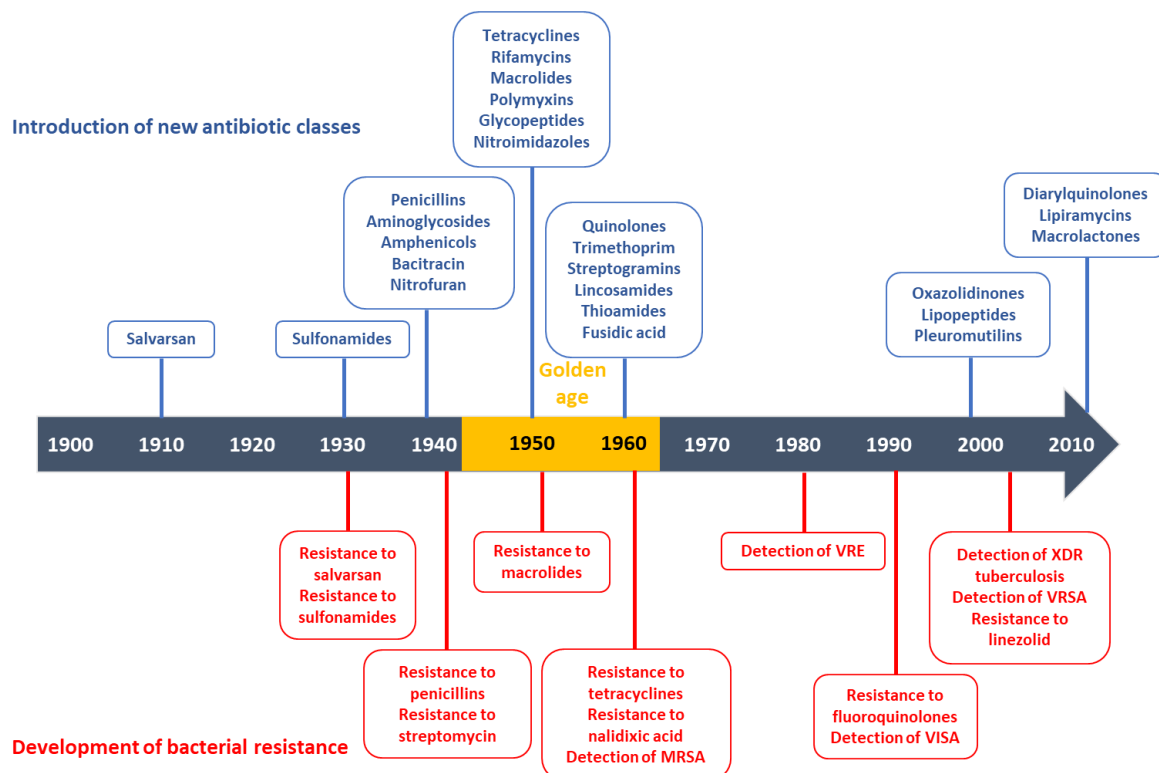


Figure 1.1. Timeline of the introduction of new antibiotic classes and the development of bacterial resistance²

These mechanisms have resulted in the appearance of several Gram-positive and Gram-negative species that are of high concern. These include the highly drug resistant ESKAPE pathogens, six nosocomial bacteria: *Enterococcus faecium*, *Staphylococcus aureus*, *Klebsiella pneumoniae*, *Acinetobacter baumannii*, *Pseudomonas aeruginosa*, and *Enterobacter* species.¹⁸⁻²⁰ In particular, drug-resistant *S. aureus* has become a major threat, with 20% of the population being persistent carriers of resistant strains of *S. aureus*, of which Methicillin-resistant *S. aureus* (MRSA) causes 19,000 deaths annually in the US.^{3,21} Vancomycin was the drug of choice for treatment of MRSA, until Vancomycin-intermediate (VISA), and Vancomycin-resistant (VRSA) strains were observed.^{21,22} Additionally, tuberculosis or TB caused 9.9 million infections and 1.5 million deaths in 2020. It is estimated that about 9.9% of the TB cases are either MDR or extensively drug-resistant (XDR-TB), which are then resistant to all first-line anti-TB agents and some second-line agents, leaving few treatment options and costing on average \$483,000 for one course of treatment.^{21,23-25} This high rate of bacterial resistance, going hand in hand with the lack of newly introduced antibacterial agents on the market necessitate the development of new scaffolds for antibiotics that act on underutilized bacterial targets.

1.2 Antibacterial Drug Classes and their Mechanisms of Action

There are four classic targets for antibacterial drugs, namely: protein synthesis, peptidoglycan biosynthesis, DNA replication, and folate biosynthesis.^{7,8,15,26} Antibacterial agents can either inhibit bacterial cell replication, hence being considered a bacteriostatic agent, or kill the cell and therefore be classified as a bactericidal antibiotic.^{27,28} β -lactams include four subclasses: penicillins, cephalosporins, carbapenems, and monobactams. They target the penicillin-binding

proteins (PBPs) involved in the cell wall synthesis.^{7,29-31} They are among the oldest and most used antibiotics to date.⁵ Other cell wall synthesis inhibitors include glycopeptide antibiotics such as vancomycin and teicoplanin which interfere with the transpeptidation step of cell wall formation by binding to the terminal D-Ala-D-Ala of lipid II (more details on the bacterial cell wall synthesis steps are in Section **1.4**).^{32,33}

Bacterial protein synthesis is extensively targeted by many classes of antibacterial agents, such as aminoglycosides, tetracyclines, macrolides, phenicols, and lincosamides binding to either the small 30S or the large 50S ribosomal subunit.^{30,34,35}

Bacterial DNA synthesis is either directly targeted by interfering with the topoisomerase enzymes as with quinolones, or indirectly targeted by interfering with the folate metabolism of the bacteria as with sulfonamides and pyrimidines.³⁶⁻³⁸

Other mechanisms of antibacterial agents include cell membrane disruption by the more recently introduced lipopeptides, and interference with LPS of Gram-negative bacteria by polymyxins.³⁹⁻⁴¹ *Figure 1.2* includes the structures of several representatives of the above-mentioned classes and *Table 1.1* summarizes most of the clinically used antibacterial drug classes, with their targets, modes of action, modes of resistance, and origin.

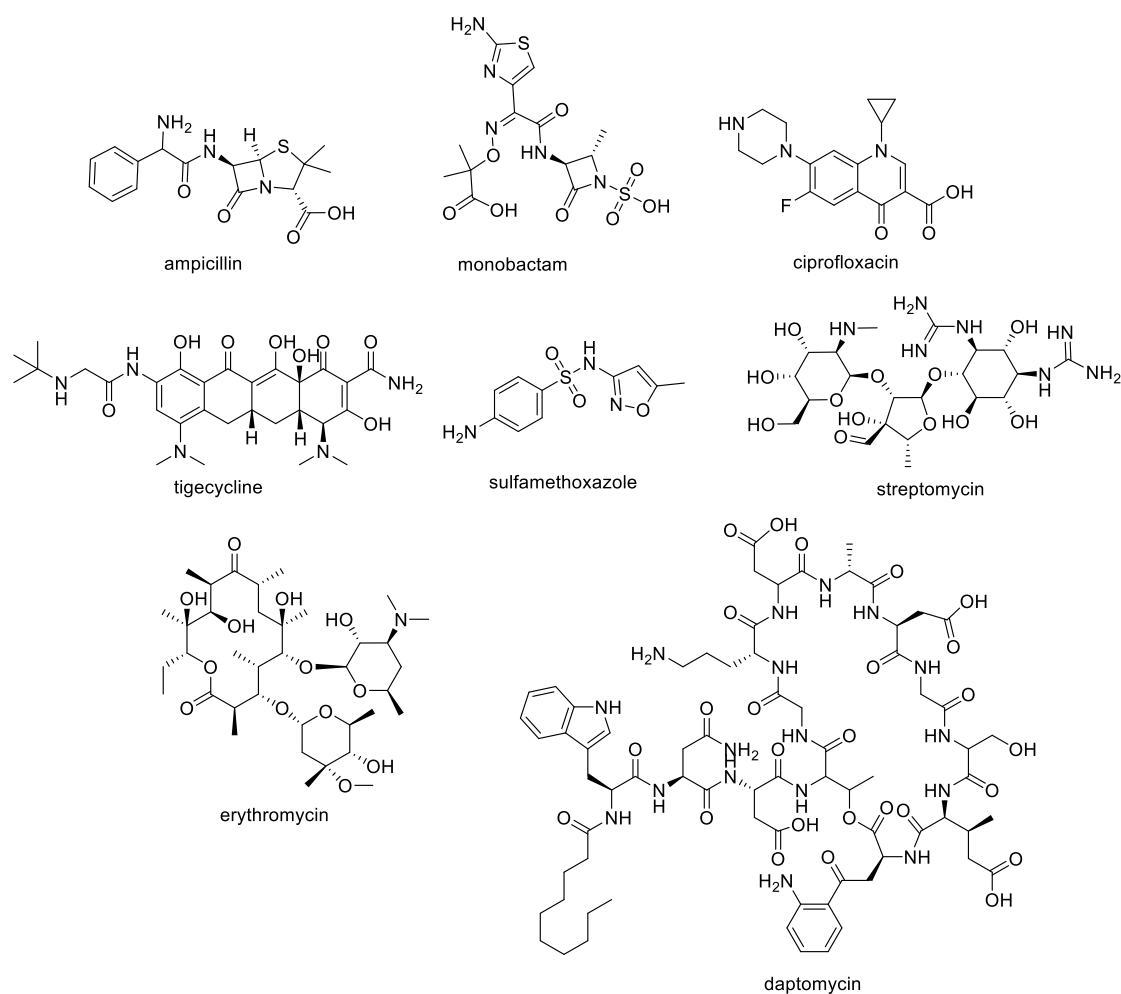


Figure 1.2. Examples of available antibiotics

Table 1.1. Classes of antibiotics with their mechanisms of action and modes of resistance^{7,15,26}

Antibiotic class	Example(s)	Target	Mode of action	Mode(s) of resistance
β-lactams^a	penicillins, cephalosporins, penems, monobactams	Peptidoglycan biosynthesis	Bactericidal	Drug hydrolysis Efflux Altered target
Aminoglycosides^a	streptomycin	Protein synthesis	Bactericidal	Drug modification Efflux Altered target
Sulfonamides^b	sulfamethoxazole	Folate biosynthesis	Bacteriostatic	Efflux Altered target

Tetracyclines^a	tigecycline	Protein synthesis	Bacteriostatic	Drug modification Efflux Altered target
Macrolides^a	erythromycin	Protein synthesis	Bacteriostatic	Drug hydrolysis Drug modification Efflux Altered target
Oxazolidinones^b	linezolid	Protein synthesis	Bacteriostatic	Efflux Altered target
Quinolones^a	ciprofloxacin	DNA synthesis	Bactericidal	Drug modification Efflux Altered target
Glycopeptides^a	vancomycin	Peptidoglycan biosynthesis	Bactericidal	Altered target
Phenicols^a	chloramphenicol	Protein synthesis	Bacteriostatic	Drug modification Efflux Altered target
Benzyl diaminopyrimidines^b	trimethoprim	Folate biosynthesis	Bacteriostatic	Efflux Altered target
Rifamycins^a	rifampin	RNA synthesis	Bactericidal	Drug modification Efflux Altered target
Lincosamides^a	clindamycin	Protein synthesis	Bacteriostatic	Drug modification Efflux Altered target
Streptogramins^a	synrecid	Protein synthesis	Bactericidal	Drug modification Efflux Altered target

Polymyxins^a	colistin	LPS	Bactericidal	Altered target Efflux
Lipopeptides^a	daptomycin	Cell membrane	Bactericidal	Altered target

^anatural origin, ^bsynthetic compound

1.3 Bacterial Cell Wall Structure

The cell wall is the main structure-maintaining feature of the bacterial cell. It provides structure and rigidity to the bacteria and helps the cells withstand the large osmotic pressure between their cytoplasm and the outside environment.⁴²⁻⁴⁵ It is present in both Gram-negative and Gram-positive bacteria and mainly consists of peptidoglycan (PG), a polymeric mesh-like structure of alternating glycan units: *N*-acetylglucosamine (GlcNAc) and *N*-acetylmuramic acid pentapeptide (MurNAc-pentapeptide), with the latter being cross-linked via peptidyl bridges.^{45,46} The PG unit structure is the same in both Gram-positive and Gram-negative bacteria, differing in the third amino acid in the pentapeptide chain, where it is *L*-Lys in Gram-positive and *meso*-diaminopimelic acid (*mDAP*) in Gram-negative bacteria.⁴⁷ This peptidoglycan layer forms 30-70% of the Gram-positive bacteria's cell wall in addition to polysaccharides, teichoic or teichuronic acids, but it represents a minor component (<10%) in Gram-negative cell walls which mainly consist of lipopolysaccharides (LPS) and lipoproteins (*Figure 1.3*).^{45,48} It is unique to prokaryotic cells, and with approximately 20 specialized enzymes involved in its synthesis and maintenance, it is therefore a rich source for targets for antibacterial drug discovery.^{44,49}

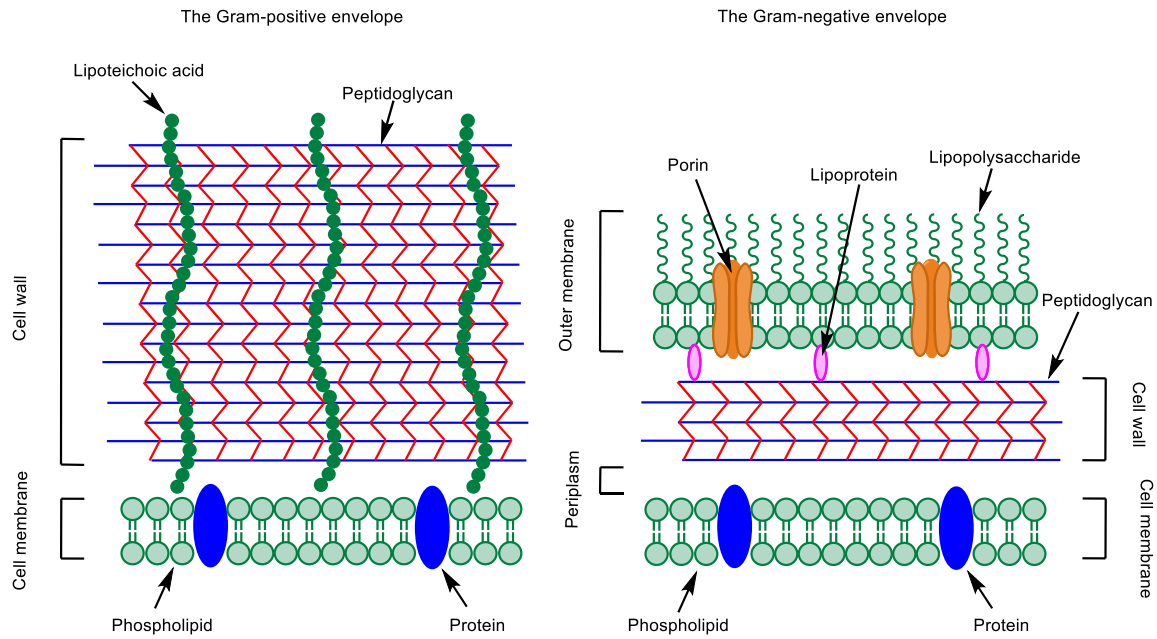


Figure 1.3. Bacterial cell wall structure in Gram-positive and Gram-negative bacteria

(Inspired by: Green; *Expert Opin. Ther. Targets.* **2002**, 6, 1-20)⁴⁷

1.4 Peptidoglycan Biosynthesis

The biosynthetic pathway of peptidoglycan involves three stages: an intracellular first stage in which the UDP-*N*-acetylmuramyl pentapeptide (UDP-MurNAc pentapeptide) building block is assembled; a second membrane-associated stage where the lipid intermediates (lipids I and II) are synthesized to transfer the synthesized building block across the cell membrane; and an extracellular last stage where this monomer is added to the growing cell wall polymer via glycosyltransferases and transpeptidases.⁵⁰⁻⁵²

1.4.1 UDP-GlcNAc Synthesis Pathway

The first stage starts with the formation of UDP-GlcNAc from fructose-6-phosphate over four steps (*Figure 1.4*).^{52,53} The first step involves the enzyme glucosamine-6-phosphate synthase (GlmS), which catalyzes the glutamine-dependent transformation of fructose-6-phosphate into glucosamine-6-phosphate (GlcN-6-P).⁵³⁻

⁵⁵ In the next step, phosphoglucosamine mutase (GlmM) reversibly converts GlcN-6-

P into glucosamine-1-phosphate (GlcN-1-P) through a glucosamine-1,6-diphosphate intermediate.⁵⁶ The last two steps of the process are the acetyl transfer and uridylyate transfer reactions, which are both performed by the bifunctional glucosamine-1-phosphate acetyl-transferase and *N*-acetylglucosamine-1-phosphate uridylyate transferase enzyme (GlmU) which uses acetyl-coenzyme A (Ac-CoA) and UTP to produce the UDP-GlcNAc building block.^{57,58}

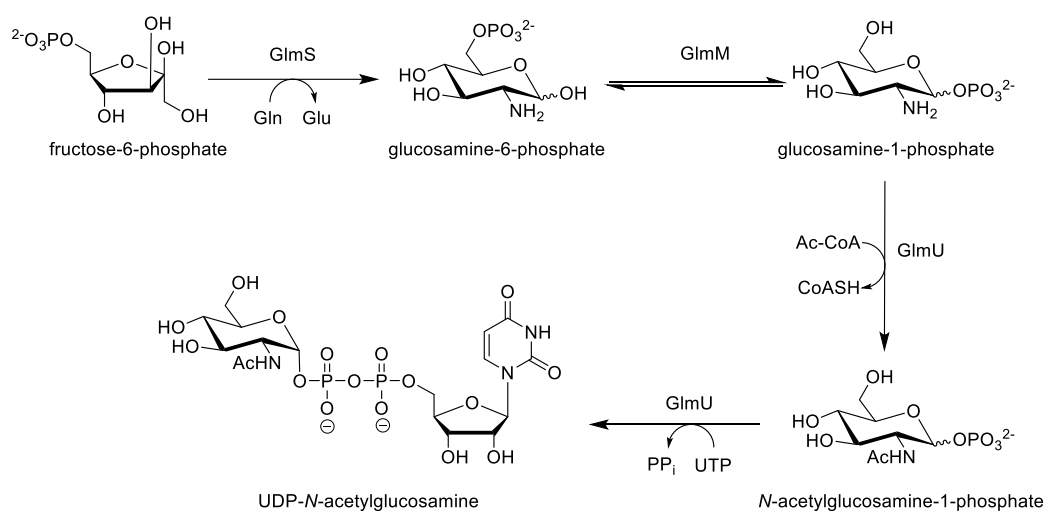


Figure 1.4. Biosynthesis of UDP-GlcNAc

1.4.2 Synthesis of UDP-MurNAc Pentapeptide

The first committed step of PG biosynthesis is the transformation of UDP-GlcNAc into UDP-MurNAc pentapeptide through the action of the Mur family of enzymes, MurA to MurF (Figure 1.5) (more details in section 1.5).⁵⁹⁻⁶¹ The biosynthesis starts through the action of the first enzyme of the series, MurA, which acts as an enolpyruvyl transferase adding an enolpyruvate moiety from phosphoenolpyruvate (PEP) to the 3-OH of UDP-GlcNAc to form EP-UDP-GlcNAc, releasing inorganic phosphate (P_i) as a second product.^{62,63}

The next enzyme in the series is MurB which acts as a reductase to produce UDP-N-acetylmuramic acid (UDP-MurNAc) through the NADPH-dependent reduction of EP-UDP-GlcNAc.^{64,65} After that, the ATP-dependent Mur ligases (MurC - MurF)

sequentially add amino acids to UDP-MurNAc to ultimately form the pentapeptide derivative of UDP-MurNAc. The amino acid residues that are added are L-Ala by MurC, D-Glu by MurD, *meso*-diaminopimelic acid (*mDAP*) in Gram-negative or L-Lys in Gram-positive bacteria by MurE, and finally a D-Ala-D-Ala dipeptide unit by MurF.^{66,67} The MurF co-substrate D-Ala-D-Ala is produced from L-Ala in two steps performed by the enzymes alanine racemase (*Alr*), which transforms L-Ala into D-Ala, and D-Ala-D-Ala ligase (*Ddl*) which forms the dipeptide.⁶⁸⁻⁷⁰

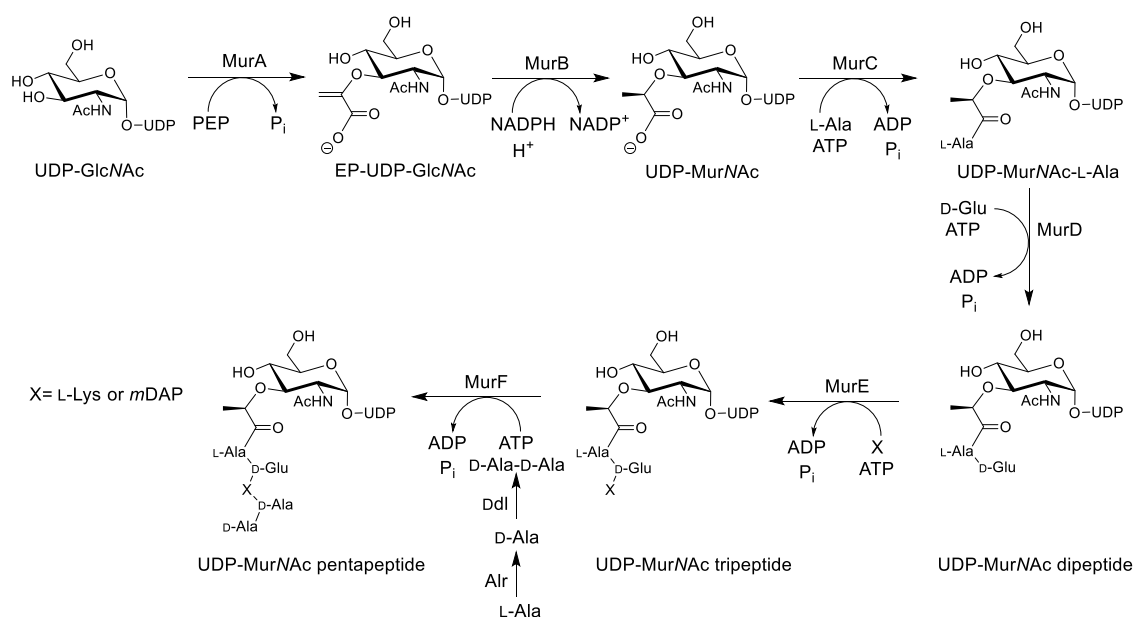


Figure 1.5. Cytoplasmic steps of PG biosynthesis

1.4.3 Membrane-associated Steps of PG Biosynthesis

The first membrane-associated steps of PG biosynthesis are the formation of lipid I and lipid II, mediated by the action of *MraY* and *MurG*.^{61,71} *MraY* or phospho-MurNAc-pentapeptide translocase is an integral membrane protein catalyzing the transfer of UDP-MurNAc pentapeptide to the lipid carrier undecaprenyl phosphate ($C_{55}\text{-P}$) to furnish undecaprenyl-pyrophosphoryl-MurNAc-pentapeptide (lipid I) releasing UMP as a by-product.⁷¹⁻⁷³ The last intracellular cell wall synthesis enzyme, *MurG* or *N*-acetylglucosaminyl transferase catalyzes the addition of *N*-acetylglucosamine

(GlcNAc) from UDP-GlcNAc to the MurNAc-pentapeptide unit, thus forming undecaprenyl-pyrophosphoryl MurNAc-pentapeptide-GlcNAc (lipid II) (Figure 1.6).⁷⁴⁻⁷⁶

The FEM ABX enzymes are involved in modification of the *S. aureus* pentapeptide chain, for which the FEM enzymes catalyze the addition of an interchain peptide consisting of five glycine residues attached to L-Lys of the pentapeptide chain.^{77,78} This interchain peptide is then involved in the transpeptidation step that occurs at the outside of the membrane.^{78,79} Additionally, in several Gram-positive organisms, the MurT/GatD enzymatic complex catalyzes the amidation of the D-Glu of the pentapeptide chain into D-Gln.^{80,81} The linked disaccharide MurNAc-pentapeptide-GlcNAc, is subsequently transferred across the cell membrane where it undergoes both polymerization and crosslinking.^{71,82}

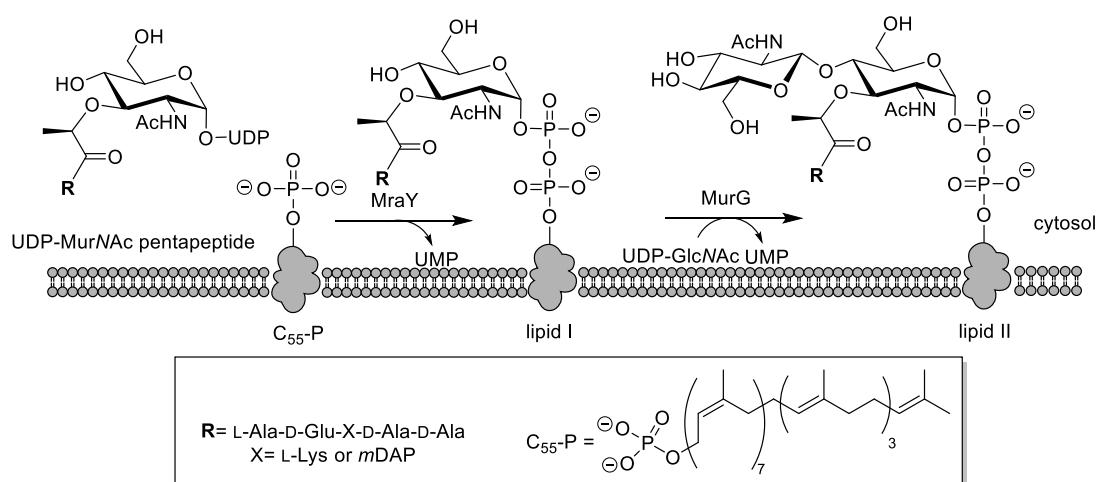


Figure 1.6. Membrane-associated steps of PG synthesis

1.4.4 Extracellular Steps of PG Biosynthesis

Lipid II is translocated across the bacterial membrane through the action of a “flippase enzyme”. The identity of this flippase enzyme has been unknown for a long time, but recently, it has been debated to either be FtsW or MurJ.⁸³⁻⁸⁵ The case for either protein

being the missing “flippase enzyme” has been presented, but a conclusion on the identity of the specific protein and whether the flipping action could be performed by both proteins together has not been reached.^{83,86–89}

After the translocation step, the glycosyltransferase enzymes (GTs) synthesize the glycan chain of the PG, while simultaneously coordinating the hydrolysis of the preexisting PG mesh to incorporate the newly synthesized material without compromising the integrity of the cell.^{84,90} Penicillin-binding proteins (PBPs) perform this GT action in addition to the transpeptidation (TP) step that follows. These proteins can be monofunctional, catalyzing either the GT or TP actions, or bifunctional, catalyzing both actions.^{46,90–92} Transpeptidation occurs between the pentapeptide chains of the growing PG and the preexisting glycopeptide chain, providing the bacterial cell wall with rigidity and structure.^{46,90} Transpeptidation involves the serine-mediated activation of D-Ala at position 4 of the pentapeptide, followed by nucleophilic attack of an amino group of the side chain and release of the terminal D-Ala (position 5 of the pentapeptide chain). The nucleophilic amino group differs according to the bacterial species.^{46,78,90} In case of *E. coli*, the mDAP at position 3 of the pentapeptide is involved, while in the case of *S. aureus*, the L-Lys-pentaglycine takes part in the cross-linking with 4-D-Ala.^{46,78,93} This TP step is the main target of β -lactams which act by mimicking the terminal D-Ala-D-Ala, forming a long-lived acyl intermediate with the active serine residue of the TP. Moreover, it is also the target of glycopeptides such as vancomycin which attaches to the D-Ala-D-Ala moiety of the substrate, preventing the recognition by the TP.^{76,93,94} Further modifications in the glycan chain or the peptide stem of the PG structure can occur in several bacterial species to help the bacteria evade the host immune system whether.^{46,95} Examples of glycan modifications are *O*-acetylation of C-6 of the MurNAc, *N*-glycolylation at C-2 of

MurNAc, *N*-deacetylation of C-2 of the GlcNAc, or covalent addition of teichoic acids at C-6 of MurNAc in Gram-positive bacteria.⁹⁶⁻⁹⁹ Modifications to the peptide stem include amidation of D-Glu at the second position of the peptide chain, amidation of *m*DAP at the third position or its replacement by L-ornithine, or the more recently discovered incorporation of non-canonical D-amino acids at the peptide chain termini.^{80,100-104}

1.5 Mur Enzymes

The Mur enzyme family is comprised of six enzymes (MurA to MurF) that catalyze the conversion of the cell wall precursor UDP-GlcNAc into UDP-MurNAc pentapeptide.^{46,51,67} They each produce the substrate of the next enzyme of the series, and their products are tightly regulated by the bacterial cells (*Table 1.2*).^{53,105-108} They represent unique targets for antibacterial agents as they are essential enzymes for the bacterial cell's survival and replication and are exclusive to the prokaryotic bacterial cells.^{60,67,93} Their X-ray crystal structures are available, showing similarities across different bacterial species in their principal architecture, and catalytic sites (*Table 1.2*).^{60,67,109}

Table 1.2. Mur enzyme family: function, substrates, products, and X-ray crystal structures.

Enzyme	Function	Substrates	Product	X-ray Crystal Structures (PDB)
MurA	Transferase	UDP-GlcNAc, PEP	EP-UDP-GlcNAc, P _i	See section 1.6.1
MurB	Reductase	EP-UDP-GlcNAc, NADPH	UDP-MurNAc, NADP ⁺	1MBT, ⁶⁵ 4JAY, ¹¹⁰ 2MBR, ¹¹¹ 2Q85 ¹¹²

MurC	Transferase/Ligase	UDP-MurNAc, L-Ala, ATP	L-Ala-UDP- MurNAc, ADP, P _i	2F00, ¹¹³ 1J6U, ¹¹⁴ 1P3D ¹¹⁵
MurD	Transferase/Ligase	L-Ala-UDP- MurNAc, D-Glu, ATP	L-Ala-D-Glu- UDP- MurNAc, ADP, P _i	2JFH, ¹¹⁶ 2Y67, ¹¹⁷ 2X50, ¹¹⁸ 2XPC, ¹¹⁹ 2UUO ¹²⁰
MurE	Transferase/Ligase	L-Ala-D-Glu- UDP-MurNAc, X*, ATP	L-Ala-D-Glu- X*-UDP- MurNAc, ADP, P _i	1E8C, ¹²¹ 2XJA, ¹²² 4C12, ¹²³ 4BUB ¹²⁴
MurF	Transferase/Ligase	L-Ala-D-Glu-X*- UDP-MurNAc, D-Ala-D-Ala, ATP	L-Ala-D-Glu- X*-D-Ala-D- Ala-UDP- MurNAc, ADP, P _i	1GG4, ¹²⁵ 3ZL8, ¹²⁴ 4QDI, ¹²⁶ 3ZM5, ¹²⁷ 2AM1 ¹²⁸

*X = mDAP in Gram-negative bacteria, and L-Lys in Gram-positive bacteria

Another advantage for Mur enzymes as targets for the development of antibacterial agents is the ease of their monitoring in activity assays. This is owed to the fact that five of the six enzymes (MurA and the Mur ligases MurC to F) release P_i as a side product of the enzymatic reaction, which can be monitored through a simple malachite green assay.^{66,129-131} This assay detects P_i by production of a green complex with the malachite green dye that can then be detected spectroscopically at 625-650 nm.^{130,132} The activity of MurB can be monitored through an NADPH-based assay, which detects the decrease in NADPH absorbance at 340 nm.¹³³ Additional activity assays for the Mur enzymes are listed in *Table 1.3*.

Table 1.3. Additional methods for activity assays for Mur enzymes.

Mur Enzyme	Assay
MurA	Capillary electrophoresis and detection of the product EP-UDP-GlcNAc ¹³⁴

MurB	Detection of decrease in NADPH fluorescence at $\lambda_{\text{ex}}=340$ nm and $\lambda_{\text{em}}=460$ nm ¹³⁵
MurC	LC-MS-based assay measuring L-Ala-UDP-MurNAc production ¹³⁶
MurD	Radioactivity-based assay, monitoring the reaction of radiolabeled D-[¹⁴ C] Glu with L-Ala-UDP-MurNAc ¹¹⁷
MurE	Radioactivity-based thin-layer chromatography (TLC) assay detecting the amount of radioactivity in the radiolabeled product L-Ala-D-Glu- <i>m</i> [¹⁴ C] DAP-UDP-MurNAc ^{137,138}
MurF	Radioactivity-based assay monitoring the formation of the radioactive product; L-Ala-D-Glu- <i>m</i> [¹⁴ C] DAP-D-Ala-D-Ala-UDP-MurNAc ¹²⁹

1.5.1 Inhibitors of Mur Enzymes

Many inhibitors have been developed over the years to target each member of the Mur family of enzymes. However, this multitude of inhibitors did not afford any new antibacterial drug, with only the MurA inhibitor fosfomycin being in clinical use.¹³⁹

MurA inhibitors are discussed in full details in section 1.6.2. MurB inhibitors (*Figure 1.7*) include 4-thiazolidinone derivatives,¹³³ imidazolinones,¹⁴⁰ and alkyl pyrazolidinediones.¹⁴¹

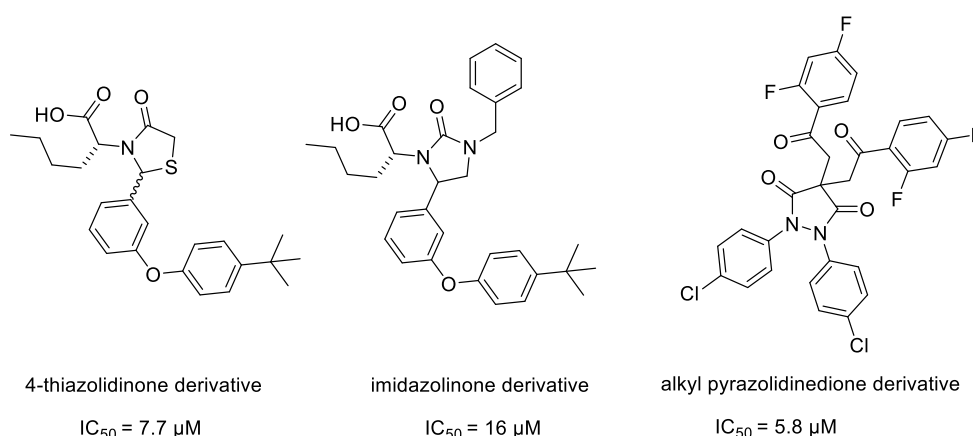


Figure 1.7. Examples of MurB inhibitors; IC₅₀ values for *E. coli* MurB

MurC inhibitors are more diverse in structure (*Figure 1.8*) and include the very potent phosphinate transition state analogues, also used for MurD and MurE inhibition,^{142,143} benzylidene rhodanines,¹⁴⁴ *N*-acylhydrazones,¹⁴⁵ benzofuran acyl-sulfonamides,¹⁴⁶ sulfonylhydrazide derivatives,¹⁴⁷ and pulvinamide.¹⁴⁸

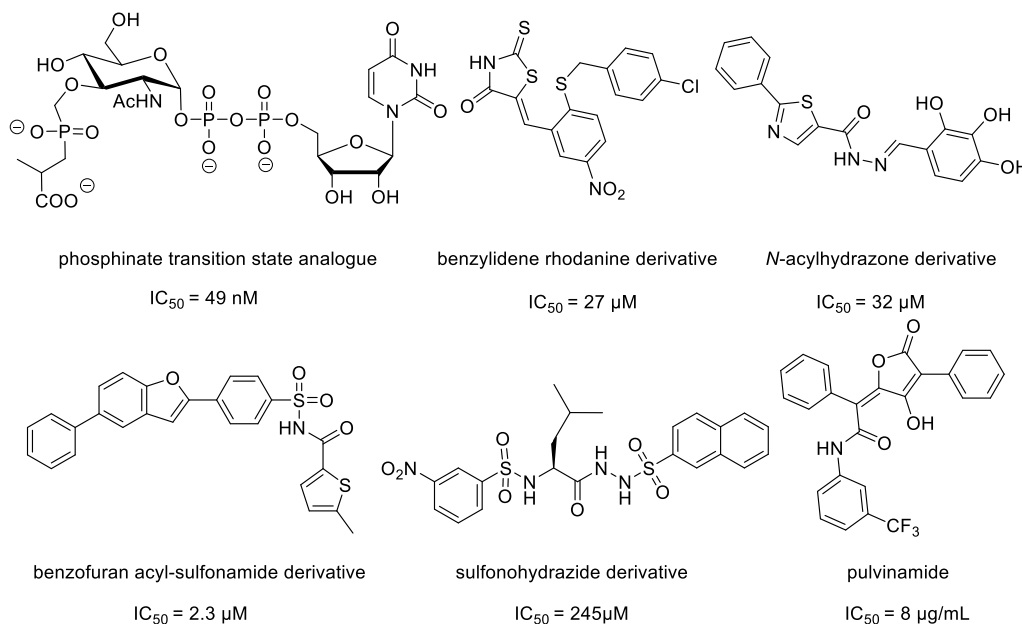


Figure 1.8. Examples of MurC inhibitors; IC₅₀ values for *E. coli* MurC.

There is also a large variety of available and potent MurD inhibitors (*Figure 1.9*) such as 9*H*-Xanthene derivatives,¹²⁹ phosphinate transition state analogues,^{149,150} naphthalene sulfonamides with and without a D-glutamic acid moiety,^{116,119,120} macrocyclic inhibitors,¹⁵¹ 5-benzylidenerhodanines,^{118,152-154} as well as peptide inhibitors.¹⁵⁵

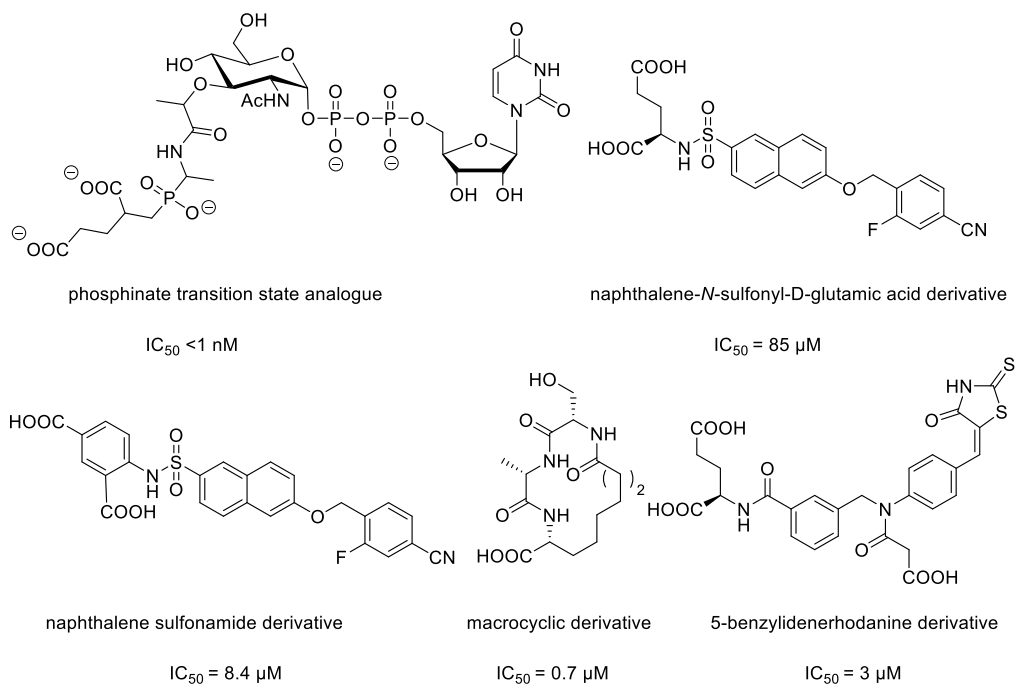


Figure 1.9. Examples of MurD inhibitors; IC_{50} values for *E. coli* MurD

There is a limited number of available MurE inhibitors (*Figure 1.10*) such as the already established phosphinate transition state analogues,¹⁵⁶ sulfonamides,¹⁵⁷ plant-derived 3-methoxynordomesticine¹⁵⁸ and olympicin,¹⁵⁹ in addition to peptide inhibitors.^{155,160}

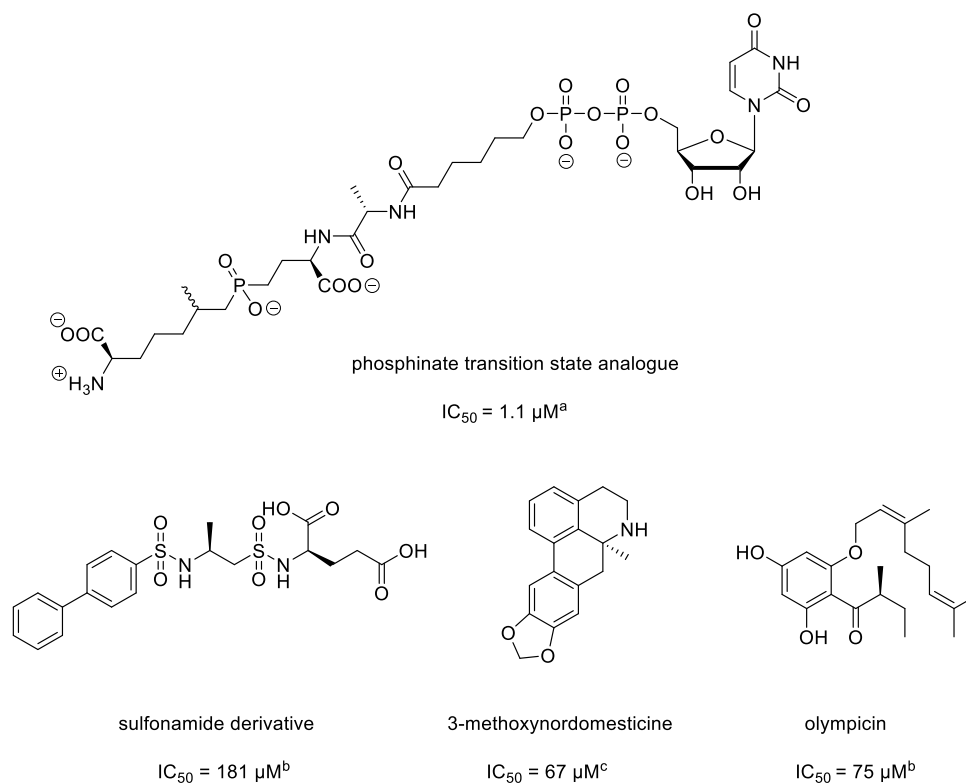


Figure 1.10. Examples of MurE inhibitors; ^aInhibition tested with *E. coli* MurE;

^bInhibition tested with *S. aureus* MurE; ^cInhibition tested with *M. tuberculosis* MurE

MurF inhibitors (Figure 1.11) include 1,3,5-triazine derivatives,¹²⁹ various cyanothiophene derivatives,^{127,128,161–163} thiazolylaminopyrimidine derivatives,¹⁶⁴ 8-hydroxy quinolines,¹⁶⁵ diarylquinolines,¹⁶⁶ in addition to pseudo-tri- and -tetrapeptide aminoalkylphosphinic acids.¹⁶⁷

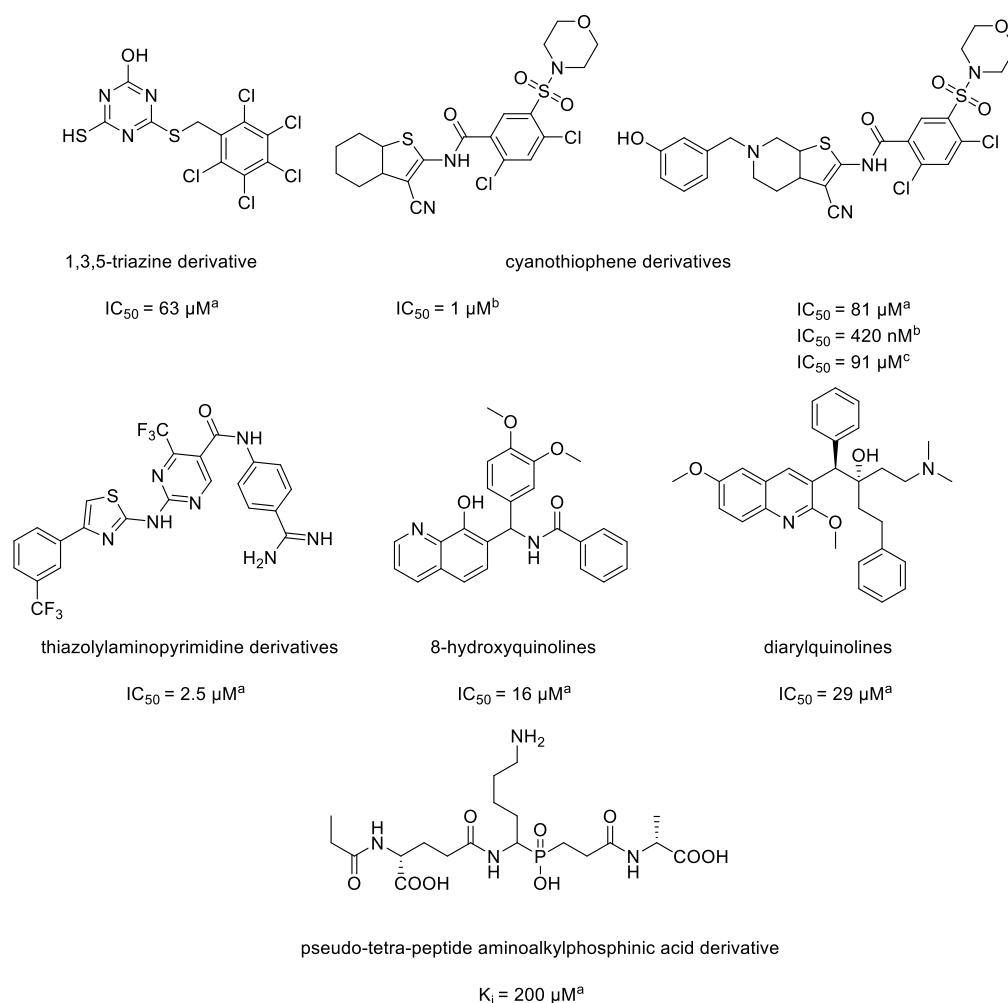


Figure 1.11. Examples of MurF inhibitors; ^aInhibition tested with *E. coli* MurF;

^bInhibition tested with *S. pneumoniae* MurF; ^cInhibition tested with *S. aureus* MurF

Finally, inhibitors of multiple Mur enzymes (*Figure 1.12*) have been developed, such as the dual MurA/MurB inhibitors: pyrazolidinedione derivatives,¹³⁸ and phenyl thiazolyl urea derivatives;¹⁶⁸ the MurC/MurD inhibitors: *N*-benzylidenesulfonohydrazide derivatives¹⁴⁷ and *N*-acylhydrazones;¹⁴⁵ the MurD/MurE inhibitors: benzene-1,3-dicarboxylic acid derivatives;¹⁶⁹ and the multiple Mur enzyme inhibitors: naphthyl tetrionic acid derivatives,¹¹² pulvinones,¹⁴⁸ phosphorylated hydroxyethylamines,¹⁷⁰ 2-phenyl-5,6-dihydro-2*H*-thieno[3,2-*c*]pyrazol-3-ol derivatives,¹⁷¹ 5-benzylidenethiazolidin-4-ones,¹⁷² and finally, benzene-1,3-dicarboxylic acid 2,5-dimethylpyrroles.^{66,169}

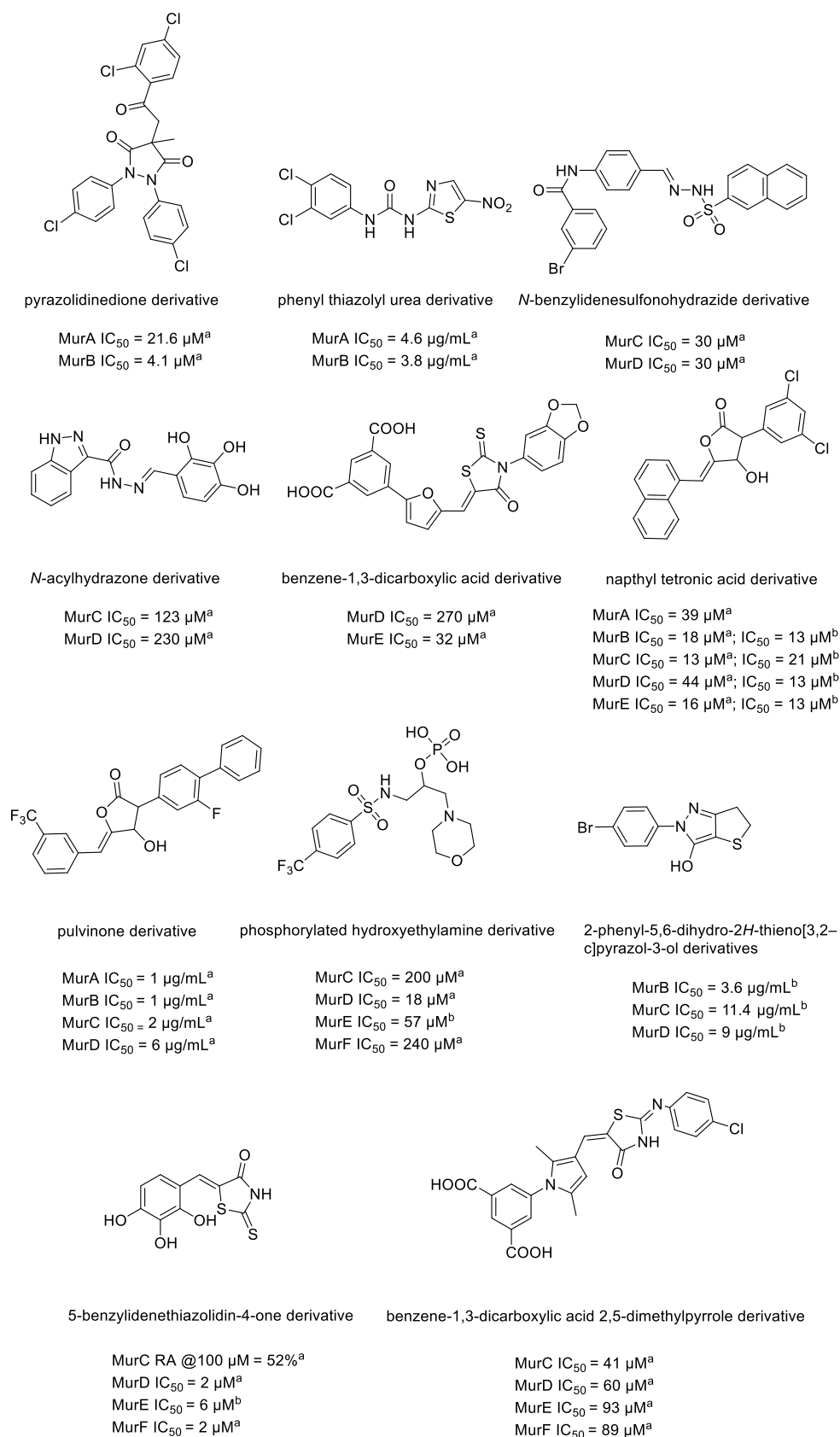


Figure 1.12. Inhibitors of multiple Mur enzymes; ^aInhibition tested with *E. coli* enzymes;

^bInhibition tested with *S. aureus* enzymes

In general, the discovered Mur inhibitors suffer from several problems which hamper their further development into clinically used antibacterials. These problems include: insufficient potency on the target enzymes,^{147,155,157,167} lack of *in vitro* antibacterial activity,^{147,173} toxicity to mammalian cells,¹⁴⁴ binding to bovine serum albumin (BSA),¹⁴⁶ and off-target inhibition.^{146,163} Also, some of the reported inhibitors can be considered pan-assay interference compounds (PAINS).^{144,145,152,174}

1.6 MurA

MurA (UDP-*N*-acetylglucosamine 1-carboxyvinyltransferase) is the first member of the Mur enzyme family. It catalyzes the conversion of UDP-GlcNAc into EP-UDP-GlcNAc, through the addition of an enolpyruvyl moiety from PEP to the 3-OH of the UDP-GlcNAc (Figure 1.13).^{63,175,176}

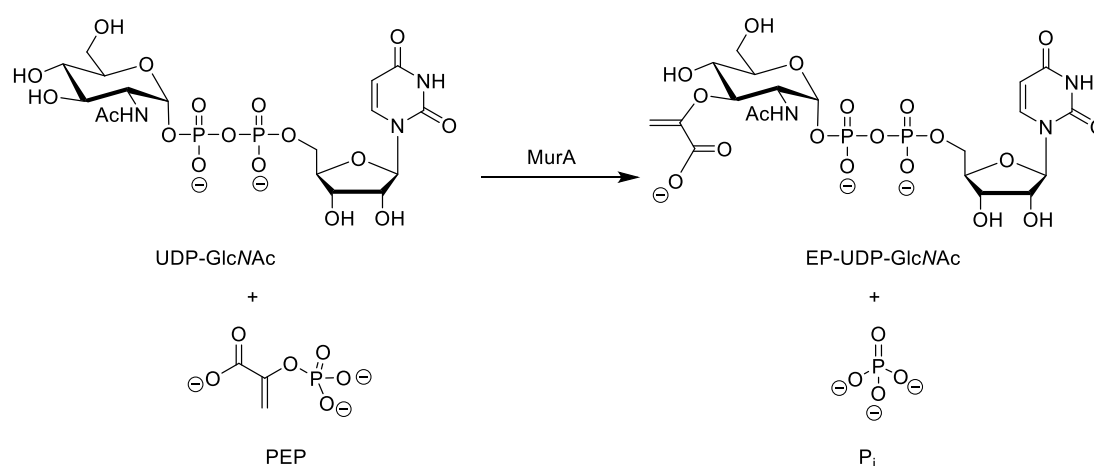


Figure 1.13. MurA-catalyzed reaction

MurA is one of only two known enolpyruvyl transferases that cleave the C–O bond of PEP, in addition to 5-enolpyruvyl-shikimate-3-phosphate (EPSP) synthase (AroA).¹⁷⁷⁻¹⁷⁹ EPSP synthase is an enzyme in the shikimic acid pathway and is therefore involved in the synthesis of aromatic amino acids in plants, fungi and bacteria.¹⁸⁰⁻¹⁸² MurA is the target of the antibiotic fosfomicin, while the herbicide glyphosate inhibits EPSP

synthase.^{139,180,183,184} MurA is an attractive target for antibacterial drug discovery, as it is the only Mur enzyme with an available, clinically used antibiotic.^{59,185}

1.6.1 MurA Structure and Catalysis

The *murA* gene is comprised of approximately 1260 base pairs and codes for the MurA enzyme which has about 419 amino acids (*E. coli* numbering) and an approximate molecular weight of 44.7 kDa.¹⁸⁶ It is a globular protein composed of two domains connected by a double-stranded linker: the catalytic domain (residues 22-229) and the C-terminal domain (residues 1-21 and 230-419).^{63,186} The main structure of both domains is very similar, with the overall structure consisting of six folding units, each consisting of two α -helices and four β -sheets (*Figure 1.14*).^{63,187} The catalytic site is located at the interphase between these domains, where the flexible surface loop (Pro111-Pro121) contains the vital Cys115 residue.^{62,188} This loop acts as a lid for the catalytic site with the residues surrounding the binding pocket forming intermolecular hydrogen bonds that are essential for the enzymatic reaction.^{186,188} It also contains three conserved glycine residues (Gly 113, 114, and 118) that aid in the transition of the loop states serving as a hinge.^{62,189}

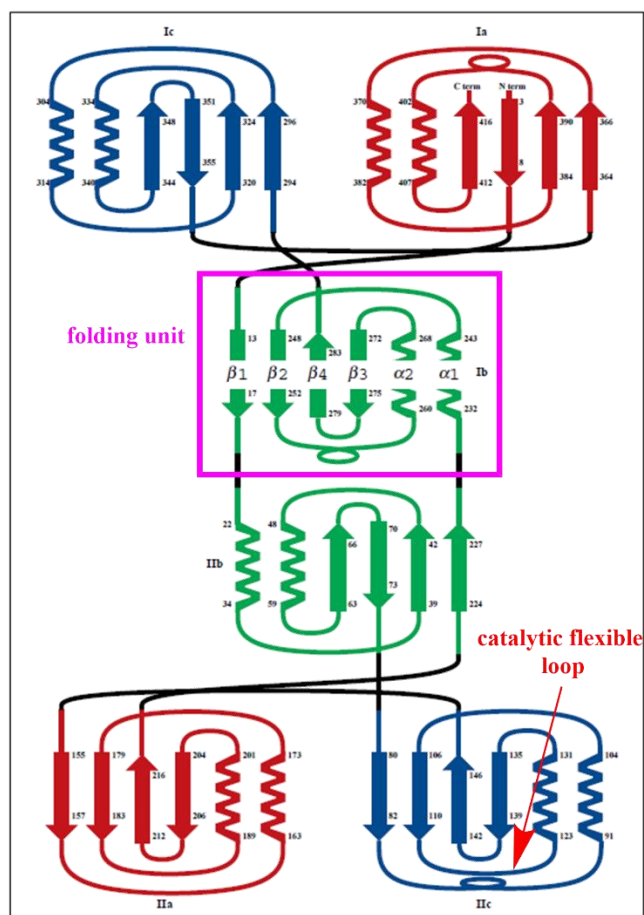


Figure 1.14. Topology sketch of *E. cloacae* MurA. The figure shows the six-fold repetition of a single folding unit. The flexible loop containing Cys115 is marked by an arrow (taken and modified from: Schönbrunn *et al.*; *Structure*. **1996**, 4, 1065-1075).¹⁸⁷

This loop was postulated to adopt an open conformation when no ligand is bound and a closed conformation upon UDP-GlcNAc binding.^{190,191} The thiol group of the catalytically important Cys115 is the target for covalent binding by both the antibiotic fosfomycin and PEP.^{192,193} The covalent modification, however, is not essential for catalysis, as evidenced by the C115D mutant which, while fully resistant to fosfomycin, is still enzymatically active.¹⁹⁴ The inactivity of the C115S and C115A mutants suggests that while the Cys115 residue might not be essential for the activity as a nucleophile, it still plays a critical role in the enzymatic process.^{176,193,194} It was suggested that the thiol group of cysteine serves as a general acid in the protonation of the C-3 of PEP.⁶³ The activity of the Asp115 mutant, albeit with a higher preferred

pH for activity than the WT enzyme, in addition to this mutation being naturally present in some bacterial species, proposes that ionization of the Asp plays a similar role to the Cys ionization.^{190,194,195} The studies by Wanke and Ammerhein, as well as, Brown, *et al.* proved that the Cys115 takes part in the formation of a covalent phospholactyl-enzyme adduct, so the overall conclusion is that Cys115 acts as both an enzyme nucleophile and a general acid in the catalytic mechanism (*Figure 1.15*).^{190,193,194,196}

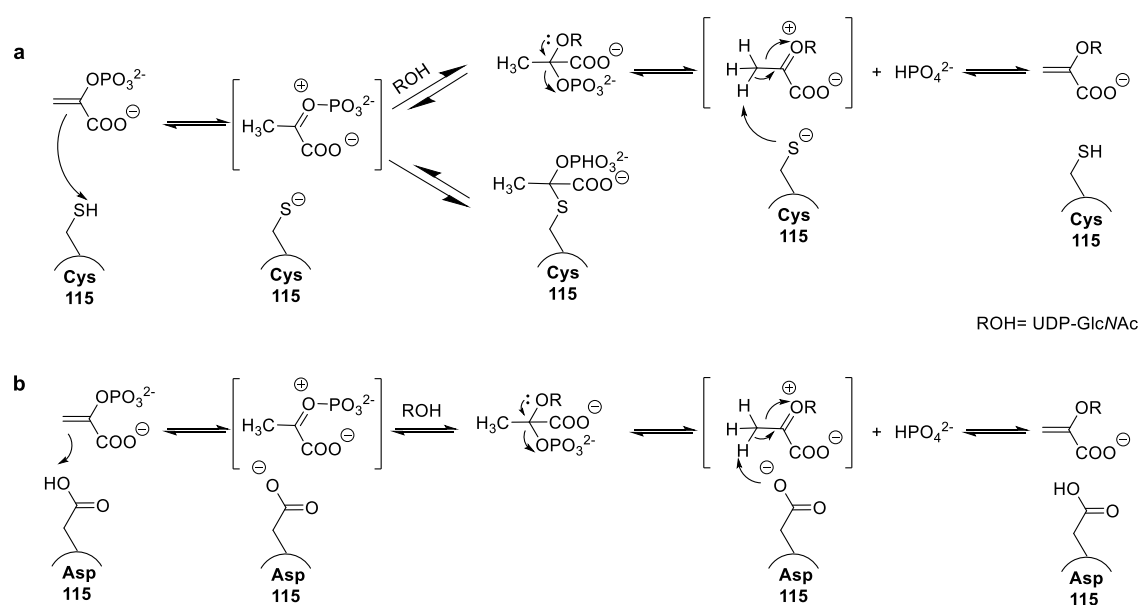


Figure 1.15. MurA catalysis in case of: **a.** WT MurA **b.** C115D MurA

Other important residues for catalysis and binding are Lys 22, Arg120, and Arg397 which interact with the phosphate group of UDP-GlcNAc, providing strong electrostatic interactions and five hydrogen bonds.^{63,189,197} Additionally, Asn23 and Asp305 stabilize the transition states of the enzyme and may help in the binding and affinity to UDP-GlcNAc and are highly conserved across bacterial species.^{189,198}

The catalytic mechanism of MurA was first hypothesized to be through an induced fit process where first, UDP-GlcNAc binds to the open form of the enzyme inducing a large conformational change of the flexible loop and transitioning the enzyme into the

closed form. This closed form can then bind to the PEP at Cys115 and start the catalytic reaction.^{63,192,199} This has been challenged by discovering that PEP could bind to the free enzyme causing conformational changes, so the strict induced fit model does not fully apply in this case.¹⁹²

It was later proposed that MurA is expressed in a dormant complex covalently bound to its substrate PEP at the Cys115 residue and in complex with the MurB product UDP-MurNAc.^{196,200} This was due to the finding that purified recombinant MurA was bound to UDP-MurNAc in absence of added MurB substrates and after several rounds of purification.^{105,200} At increased UDP-GlcNAc concentrations, the bound UDP-MurNAc is displaced and the enzyme forms the tetrahedral intermediate (THI), which breaks down into the reaction products EP-UDP-GlcNAc and P_i. The enzymatic reaction is renewed when PEP displaces the P_i and UDP-GlcNAc replaces EP-UDP-GlcNAc (*Figure 1.16*). This proposal suggests that the binding of the UDP-MurNAc is a form of feedback regulation when the MurB product is increasingly formed and the UDP-GlcNAc is depleted.²⁰⁰

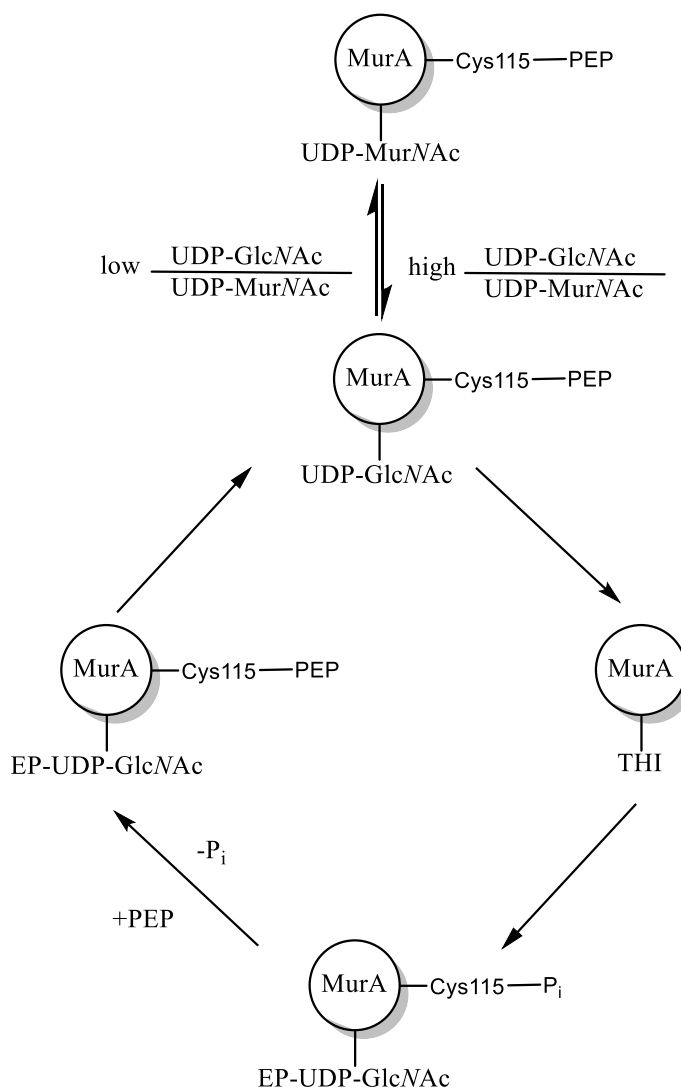


Figure 1.16. Schematic mechanism of MurA catalysis

There are several available X-ray crystal structures for MurA in different states (*Table 1.4*) whether ligand-free, in the dormant complex form with UDP-MurNAc and the covalent Cys-PEP adduct, or bound to its substrates or products or finally in complex with several of its inhibitors. It is noteworthy that despite the many crystal structures of MurA from Gram-negative bacteria, not a single crystal structure of the protein from Gram-positive organisms has been reported.¹⁸⁸ Additionally, several previously published MurA structures were revised and corrected, as they had incorrectly labelled the UDP-MurNAc in the dormant form as UDP-GlcNAc.²⁰⁰ This dormant complex was able to withstand many of the solvents used in crystallization, and only

preincubating the enzyme with UDP-GlcNAc or in a phosphate buffer could give the active form of the enzyme.²⁰⁰

Table 1.4. Available X-ray crystal structures of MurA

PDB entry	Organism (MurA subtype)	Ligand(s)	R (Å)
1EJD ¹⁹¹	<i>E. cloacae</i> (WT)	unliganded	1.55
1EJC ¹⁹¹	<i>E. cloacae</i> (WT)	unliganded	1.80
1NAW ¹⁸⁷	<i>E. cloacae</i> (WT)	unliganded	2.00
3SPB ²⁰⁰	<i>E. cloacae</i> (WT)	unliganded	2.30
3V5V ²⁰⁰	<i>E. cloacae</i> (C115D)	unliganded	2.70
1DLG ¹⁹²	<i>E. cloacae</i> (C115S)	unliganded	1.90
3SWD ²⁰⁰	<i>E. coli</i> (WT)	UDP-MurNAc, PEP-Cys115*	2.50
3SU9 ²⁰⁰	<i>E. cloacae</i> (WT)	UDP-MurNAc, PEP-Cys115*	2.20
3SWE ²⁰⁰	<i>H. influenzae</i> (WT)	UDP-MurNAc, PEP-Cys117*	2.20
3SWG ²⁰⁰	<i>A. aeolicus</i> (WT)	UDP-MurNAc, PEP-Cys124*	1.81
3KQJ ²⁰¹	<i>E. coli</i> (WT)	UDP-GlcNAc	1.70
3UPK ²⁰⁰	<i>E. cloacae</i> (WT)	UDP-GlcNAc	2.00
3V4T ²⁰⁰	<i>E. cloacae</i> (C115D)	UDP-GlcNAc	2.50
3SWA ²⁰⁰	<i>E. cloacae</i> (R120A)	UDP-GlcNAc, PEP-Cys115*	1.90
1Q3G ¹⁸¹	<i>E. cloacae</i> (D305A)	Tetrahedral reaction intermediate	2.65
1A2N ¹⁷⁶	<i>E. coli</i> (C115A)	Fluorinated tetrahedral reaction intermediate	2.80
1RYW ²⁰²	<i>E. cloacae</i> (C115S)	EP-UDP-GlcNAc	2.30
3SWQ ²⁰⁰	<i>E. cloacae</i> (WT)	EP-UDP-GlcNAc	1.83
3SWI ²⁰⁰	<i>E. cloacae</i> (WT)	EP-UDP-GalNAc, PEP-Cys115*	2.80
1UAE ⁶³	<i>E. coli</i> (WT)	UDP-GlcNAc, fosfomycin-Cys115*	1.80
3KR6 ²⁰¹	<i>E. cloacae</i> (WT)	UDP-GlcNAc, fosfomycin-Cys115*	1.70
3LTH ²⁰¹	<i>E. cloacae</i> (WT)	UDP-GlcNAc, fosfomycin-Cys115*	1.75
3KQA ²⁰¹	<i>E. cloacae</i> (WT)	Terreic acid-Cys115*	2.25
2Z2C ²⁰³	<i>E. coli</i> (WT)	UNAG-cnicin adduct	2.05
1YBG ¹⁷⁹	<i>E. cloacae</i> (WT)	5-sulfonyl-anthranilic derivative (T6361)	2.60
1EYN ²⁰⁴	<i>E. cloacae</i> (WT)	ANS	1.70

*covalent adduct with the catalytic Cys residue of the enzyme.

1.6.2 MurA Inhibitors

1.6.2.1 Fosfomycin

Fosfomycin, originally called phosphonomycin, is the first and only reported Mur inhibitor in clinical use.^{139,205} It is a naturally occurring broad-spectrum antibiotic produced by *Streptomyces* species that was discovered by Hendlin *et al.* in 1969.^{183,206} It has been clinically used since the 1980s to treat lower urinary tract infections (UTIs), primarily cystitis in women, in addition to the treatment of pediatric gastrointestinal infections with Shiga-like-toxin-producing *E. coli* in Japan.^{59,205,207,208} It is an irreversible covalent inhibitor of MurA, binding in a time-dependent manner to the catalytic Cys115 residue (*Figure 1.17*).^{139,209} It acts as a competitive inhibitor, competing with PEP for the active site, and depends on the presence of UDP-GlcNAc for its binding and activity, with a reported IC₅₀ value of 8.8 μM against *E. coli* MurA.^{139,209,210} It binds between UDP-GlcNAc and the enzyme through a series of hydrogen bonds, and its phosphonate group is surrounded by three positively charged residues (Lys22, Arg120 and Arg 397) providing strong electrostatic interactions.⁶³

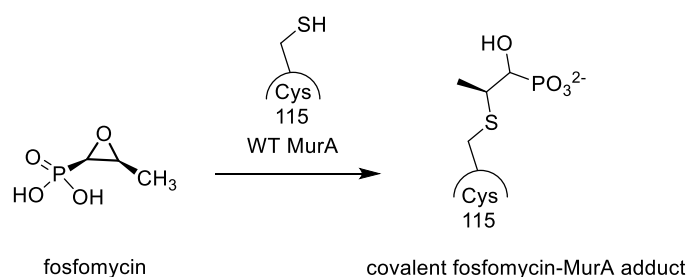


Figure 1.17. Mechanism of MurA inhibition by fosfomycin

There are several resistance mechanisms that bacteria use to evade the effect of fosfomycin. The first of these is the natural resistance of species such as *Mycobacterium tuberculosis* and *Chlamydia trachomatis* which contain an Asp residue

instead of the catalytic Cys.^{194,195,211} The second mechanism of inhibition involves decreased uptake of fosfomicin into bacterial cells through mutations of the responsible systems in the bacteria, namely, the glycerol-3-phosphate transporter (GlpT) and the hexose phosphate transporter (UhpT).^{212,213} Another mechanism for resistance is the overexpression of MurA.^{208,214} Moreover, the presence of enzymes that inactivate fosfomicin by reacting its oxirane ring with either glutathione, L-cysteine, or water confers resistance to fosfomicin, with the *fosA*, *fosB*, and *fosX* genes encoding these inactivating transferases.^{212,215} A second group of inactivating enzymes are the Fom A, FomB, and FosC enzymes which act in a similar manner to eukaryotic protein kinases, transferring one or more phosphate groups to the structure of fosfomicin.^{212,216} This last mechanism is hypothesized to be the method by which fosfomicin-expressing *Streptomyces* species resist the harmful effect of the antibiotic.^{217,218}

In general, the resistance to fosfomicin is spreading across different clinical bacterial isolates and in different geographical locations.^{183,219,220} However, as fosfomicin has low human toxicity and a low allergenic potential, in addition to its broad-spectrum activity even against MDR organisms, using fosfomicin against resistant infections outside the UTI indication has been attractive.^{183,205,206} This is strengthened by the fact that fosfomicin combination treatments with several antibiotics showed great potential, such as with β -lactams,²²¹ quinolones,²²² vancomycin,²²³ and aminoglycosides.²²⁴

1.6.2.2 Other MurA Inhibitors

The development of further MurA inhibitors has been ongoing since 2001 with the introduction of three chemically diverse inhibitors by Baum *et al.* (compounds **1**, **2**, and **3**; *Figure 1.18*). **1** is a cyclic disulfide, **2** is a pyrazolopyrimidine derivative, and **3**

is a purine derivative. All three were active against *E. coli* MurA at a sub-micromolar level, however, it was observed that the thiol group-containing dithiothreitol (DTT) abolished their MurA inhibition, hinting towards a general reactivity to sulfhydryl groups. They also inhibited DNA, RNA, and protein synthesis in bacteria, indicating a nonspecific antimicrobial mechanism.²¹⁰ Compound **4** showed time-dependent inhibition of MurA in a whole-cell assay for PG biosynthesis inhibition, but inactivation of other bacterial enzymes could not be ruled out.²²⁵ The phenyl thiazolyl urea derivative **5** has been synthesized to be used as a reference compound for MurB inhibition as it is a dual inhibitor on both MurA and MurB. However, when tested in our standard MurA assay, it didn't show any MurA inhibition.¹⁶⁸ Eschenburg *et al.* synthesized **6**, a 5-sulfonyl anthranilic acid derivative, and co-crystallized it with *E. cloacae* MurA (1YBG). The co-crystal showed that **6** obstructed the enzyme's transition from an open state to a closed UDP-GlcNAc-bound state.¹⁷⁹ Cnicin **7**, a sesquiterpene lactone derivative was active on both *E. coli* and *P. aeruginosa* MurA. Its co-crystal with MurA (2Z2C) showed that it follows a non-covalent suicide inhibition pattern, binding to UDP-GlcNAc and inhibiting the enzyme. Despite the co-crystal showing that there was no interaction between Cys115 and cnicin, it was inactive on C115D MurA.^{226,227} Peptide **8** modestly inhibited *P. aeruginosa* MurA exhibiting a time-independent UDP-GlcNAc-competitive mechanism.²²⁸

Aminotetralones such as **9** were introduced as MurA inhibitors by Dunsmore *et al.*, and they showed tight binding to MurA which suggested a possible covalent inhibition. They were moderately active on bacteria but were inactive against C115D MurA. Ebselen **10**, a non-toxic seleno-organic compound, has antiinflammatory properties and inhibits several mammalian enzymes such as lipoxygenases, NO synthases, NADPH oxidase, and protein kinase C.²²⁹ It also inhibits *H. influenzae* MurA

at an IC_{50} value of 0.1 μ M, covalently modifying the catalytic Cys117 of the enzyme. However, it was able to modify the surface-exposed Cys residues of the protein and it lost its activity in the presence of DTT.²³⁰ Mendgen *et al.* discovered that tulipalines and tuliposides such as compound **11** showed strong covalent MurA inhibition in addition to antibacterial activity on *E. coli*, however, these compounds were again inactive on C115D MurA.^{231,232} Benzothioxalone derivatives such as **12**, were identified in 2010 after screening a library of more than 650000 compounds. They irreversibly inhibit MurA, but are inactive on C115D MurA and show weak Gram-negative antibacterial activity. The fungal product terreic acid **13** covalently inhibits MurA, lacking enzymatic inhibition on the C115D mutant. However, it still retains its antibacterial properties in strains that overexpress MurA and strains with a C115D mutation, which indicates a different antibacterial mechanism than MurA inhibition.^{201,233} Another class of irreversible inhibitors are quinoline derivatives such as **14**. While they were potent nanomolar inhibitors, they suffered from unspecific binding to thiol groups as they lost their effect when DTT was added and covalently bound to all the cysteine residues in the protein.²³⁴ Bromonitrovinylfuran **15**, was reported as an irreversible inhibitor of MurA acting on several MurA subtypes from different bacteria, and it had a very good antibacterial profile. However, it bound to all cysteine residues of MurA, in addition to forming adducts with glutathione (GSH). It was also found to be cytotoxic to both cancer and non-cancer cell lines.²³⁵

Avenaciolides such as **16** were isolated from *Neosartorya fischeri*. They possess an α,β -unsaturated carbonyl system which was essential for their inhibitory effect. They were active on both Gram-negative and Gram-positive MurA and retained their activity when the catalytic Cys residue in MRSA MurA was changed to Asp, but they are known inhibitors of glutamate transport in rat liver microsomes.²³⁶⁻²⁴⁰ **17** is a

triazole benzoic acid derivative with a good potency against *E. coli* MurA. It was discovered by induced fit simulation and molecular modelling, but had no antibacterial effect.²⁴¹ A screening of several small heterocycles with an electrophilic warhead led to the discovery of compound **18**, which exhibited time-independent reversible MurA inhibition. Nevertheless, it is suspected to be a promiscuous protein binder as it completely inhibited the serine protease thrombin.¹³¹ Quercetin-3-*O*-*D*-glucuronide **19** is a known anti-inflammatory agent. Its inhibition of MurA was discovered through structure-based virtual screening (SBVS), where it showed an uncompetitive mode of inhibition, binding to the enzyme-UDP-GlcNAc complex. Due to its high K_i value relative to other known MurA inhibitors, it still needs further optimization to be considered an effective MurA inhibitor.²⁴² The diterpene derivative 20-methyl carnosate **20** was shown to possess antibacterial properties against both MSSA (Methicillin-susceptible *S. aureus*) and MRSA in addition to *E. coli* in the presence of polymyxin B nonapeptide (PMBN) as a membrane perturbing agent. Its anti-MurA activity was tested, and it was revealed to be a time-dependent inhibitor of both *E. coli* and *S. aureus* MurA. Its mode of inhibition was postulated to be similar to cnicin **7**, in that it acts as a non-covalent suicide inhibitor at the UDP-GlcNAc binding site.^{227,243} Lastly, the benzohydrazide compound **21** is an uncompetitive inhibitor of *E. coli* MurA, showing antibacterial activity on *S. aureus* and *E. coli* in the presence of EDTA, which acts as an outer membrane permeabilizer.²⁴⁴

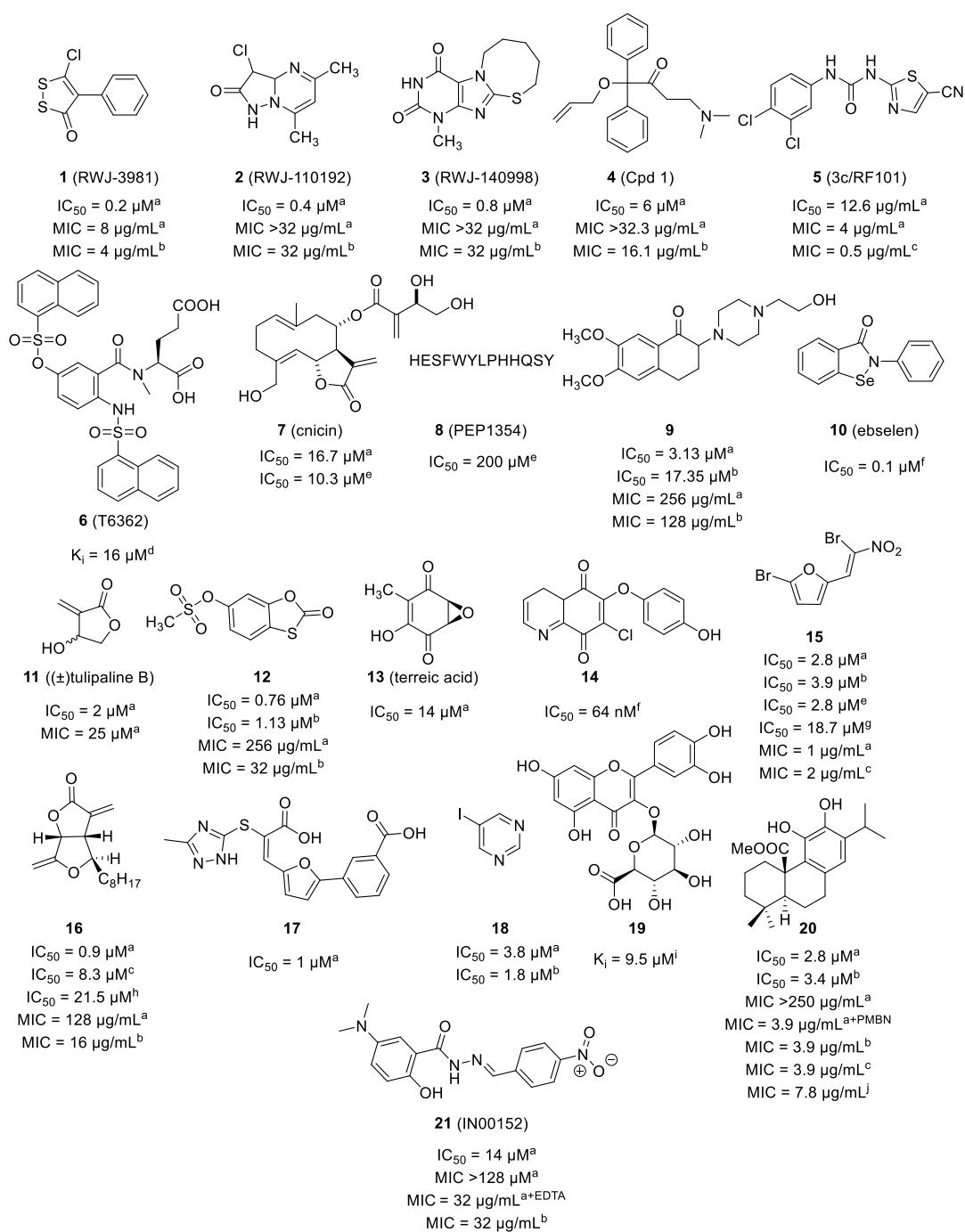


Figure 1.18. MurA inhibitors. ^atested with *E. coli*; ^btested with *S. aureus*; ^ctested with MRSA; ^dtested with *E. cloacae*; ^etested with *P. aeruginosa*; ^ftested with *H. influenzae*; ^gtested with C115D *E. coli*; ^htested with C119D MRSA; ⁱtested with *F. nucleatum*; ^jtested with *E. faecalis*.

1.7 ANS

8-Anilidonaphthalene-1-sulfonic acid (ANS) is a dye that has been used to study biological systems due to its fluorescent properties and its sensitivity to its surrounding environment (*Figure 1.19*).^{204,245} It possesses weak fluorescence in aqueous media, but this fluorescence is greatly enhanced with a blue shift in maximum emission wavelength in less polar solvents and when bound to hydrophobic pockets of proteins.²⁴⁵⁻²⁴⁷ It is able to bind to a wide range of proteins, interacting with Arg and Lys residues through its anionic sulfonate group, in addition to anchoring its anilidonaphthalene structure at the hydrophobic pockets of proteins.^{248,249} It has been used since 1965 to study the structures of apomyoglobin, apohaemoglobin and calf thymus histone fractions.^{246,250} In general, it is used to study hydrophobic patches in proteins,²⁵¹ substrate-protein interactions,^{252,253} protein folding events,^{254,255} protein aggregation,^{256,257} molten globule detection,²⁵⁸ and general conformational changes.²⁰⁴

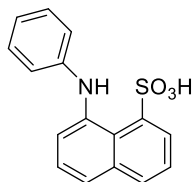


Figure 1.19. Structure of ANS

ANS has been co-crystallized with various proteins such as transthyretin,²⁵⁹ DAPK1,²⁶⁰ LmaPBP,²⁶¹ Bet v 1,²⁶² Hyp-1,²⁶³ S100A7,²⁶⁴ human heart fatty acid binding protein,²⁶⁵ CDK2,²⁶⁶ and Ppm1p.²⁶⁷ Additionally, it was extensively used to study the structure and binding of ligands and inhibitors to MurA such as UDP-GlcNAc, PEP, UDP-MurNAc, fosfomycin, and several other small molecules through a fluorescence-based assay.^{105,179,199,230} This assay depends on detection of the fluorescent ANS-MurA complex, and monitoring the fluorescence intensity upon addition of the respective

ligand/inhibitor.¹⁹⁹ This change in fluorescence (usually quenching) corresponds to the structural changes that occur, and the changing of the flexible loop orientation resulting in displacement of the bound ANS.^{199,204} The quenching effect was used to calculate the K_d values for various MurA ligands such as PEP, UDP-GlcNAc, and UDP-MurNAc.^{105,199} This effect was also exploited to study the inhibition and binding of several MurA inhibitors such as fosfomicin, ebselen, and the 5-sulfonyl-anthranilic acid derivative T6362.^{179,199,230}

ANS was successfully co-crystallized with *E. cloacae* MurA by Schönbrun *et al.* (PDB code: 1EYN).²⁰⁴ The X-ray crystal structure revealed that ANS is able to specifically bind to MurA in the solvent-exposed region of the enzyme away from the catalytic site, inducing the formation of a hydrophobic environment for its anilinonaphthalene core. It induces a conformational change in the flexible loop of MurA, normally stabilized through a series of hydrogen bonds between its residues, leading to its unwinding and disruption of the hydrogen bonds (*Figure 1.20*). The naphthalene ring of ANS is located between Pro112 and Arg91, the anilino ring is located opposite to the α -C of Gly113, and the sulfonate group is connected via three hydrogen bonds: the first with the main chain amide of Gly113, and the other two via two water molecules to the guanidine of Arg91 (*Figure 1.21*).²⁰⁴

Despite the specific binding of ANS to *E. cloacae* MurA, when tested in a functional assay against *E. cloacae* MurA, ANS did not show any inhibition of the enzyme in concentrations up to 1 mM.¹⁹⁹

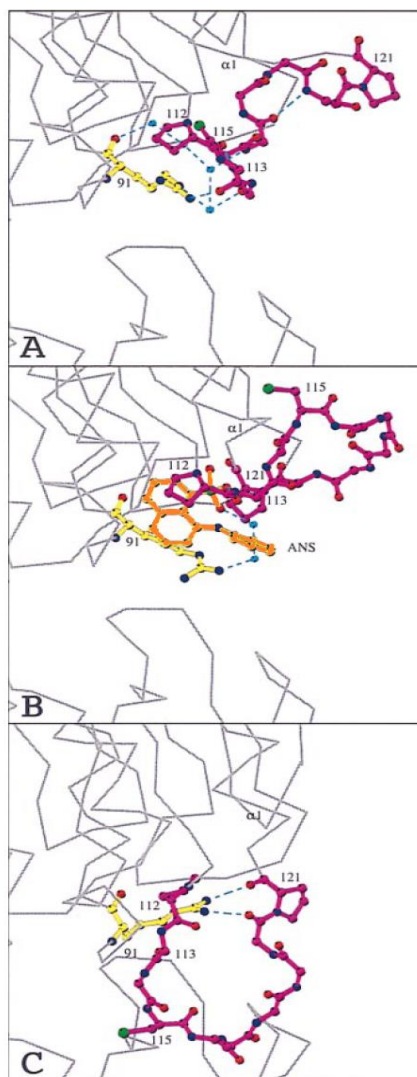


Figure 1.20. Conformational changes of the MurA flexible loop. **A.** unliganded MurA; **B.** ANS-bound MurA; **C.** closed-form MurA. [Arg91 is shown as yellow sticks, ANS is shown as orange sticks, the flexible loop is depicted as magenta sticks, water molecules are represented as turquoise spheres, the hydrogen bonds are represented as dashed lines, and the surrounding protein is shown as a gray α -carbon trace]. (Taken and modified from: Schönbrunn *et al.*; *Proc. Natl. Acad. Sci. U.S.A.* **2000**, 97, 6345-6349)²⁰⁴

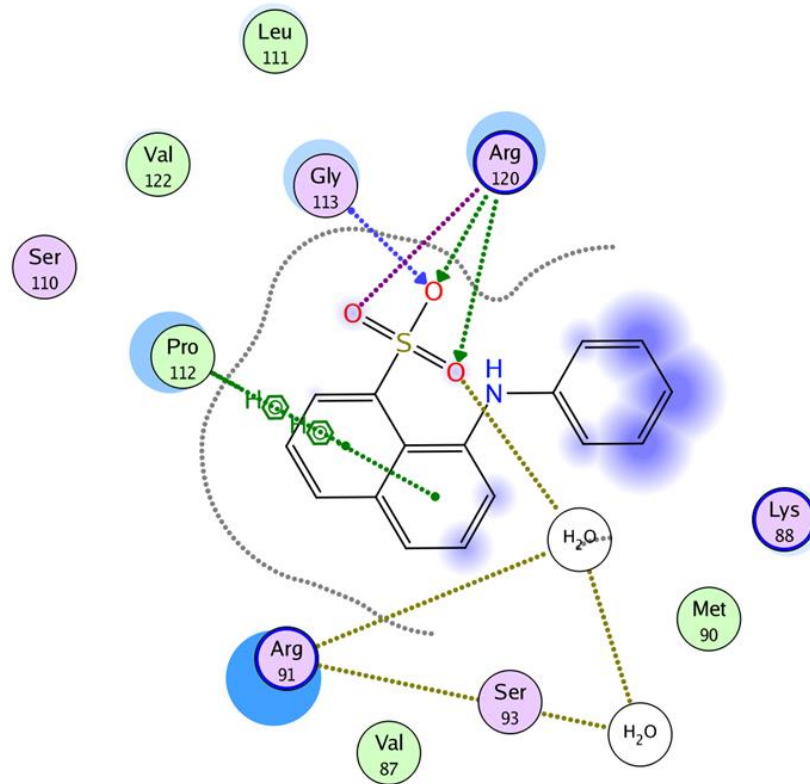


Figure 1.21. Binding mode of ANS to MurA. (based on the ANS-MurA X-ray co-crystal structure, PDB code: 1EYN)²⁰⁴

2. Objectives

The main aim of this work was to discover inhibitors for one or more of the Mur enzymes. Our work first started with reviewing the available inhibitors of the various members of the Mur enzyme family, which led to the observation that most of the available inhibitors suffer from various problems such as lack of potency, toxicity to human cells, non-specific inhibitory activity, and inactivity on bacterial cells. We decided to focus on the first two members of the Mur family, so both MurA and MurB enzymes from *E. coli* were expressed. While the MurA substrates are commercially available, the MurB substrate EP-UDP-GlcNAc needed to be synthesized using enzymatic synthesis using MurA and its two substrates UDP-GlcNAc and PEP. With all the needed substrates in hand, we then developed reliable assays for MurA and MurB activity based on the methods described in literature.^{130,138,226} The developed assays were modified and perfected to give more reproducible, and reliable results.

Our first project focused on testing and synthesizing 1,2-diarylpyrazolidin-3-one derivatives (*Figure 2.1*) as potential inhibitors for both MurA and MurB enzymes. These structures were similar to the published dual MurA/MurB inhibitors, the pyrazolidine-3,5-diones, but they lacked the carbonyl group at position 5 of the ring and had a more diverse substitution pattern on the pyrazolidinone ring.^{138,141,268} The effect of these chemical modifications was tested using the established MurA and MurB assays, in addition to testing against Gram-positive *S. aureus* and *Bacillus subtilis*, as well as Gram-negative *E. coli* $\Delta tolC$.

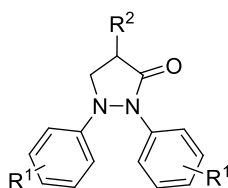


Figure 2.1. General structure of the investigated 1,2-diarylpyrazolidine-3-one derivatives

Next, we started a MurA screening campaign on a library of pyrrolidinedione derivatives (*Figure 2.2*) based on the published MurA inhibitory effect of pyrazolidinediones.^{138,141,268} These pyrrolidinediones were first synthesized as inhibitors of protein kinase C (PKC), with some derivatives showing moderate inhibition against the target enzyme.²⁶⁹ These compounds were tested against both WT and C115D MurA on several stages, then they were tested against *E. coli* $\Delta tolC$ (with and without PMBN) and *S. aureus*. Several additional assays were performed on the most active derivatives, including determination of enzyme kinetics, fluorescence binding assays in combination with ANS, protein NMR, native MS, metabolic stability assays, and MTT assays to test their toxicity to human cells.

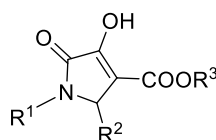


Figure 2.2. General structure of the investigated pyrrolidinediones

The fluorescence binding assays performed with the pyrrolidinedione derivatives in combination with ANS (*Figure 2.3*) piqued our interest towards ANS as a potential MurA inhibitor. The binding of ANS to MurA has been well characterized, but ANS had been reported not to be a MurA inhibitor when tested in concentrations up to 1 mM on *E. cloacae* MurA.¹⁹⁹ However, we decided to test ANS on *E. coli* MurA to verify its lack of inhibitory activity. ANS was discovered to be a strong inhibitor of *E. coli* MurA

so we decided to test some commercially available simplified ANS derivatives against *E. coli* MurA. After that, we decided to further test the compounds against C115D *E. coli* and *E. cloacae* MurA. The compounds were again tested against *E. coli* $\Delta tolC$ and *S. aureus* bacteria.

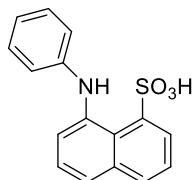


Figure 2.3. Structure of ANS

We last decided to synthesize the reference 5-cyanothiazolyl urea compound **RF101** (referred to as compound **3c** in chapter 3.5) (Figure 2.4), which had been reported to be potent on both MurA and MurB enzymes and active in antibacterial cell assays.¹⁶⁸ We tested **RF101** in both the MurA and MurB assays, to discover that while it was indeed a MurB inhibitor, it showed little inhibitory effect on MurA in our test. It was also active on both Gram-negative and Gram-positive bacterial cells. We attempted to further improve the uptake of **RF101** into bacterial cells to achieve better antibacterial effects by incorporating it into liposomes loaded with nanoparticles which had the additional benefit of decreasing mammalian cell toxicity.

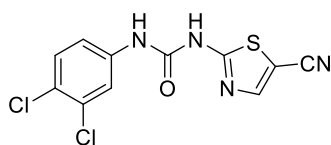


Figure 2.4. Structure of **RF101**

The four projects, their corresponding experimental work and the respective results are summarized in the following sections: 3.2, 3.3, 3.4, 3.5. The experimental details of sections 3.3 and 3.4 are provided in section 5, and supplementary information for sections 3.3, 3.4, and 3.5 are in sections 7.6, 7.7, and 7.8, respectively.

3. Results

3.1 General Comments

All projects are presented in the following four chapters. At the beginning of each chapter, a contribution overview is presented to indicate who has been involved in the different parts of the work. At the end of each chapter, a short conclusion and an outlook are given. The discussion for each chapter is included in chapter 4. Numbering of the compounds, figures and tables starts again at the beginning of each chapter in the interest of readability. The references for each chapter are included after the chapter itself. The experimental parts for chapters 3.3 and 3.4 are included in chapter 5. Numbering in the supplementary materials follows the numbering of the respective chapters. Supporting information for chapters 3.3, 3.4, and 3.5 are found at the end of the thesis in the appendix in sections 7.6, 7.7 and 7.8, respectively.

3.2 Synthesis of Novel 1,2-Diarylpyrazolidin-3-one-based Compounds and their Evaluation as Broad spectrum Antibacterial Agents

This part of the thesis has been published in *Bioorg. Chem.* in 2020

S. A. Mokbel, R. K. Fathalla, L. Y. El-Sharkawy, A. H. Abadi, M. Engel, and M. Abdel-Halim, *Bioorg. Chem.* **2020**, *99*, 103759, DOI: 10.1016/j.bioorg.2020.103759.

The contributions of each author to this chapter are listed below:

Salma A. Mokbel: She synthesized some of the test compounds, in addition to conceiving and writing the manuscript.

Reem K. Fathalla: She planned most of the biological assays in this publication. She tested the compounds on *E. coli* $\Delta tolC$ and *S. aureus*. She developed and performed the MurA and MurB assays for the tested compounds and calculated the IC₅₀ and MIC values. Finally, she was involved in the writing process of the manuscript.

Lina Y. El-Sharkawy: She synthesized some of the test compounds.

Ashraf H. Abadi: He was responsible for the supervision and administration of the project.

Matthias Engel: He was responsible for co-supervision of the project and was involved in writing and editing the manuscript.

Mohammad Abdel-Halim: He was responsible for the conceptualization and co-supervision of the project and was involved in writing and editing the manuscript.

3.2.1 Abstract

There is a continuous need to develop new antibacterial agents with non-traditional mechanisms to combat the nonstop emerging resistance to most of the antibiotics used in clinical settings. We identified novel pyrazolidinone derivatives as antibacterial hits in an in-house library screening and synthesized several derivatives in order to improve the potency and increase the polarity of the discovered hit compounds. The oxime derivative **24** exhibited promising antibacterial activity against *E. coli* TolC, *B. subtilis* and *S. aureus* with MIC values of 4, 10 and 20 µg/mL, respectively. The new lead compound **24** was found to exhibit a weak dual inhibitory activity against both the *E. coli* MurA and MurB enzymes with IC₅₀ values of 88.1 and 79.5 µM, respectively, which could partially explain its antibacterial effect. A comparison with the previously reported, structurally related pyrazolidinediones suggested that the oxime functionality at position 4 enhanced the activity against MurA and recovered the activity against the MurB enzyme. Compound **24** can serve as a lead for further development of novel and safe antibiotics with potential broad spectrum activity.

3.2.2 Introduction

The extensive appearance of resistant bacterial strains represents an alarming threat to public health. This resistance has been exacerbated by the decrease in industrial efforts to discover and develop new antibacterial agents during the last decades.[1] In light of this situation, efforts toward the discovery of new antibacterial agents with novel mechanisms of action need to be strengthened which represents one of the greatest challenges in drug discovery. The inhibition of bacterial peptidoglycan synthesis is an established strategy for the development of new antibacterial agents.[2-4] To date, the focus was on the late steps of peptidoglycan biosynthesis

that are catalyzed by transpeptidases and led to important inhibitors, such as the β -lactam antibiotics.[5-7] Only in the last decade, drug discovery efforts increasingly turned towards the cytoplasmic steps of the peptidoglycan biosynthesis, which are catalyzed by the Mur enzymes MurA-F.[2, 3] Starting with MurA, the cytoplasmic Mur enzymes synthesize the final peptidoglycan biosynthesis precursor uridine 5'-diphosphate (UDP)-*N*-acetylmuramyl-pentapeptide.[8, 9]

In previous studies, several pyrazolidine-3,5-diones were reported as inhibitors of bacterial cell wall biosynthesis through inhibition of the MurB enzyme (UDP-*N*-acetylenolpyruvyl glucosamine reductase), [10-12] with some derivatives showing activity also against MurA and MurC enzymes (Figure 1). The 4-alkyl and 4,4-dialkyl pyrazolidinediones were described as weak inhibitors of *S. aureus* and *E. coli* MurB, and were shown to have modest antibacterial activity against Gram-positive bacteria, particularly against penicillin-resistant *Streptococcus pneumoniae* (PRSP), compound A in Figure 1 is an example.[11] A second series of related pyrazolidinediones with 4-benzoyl and 4-arylamido substituents was reported to inhibit *E. coli* MurB in the low micromolar range, and also showed moderate inhibitory activity against MurA and MurC (cpds. B and C, Figure 1).[10, 12]

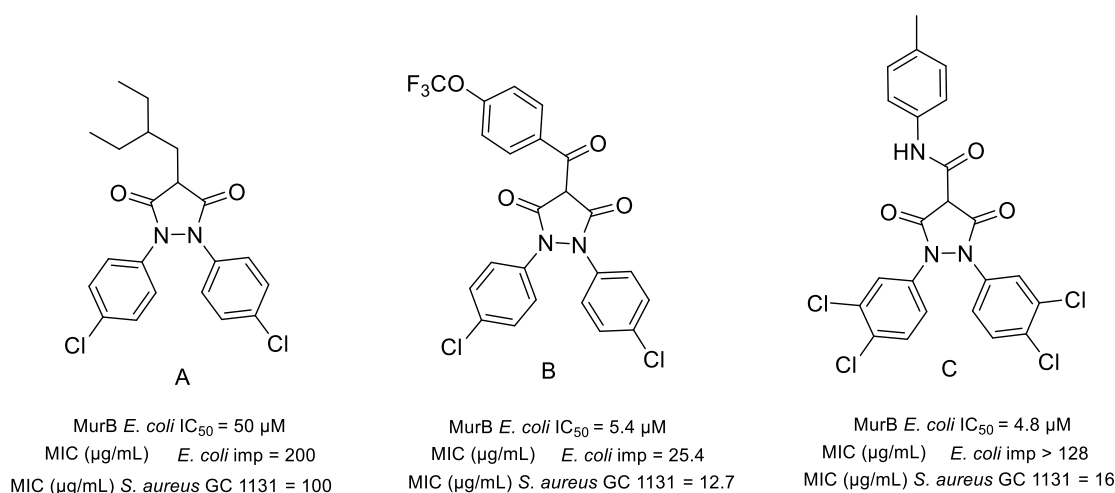


Figure 1. Representative examples of the previously reported pyrazolidine-3,5-diones

The latter group of compounds was shown to inhibit biosynthesis of peptidoglycan, as evaluated by measuring the amount of accumulated soluble peptidoglycan after incubating the compounds with *Streptococcus epidermidis*. [10] However, the inhibitors suffered from the following drawbacks: i) activity against Gram-positive bacteria but much less against Gram-negative ones ii) loss of activity in the presence of 4% bovine serum albumin (BSA), indicative of a strong BSA binding. [10-12] It can be assumed that the strong BSA binding was caused by the high lipophilicity of the structures, which required three aryl systems for biological activity. The replacement of the aryl system in position 4 by branched alkyl chains had previously resulted in almost inactive compounds against Gram-negative bacteria (compound A, Figure 1). Thus, the pyrazolidinedione scaffold gave promising MurB inhibitors with a good activity against Gram-positive bacteria in vitro, but was not suitable for in vivo applications. In the present study, novel, structurally related pyrazolidin-3-one derivatives with anti-bacterial activity were developed from initial hits identified in a screening of an in-house library.

3.2.3 Results and Discussion

3.2.3.1 Compound Design

Inspired by the reported pyrazolidine-3,5-dione series, we decided to screen an in-house library of compounds with some structural similarities, but one major difference, which is the absence of the second carbonyl group at position 5 of the pyrazolidine ring (compounds **D-I**, Figure 2). Since this also disrupted the coplanarity of the bis-aryl-pyrazolidine-3,5-dione core, it seemed interesting to investigate the effect of the changed shape on target inhibition and anti-bacterial activity. In spite of their limited size, the screened small library of compounds offered some diversity of

functional group variations. In particular, it allowed us to evaluate the potential influence of the substituent at position 4 of the pyrazolidinone ring.

Compounds **D-I** were screened for their ability to inhibit the growth of several bacterial species including *S. aureus* (strain Newman), *B. subtilis* (ATCC 6633) and *E. coli* (both *E. coli* BL-21 and a TolC mutant in which the AcrAB-TolC multidrug efflux pump gene is deleted). The results are shown in *Table 1*. Interestingly, our preliminary screening results showed that a plain methyl group (compound **D**) rather than the bulky and lipophilic benzoyl (compound **E**) or pivaloyl (compound **H**) moieties in position 4 gave the highest overall potency. This was a significant progress compared to the pyrazolidinedione scaffold that required such substituents to achieve a significant activity.^[10-12] Compound **D** even seemed to be active against a wider bacterial spectrum when compared to the most relative compounds in the previously reported 4-alkylpyrazolidinedione series,^[11] as it showed improved activity against the Gram-negative *E. coli* TolC. Although its activity was reduced against the *E. coli* BL-21 (non-efflux pump deficient), the 3-fold drop of activity (*Table1*) is less pronounced than found with some antibacterial drugs in the market: e.g., a 60-fold drop in activity was reported for the macrolide antibiotics erythromycin and clarithromycin between *E. coli* TolC and wild type strains.^[13] This suggested that the hit compound **D** is a weaker substrate of the AcrAB-TolC pump and sufficiently active compounds can be obtained after optimization of the potency.

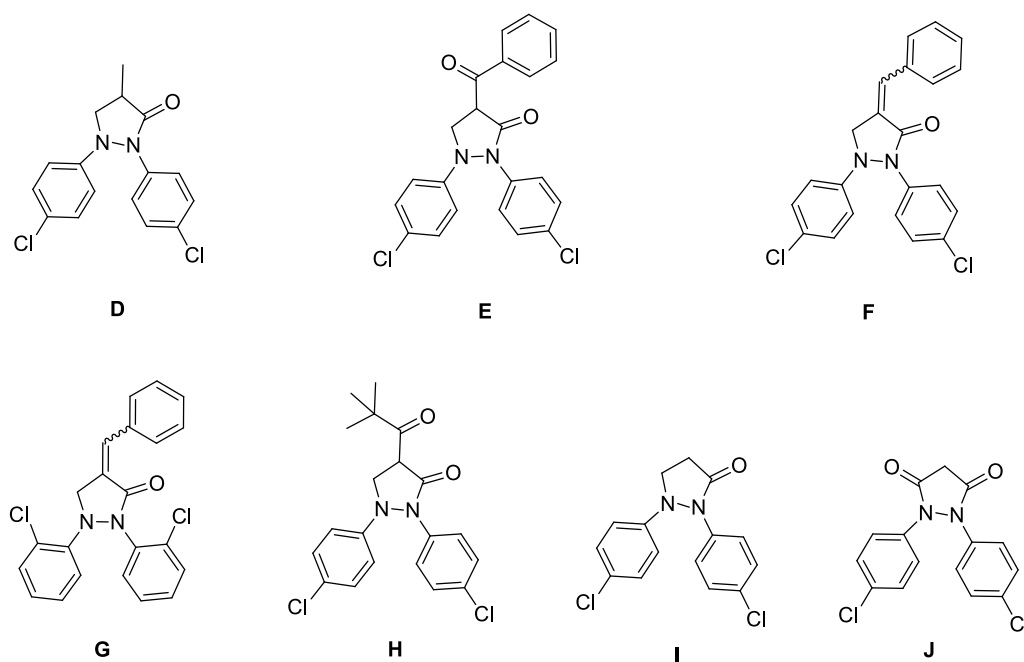


Figure 2. The small library of pyrazolidinone derivatives (compounds **D-I**) and the reference compound **J**

A comparison of compound **D** with its 4-unsubstituted precursor **I** proved that the 4-methyl substituent enhanced the activity against *E. coli* TolC (MIC₅₀: 2.6 vs. 4.9 µg/mL respectively). Nevertheless, compound **I** still inhibited the bacterial growth (MIC=20 µg/mL), whereas the unsubstituted pyrazolidinedione **J** (compound **17** in ref [10]) - prepared for comparison - was much less active against *E. coli* TolC (MIC > 50 µg/mL in our assays). This result demonstrated that the new scaffold might be superior for the development of new antibacterial drugs especially against Gram-negative bacteria, because the core structure **I** already showed significant activity compared to **J**. Although the pyrazolidinedione derivative **J** showed higher potency against Gram-positive bacteria when compared to compound **I** (in accordance with the data reported in ref [10]), this was overcome already by the plain methyl substitution in **D**. Thus, the 1,2-diarylpyrazolidin-3-one core was identified as a new anti-bacterial scaffold with potential broad spectrum activity. On the other hand, it was noted that introduction of the methyl group markedly decreased the solubility of

D in the growth medium compared with **I**, precluding the use of higher concentration to determine the MIC for compound **D**. An enlarged aryl system as in compound **F** (Table 1) aggravated the solubility issue, so that its potency to inhibit bacterial growth could not be precisely evaluated.

Table 1. MIC₅₀ values of the new pyrazolidinone inhibitors (µg/mL)*

		Compound no.						
		D	E	F	G	H	I	J
MIC ₅₀ (µg/mL) ^a	<i>S. aureus</i>	3.6	>25	n. d ^b	>25	>25	>25	4.6
	<i>B. subtilis</i>	4.4	>25	n. d	>25	>25	8.5	6.8
	<i>E. coli</i> TolC	2.6	>25	n. d	7.3	>25	4.9	>25
	<i>E. coli</i> BL-21	7.8	>25	n. d	>25	>25	>25	>25

^aMIC₅₀ were used for initial comparison to overcome solubility problems of some compounds;

^bn.d.: not determined because of poor solubility in the assay medium. *Experiments were made at least two times and standard deviation was less than 20 % (most cases: < 15 %).

Hence, one of the major goals of this work is to synthesize derivatives of **D** and **I** with higher polarity along with improved potency. This was planned through the variation of both the 1,2-diaryl substituents and the 4-substituent at the pyrazolidine ring. Additionally, we wanted to test whether the MurA/MurB enzymes were still the cellular targets of the novel compounds, and finally, we aimed at evaluating the cytotoxicity against human cells.

3.2.3.2 Chemistry

The synthesis of the desired 3-pyrazolidinones (compounds **1-8**) was accomplished via a three-step sequence as shown in Scheme 1. The procedure was started by oxidative coupling of the aniline derivative using manganese IV oxide under reflux in toluene for 8 hours and a water trap (Dean-Stark apparatus) was used to separate water released from the reaction. The coloured diazene was then reduced to the respective hydrazine using Zn/NH₄Cl in acetone at room temperature (Scheme 1).

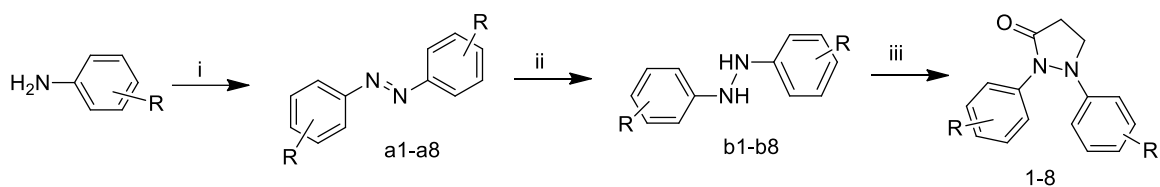
The cyclization reaction was performed through reacting the diaryl hydrazine derivatives with 3-chloropropionyl chloride in the presence of potassium carbonate as a base at room temperature. The cyclization was completed after 72 hours. Under the same reaction conditions, the use of 1,2-bis(2-chlorophenyl)hydrazine (compound **b2**) did not give rise to a new product, which can be attributed to the steric hindrance caused by the bulky *ortho*-chloro substituents. In the latter case, harsher reaction conditions were used to get the respective pyrazolidinone, where the diaryl hydrazine was deprotonated by sodium hydride in DMF, followed by the addition of 3-chloropropionyl chloride and heating at 60 °C for 3 hours, to obtain the desired product in a poor yield (15%) (Scheme 1).

The bis-(bromophenyl) derivatives, compounds **5** and **6**, were subjected to Suzuki coupling in order to replace the bromine atoms with phenyl, 3-thienyl, or 2-furyl rings (Scheme 2). The coupling was achieved by the reaction of compounds **5** or **6** with the respective aryl boronic acid derivative in the presence of Cs₂CO₃ as a base, tetrakis(triphenylphosphine) palladium as catalyst and dioxane/water as solvent; the same reaction conditions did not give successful coupling with pyridine and pyrazole boronic acids, however.

Substitution of the pyrazolidinone derivative (**3**) at position 4 was initiated by the deprotonation of this acidic methylene by using lithium diisopropyl amide (LDA) at -78 °C for 1 hour, followed by trapping the anion by adding the suitable electrophiles like methyl iodide to give compound **13** (Scheme 3). Carboxylation of position 4 was similarly achieved by treating the anion with carbon dioxide (dry ice) to give the 4-carboxy derivative **14**, basically as described in ref[14]. It is worth mentioning that lithium bis(trimethylsilyl)amide (LiHMDS) could also do the required deprotonation successfully under the same conditions. Several amide derivatives were prepared by

reacting the carboxylic acid derivative **14** with different amines using HBTU as coupling agent in the presence of TEA as shown in Scheme 3. Synthesis of the oxime (compound **24**) was accomplished by treatment of **14** with sodium nitrite and HCl as in ref [14] (Scheme 3). Reduction of the oxime group in **24** was achieved using Zn dust in acetic acid to yield the respective primary amine **25** (Scheme 3). It is worth mentioning that trials to prepare the ester derivatives of **14** in the presence of an acid catalyst did not give the desired product but mainly returned the decarboxylated precursor **3**. This can be explained by the decarboxylation mechanism of β -ketoacids under acidic conditions.[15]

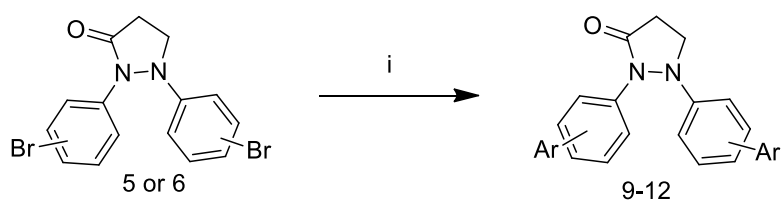
Scheme 1



Reagents and conditions i) MnO₂, toluene, reflux. ii) Zn, NH₄Cl, acetone, RT. iii) acetone, K₂CO₃ followed by 3-chloropropionyl chloride, rt (or DMF, NaH, followed by 3-chloropropionyl chloride, heat at 60 °C for 3h to get compound **2**).

Cpd #	R	Cpd #	R	Cpd #	R
a1, b1, 1	H	a4, b4, 4	4-fluoro	a7, b7, 7	4-methyl
a2, b2, 2	2-chloro	a5, b5, 5	3-bromo	a8, b8, 8	3,4-dimethyl
a3, b3, 3	3-chloro	a6, b6, 6	4-bromo		

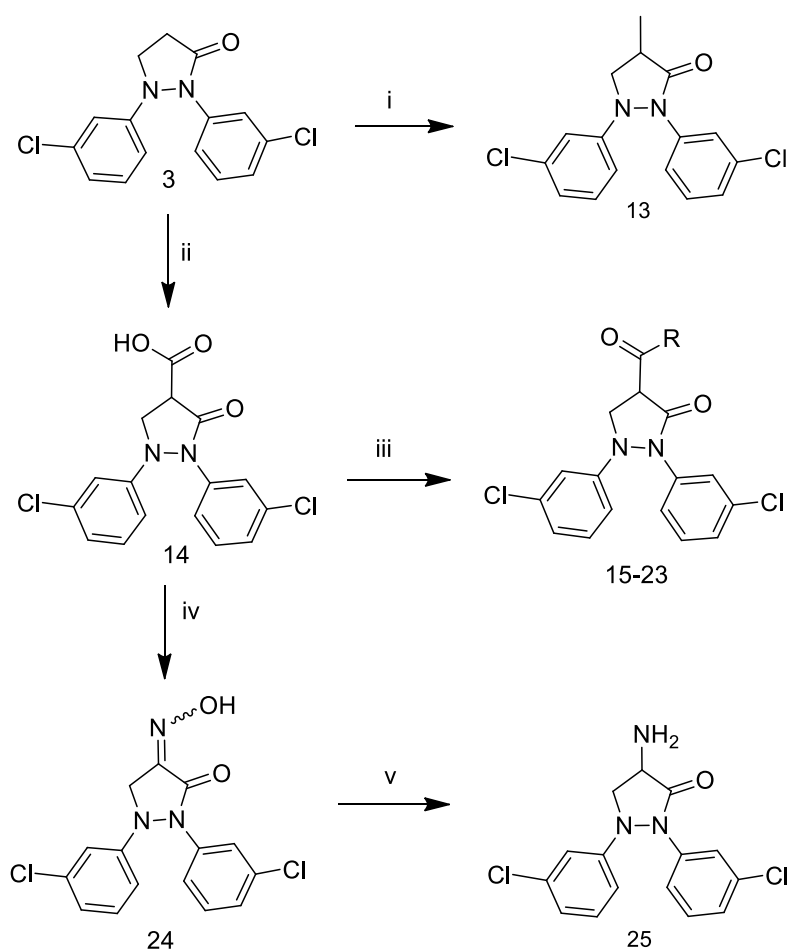
Scheme 2



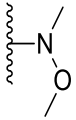
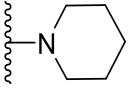
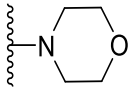
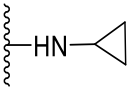
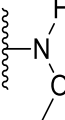
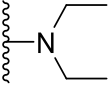
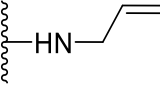
Reagents and conditions i) $\text{Pd}(\text{PPh}_3)_4$, Cs_2CO_3 , dioxane: water (4:1), reflux overnight.

Cpd#	Attachment	Ar	Cpd#	Attachment	Ar
9	<i>para</i>		11	<i>meta</i>	
10	<i>para</i>		12	<i>para</i>	

Scheme 3

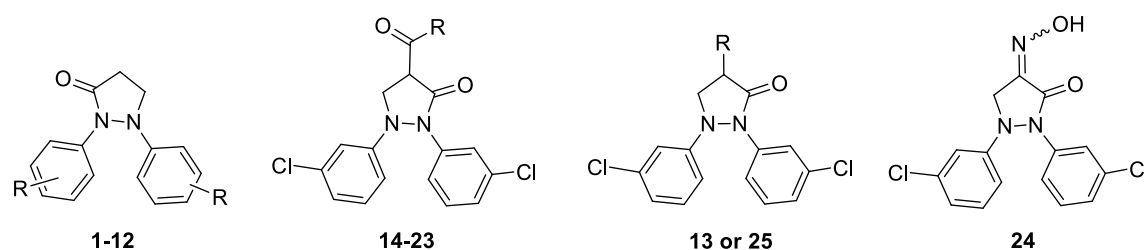


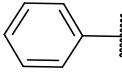
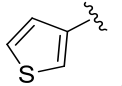
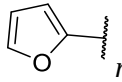
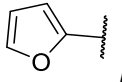
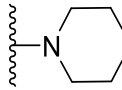
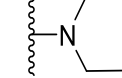
Reagents and conditions i) 1.5 equiv of LDA, 1.5 equiv of MeI, THF, $-78\text{ }^{\circ}\text{C}$ then room temperature for 20 h. ii) 14 equiv of LDA, excess CO_2 , THF, $-78\text{ }^{\circ}\text{C}$ then room temperature for 1 h. iii) HBTU, TEA, amine derivative, DCM, room temperature, 5h. iv) NaNO_2 , HCl, $\text{Et}_2\text{O}/\text{H}_2\text{O}$. v) Zn dust, acetic acid, NH_4Cl , heat at $50\text{ }^{\circ}\text{C}$, overnight.

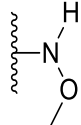
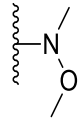
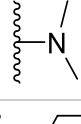
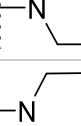
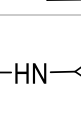
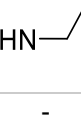
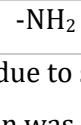
Cpd#	R	Cpd#	R	Cpd#	R
15		18		21	
16		19		22	
17		20		23	

3.2.3.3 Biological Evaluation

Bacterial Growth Inhibition. The synthesized compounds were tested against Gram-positive and negative bacteria for growth inhibition, using serial dilutions of each compound with a maximum concentration of $25\text{ }\mu\text{g}/\text{mL}$ to minimize solubility problems during the assay. The results are listed in *Table 2*. For the more potent compounds, the assay was repeated with an adapted concentration range to allow a more precise evaluation of the MIC values. However, some of the compounds possessed a poor solubility, leading to precipitation above a certain concentration threshold; for some of these compounds, a strong initial inhibition was observed at low concentrations, allowing determining a MIC_{50} value, while a plateau was reached at the higher concentrations. Therefore, we included in *Table 1* the MIC_{50} values to allow a comparison of potency between all compounds, and the MIC where it could be determined.

Table 2. Biological activity of the synthesized compounds against bacteria*

Cpd #	R	<i>E. coli</i> tolC MIC ₅₀ µg/mL	<i>E. coli</i> tolC MIC µg/mL	<i>B. Subtilis</i> MIC ₅₀ µg/mL	<i>B. Subtilis</i> MIC µg/mL	<i>S. aureus</i> MIC µg/mL
1	-H	>25	>25	>25	>25	>25
2	2-chloro	13	43	>25	>25	>25
3	3-chloro	2.7	10	4.9	NR	>25
4	4-fluoro	>25	>25	>25	>25	>25
5	3-bromo	2.8	NR	4.2	NR	>25
6	4-bromo	2.2	NR	7.7	NR	>25
7	4-methyl	6.2	24	18.2	>25	25
8	3,4-dimethyl	3.8	14	5.5	>25	25
9	 <i>para</i>	>25	>25	>25	>25	>25
10	 <i>para</i>	>25	>25	>25	>25	>25
11	 <i>meta</i>	14.5	25	16	>25	>25
12	 <i>para</i>	16.5	25	12	>25	>25
13	-CH ₃	1.8	NR	3.8	NR	>25
14	-OH	19.5	>25	>25	>25	>25
15		23	>25	>25	>25	>25
16		>25	>25	>25	>25	>25

17		>25	>25	>25	>25	>25
18		>25	>25	>25	>25	>25
19		>25	>25	>25	>25	>25
20		>25	>25	>25	>25	>25
21		>25	>25	>25	>25	>25
22		4.6	>25	>25	>25	>25
23		>25	>25	>25	>25	>25
24	-	1.8	4	4	10	20
25	-NH ₂	8	25	15	44	>25

NR: Not reached due to solubility problems. *Experiments were made at least two times and standard deviation was less than 20 % (most cases: < 15 %).

3.2.3.3.1 Activity Against *E. coli* TolC

First round of structural optimization. Since our main focus was to take advantage of the new scaffold's improved activity against the Gram-negative *E. coli* TolC, we based our rounds of optimisation and SAR analysis on the assay results obtained from this phenotypic screen. The first round of structural optimization for the discovered hits involved the synthesis of several 4-unsubstituted pyrazolidinone derivatives to determine the optimum substitution type and pattern at the 1,2-diaryl system. To this end, several analogues of compound **I** (MIC = 20 µg/mL) were prepared, starting with compound **1**, in which the halogen substituents were removed. This almost led to abolishing the antibacterial activity against *E. coli* TolC, indicating that a halogen or at

least hydrophobic substitution is essential for the antibacterial efficacy. Shifting the chloro substituents to the *ortho* positions greatly reduced the antibacterial activity as well (compound **2**). Contrastingly, the shift of the chloro substituents from the *para* (compound **I**) to the *meta* positions gave compound **3**, showing a two-fold increase in antibacterial potency (MIC = 10 µg/mL). Compound **4**, bearing fluorine which is smaller and less lipophilic than chlorine, almost lost the activity against *E. coli* TolC. On the other hand, compounds **5** and **6**, endowed with the bulkier and more lipophilic bromine, at the *meta* or *para* position of the aromatic rings, respectively, showed somewhat lower MIC₅₀ values compared to that of the respective chloro congeners (compounds **2** and **I**). However, the poor water solubility did not permit to determine a MIC value for **5** and **6**. Replacing the *p*-chloro substitution in compound **I** with the lipophilic, electron-donating methyl kept the antibacterial activity with almost similar potency (compound **7** compared with compound **I**). A slight increase of the antibacterial activity was observed when compound **7** was substituted with an additional methyl group at the *meta*-positions of the 1,2-bisphenyl system (compound **8**, MIC = 14 µg/mL).

As the bulky bromo substitution in compounds **5** and **6** retained the antibacterial activity, it was conceivable that aryl systems having steric requirements comparable to bromine might also be tolerated and lead to an improved potency and/or water solubility. While the replacement of bromine at position 4 with phenyl or the bioisosteric thiophene rings had a negative impact on the biological activity (compare **9** and **10** with compound **6**), the more polar furan ring system in compounds **11** and **12** recovered some of the antibacterial potency but with about 3-6 fold increase in the MIC₅₀ values compared to their bromo precursors. The furan derivatives exhibited almost full inhibition of bacterial growth at 25 µg/mL, which is most probably

attributed to their improved solubility in the assay medium compared to their respective bromo analogues. However, the bi-aryl systems did not appear promising with respect to increasing the potency. In summary, the 3-chloro-substituted analogue **3** showed the best balance between potency (MIC = 10 µg/mL) and solubility and was chosen for further optimization

Second round of optimization. Keeping bis-(*m*-chlorophenyl) rings of compound **3** constant, different substituents were tested at position 4 of the pyrazolidine ring. Like in hit compound **D**, the 4-methyl substituent showed some improvement in the antibacterial potency as indicated by the reduction in the MIC₅₀ (compound **13**), however, solubility remained a limiting factor for further development of other 4-alkyl derivatives. Hence, we decided to move towards developing new compounds with more polar substituents at position **4**. This was primarily achieved by the carboxylation of position 4 to give compound **14**. Unfortunately, the carboxyl function led to a tenfold decrease in potency (MIC₅₀) compared with the methylated analogue **13**. In an attempt to regain the potency, several amide derivatives were synthesized, including the polar alicyclic amides **15** and **16**, which were virtually inactive. The methoxy, alkyl, cycloalkyl and allyl amide series (**17-23**), also did not yield active congeners except the cyclopropyl amide derivative **22**, however, MIC values were not reached within the tested concentration range.

In a different trial to boost the activity of compound **3** with a more polar analogue, the oxime derivative **24** was synthesized. Compound **24** showed an MIC value of 4 µg/mL, representing the most potent antibacterial agent against *E. coli* TolC among the present series.

Since incorporation of a primary amine was reported to increase accumulation of compounds inside *E. coli*,^[16] and was also assumed to significantly increase the

polarity similar to the active oxime derivative **24**, we finally synthesized compound **25**. Although the primary amine showed a better activity than the carboxylic acid in compound **14**, adding this amino deteriorated the MIC by 2.5-fold compared to the unsubstituted compound **3**.

3.2.3.3.2 Activity Against *E. coli* with Wild Type Efflux Pump

Compounds **3** and **24**, the most potent compounds against *E. coli* TolC, were also tested against the non-efflux pump deficient *E. coli* BL-21 strain. The activity of the compounds was found to be greatly reduced, as only a weak inhibition was observed at 25 µg/mL, indicating that the compounds' activity is aborted by efflux transport. This adds an extra goal in the future optimization of this class of compounds which is developing new structures that are not substrates for efflux pumps which represents one of the major problems in antibiotics' development. [17, 18]

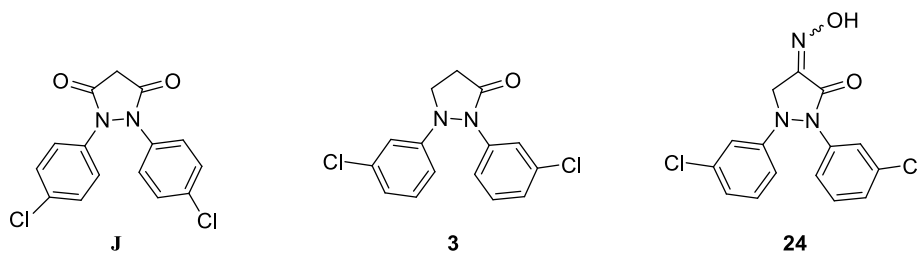
3.2.3.3.3 Activity Against Gram-positive Bacteria

All new compounds were tested against *B. subtilis* and *S. aureus*. Altogether, the activity pattern of the compounds against *B. subtilis* was very similar to that obtained against *E. coli* TolC, although the MIC values tended to be somewhat increased. It is possible that the compounds hit the same conserved target in both the Gram-positive and Gram-negative bacteria, so that they have the potential to be developed to broad spectrum antibiotics. The oxime derivative **24** showed the highest potency against *B. subtilis* with a MIC value of 10 µg/mL. Additionally, **24** was also the most potent compound against *S. aureus* with MIC value of 20 µg/mL. Interestingly, methyl substitution on both the 1,2-diphenyl rings enhanced the antibacterial activity against *S. aureus* as can be seen from the MIC values of compounds **7** and **8** (MIC = 25 µg/mL for both compounds).

3.2.3.3.4 Investigation of MurA and MurB Inhibition as a Possible Mechanism of Action.

As the newly presented series possess a structural similarity to the previously reported pyrazolidinedione type MurB inhibitors,[10-12] we screened both compounds **3** and **24** for their ability to inhibit recombinant MurA and MurB *E. coli* enzymes at 100 μ M concentration. Fosfomycin and compound **J** from ref [10] were used as positive controls for the MurA and MurB assay, respectively (Table 3). Compound **3** showed a weak effect against both MurA and MurB at 100 μ M (30.7 μ g/mL), indicating that its antibacterial effect is likely due to other mechanisms. Its dicarbonyl analogue **J** had more potent MurB inhibition, indicating that the additional carbonyl (at position 5) in compound **J** enhanced the MurB inhibition. On the other hand, the oxime derivative **24** showed a dual inhibition of both MurA and MurB enzymes (IC_{50} 's were 88.1 μ M and 79.5 μ M against MurA and MurB, respectively), which can be directly attributed to the oxime group at position 4 that might recover the potency against MurB and boost the activity against MurA. Nevertheless, the weak inhibitory potency of compound **24** against MurA and MurB enzymes can only partially explain the antibacterial activity against *E.coli* TolC and *B. Subtilis* (MIC = 4 μ g/mL and 10 μ g/mL respectively). It is likely that **24** is affecting bacterial growth through additional, unknown mechanisms.

Table 3: *E. coli* MurA and MurB Inhibition for compounds **3** and **24***



Cpd #	MurA		MurB	
	% inhibition at 100 μ M	IC ₅₀ (μ M)	% inhibition at 100 μ M	IC ₅₀ (μ M)
3	28.3	ND	26.9	ND
24	54.7	88.1	58.9	79.5
J	13.2	ND	39.7	122
Fosfomycin	76	22.3	NT	NT

*Values are mean values of at least two experiments; standard deviation <10%; NT: not tested.

3.2.3.3.5 Cytotoxicity Assay against HepG2 Cells

To evaluate the suitability of the scaffold as potential antibiotics, we evaluated the cytotoxicity of the lead compound **24** against the HepG2 human liver cancer cell line using the MTT assay. Compound **24** showed only low toxicity towards HepG2 cells (LD₅₀ > 50 μ g/mL, 16 % growth inhibition at 50 μ g/mL). This indicates that this new lead compound is not particularly cytotoxic against mammalian cells, leaving a sufficient therapeutic window for further optimization.

3.2.4 Conclusion

In the present study, a new antibacterial lead compound, **24**, was developed based on an initial screening hit. The still low molecular weight of 336 g/mol leaves room for further optimizations while it already displayed good broad spectrum potency. Importantly, **24** showed promising activity against Gram-negative *E. coli* TolC, and the related hit compound **D** even against the non-efflux pump defective *E. coli* BL-21, suggesting that the new 1,2-diarylpyrazolidin-3-one scaffold can be optimized to a new antibiotic agent against Gram-negative bacteria, for which there is a very high

medical need.[19] While the targets of the new inhibitors could only be partially identified, they were sufficiently selective for the bacterial cells.

3.2.5 Experimental Section

3.2.5.1 Chemistry

All reagents and solvents were obtained from commercial suppliers and were used as received. ^1H NMR and ^{13}C NMR spectra were measured using A Bruker DRX 500 spectrometer, for some compounds Varian Mercury VX 400 spectrometer was used. The chemical shifts are referenced to the residual protonated solvent signals. All the tested compounds had at least 95% purity as obtained by means of HPLC-MS. Mass spectra (HPLC-ESI-MS) were obtained using a TSQ quantum (Thermo Electron Corporation) instrument with a triple quadrupole mass detector (Thermo Finnigan) and an ESI source. All samples were inserted using an autosampler (Surveyor, Thermo Finnigan) by an injection volume of 10 μL . The MS detection was determined using a source CID of 10 V and carried out at a spray voltage of 4.2 kV, a nitrogen sheath gas pressure of 4.0×10^5 Pa, a capillary temperature of 400 $^\circ\text{C}$, a capillary voltage of 35 V and an auxiliary gas pressure of 1.0×10^5 Pa. Reversed phase C18 NUCLEODUR 100-3 (125 X 3 mm) column (Macherey-Nagel) was used to separate analytes. The mobile phase consisted of water containing 0.1% TFA (A) and acetonitrile containing 0.1% TFA (B). HPLC-Method: flow rate 0.4 mL/min. The percentage of B started at an initial of 5%, was increased up to 100% during 16 min, kept at 100% for 2 min, and flushed back to 5% in 2 min. Melting points were measured by a Mettler FP1 melting point apparatus and are uncorrected.

3.2.5.1.1 General Synthetic Procedure and Experimental Details

General procedure for synthesis of the diazene derivatives (a1-a8). To a suspension of the aniline derivative (100 mmol) in toluene (350 mL), manganese (IV) oxide (500 mmol, 43.45 g) was added while stirring. The mixture was refluxed with water removal using (Dean-Stark apparatus) for 8 hours. The mixture was left to cool then filtered through a pad of silica gel. The filter cake was washed with several portions of toluene and methylene chloride. The collected wash and the filtrate were evaporated under reduced pressure to afford the diazene derivative as an orange to red solid. The product was used in the next step with no need for further purification.

1,2-Bisphenyldiazene (a1). Synthesized according to the general procedure for diazene synthesis using aniline; mp 68-69 °C; MS (ESI): $m/z = 183$ (M+H)⁺.

1,2-Bis(2-chlorophenyl)diazene (a2). Synthesized according to the general procedure for diazene synthesis using 2-chloroaniline; mp 135-137 °C; MS (ESI): $m/z = 251$ (M+H)⁺.

1,2-Bis(3-chlorophenyl)diazene (a3). Synthesized according to the general procedure for diazene synthesis using 3-chloroaniline; mp 101-103 °C; MS (ESI): $m/z = 251$ (M+H)⁺.

1,2-Bis(4-fluorophenyl)diazene (a4). Synthesized according to the general procedure for diazene synthesis using 4-fluoroaniline; mp 101-102 °C; MS (ESI): $m/z = 219$ (M+H)⁺.

1,2-Bis(3-bromophenyl)diazene (a5). Synthesized according to the general procedure for diazene synthesis using 3-bromoaniline; mp 150-151 °C; MS (ESI): $m/z = 340.8$ (M+H)⁺.

1,2-Bis(4-bromophenyl)diazene (a6). Synthesized according to the general procedure for diazene synthesis using 4-bromoaniline; mp 203-204 °C; MS (ESI): $m/z = 340.8$ (M+H)⁺.

1,2-Bis-*p*-tolylidiazene (a7). Synthesized according to the general procedure for diazene synthesis using *p*-toluidine; mp 143-145 °C; MS (ESI): $m/z = 211$ (M+H)⁺.

1,2-Bis(3,4-dimethylphenyl)diazene (a8). Synthesized according to the general procedure for diazene synthesis using 3,4-dimethylaniline; mp 210-211 °C; MS (ESI): $m/z = 239$ (M+H)⁺.

General procedure for synthesis of the hydrazine compounds (b1-b8). To a suspension of the diazene derivative (22.5 mmol) in acetone (100 mL) saturated aqueous ammonium chloride (30 mL) and zinc dust (172.3 mmol, 11.3 g) were added. The suspension was stirred at room temperature for 5 h and filtered through a pad of silica gel. The silica cake was washed with acetone till obtaining a clear filtrate. The filtrate was collected, and the solvent was evaporated under reduced pressure till reaching half of the initial volume. The residue was diluted with ice/water (150 mL) to form a precipitate. The precipitate was filtered off, dried and stored under inert atmosphere. The product was used in the next step without further purification.

1,2-Bisphenylhydrazine (b1). Synthesized according to the general procedure for hydrazine synthesis using 1,2-bisphenyldiazene (**a1**); m.p 131-132°C; MS (ESI): $m/z = 185$ (M+H)⁺.

1,2-Bis(2-chlorophenyl)hydrazine (b2). Synthesized according to the general procedure for hydrazine synthesis using 1,2-bis(2-chlorophenyl)diazene (**a2**); m.p 87-88 °C; MS (ESI): $m/z = 253$ (M+H)⁺.

1,2-Bis(3-chlorophenyl)hydrazine (b3). Synthesized according to the general procedure for hydrazine synthesis using 1,2-bis(3-chlorophenyl)diazene (**a3**); m.p 97-99 °C; MS (ESI): $m/z = 253$ (M+H)⁺.

1,2-Bis(4-fluorophenyl)hydrazine (b4). Synthesized according to the general procedure for hydrazine synthesis using 1,2-bis(4-fluorophenyl)diazene (**a4**); m.p 94-95 °C; MS (ESI): $m/z = 221$ (M+H)⁺.

1,2-Bis(3-bromophenyl)hydrazine (b5). Synthesized according to the general procedure for hydrazine synthesis using 1,2-bis(3-bromophenyl)diazene (**a5**); m.p 160-161 °C; MS (ESI): $m/z = 340.8$ (M+H)⁺.

1,2-Bis(4-bromophenyl)hydrazine (b6). Synthesized according to the general procedure for hydrazine synthesis using 1,2-bis(4-bromophenyl)diazene (**a6**); m.p 123-125 °C; ;MS (ESI): $m/z = 340.8$ (M+H)⁺.

1,2-Bis-*p*-tolylhydrazine (b7). Synthesized according to the general procedure for hydrazine synthesis using 1,2-bis-*p*-tolyl diazene (**a7**); m.p 39-40 °C; MS (ESI): $m/z = 213$ (M+H)⁺.

1,2-Bis(3,4-dimethylphenyl)hydrazine (b8). Synthesized according to the general procedure for hydrazine synthesis using 1,2-bis(3,4-dimethylphenyl)diazene (**a8**); m.p 125- 126 °C; MS (ESI): $m/z = 241$ (M+H)⁺.

General procedures for synthesis of the pyrazolidinone derivatives (1–8).

Procedure A. The hydrazine derivative (2 mmol) was dissolved in 30 mL acetone and K₂CO₃ (2.5 equivalent, 5 mmol, 0.8 g) was added. The mixture was stirred under ice cooling for 15 minutes. 3-Chloropropionyl chloride (1.5 equivalent, 5 mmol, 0.69 g) was added. The mixture was stirred for 3 days at room temperature. Afterwards, acetone was evaporated under reduced pressure till half of the initial volume was reached. The mixture was poured into an ice/water mixture (100 mL) to form a

precipitate. The product was collected after vacuum filtration and was purified by silica gel column chromatography.

Procedure B. The hydrazine derivative (2 mmol) was dissolved in 20 mL DMF then NaH (4 mmol, 0.096 g) was added under ice cooling. The mixture was stirred for 15 min then 3-chloropropionyl chloride (1.5 equivalent, 5 mmol, 0.69 g) was added. After that, the resulting solution was heated at 60 °C under argon atmosphere for 3h. The dark solution was poured on ice/water mixture and the obtained solid was collected using vacuum filtration and was purified by silica gel column chromatography.

1,2-Diphenylpyrazolidin-3-one (1). Synthesized according to method **A** for pyrazolidinone synthesis using 1,2-bisphenylhydrazine (**b1**); dark brown solid; yield: 56%; mp 126.3-129 °C; ¹H NMR (400 MHz, CDCl₃) δ 7.82 – 7.77 (m, 2H), 7.34 – 7.27 (m, 4H), 7.12 – 7.01 (m, 2H), 7.01 – 6.96 (m, 2H), 4.02 (t, *J* = 7.3 Hz, 2H), 2.73 (t, *J* = 7.3 Hz, 2H); ¹³C NMR (101 MHz, CDCl₃) δ 172.29, 150.18, 138.62, 129.70, 129.33, 124.88, 124.14, 118.92, 118.85, 55.41, 30.17; MS (ESI): *m/z* = 239.01 (M+H)⁺.

1,2-Bis(2-chlorophenyl)pyrazolidin-3-one (2). Synthesized according to method **B** for pyrazolidinone synthesis using 1,2-bis(2-chlorophenyl)hydrazine (**b2**); white solid; yield: 15%; mp 72-74 °C; ¹H NMR (500 MHz, CDCl₃) δ 7.57 – 7.49 (m, 2H), 7.45 – 7.39 (m, 1H), 7.37 (dt, *J* = 5.7, 2.5 Hz, 1H), 7.24 – 7.20 (m, 2H), 7.20 – 7.16 (m, 1H), 7.08 – 7.01 (m, 1H), 4.01 (dd, *J* = 7.7, 6.5 Hz, 2H), 2.81 (t, *J* = 7.7 Hz, 2H); MS (ESI): *m/z* = 307.06 (M+H)⁺.

1,2-Bis(3-chlorophenyl)pyrazolidin-3-one (3). Synthesized according to method **A** for pyrazolidinone synthesis using 1,2-bis(3-chlorophenyl)hydrazine (**b3**); yellow solid; yield: 83%; mp 84-86 °C; ¹H NMR (500 MHz, CDCl₃) δ 7.87 (t, *J* = 2.1 Hz, 1H), 7.72 – 7.67 (m, 1H), 7.31 – 7.27 (m, 1H), 7.27 – 7.21 (m, 1H), 7.14 – 7.06 (m, 2H), 7.03 – 6.99 (m, 1H), 6.89 – 6.83 (m, 1H), 4.05 (t, *J* = 7.3 Hz, 2H), 2.77 (t, *J* = 7.3 Hz, 2H); ¹³C

NMR (126 MHz, CDCl₃) δ 171.16, 147.32, 136.79, 132.74, 132.52, 130.29, 129.66, 125.15, 124.39, 120.80, 118.77, 116.24, 115.35, 49.59, 31.32; MS (ESI): m/z = 307.03 (M+H)⁺.

1,2-Bis(4-fluorophenyl)pyrazolidin-3-one (4). Synthesized according to the method A for pyrazolidinone synthesis using 1,2-bis(4-fluorophenyl)hydrazine (**b4**); beige solid; yield: 75%; mp 114-116 °C; ¹H NMR (500 MHz, CDCl₃) δ 7.88 – 7.56 (m, 2H), 7.04 – 6.86 (m, 6H), 3.93 (t, J = 7.4 Hz, 2H), 2.71 (t, J = 7.4 Hz, 2H); ¹³C NMR (126 MHz, CDCl₃) δ 171.37, 159.38 (d, J = 243.2 Hz), 159.36 (d, J = 244.4 Hz), 145.47 (d, J = 2.5 Hz), 133.94 (d, J = 2.7 Hz), 120.15 (d, J = 7.9 Hz), 120.04 (d, J = 8.1 Hz), 116.04 (d, J = 22.8 Hz), 115.57 (d, J = 22.5 Hz), 55.07, 31.14; MS (ESI): m/z = 275.02 (M+H)⁺.

1,2-Bis(3-bromophenyl)pyrazolidin-3-one (5). Synthesized according to the method A for pyrazolidinone synthesis using 1,2-bis(3-bromophenyl)hydrazine (**b5**); brown solid; yield: 81%; mp 97-99 °C; ¹H NMR (500 MHz, CDCl₃) δ 8.09 (t, J = 2.0 Hz, 1H), 7.83 – 7.76 (m, 1H), 7.33 (ddd, J = 8.0, 1.9, 1.1 Hz, 1H), 7.31 – 7.27 (m, 2H), 7.23 (td, J = 7.9, 6.0 Hz, 2H), 6.99 – 6.93 (m, 1H), 4.11 (t, J = 7.3 Hz, 2H), 2.83 (t, J = 7.3 Hz, 2H); ¹³C NMR (126 MHz, CDCl₃) δ 171.62, 150.77, 138.90, 130.53, 130.22, 127.54, 126.93, 123.12, 122.64, 121.44, 120.84, 116.64, 116.63, 54.87, 31.33.; MS (ESI): m/z = 394.8 (M+H)⁺.

1,2-Bis(4-bromophenyl)pyrazolidin-3-one (6). Synthesized according to the method A for pyrazolidinone synthesis using 1,2-bis(4-bromophenyl)hydrazine (**b6**); light brown solid; yield: 75%; mp 180-181 °C; ¹H NMR (500 MHz, CDCl₃) δ 7.69 – 7.63 (m, 2H), 7.43 – 7.35 (m, 4H), 6.85 – 6.79 (m, 2H), 3.98 (t, J = 7.3 Hz, 2H), 2.72 (t, J = 7.3 Hz, 2H); ¹³C NMR (126 MHz, CDCl₃) δ 171.66, 148.58, 137.02, 132.46, 132.10, 120.21, 119.95, 117.54, 116.88, 54.96, 31.55; MS (ESI): m/z = 394.8 (M+H)⁺.

1,2-Bis-*p*-tolylpyrazolidin-3-one (7). Synthesized according to method **A** for pyrazolidinone synthesis using 1,2-bis-*p*-tolylhydrazine (**b7**); dark brown solid; yield: 42%; mp 108-110 °C; ¹H NMR (500 MHz, CDCl₃) δ 7.69 – 7.68 (m, 1H), 7.68 – 7.66 (m, 1H), 7.12 – 7.10 (m, 1H), 7.08 (tdd, *J* = 1.8, 0.8 Hz, 2H), 7.07 – 7.04 (m, 1H), 6.90 – 6.88 (m, 1H), 6.88 – 6.86 (m, 1H), 3.95 (t, *J* = 7.3 Hz, 2H), 2.71 (t, *J* = 7.3 Hz, 2H), 2.28 (d, *J* = 3.1 Hz, 6H); ¹³C NMR (126 MHz, CDCl₃) δ 171.70, 147.48, 135.84, 134.08, 133.42, 129.90, 129.49, 118.70, 118.58, 55.10, 31.66, 20.97, 20.74; MS (ESI): *m/z* = 267.04 (M+H)⁺.

1,2-Bis(3,4-dimethylphenyl)pyrazolidin-3-one (8). Synthesized according to method **A** for pyrazolidinone synthesis using 1,2-bis(3,4-dimethylphenyl)hydrazine (**b8**); brown solid; yield: 35%; mp 86-87 °C; ¹H NMR (500 MHz, DMSO-*d*₆) δ 7.54 (d, *J* = 2.0 Hz, 1H), 7.39 (dd, *J* = 8.3, 2.2 Hz, 1H), 7.05 (t, *J* = 6.9 Hz, 1H), 6.99 (t, *J* = 8.3 Hz, 1H), 6.82 (t, *J* = 3.9 Hz, 1H), 6.67 – 6.59 (m, 1H), 3.92 (t, *J* = 7.3 Hz, 2H), 2.61 (t, *J* = 7.3 Hz, 2H), 2.14 (m, 12H); ¹³C NMR (126 MHz, DMSO-*d*₆) δ ¹³C NMR (101 MHz, DMSO-*d*₆) δ 171.91, 148.24, 137.52, 136.96, 136.56, 132.42, 131.69, 130.34, 130.14, 120.20, 119.46, 116.12, 115.83, 54.90, 31.39, 20.21, 20.18, 19.21, 19.01; MS (ESI): *m/z* = 295.13 (M+H)⁺.

General procedure for Suzuki coupling (9-12). The aryl boronic acid derivative (1.5 mmol) was added to a mixture of the bis-bromophenyl derivative (0.5 mmol, 0.2 g), caesium carbonate (4 equivalent, 0.65 g, 2 mmol) and tetrakis (triphenylphosphine) palladium (0.05 equivalent, 0.025 mmol, 0.02 g) in 30 mL of dioxane/water (4 : 1). The mixture was refluxed overnight at 100 °C. The solvent was evaporated under reduced pressure, then brine was added and the product was extracted with EtOAc (3×40 mL). The combined organic extracts were dried with

Mg₂SO₄, evaporated to dryness under reduced pressure and purified by silica gel column chromatography.

1,2-Bis([1,1'-biphenyl]-4-yl)pyrazolidin-3-one (9). Synthesized according to the method outlined above using phenylboronic acid and 1,2-bis(4-bromophenyl)pyrazolidin-3-one (**6**); beige solid; yield: 30%; mp 155-157 °C; ¹H NMR (500 MHz, CDCl₃) δ 7.77 (d, *J* = 8.7 Hz, 2H), 7.46 – 7.33 (m, 8H), 7.26 (t, *J* = 7.6 Hz, 4H), 7.20 – 7.12 (m, 2H), 6.93 (d, *J* = 8.6 Hz, 2H), 3.91 (t, *J* = 7.3 Hz, 2H), 2.63 (t, *J* = 7.2 Hz, 2H); ¹³C NMR (126 MHz, CDCl₃) δ 172.19, 149.28, 140.74, 140.60, 137.74, 137.57, 137.10, 129.15, 129.12, 128.31, 127.91, 127.48, 127.20, 127.15, 119.15, 119.04, 115.73, 55.33, 32.06; MS (ESI): *m/z* = 391.32 (M+H)⁺.

1,2-Bis(4-(thiophen-3-yl)phenyl)pyrazolidin-3-one (10). Synthesized according to the method outlined above using 3-thiophene boronic acid and 1,2-bis(4-bromophenyl)pyrazolidin-3-one (**6**); light brown solid; yield: 35%; mp 176-177 °C; ¹H NMR (500 MHz, CDCl₃) δ 7.88 – 7.83 (m, 2H), 7.57 – 7.53 (m, 2H), 7.53 – 7.49 (m, 2H), 7.39 (dd, *J* = 2.8, 1.4 Hz, 1H), 7.37 – 7.32 (m, 4H), 7.32 – 7.30 (m, 1H), 7.04 – 7.00 (m, 2H), 4.05 (t, *J* = 7.3 Hz, 2H), 2.77 (t, *J* = 7.3 Hz, 2H); ¹³C NMR (126 MHz, CDCl₃) δ 171.58, 148.49, 141.50, 141.32, 136.94, 131.91, 131.53, 127.18, 126.76, 126.19, 126.11, 126.02, 125.98, 119.76, 119.64, 118.71, 118.54, 54.76, 31.58; MS (ESI): *m/z* = 403.33 (M+H)⁺.

1,2-Bis(3-(furan-2-yl)phenyl)pyrazolidin-3-one (11). Synthesized according to the method outlined above using 2-furan boronic acid and 1,2-bis(3-bromophenyl)pyrazolidin-3-one (**5**); dark brown solid; yield: 18%; mp 121-123 °C; ¹H NMR (500 MHz, CDCl₃) δ 7.66 – 7.60 (m, 2H), 7.58 – 7.50 (m, 1H), 7.48 – 7.40 (m, 2H), 7.09 – 6.98 (m, 3H), 6.94 – 6.90 (m, 2H), 6.87 (t, *J* = 2.0 Hz, 1H), 6.77 (ddd, *J* = 8.3, 2.5, 0.8 Hz, 1H), 6.62 (ddd, *J* = 8.1, 2.2, 1.0 Hz, 1H), 6.16 (s, 1H), 3.81 – 3.70 (m, 2H),

2.69 (s, 2H); ^{13}C NMR (126 MHz, CDCl_3) δ 176.09, 149.91, 148.50, 132.24, 132.22, 132.16, 132.08, 131.94, 131.11, 130.78, 130.65, 128.65, 128.55, 123.56, 123.41, 122.96, 122.03, 115.70, 115.26, 111.35, 111.15, 46.99, 31.24.; MS (ESI): $m/z = 371.22$ (M+H) $^+$.

1,2-Bis(4-(furan-2-yl)phenyl)pyrazolidin-3-one (12). Synthesized according to the method outlined above using 2-furan boronic acid and 1,2-bis(4-bromophenyl)pyrazolidin-3-one (**6**); brown solid; yield: 15%; mp 158-160 °C; ^1H NMR (500 MHz, CDCl_3) δ 7.88 – 7.83 (m, 2H), 7.57 – 7.49 (m, 4H), 7.40 – 7.28 (m, 6H), 7.04 – 7.00 (m, 2H), 4.05 (t, $J = 7.3$ Hz, 2H), 2.77 (t, $J = 7.3$ Hz, 2H); ^{13}C NMR (126 MHz, CDCl_3) δ 171.67, 148.58, 141.59, 141.41, 137.03, 132.00, 131.62, 127.28, 126.85, 126.28, 126.20, 126.11, 126.07, 119.85, 119.74, 118.80, 118.63, 54.85, 31.67.; MS (ESI): $m/z = 371.26$ (M+H) $^+$.

1,2-Bis(3-chlorophenyl)-4-methylpyrazolidin-3-one (13). To a three-necked flask, lithium diisopropylamide (LDA) (0.6 mL) (2M in THF/n-heptane/ethylbenzene) was added and mixed with THF (10 mL) under argon atmosphere. The solution was stirred for 20 min at 0 °C, and further cooled to -78 °C. A solution of compound **3** (1 mmol, 0.306 g) dissolved in THF (10 mL) was added to the mixture via a syringe dropwise. After stirring for 1 h at -78 °C, methyl iodide (2 mmol, 0.12 mL) was added. The mixture was left to stir for additional 30 min at -78 °C, then left to attain room temperature and left to stir overnight. Afterwards, the solvent was evaporated to dryness under reduced pressure and the residue was partitioned between brine and EtOAc. The EtOAc layer was separated and the aqueous layer was washed with 50 mL EtOAc for two times. The combined organic layers were dried over anhydrous MgSO_4 , evaporated under vacuum and the residue was purified using silica gel column chromatography to give the title compound as a yellow solid; yield: 52%; mp 141-

142; ^1H NMR (500 MHz, CDCl_3) δ 7.83 (dd, $J = 3.1, 1.1$ Hz, 1H), 7.68 – 7.65 (m, 1H), 7.25 – 7.22 (m, 1H), 7.21 – 7.17 (m, 1H), 7.08 (ddd, $J = 8.0, 2.0, 1.0$ Hz, 1H), 7.02 (tdd, $J = 3.8, 1.9, 0.9$ Hz, 1H), 6.97 – 6.95 (m, 1H), 6.81 (ddd, $J = 8.2, 2.3, 0.9$ Hz, 1H), 4.07 (dd, $J = 11.5, 7.5$ Hz, 1H), 3.71 (t, $J = 11.5$ Hz, 1H), 2.95 (dp, $J = 11.5, 7.1$ Hz, 1H), 1.21 (d, $J = 7.0$ Hz, 3H); ^{13}C NMR (126 MHz, CDCl_3) δ 174.21, 150.85, 139.01, 135.10, 134.68, 130.25, 129.96, 124.52, 123.74, 118.34, 118.00, 116.08, 115.98, 62.11, 36.06, 12.63; MS (ESI): $m/z = 321.10$ M+H) $^+$.

1,2-Bis(3-chlorophenyl)-3-oxopyrazolidine-4-carboxylic acid (14). To a three-necked flask, lithium diisopropylamide (LDA) (35 mL) (2 M in THF/n-heptane/ethylbenzene) was added and mixed with THF (10 mL) under argon atmosphere. The solution was stirred for 20 minutes at 0 °C, and further cooled to -78 °C. A solution of compound **3** (5 mmol, 1.53 g) dissolved in THF (10 mL) was added via a syringe dropwise. After stirring for 1 h at -78 °C, crushed dry ice was added until excess solid dry ice was observed, and left till no effervescence remains in the flask (about 1 h). The mixture was evaporated to dryness then brine was added. The medium was acidified using 2M HCl. The separated yellow residue was extracted with EtOAc. The aqueous layer was washed with 50 mL EtOAc for two times. The combined organic layers were dried over anhydrous MgSO_4 , evaporated under vacuum and the residue was purified using silica gel column chromatography, using (CH_2Cl_2 , 1% HCOOH) as mobile phase to give the title compound as a yellow solid; yield: 89%; mp 160-162 °C; ^1H NMR (500 MHz, $\text{DMSO}-d_6$) δ 13.15 (s, 1H), 7.79 (t, $J = 2.1$ Hz, 1H), 7.57 (ddd, $J = 8.3, 2.1, 1.0$ Hz, 1H), 7.37 (dt, $J = 35.9, 8.1$ Hz, 2H), 7.24 (ddd, $J = 8.0, 2.1, 1.0$ Hz, 1H), 7.14 – 7.05 (m, 2H), 6.92 (ddd, $J = 8.2, 2.3, 1.0$ Hz, 1H), 4.34 (qd, $J = 12.0, 7.8$ Hz, 2H), 3.94 (t, $J = 7.7$ Hz, 1H); ^{13}C NMR (126 MHz, $\text{DMSO}-d_6$) δ 168.68, 168.14,

150.90, 138.95, 133.86, 133.66, 131.15, 130.96, 124.90, 123.43, 117.98, 117.88, 116.92, 116.53, 57.20, 48.62; MS (ESI): $m/z = 351.12$ (M+H)⁺.

General procedure for amide synthesis (15- 23). To a solution of compound **14** (1.2 mmol, 0.4 g) in 20 mL CH₂Cl₂, HBTU (1.3 mmol, 0.5 g), triethylamine (0.4 mL) and the respective amine (4 equivalent, 4.8 mmol) were added sequentially. The mixture was stirred for 5 h at room temperature. The solvent was evaporated under reduced pressure then purification was done using silica gel column chromatography.

1,2-Bis(3-chlorophenyl)-4-(4-methylpiperazine-1-carbonyl)pyrazolidin-3-one (15). Synthesized according to the general procedure for amide synthesis using *N*-methylpiperazine; white solid; yield: 76%; mp 159-161 °C; ¹H NMR (400 MHz, DMSO-*d*₆) δ 7.77 (t, *J* = 2.0 Hz, 1H), 7.54 (ddd, *J* = 8.3, 2.0, 1.0 Hz, 1H), 7.41 (t, *J* = 8.2 Hz, 1H), 7.31 (t, *J* = 8.0 Hz, 1H), 7.22 (ddd, *J* = 8.0, 2.0, 1.0 Hz, 1H), 7.12 – 6.99 (m, 2H), 6.96 – 6.88 (m, 1H), 4.63 (dd, *J* = 9.7, 7.8 Hz, 1H), 4.56 – 4.37 (m, 1H), 4.21 (dd, *J* = 11.7, 7.8 Hz, 1H), 3.75 – 3.46 (m, 3H), 3.46 – 3.23 (m, 3H), 2.40 (s, *J* = 16.1 Hz, 2H), 2.21 (s, 3H); ¹³C NMR (101 MHz, DMSO-*d*₆) δ 168.88, 164.05, 150.91, 138.84, 133.58, 133.47, 130.97, 130.71, 124.63, 122.98, 117.70, 117.54, 116.57, 116.45, 56.92, 54.80, 54.11, 44.55, 41.57; MS (ESI): $m/z = 433.13$ (M+H)⁺.

1,2-Bis(3-chlorophenyl)-4-(morpholine-4-carbonyl)pyrazolidin-3-one (16). Synthesized according to the general procedure for amide synthesis using morpholine; white solid; yield: 77%; mp 93-95 °C; ¹H NMR (500 MHz, DMSO-*d*₆) δ 7.78 (t, *J* = 2.0 Hz, 1H), 7.54 (ddd, *J* = 8.4, 2.1, 0.9 Hz, 1H), 7.41 (t, *J* = 8.2 Hz, 1H), 7.31 (t, *J* = 8.1 Hz, 1H), 7.23 (ddd, *J* = 8.0, 2.1, 0.9 Hz, 1H), 7.13 – 7.02 (m, 2H), 6.93 (ddd, *J* = 8.3, 2.3, 0.8 Hz, 1H), 4.64 (dd, *J* = 10.0, 7.8 Hz, 1H), 4.46 (dd, *J* = 11.7, 10.2 Hz, 1H), 4.21 (dd, *J* = 11.8, 7.7 Hz, 1H), 3.74 – 3.46 (m, 7H), 3.39 – 3.34 (m, 1H); ¹³C NMR (126 MHz, DMSO-*d*₆) δ 168.84, 164.18, 150.91, 138.81, 133.61, 133.48, 131.00, 130.75, 124.68,

123.04, 117.72, 117.57, 116.60, 116.49, 66.44, 56.86, 46.07, 44.42; MS (ESI): m/z = 420.4 (M+H)⁺.

1,2-Bis(3-chlorophenyl)-*N*-methoxy-3-oxopyrazolidine-4-carboxamide (17).

Synthesized according to the general procedure for amide synthesis using methoxyamine hydrochloride ; white creamy semisolid; yield: 25.1%; ¹H NMR (400 MHz, DMSO- *d*₆) δ 11.35 (s, 1H), 7.79 (t, *J* = 2.0 Hz, 1H), 7.56 (ddd, *J* = 8.3, 2.0, 0.9 Hz, 1H), 7.42 (t, *J* = 8.2 Hz, 1H), 7.33 (t, *J* = 8.1 Hz, 1H), 7.24 (ddd, *J* = 8.0, 2.0, 0.9 Hz, 1H), 7.12 (dd, *J* = 7.6, 1.5 Hz, 1H), 7.07 (t, *J* = 2.1 Hz, 1H), 6.91 (dd, *J* = 7.9, 1.9 Hz, 1H), 4.29 (dd, *J* = 14.3, 6.6 Hz, 2H), 3.68 (dd, *J* = 9.7, 8.2 Hz, 1H), 3.58 (s, 3H); ¹³C NMR (101 MHz, DMSO-*d*₆) δ 169.22, 163.13, 151.39, 139.24, 134.32, 134.05, 131.59, 131.47, 125.33, 124.07, 118.50, 118.12, 117.14, 117.00, 63.98, 57.25, 46.55; MS (ESI): m/z = 380 (M+H)⁺.

1,2-Bis(3-chlorophenyl)-*N*-methoxy-*N*-methyl-3-oxopyrazolidine-4-

carboxamide (18). Synthesized according to the general procedure for amide synthesis using *N*-methoxy-*N*-methylamine hydrochloride; white solid; yield: 53%; mp 112-114; ¹H NMR (400 MHz, DMSO- *d*₆) δ 7.78 (t, *J* = 2.0 Hz, 1H), 7.55 (ddd, *J* = 8.3, 2.0, 0.9 Hz, 1H), 7.42 (t, *J* = 8.2 Hz, 1H), 7.31 (t, *J* = 8.0 Hz, 1H), 7.24 (ddd, *J* = 8.0, 2.0, 0.9 Hz, 1H), 7.09 (dt, *J* = 4.2, 1.5 Hz, 2H), 6.94 – 6.87 (m, 1H), 4.52 (t, *J* = 8.8 Hz, 1H), 4.32 (dd, *J* = 11.4 Hz, 2H), 3.73 (s, 3H), 3.14 (s, 3H); ¹³C NMR (101 MHz, DMSO- *d*₆) δ 169.14, 167.11, 151.31, 139.23, 134.18, 133.99, 131.50, 131.29, 125.27, 123.69, 118.35, 118.17, 117.18, 116.80, 62.08, 57.34, 45.10, 32.22; MS (ESI): m/z = 394.10 (M+H)⁺.

1,2-Bis(3-chlorophenyl)-*N,N*-dimethyl-3-oxopyrazolidine-4-carboxamide (19).

Synthesized according to the general procedure for amide synthesis using dimethylamine; light yellow powder; yield: 39.7%; mp 152-154 °C; ¹H NMR (400

MHz, DMSO- d_6) δ 7.77 (t, J = 2.0 Hz, 1H), 7.54 (ddd, J = 8.3, 2.0, 1.0 Hz, 1H), 7.46 – 7.37 (m, 1H), 7.31 (dd, J = 10.5, 5.6 Hz, 1H), 7.22 (ddd, J = 7.9, 2.0, 1.0 Hz, 1H), 7.07 (ddd, J = 5.4, 3.1, 1.3 Hz, 2H), 6.91 (ddd, J = 8.3, 2.2, 0.8 Hz, 1H), 4.59 (dd, J = 9.7, 7.9 Hz, 1H), 4.41 (dd, J = 11.5, 9.9 Hz, 1H), 4.22 (dd, J = 11.6, 7.9 Hz, 1H), 3.10 (s, 3H), 2.86 (s, 3H); ^{13}C NMR (100 MHz, DMSO- d_6) δ 168.71, 165.39, 150.70, 138.54, 133.34, 133.18, 130.68, 130.45, 124.36, 122.71, 117.45, 117.31, 116.32, 116.09, 56.72, 44.55, 36.81, 35.10; MS (ESI): m/z = 378.15 (M+H) $^+$.

1,2-Bis(3-chlorophenyl)-*N,N*-diethyl-3-oxopyrazolidine-4-carboxamide (20).

Synthesized according to the general procedure for amide synthesis using diethylamine; beige solid; yield: 43%; mp 117-119 °C; ^1H NMR (400 MHz, DMSO- d_6) δ 7.78 (t, J = 2.0 Hz, 1H), 7.54 (ddd, J = 8.3, 2.1, 1.0 Hz, 1H), 7.42 (dd, J = 10.8, 5.5 Hz, 1H), 7.31 (t, J = 8.1 Hz, 1H), 7.23 (ddd, J = 7.9, 2.1, 1.0 Hz, 1H), 7.11 – 7.02 (m, 2H), 6.91 (ddd, J = 8.2, 2.3, 0.8 Hz, 1H), 4.42 (dd, J = 18.9, 8.3 Hz, 2H), 4.29 (dd, J = 10.3, 6.9 Hz, 1H), 3.60 – 3.49 (m, 1H), 3.45 – 3.34 (m, 1H), 3.33 – 3.16 (m, 2H), 1.12 (t, J = 7.1 Hz, 3H), 0.99 (t, J = 7.0 Hz, 3H); ^{13}C NMR (101 MHz, DMSO- d_6) δ 169.69, 165.66, 151.48, 139.38, 134.06, 133.97, 131.46, 131.18, 125.11, 123.38, 118.21, 118.05, 117.06, 116.82, 57.71, 45.45, 42.10, 14.32, 13.23; MS (ESI): m/z = 406.1 (M+H) $^+$.

1,2-Bis(3-chlorophenyl)-4-(piperidine-1-carbonyl)pyrazolidin-3-one (21).

Synthesized according to the general procedure for amide synthesis using piperidine; beige solid; yield: 34%; mp 163-165 °C; ^1H NMR (400 MHz, DMSO- d_6) δ 7.77 (t, J = 2.0 Hz, 1H), 7.54 (ddd, J = 8.3, 1.9, 0.7 Hz, 1H), 7.41 (t, J = 8.2 Hz, 1H), 7.30 (t, J = 8.1 Hz, 1H), 7.22 (ddd, J = 8.0, 2.0, 0.8 Hz, 1H), 7.09 – 7.02 (m, 2H), 6.94 – 6.88 (m, 1H), 4.61 (dd, J = 9.6, 7.9 Hz, 1H), 4.44 (dd, J = 11.5, 9.9 Hz, 1H), 4.21 (dd, J = 11.7, 7.8 Hz, 1H), 3.63 – 3.42 (m, 3H), 3.39 – 3.30 (m, 1H), 1.67 – 1.46 (m, 4H), 1.46 – 1.35 (m, 2H); ^{13}C NMR (101 MHz, DMSO- d_6) δ 169.50, 164.22, 151.40, 139.33, 134.01, 133.91,

131.41, 131.14, 125.03, 123.36, 118.12, 117.96, 116.99, 116.85, 57.48, 46.91, 45.03, 43.11, 26.62, 25.75, 24.38; MS (ESI): $m/z = 418.04$ (M+H)⁺,

1,2-Bis(3-chlorophenyl)-N-cyclopropyl-3-oxopyrazolidine-4-carboxamide

(22). Synthesized according to the general procedure for amide synthesis using cyclopropylamine; brown solid; yield: 63%; mp 138-140 °C; ¹H NMR (500 MHz, DMSO- *d*₆) δ 8.24 (d, *J* = 4.2 Hz, 1H), 7.79 (t, *J* = 2.0 Hz, 1H), 7.55 (ddd, *J* = 8.4, 2.1, 0.9 Hz, 1H), 7.44 – 7.38 (m, 1H), 7.35 – 7.29 (m, 1H), 7.23 (ddd, *J* = 8.0, 2.1, 0.9 Hz, 1H), 7.13 – 7.08 (m, 1H), 7.05 (t, *J* = 2.1 Hz, 1H), 6.90 (ddd, *J* = 8.3, 2.3, 0.8 Hz, 1H), 4.24 (dd, *J* = 19.2, 9.3 Hz, 2H), 3.78 (dd, *J* = 9.9, 8.1 Hz, 1H), 2.68 – 2.58 (m, 1H), 0.69 – 0.54 (m, 2H), 0.43 – 0.27 (m, 2H); ¹³C NMR (126 MHz, DMSO- *d*₆) δ 169.31, 166.64, 150.97, 138.80, 133.76, 133.49, 131.01, 130.90, 124.61, 123.43, 117.86, 117.43, 116.45, 116.44, 57.13, 48.16, 22.49, 5.79, 5.69; MS (ESI): $m/z = 390.08$ (M+H)⁺.

N-Allyl-1,2-bis(3-chlorophenyl)-3-oxopyrazolidine-4-carboxamide (23).

Synthesized according to the general procedure for amide synthesis using allylamine; grey solid; yield: 42.9%; mp 93-95 °C; ¹H NMR (400 MHz, DMSO- *d*₆) δ 8.33 (t, *J* = 5.7 Hz, 1H), 7.80 (t, *J* = 2.0 Hz, 1H), 7.57 (ddd, *J* = 8.3, 2.1, 1.0 Hz, 1H), 7.45 – 7.29 (m, 2H), 7.23 (ddd, *J* = 8.0, 2.1, 1.0 Hz, 1H), 7.14 – 7.04 (m, 2H), 6.91 (ddd, *J* = 8.2, 2.3, 0.8 Hz, 1H), 5.77 (ddt, *J* = 17.2, 10.1, 4.9 Hz, 1H), 5.21 (dd, *J* = 17.2, 1.8 Hz, 1H), 5.06 (dd, *J* = 10.3, 1.7 Hz, 1H), 4.28 (dd, *J* = 9.1, 3.8 Hz, 2H), 3.96 (t, *J* = 9.1 Hz, 1H), 3.80 – 3.65 (m, 2H); ¹³C NMR (101 MHz, DMSO- *d*₆) δ 169.38, 165.45, 150.98, 138.81, 134.48, 133.78, 133.50, 131.02, 130.92, 124.64, 123.45, 117.89, 117.46, 116.50, 116.44, 115.20, 57.10, 48.22, 41.03; MS (ESI): $m/z = 390.00$ (M+H)⁺.

1,2-Bis(3-chlorophenyl)-4-(hydroxyimino)pyrazolidin-3-one (24). To a stirred solution of compound **14** in 5:1 Et₂O/H₂O (10 mL) cooled at 0 °C, NaNO₂ (400 mg, 5.8 mmol) was added followed by conc. HCl (3 mmol, 0.25 mL) cautiously divided on four

portions for 3 h. After stirring for 2.5 hours at room temperature, saturated aqueous ammonium chloride was added (15 mL). The mixture was stirred for 1 more hour. The mixture was extracted with EtOAc (4 times). Organic layers were collected, dried over MgSO₄ and the solvent was evaporated under reduced pressure. Then the resulting residue was purified by silica gel column chromatography to afford the title compound as a yellow oil; yield: 19%; ¹H NMR (500 MHz, DMSO- *d*₆) δ 12.83 (s, 1H), 7.88 (t, *J* = 2.0 Hz, 1H), 7.63 (ddd, *J* = 8.4, 2.1, 0.9 Hz, 1H), 7.46 – 7.40 (m, 1H), 7.34 – 7.28 (m, 1H), 7.28 – 7.24 (m, 1H), 7.12 (dtt, *J* = 2.9, 2.0, 1.0 Hz, 2H), 6.95 (ddd, *J* = 8.3, 2.2, 1.0 Hz, 1H), 4.68 (s, 2H); ¹³C NMR (126 MHz, DMSO- *d*₆) δ 160.27, 151.93, 148.32, 139.15, 133.90, 133.40, 131.07, 130.90, 125.19, 123.99, 118.46, 118.12, 117.07, 116.76, 66.34; MS (ESI): *m/z* = 336.05 (M+H)⁺.

4-Amino-1,2-bis(3-chlorophenyl)pyrazolidin-3-one (25). To a stirred solution of oxime **24** (0.167 g, 0.5 mmol) in acetic acid (20 ml) at room temperature was added zinc dust (1.29 g, 19.8 mmol) and NH₄Cl (0.56 g, 10.5 mmol). After stirring at 50 °C overnight, the mixture was filtered over a pad of silica gel and the filtrate was concentrated under reduced pressure. To the resulting residue, saturated aq. NaHCO₃ was added and the mixture was extracted with methylene chloride. The combined organic layers were dried over anhydrous Na₂SO₄. The solvent was removed under reduced pressure then resulting residue was purified by silica gel chromatography to afford the title compound as white solid; yield: 42%; mp 180-182; ¹H NMR (500 MHz, DMSO-*d*₆) δ 7.80 (t, *J* = 2.0 Hz, 1H), 7.54 (ddd, *J* = 8.4, 2.1, 0.9 Hz, 1H), 7.41 (t, *J* = 8.2 Hz, 1H), 7.30 (t, *J* = 8.1 Hz, 1H), 7.24 – 7.14 (m, 1H), 7.13 – 7.03 (m, 2H), 6.90 (ddd, *J* = 8.3, 2.2, 0.8 Hz, 1H), 4.21 (dd, *J* = 11.2, 7.1 Hz, 1H), 3.82 (dd, *J* = 11.4, 7.1 Hz, 1H), 3.72 (t, *J* = 11.3 Hz, 1H), 2.05 (s, 2H); ¹³C NMR (126 MHz, DMSO-*d*₆) δ 174.58, 150.99,

139.36, 133.78, 133.40, 130.90, 130.85, 124.14, 122.88, 117.40, 117.03, 116.04, 115.93, 61.46, 51.64. MS (ESI): $m/z = 322.02$ (M+H)⁺.

3.2.5.2 Biology

3.2.5.2.1 Minimal Inhibitory Concentration (MIC) Determination

MIC values for *E. coli* TolC, *S. aureus* (strain Newman), *B. subtilis* (ATCC 6633) and *E. coli* BL-21 were determined for all compounds with a maximal DMSO concentration of 1% as previously described in ref [20]. Final compound concentrations prepared from serial dilutions ranged from 1 to 25 $\mu\text{g}/\text{mL}$ and were adapted for each compound depending on their antibacterial activity and the observation of compound precipitation in the growth medium. The ODs were determined after addition of the compounds and again after incubation for 16 h at 37 °C and 50 rpm in 96 well plates using a POLARstar Omega Microplate Reader (BMG LABTECH). Given MIC values are means of two independent determinations. They are defined as the lowest concentration of compounds that reduced OD₆₀₀ by $\geq 95\%$ and were read off the inhibition curves. Experiments were made at least two times and standard deviation was less than 20 % (most cases: < 15 %). LB broth was used for *E. coli* and *B. subtilis*, and Müller Hinton medium was used for *S. aureus*.

3.2.5.2.2 Determination of Cytotoxicity

HepG2 cells were cultured in DMEM supplemented with 10% fetal bovine serum (FBS), 100 units/mL penicillin, and 100 $\mu\text{g}/\text{mL}$ streptomycin. Cells were cultured in a 96-well plate at a density of 3×10^4 cell/well, and then incubated in 5% CO₂ at 37°C for 12 hours. Media was replaced with a fresh one containing variable concentrations of the tested compounds dissolved in DMSO and left for 36 hours in 5% CO₂ at 37°C. To access the cytotoxicity a MTT assay was performed. The media was replaced with a

fresh one containing MTT (5mg/mL) and incubated for 3 hours. The precipitate was dissolved in DMSO and measured at 570 nm using a POLARstar Omega Microplate Reader (BMG LABTECH). 0.1% DMSO was used as a control and the samples were assayed in triplicates in 4 different cultures. To determine the LD₅₀ probit analysis was used.

3.2.5.2.3 Expression of MurA and MurB

MurA and MurB enzymes from *E. coli* K12 were overexpressed as His-tag fusion proteins in *E. coli* BL21. The expression plasmids pAB3 (MurA) and pJMP (MurB) were a kind gift from Prof. Christian Klein, Universität Heidelberg.[[21](#), [22](#)] The transformed *E. coli* cells were grown in LB broth (containing 50 µg/mL kanamycin for MurA and 50 µg/mL Ampicillin for MurB) on a shaker at 37 °C until a cell density (OD_{600 nm}) of 0.8 was reached, then 1 mM isopropyl-D-thiogalactopyranoside was added and shaking continued for 2 h at 37 °C. The cells were harvested by centrifugation at 4000 rpm for 30 min. The cell pellets were suspended in lysis buffer containing 20 mM Tris-HCl (pH 7.5), 250 mM NaCl, 5 mM imidazole and a protease inhibitor cocktail (cOmplete™, Roche), followed by sonication on ice for 10 min. The lysate was centrifuged at 4000 rpm for 30 minutes at 4 °C, and the obtained supernatant was loaded on a Ni²⁺-NTA agarose column (Qiagen) equilibrated with lysis buffer. The column was washed several times using lysis buffer, and the His-tagged proteins were eluted using lysis buffer also containing 750 mM imidazole. The protein fractions were dialyzed to remove the excess imidazole in a dialysis buffer containing 20 mM Tris-HCl (pH 8.0), 150 mM NaCl, 1mM DTT, protease inhibitor cocktail (cOmplete™, Roche) and 10 % glycerol. The resulting protein concentrations were 5 µg/µL for MurA and 5.3 µg/µL for MurB as determined by the NanoDrop 2000

(Thermo Scientific). The aliquoted proteins were snap frozen in liquid nitrogen and stored at -80 °C until needed.

3.2.5.2.4 MurA Assay

The assay was performed in 96 well plates in a final volume of 100 μ L. MurA (27 pmoles) was preincubated with inhibitors (or DMSO as a control) for 10 minutes at room temperature prior to addition of the substrates. A master mix consisting of 150 μ M UDP-N-acetylglucosamine (UNAG), 150 μ M PEP, 2 mM Dithiothreitol (DTT) and 25 mM Tris-HCl (pH 7.5) (final concentrations) was then added and the mixture incubated at 37 °C for 30 min. The reaction was stopped by addition of 100 μ L of a solution containing malachite green solution (0.045 % (w/v) in a 1 % PVA solution) and sodium molybdate (4.8% (w/v) in 5 N HCl) at a ratio of 3:1. After 5 min, the absorbance at 625 nm was measured using a POLARstar Omega Microplate Reader (BMG LABTECH). The background absorbance (same reaction without addition of MurA) was subtracted from the measured absorbances.

3.2.5.2.5 Enzymatic synthesis of UDP-N-acetylglucosamine Enolpyruvate (UNAGEP)

The synthesis of UNAGEP was performed on a small scale and used as a crude product in the subsequent MurB assay. It was done in a 3 mL final volume containing 50 mM Tris-HCl (pH 7.5), 1 mM DTT, 2 mM PEP, 2 mM UNAG and 620 μ g MurA . The reaction proceeded at 37 °C for 5 hours, the protein was filtered out using a 10 kDa Vivaspin 6 centrifugal filter (Sartorius Stedim), and the product was aliquoted and stored at -80 °C.

3.2.5.2.6 MurB Assay

The assay was performed in 96 well plates in a final volume of 200 μ L. The compounds (or DMSO as a control) were added to a mixture containing (as final concentrations):

20 mM KCl, 0.5 mM DTT and 50 mM Tris-HCl (pH 7.5). 26 μ L of the crude UNAGEP solution (obtained as described above) were then added, followed by MurB (26 pmoles). The mixture allowed to stand for 15 min at room temperature. The reaction was started by the addition of 150 μ M NADPH and the activity of the enzyme measured by monitoring the decrease in absorbance at 340 nm for 2 min using a POLARstar Omega Microplate Reader (BMG LABTECH).

Notes

The authors declare no competing financial interest.

Acknowledgement

ME and MA-H would like to thank Prof. Christian Ducho (Saarland University) for generously providing the lab space and for the financial support. We also thank Martina Jankowski for the excellent technical assistance.

3.2.6 References

- (1) G. Kapoor, S. Saigal, A. Elongavan, Action and resistance mechanisms of antibiotics: A guide for clinicians, *J. Anaesthesiol. Clin. Pharmacol.* 33(3) (2017) 300.
- (2) T.D.H. Bugg, D. Braddick, C.G. Dowson, D.I. Roper, Bacterial cell wall assembly: still an attractive antibacterial target, *Trends Biotechnol.* 29(4) (2011) 167-73.
- (3) A. Gautam, R. Vyas, R. Tewari, Peptidoglycan biosynthesis machinery: a rich source of drug targets, *Crit. Rev. Biotechnol.* 31(4) (2011) 295-336.
- (4) D.W. Green, The bacterial cell wall as a source of antibacterial targets, *Expert Opin. Ther. Targets* 6(1) (2002) 1-19.
- (5) E. Sauvage, F. Kerff, M. Terrak, J.A. Ayala, P. Charlier, The penicillin-binding proteins: structure and role in peptidoglycan biosynthesis, *FEMS Microbiol. Rev.* 32(2) (2008) 234-58.
- (6) K.-F. Kong, L. Schneper, K. Mathee, Beta-lactam antibiotics: from antibiosis to resistance and bacteriology, *APMIS* 118(1) (2009) 1-36.

- (7) T. Schneider, H.-G. Sahl, An oldie but a goodie - cell wall biosynthesis as antibiotic target pathway, *Int. J. Med. Microbiol.* 300(2-3) (2010) 161-9.
- (8) A.L. Lovering, S.S. Safadi, N.C.J. Strynadka, Structural perspective of peptidoglycan biosynthesis and assembly, *Annu. Rev. Biochem.* 81 (2012) 451-78.
- (9) M. Hrast, I. Sosič, R. Sink, S. Gobec, Inhibitors of the peptidoglycan biosynthesis enzymes MurA-F, *Bioorg. chem.* 55 (2014) 2-15.
- (10) A.M. Gilbert, A. Failli, J. Shumsky, Y. Yang, A. Severin, G. Singh, W. Hu, D. Keeney, P.J. Petersen, A.H. Katz, Pyrazolidine-3,5-diones and 5-hydroxy-1*H*-pyrazol-3(2*H*)-ones, inhibitors of UDP-*N*-acetylenolpyruvyl glucosamine reductase, *J. Med. Chem.* 49(20) (2006) 6027-36.
- (11) K.M.K. Kutterer, J.M. Davis, G. Singh, Y. Yang, W. Hu, A. Severin, B.A. Rasmussen, G. Krishnamurthy, A. Failli, A.H. Katz, 4-Alkyl and 4,4'-dialkyl 1,2-bis(4-chlorophenyl)pyrazolidine-3,5-dione derivatives as new inhibitors of bacterial cell wall biosynthesis, *Bioorg. Med. Chem. Lett.* 15(10) (2005) 2527-31.
- (12) Y. Yang, A. Severin, R. Chopra, G. Krishnamurthy, G. Singh, W. Hu, D. Keeney, K. Svenson, P.J. Petersen, P. Labthavikul, D.M. Shlaes, B.A. Rasmussen, A.A. Failli, J.S. Shumsky, K.M.K. Kutterer, A. Gilbert, T.S. Mansour, 3,5-Dioxopyrazolidines, novel inhibitors of UDP-*N*-acetylenolpyruvylglucosamine reductase (MurB) with activity against gram-positive bacteria, *Antimicrob. Agents. Chemother.* 50(2) (2006) 556-64.
- (13) R. Chollet, J. Chevalier, A. Bryskier, J.-M. Pages, The AcrAB-TolC pump is involved in macrolide resistance but not in telithromycin efflux in *Enterobacter aerogenes* and *Escherichia coli*, *Antimicrob. Agents Chemother.* 48(9) (2004) 3621-4.
- (14) T. Kan, T. Fujimoto, S. Ieda, Y. Asoh, H. Kitaoka, T. Fukuyama, Stereocontrolled total synthesis of potent immunosuppressant FR901483, *Org. Lett.* 6(16) (2004) 2729-2731.
- (15) R.J. Ouellette, J.D. Rawn, 20 - Carboxylic Acids, in: R.J. Ouellette, J.D. Rawn (Eds.), *Organic Chemistry*, Elsevier, Boston, 2014, pp. 659-698.
- (16) M.F. Richter, B.S. Drown, A.P. Riley, A. Garcia, T. Shirai, R.L. Svec, P.J. Hergenrother, Predictive compound accumulation rules yield a broad-spectrum antibiotic, *Nature* 545(7654) (2017) 299-304.

- (17) H. Nikaido, H.I. Zgurskaya, AcrAB and related multidrug efflux pumps of *Escherichia coli*, *J. Mol. Microbiol. Biotechnol.* 3(2) (2001) 215-218.
- (18) N. Jackson, L. Czaplewski, L.J.V. Piddock, Discovery and development of new antibacterial drugs: learning from experience?, *J. Antimicrob. Chemother.* 73(6) (2018) 1452-1459.
- (19) E. Tacconelli, E. Carrara, A. Savoldi, S. Harbarth, M. Mendelson, D.L. Monnet, C. Pulcini, G. Kahlmeter, J. Kluytmans, Y. Carmeli, M. Ouellette, K. Outtersson, J. Patel, M. Cavaleri, E.M. Cox, C.R. Houchens, M.L. Grayson, P. Hansen, N. Singh, U. Theuretzbacher, N. Magrini, Discovery, research, and development of new antibiotics: the WHO priority list of antibiotic-resistant bacteria and tuberculosis, *Lancet Infect. dis.* 18(3) (2018) 318-327.
- (20) A.P. Spork, M. Büschleb, O. Ries, D. Wiegmann, S. Boettcher, A. Mihalyi, T.D.H. Bugg, C. Ducho, Lead structures for new antibacterials: stereocontrolled synthesis of a bioactive muraymycin analogue, *Chemistry – A European Journal* 20(47) (2014) 15292-15297.
- (21) A. Steinbach, A.J. Scheidig, C.D. Klein, The unusual binding mode of cnicin to the antibacterial target enzyme MurA revealed by X-ray crystallography, *J. Med. Chem.* 51(16) (2008) 5143-5147.
- (22) C. Jöst, C. Nitsche, T. Scholz, L. Roux, C.D. Klein, Promiscuity and selectivity in covalent enzyme inhibition: a systematic study of electrophilic fragments, *J. Med. Chem.* 57(18) (2014) 7590-7599.

3.3 Identification and Biochemical Characterization of Pyrrolidinediones as Novel Inhibitors of the Bacterial Enzyme MurA

This part of the thesis has been accepted for publication in *J. Med. Chem.* in 2022.

Reem K. Fathalla, Wolfgang Fröhner, Chantal D. Bader, Patrick D. Fischer, Charlotte Dahlem, Deep Chatterjee, Sebastian Mathea, Alexandra K. Kiemer, Haribabu Arthanari, Rolf Müller, Mohammad Abdel-Halim, Christian Ducho, and Matthias Engel, *J. Med. Chem.* **2022**, DOI: 10.1021/acs.jmedchem.2c01275.

The contributions of each author to this chapter are listed below:

Reem K. Fathalla: She planned and performed all enzymatic assays and screenings in this work. She also performed the Michaelis-Menten kinetics experiments and the synergism testing, as well as all the small molecule NMR analyses in the manuscript. She planned for all the other experiments in the publication, including the native MS and protein NMR experiments, as well as the testing of the compounds on bacterial cells, toxicity tests, and metabolic stability assays. She prepared the corresponding figures and conceived and wrote the text.

Wolfgang Fröhner: He synthesized the in-house compound library.

Chantal D. Bader: She performed the native MS experiments in this text and was involved in the editing process.

Patrick D. Fischer: He performed the protein NMR experiments and analyzed their results.

Charlotte Dahlem: She performed the cell toxicity assays.

Deep Chatterjee: He performed the co-crystallography experiments (results not shown).

Sebastian Mathea: He planned and supervised the co-crystallography experiments (results not shown).

Alexandra K. Kiemer: She was involved in reviewing the text.

Haribabu Arthanari: He helped in the planning of the protein NMR experiments.

Rolf Müller: He was involved in reviewing the text.

Mohammad Abdel-Halim: He was involved in the initial planning phase of this work. He performed the UPLC-MS and purity analyses for the compounds. He was also involved in the editing process.

Christian Ducho: He was co-responsible for the project supervision and administration and reviewed and edited the work.

Matthias Engel: He conceived the main idea for this work. He was co-responsible for the project supervision. Finally, he was involved in the writing process, and reviewed and edited the chapter.

3.3.1 Abstract

To develop novel antibiotics, targeting the early steps of the cell wall peptidoglycan biosynthesis seems to be a promising strategy that is still under-utilized. MurA, the first enzyme in this pathway, is targeted by the clinically used irreversible inhibitor fosfomicin. However, mutations in its binding site can cause bacterial resistance. We herein report a series of novel reversible pyrrolidinedione-based MurA inhibitors that equally inhibit wild type (WT) MurA and the fosfomicin-resistant MurA C115D mutant, showing an additive effect with fosfomicin for the inhibition of WT MurA. For the most potent inhibitor **46** ($IC_{50} = 4.5 \mu\text{M}$), the mode of inhibition was analyzed using native mass spectrometry and protein NMR spectroscopy. The compound class was non-toxic against human cells and highly stable in human S9 fraction, human plasma and bacterial cell lysate. Taken together, this novel compound class might be further developed towards antibiotic drug candidates that inhibit cell wall synthesis.

3.3.2 Introduction

The rapidly rising issue of bacterial resistance to many known antibiotics has necessitated the discovery of antibacterial drug classes with novel mechanisms of action.¹⁻⁴ Peptidoglycan is an essential part of prokaryotic cell walls, playing an integral role in preserving the integrity and structure of bacterial cells.^{5,6} Consequently, its biosynthesis has been the target of many efforts for antibacterial drug discovery.⁷⁻⁹ The early cytoplasmic steps of peptidoglycan biosynthesis in particular have recently been considered with growing interest as potential targets, since the older, more established β -lactam antibiotics mainly acting in the bacterial periplasm, which is more accessible to small molecules, suffer from extensive bacterial resistance.¹⁰⁻¹² The early steps of peptidoglycan synthesis are performed by the Mur family of enzymes, comprising six intracellular enzymes (MurA to F) that

furnish the main cytosolic peptidoglycan precursor uridine-5-diphosphate-*N*-acetylmuramyl-pentapeptide (Park's nucleotide).^{7,9,10}

MurA is the first enzyme of this cascade and catalyzes the conversion of UDP-*N*-acetylglucosamine (UDP-GlcNAc, UNAG) into UDP-*N*-acetylglucosamine enolpyruvate (UNAGEP) through addition of an enolpyruvate moiety from the co-substrate phosphoenolpyruvate (PEP, *Figure 1*).^{10,13,14} It is an essential enzyme that is conserved across both Gram-positive and Gram-negative bacteria with no mammalian homolog.^{15,16} Hence, inhibitors directed against bacterial MurA have potential to act as broad spectrum antibiotics without affecting a related enzyme in humans. At present, the only approved antibiotic targeting MurA is fosfomycin, which has been in clinical use since the early 1970s for the treatment of uncomplicated urinary tract infections and pediatric gastrointestinal infections resulting from Shiga toxin-producing *Escherichia coli* (STEC) in Japan.^{9,17-19} Fosfomycin acts as an analogue of PEP that competitively inhibits MurA by covalent alkylation of Cys115 (*E. coli* numbering), the main catalytic residue involved in PEP binding (*Figure 1*).¹⁹⁻²² However, there is a high incidence of resistance to fosfomycin through decreased uptake,^{23,24} enzymatic modification of the antibiotic,^{25,26} MurA overexpression,^{27,28} and finally mutation of the key Cys residue to Asp. This MurA mutant is naturally present in several bacteria such as *Mycobacterium tuberculosis* (*M. tuberculosis*).^{29,30}

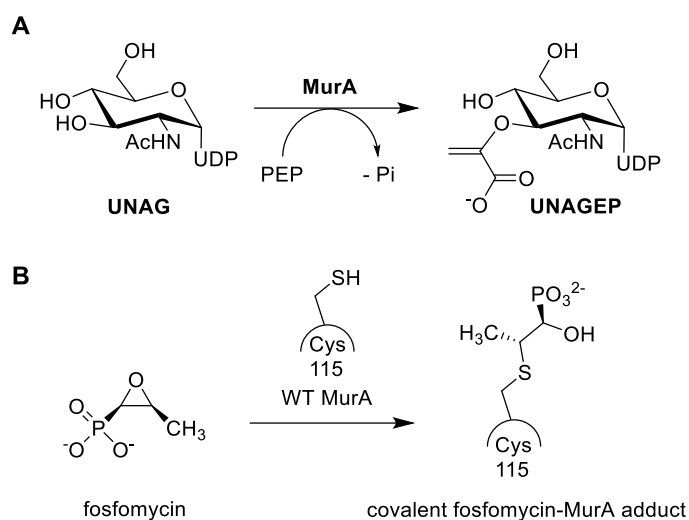


Figure 1. A. MurA-catalyzed reaction. **B.** Mechanism for the inhibition of WT MurA by fosfomicin.

Screening campaigns to identify MurA inhibitors (*Figure 2*) have been performed by various groups and led to the discovery of several low micromolar inhibitors including avenaciolides (I),²⁰ tulipalines (II),³¹ the sesquiterpene lactone cnicin (III),^{32,33} the cyclic disulfide RWJ-3981 (IV),³⁴ and ebselen (V).³⁵ These inhibitors usually possess highly electrophilic moieties that target MurA by irreversible interactions in its active site through several mechanisms ranging from reaction of the Cys key residue in a Michael addition such as in the case of I, and II, (avenaciolides and tulipalines respectively)^{20,31,36} to formation of a suicide inhibitor of the MurA active site via covalent binding to UNAG with III (cnicin).^{32,33} V (ebselen) targets MurA through covalent binding to the active-site Cys key residue,³⁵ and IV (RWJ-3981) acts by irreversible non-covalent attachment near the PEP binding site.^{37,38} While targeting the catalytic Cys residue in the active site results in effective inhibition of MurA, this mechanism also implies that most of these compounds are inactive against the naturally occurring MurA C115D mutant.^{31,32,35,37} In addition, several of these inhibitors have been shown to react non-specifically with thiol-containing

compounds such as dithiothreitol (DTT) and also the cellular antioxidant glutathione (GSH).^{20,31,35,37} Moreover, the highly electrophilic structures also raise concerns about their specificity and safety as they have been shown to undergo several off-target interactions such as the inhibition of glutamate transport in rat liver mitochondria (III, avenaciolides)³⁹⁻⁴¹ and the nonspecific inhibition of several bacterial targets in addition to failing to protect mice from death in a lethal *Staphylococcus aureus* (*S. aureus*) infection model (IV, RWJ-3981).³⁷ Therefore, it is of great importance to develop new scaffolds that inhibit MurA specifically and have proven safety on mammalian cells.

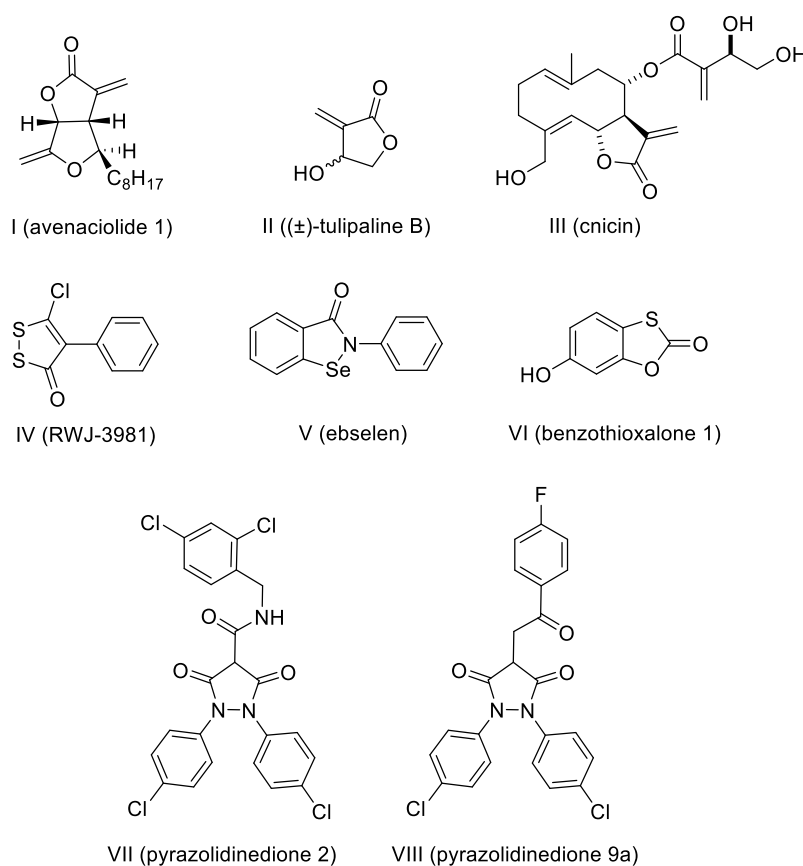


Figure 2. Previously reported MurA inhibitors.

In a high-throughput screening campaign, Miller and coworkers identified benzothioxalones (Figure 2, VI) as MurA inhibitors, displaying IC₅₀ values against MurA between 0.25 and 51 μM. The compounds were also found to form covalent

adducts due to reaction of Cys115 with the cyclic thiocarbonate unit.⁴² Consequently, binding was not detected with the C115D mutant MurA protein. Additionally, the cyclic thiocarbonate motif might react with other enzymes having a reactive cysteine in the active site, similar to the aforementioned Michael acceptor-type inhibitors.

Another class of reported inhibitors are pyrazolidinediones (*Figure 2*, VII, and VIII) that act as dual MurA/B inhibitors with MurB (i.e., the subsequent enzyme from the peptidoglycan biosynthesis cascade) as their main target.^{6,43–45} We had an in-house library of aryl-substituted pyrrolidinediones available that had formerly provided moderately active inhibitors of active atypical protein kinase C (PKC).⁴⁶ The structural similarity of this compound class to the aforementioned pyrazolidinedione-type MurA/B inhibitors prompted us to initiate a screening campaign for MurA inhibition with some selected pyrrolidinediones from our in-house library. In this study, we report the unprecedented identification of a diarylpyrrolidinedione scaffold that inhibits MurA without any reaction with the key active-site Cys115 residue. Therefore, inhibitory activities towards the *E. coli* MurA C115D mutant and the wild type (WT) MurA enzyme were identical. As this new class of MurA inhibitors also showed no toxicity to human cell lines, it overcomes many limitations of previously reported MurA inhibitors and might serve as a useful starting point for the development of novel antibiotics targeting MurA.

3.3.3 Results and Discussion

3.3.3.1 Chemistry

The synthesis of all target pyrrolidinediones **1–46** (*Table 1*) was carried out using an efficient three-component one-pot procedure (*Scheme 1*) that had been described by Merchant and Schiff.^{47,48} A major advantage of this method was that all three required reagents were usually commercially available in a large variety. For a first series of

target compounds, several amines (1–7a, 14a, and 15a) were reacted with aldehydes (1–7b, 14b, and 15b) to furnish the respective imines (1–7c, 14c, and 15c), which were converted to pyrrolidinediones **1–7**, **14** and **15** with tricarbonyl reagents (1–7e, 14e, and 15e) generated by Claisen condensation with diethyl oxalate. For a second series of target pyrrolidinediones **8–13** and **16–46**, the same protocol was applied using aminobenzothiazoles as amine components (8–13a, and 16–46a). The depicted structure of pyrrolidinediones **1–7**, **14** and **15** with residues R¹, R² and R³ (Scheme 1, Table 1) will subsequently be referred to as 'general structure' of the pyrrolidinedione scaffold when structure-activity relationship data are discussed (*vide infra*).

Scheme 1. Synthesis of pyrrolidinediones **1–46** (see Table 1 for exact structures).

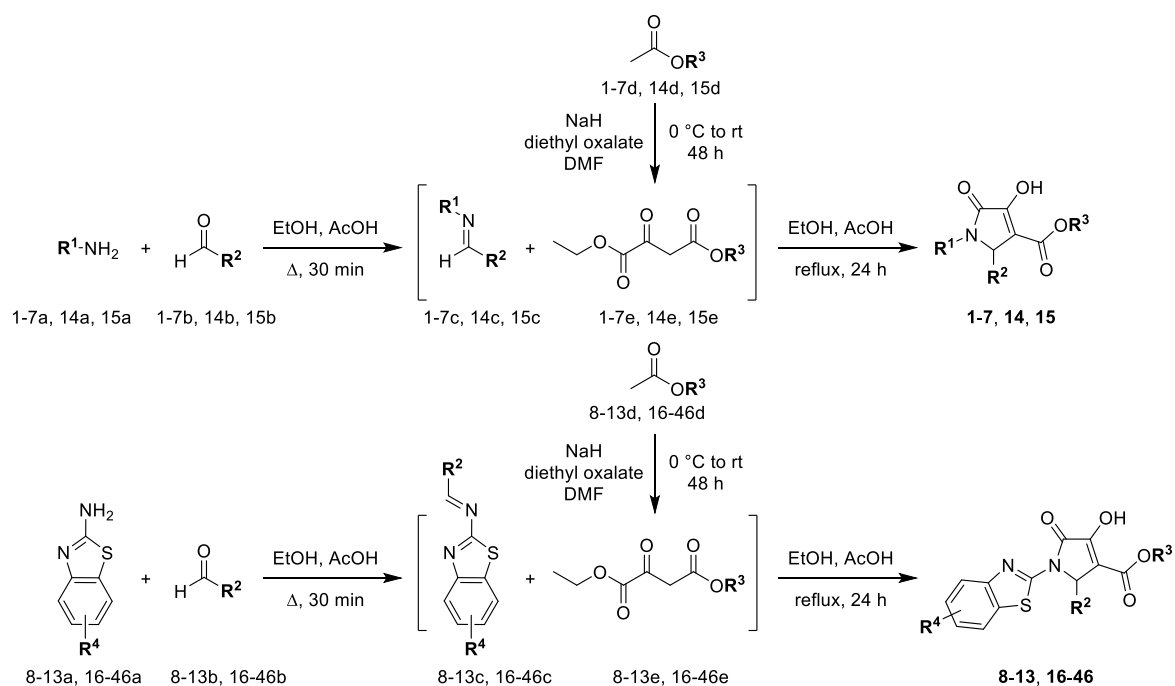
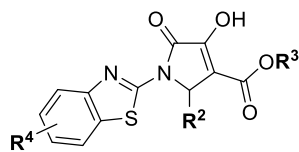


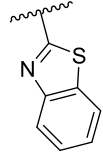
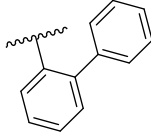
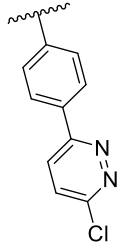
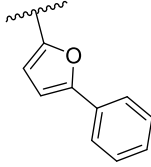
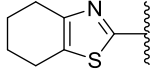
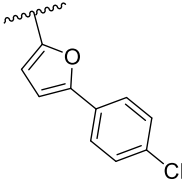
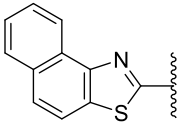
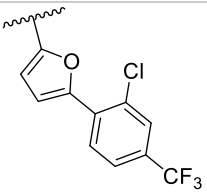
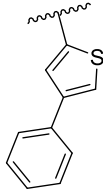
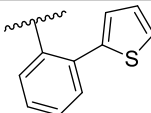
Table 1. Structures and substitution patterns of the synthesized pyrrolidinedione derivatives.

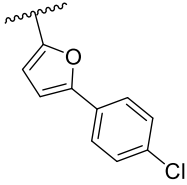
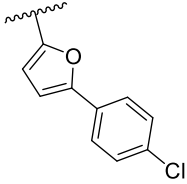
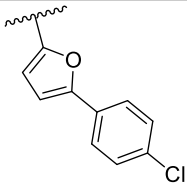
1-7, 14, 15



8-13, 16-46

No.	R ¹ /R ⁴	R ²	R ³	No.	R ¹ /R ⁴	R ²	R ³
1		4-Cl Ph	Et	24	5,6-diMe	Biph	Et
2		4-Cl Ph	Et	25	6-Me	4-OH Ph	Et
3	Biph	Ph	Et	26	6-Me		Et
4	4-Cl Ph	4-Cl Ph	Et	27	6-Me		Et
5	Ph	Biph	Et	28	6-Me		Et
6		Biph	Et	29	6-Me		Et
7		Biph	Et	30	6-Me		Et
8	H	Ph	Et	31	6-Me		Et
9	4-Me	Ph	Et	32	6-Me		Et

10	6-Me	Ph	Et	33	6-Me		Et
11	4-Cl	Ph	Et	34	6-Me		Et
12	6-Cl	Ph	Et	35	6-Me		Et
13	O-Phe	Ph	Et	36	6-Me		Et
14		Ph	Et	37	6-Me		Et
15		Ph	Et	38	6-Me		Et
16	H	Biph	Et	39	6-Me		Et
17	6-Br	Biph	Et	40	6-Me		Et
18	6-CF ₃	Biph	Et	41	4-Me	Ph	<i>t</i> Bu
19	6-Me	Biph	Et	42	6-Me	Ph	<i>t</i> Bu

20	6-OMe	Biph	Et	43	6-Cl	Ph	tBu
21	4-Cl	Biph	Et	44	6-Me		EtOH
22	4-OMe	Biph	Et	45	6-Me		Me
23	4,6-diF	Biph	Et	46	6-Me		tBu

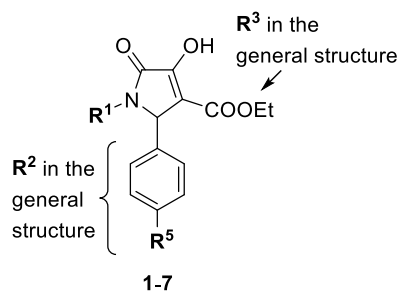
3.3.3.2 Biological Evaluation

3.3.3.2.1 Inhibition of MurA

We started the screening campaign with some selected compounds (*Table 2*) from our in-house library of aryl-substituted pyrrolidinediones against *E. coli* MurA. For the initial screening, we selected a small set of compounds covering the chemical diversity present in the positions R¹ and R² of the 'general structure' (*vide supra*, *Table 1*). The activity of MurA was tested using a standard malachite green assay measuring the amount of released inorganic phosphate using malachite green and sodium molybdate. Together, the phosphate and these reagents form a green complex that is then quantified spectrophotometrically.⁴⁹ When tested at a fixed concentration of 20 μM in this *in vitro* MurA assay, we observed inhibitory activity for several compounds, dependent on the type of the substituents (*Table 2*). In particular, compound **7** showed a remarkable activity with an IC₅₀ of 5 μM, thus being equipotent to the established MurA inhibitor fosfomicin under the assay conditions –

notwithstanding that the IC_{50} values are only comparable to a limited extent because of the irreversible binding mode of fosfomycin. Altogether, the aryl-substituted pyrrolidinedione system proved to be a new scaffold for the development of MurA inhibitors.

Table 2. Results from the screening of the initial set of aryl-substituted pyrrolidinediones against MurA.

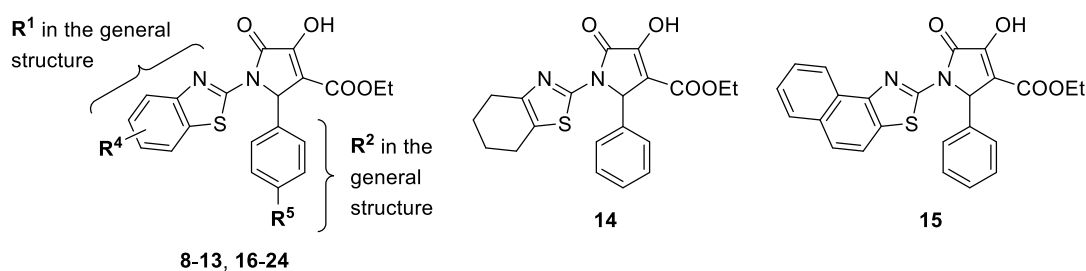


Compound	R ¹	R ⁵	Inhibition at 20 μ M \pm SD, (IC_{50} (μ M) \pm SD) ^a
1		Cl	34 \pm 6%
2		Cl	15 \pm 9%
3	Biph	H	19 \pm 1%
4	4-Cl Ph	Cl	14 \pm 3%
5	Ph	Ph	13 \pm 6%
6		Ph	40 \pm 6%
7		Ph	78 \pm 6% (5.1 \pm 0.4)
fosfomycin	-----	-----	78 \pm 3% (5.3 \pm 1.7)

^a IC_{50} values were determined for all compounds that showed more than 50% inhibition at 20 μ M

In the following rounds of screening, we explored the effect of changing one structural feature of the scaffold while preserving the others to derive structure-activity relationships (SAR) for each feature. As observed with **7**, a 6-chlorobenzothiazole unit conveyed the strongest MurA inhibition from all the different aryl moieties in the N1-position (R^1 in the general structure). Therefore, further benzothiazole motifs at this position were explored in the next round of screening, in combination with either a plain phenyl or a biphenyl side chain at position 2 (R^2 in the general structure, *Table 3*).

Table 3. MurA inhibition of benzothiazole-substituted pyrrolidinediones (variations in position R^1 of the general structure).



Compound	R^4	R^5	Inhibition at 20 μM (\pm SD)	IC_{50} (μM) (\pm SD) ^a
8	H	H	0	n.d.
9	4-Me	H	0 \pm 2%	n.d.
10	6-Me	H	26 \pm 4%	n.d.
11	4-Cl	H	18 \pm 4%	n.d.
12	6-Cl	H	14 \pm 7%	n.d.
13	6-OPh	H	53 \pm 8%	17 \pm 3
14	-----	-----	14 \pm 6%	n.d.
15	-----	-----	36 \pm 3%	n.d.
16	H	Ph	45 \pm 1%	n.d.
17	6-Br	Ph	52 \pm 2%	21 \pm 1
18	6-CF ₃	Ph	70 \pm 5%	6.1 \pm 0.7
19	6-Me	Ph	76 \pm 4%	8.5 \pm 1.9
20	6-OMe	Ph	51 \pm 4%	22 \pm 8

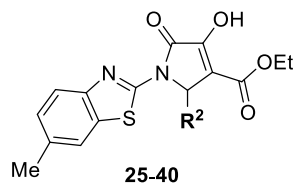
21	4-Cl	Ph	73 ± 3%	7.0 ± 0.7
22	4-OMe	Ph	31 ± 3%	25 ± 2
23	4,6-diF	Ph	76 ± 5%	7.5 ± 0.4
24	5,6-diMe	Ph	85 ± 2%	5.8 ± 0.7

^aIC₅₀ values were determined for all compounds that showed more than 50% inhibition at 20 μM; n.d. = not determined.

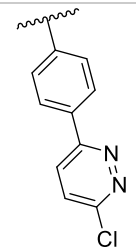
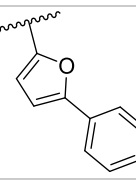
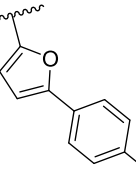
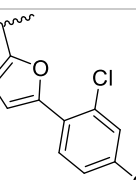
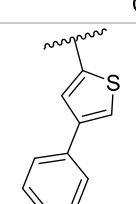
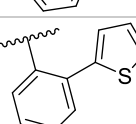
The results of the second round of screening revealed that the presence of a biphenyl moiety (R⁵ = phenyl) was a major determinant of activity (compounds **16 -14**, *Table 3*); compound **13** was the only compound lacking the additional phenyl at R⁵ to show pronounced activity (IC₅₀ = 17 μM), probably because the 6-phenoxy substituent at R¹ compensated for the absence of the biphenyl system by establishing additional aromatic interactions. Among the biphenyl compounds, an additional gain in activity of up to five-fold was achieved by the substituent R¹ at the benzothiazole. Generally, a methyl or chloro substituent at the 4- or 6-position of the benzothiazole was favorable for MurA inhibition as seen with compounds **7** (*Table 2*), **19** and **21** (*Table 3*). Bulkier substituents such as bromo or methoxy groups were slightly detrimental to the activity as demonstrated when comparing compounds **17** (6-Br) and **20** (6-OMe) with compound **19** (6-Me).

This strong dependency of the activity on the aromatic moiety at R² led us to explore a broader range of differently substituted phenyl, various simple heteroaryl and extended biaryl and naphthyl derivatives (*Table 4*). The 6-methylbenzothiazole motif at position R¹ was kept constant in this series.

Table 4. MurA inhibition of benzothiazole-aryl-substituted pyrrolidinediones (variations in position R² of the general structure).



Compound	R ²	Inhibition at 20 μM (\pm SD)	IC ₅₀ (μM) (\pm SD) ^a
25		23 \pm 13%	n.d.
26		21 \pm 1%	n.d.
27		14 \pm 2%	n.d.
28		29 \pm 2%	n.d.
29		44 \pm 3%	n.d.
30		43 \pm 4%	n.d.
31		54 \pm 4%	15 \pm 3
32		74 \pm 2%	9.5 \pm 0.3
33		12 \pm 4%	n.d.
34		57 \pm 5%	17 \pm 3

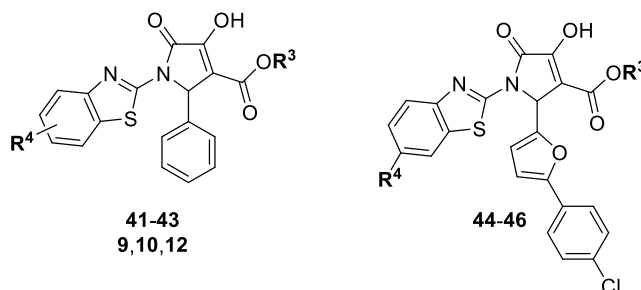
35		$36 \pm 3\%$	n.d.
36		$37 \pm 4\%$	n.d.
37		$75 \pm 3\%$	9.9 ± 1.2
38		$94 \pm 2\%$	4.8 ± 0.2
39		$72 \pm 1\%$	9.9 ± 2.1
40		$50 \pm 6\%$	22 ± 5

^aIC₅₀ values were determined for all compounds that showed more than 50% inhibition at 20 μM; n.d. = not determined.

This round of screening confirmed that a more extended aromatic system at R², e.g. the biaryl moieties in compounds **19** (Table 3), **38** and **39** (Table 4), enhanced the inhibitory activity against MurA. As seen with the 5-aryl-furan-2-yl derivatives **36–38**, further lipophilic substituents on the phenyl ring modulated the activity. The disubstitution pattern in **38** led to the strongest increase of potency, however, this was at the cost of increased lipophilicity, which in general was the main problem with the extended aryl systems at R². Unfortunately, the more polar pyridazine analog **35**

was much less active, possibly indicating the correlation of potency with the degree of lipophilicity.

Table 5. MurA inhibition of benzothiazole-substituted pyrrolidinediones with different ester moieties (variations in position R³ of the general structure).



Compound	R ⁴	R ³	Inhibition at 20 μM (± SD)	IC ₅₀ (μM) (± SD) ^a
41	4-Me	tBu	67 ± 5%	11 ± 1
9^b	4-Me	Me	0 ± 2%	n.d.
42	6-Me	tBu	38 ± 2%	n.d.
10^b	6-Me	Me	26 ± 4%	n.d.
43	6-Cl	tBu	38 ± 14%	n.d.
12^b	6-Cl	Me	14 ± 7%	n.d.
44	Me	2-OH-Et	43 ± 5%	n.d.
45	Me	Me	59 ± 5%	16 ± 5
46	Me	tBu	88 ± 3%	4.5 ± 0.5

^aIC₅₀ values were determined for all compounds that showed more than 50% inhibition at 20 μM; ^bvalues for compounds **9**, **10**, and **12** were taken from Table 2 for comparison; n.d. = not determined.

In the last round of screening, the ethyl ester side chain in position R³ of the general structure was changed to other alkyl esters (Table 5). It was found that a *t*-butyl ester led to slightly or even pronounced increases of inhibitory activity (**41** vs. **9**, **42** vs. **10**, and **43** vs. **12**, Table 5). This is most clearly demonstrated when comparing compounds **9** and **41**, where even in absence of an extended aryl system in position R², compound **41** showed an IC₅₀ value of 11 μM. However, we still observed a dependency on the substitution pattern of the benzothiazole unit, as there was only

weak additive enhancement of activity for compounds **42** and **43** over compounds **10** and **12**, respectively. In the case of the rather active 5-aryl-furan-2-yl derivatives, the ester side chain also had a noticeable influence on the activity (compounds **44–46**, *Table 5*). Changing the ethyl to the more hydrophilic 2-hydroxyethyl ester in compound **44** led to a significant decrease in activity, suggesting that the alkyl residue interacts with MurA in a hydrophobic environment. The dependency of potency of the derivative on the size of the ester moiety is confirmed by the fact that changing the ethyl ester of **37** (*Table 4*) to a methyl congener (**45**, *Table 5*) resulted in decreased inhibition. We achieved maximum MurA inhibition with the bulkier *t*-butyl ester in compound **46** (*Table 5*) as the most active derivative in the series alongside **38** (*Table 4*), which had been found to be too lipophilic (cf. *Table S3* for more information regarding the lipophilic properties and ligand efficiency of some selected compounds).

Taken together, the results obtained for pyrrolidinediones as potent MurA inhibitors with a clear SAR demonstrated that the re-screening of a compound library for activities against microbial targets can be a viable option in the discovery process for potential antibacterial agents. Compound **46** was chosen as the best-in-class derivative of the series for more detailed subsequent studies. Keeping in mind that the compounds are structurally similar to the published pyrazolidinedione type of dual MurA/MurB inhibitors (e. g., VII and VIII in *Figure 2*), we also tested compound **46** in a specific MurB assay. However, we found only a weak activity against MurB (46% inhibition at 20 μ M), confirming MurA as being the major target of compound **46** in the early steps of peptidoglycan synthesis.

3.3.3.2.2 Compound 46 Showed Equal Potency against the Clinical MurA C115D mutant

With respect to the frequent occurrence of drug-resistant mutants, it is advantageous for new inhibitors of established bacterial targets to address alternative binding sites on such a target. Therefore, we tested compound **46** for its inhibitory properties *in vitro* towards the C115D MurA mutant, which shows resistance against fosfomycin.³⁰ Remarkably, we obtained an IC₅₀ value of 4.9 μM, which was identical to the IC₅₀ value against WT MurA (4.5 μM, *Table 5*). This demonstrated that **46** inhibited MurA via an alternative binding mode or a different binding site, and that the pyrrolidinedione scaffold might have the potential to break fosfomycin resistance.

3.3.3.2.3 Reversibility of MurA Binding of Compound 46

Compound **46** was tested for its binding reversibility to MurA, using fosfomycin as a control. When employed in a dilution assay, **46** was shown to be a reversible binder, as it lost its MurA inhibitory activity when the assay mixture was diluted after an initial preincubation period with the enzyme. This was different from the irreversible inhibitor fosfomycin which retained its inhibitory effect even after the 1:50 dilution step (*Figure 3*). For these experiments, three assay conditions were used: a 1:50 diluted assay (A) for which the assay mixture with MurA, UNAG and the respective compound (10 μM initial concentration) was diluted to reach a 0.2 μM final concentration of the inhibitor; a concentrated assay (B) with a 10 μM final concentration of both compounds; and a directly diluted assay (C) without a preincubation step with a final compound concentration of 0.2 μM.

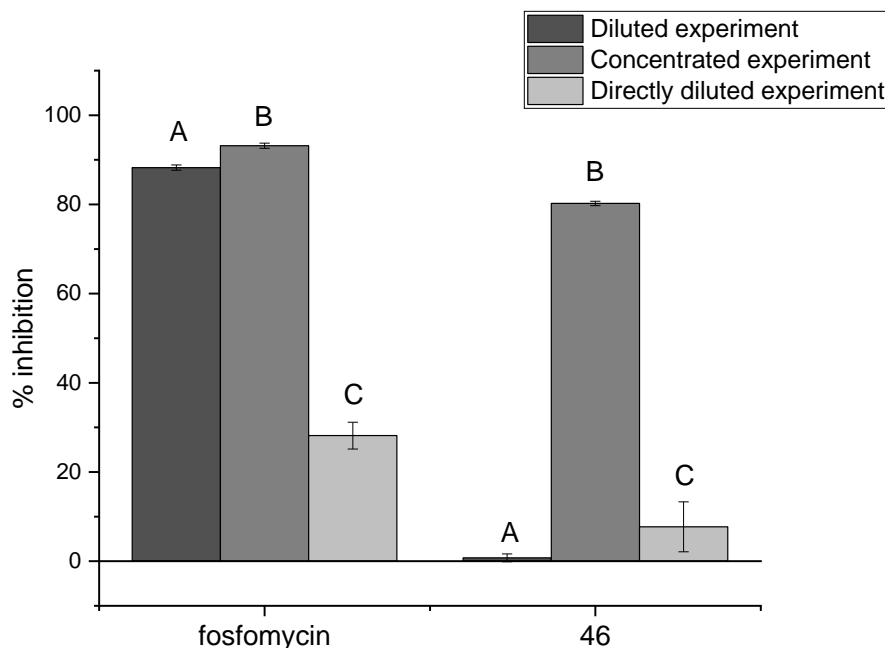


Figure 3. Assays on the reversibility of binding of fosfomycin and compound **46** to MurA. The data shown are the mean of three independent experiments, and the error bars represent \pm SD. **A.** Diluted assay with a final compound concentration of 0.2 μ M; **B.** Concentrated assay performed under the same conditions as the diluted assay, but compound concentrations were adjusted to reach a final concentration of 10 μ M; **C.** The assay conditions from **A** were directly reproduced, but without a preincubation step.

3.3.3.2.4 Analysis of Potential Cooperative Effects of Compound **46** and Fosfomycin

The observation that the potency of **46** was not reduced with the fosfomycin-insensitive C115D mutant of MurA may suggest that both compounds might target different sites. To investigate this further, we looked into a potential synergism of inhibition between both inhibitors. Indeed, compound **46** showed an additive effect with fosfomycin when they were applied together in the enzymatic assay (*Figure 4*). This additive effect disappeared, but the inhibition by **46** was retained, when the same assay was performed using the fosfomycin-resistant C115D MurA mutant. This demonstrated the potential of a combination treatment approach with a pyrrolidinedione MurA inhibitor (such as **46**) and fosfomycin and also confirmed that

the binding site of **46** did not significantly overlap with that of fosfomycin. More importantly, simultaneous blocking of MurA at two different sites might impede the occurrence of resistant mutants in a clinical setting, which is a major advantage for our suggested combination.

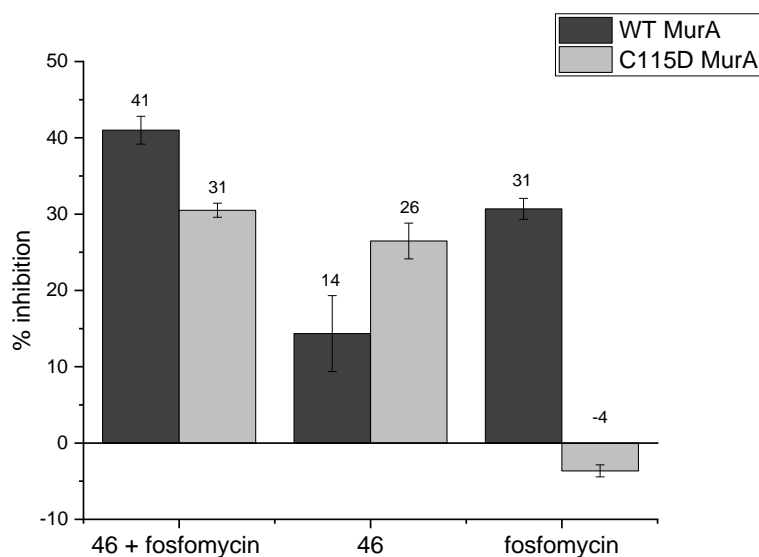


Figure 4. Additive effect of the coadministration of compound **46** and fosfomycin on WT MurA. Fosfomycin had no effect on C115D MurA while compound **46** retained its activity. The data shown are the mean of three independent experiments, and the error bars represent \pm SD; final concentrations of both compounds were 2 μ M.

3.3.3.2.5 Investigation of the Mode of Inhibition of Compound **46**

We first performed an enzyme kinetics study of the binding of **46** to MurA. While a strict Michaelis-Menten model probably could not be fully applied to MurA (as the enzyme has two substrates), we attempted to study the interplay of the binding of **46** and the concentration of UNAG in the assay. This was done by modifying the MurA malachite green assay, which is an endpoint assay, to a continuous assay measured over a time period of 30 minutes. For each tested concentration of **46**, four different concentrations of UNAG were examined (25, 100, 250 and 363 μ M). The Malachite green absorbance vs. time was plotted for each UNAG concentration, and the slope

was calculated for each resultant line. The Lineweaver-Burk plot (*Figure 5*) was then obtained by plotting the reciprocal of the slope (representing $1/V_o$) vs. the reciprocal of the UNAG concentration (representing $1/S$). The lines for each concentration of **46** were almost parallel to each other, indicating an uncompetitive binding.⁵⁰ So far, the enzyme kinetics data seemed to support a binding of **46** to the MurA-UNAG complex, thus preventing the formation of the MurA product UNAGEP.

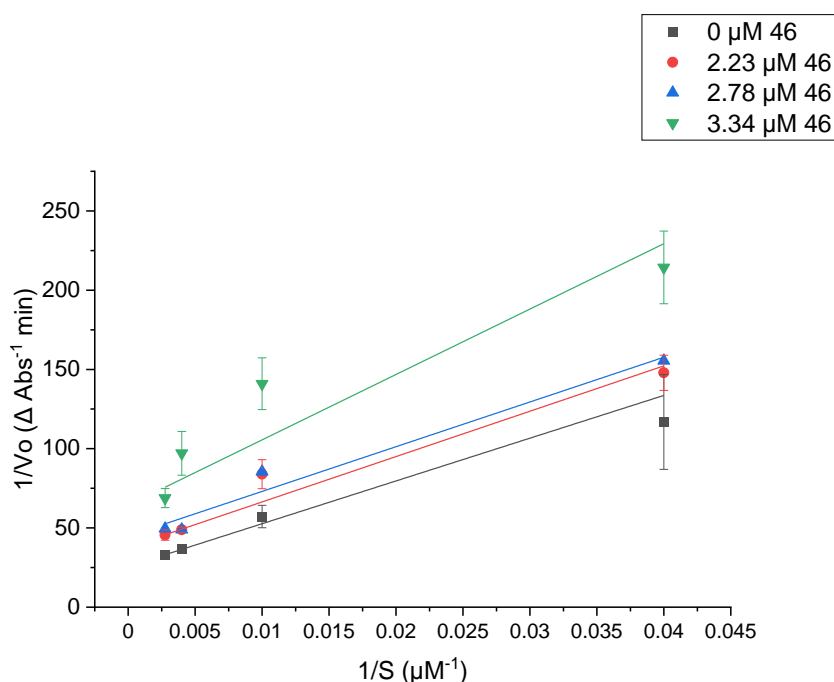


Figure 5. Lineweaver-Burk plot for the relationship of MurA activity and UNAG concentration at different concentrations of **46**. The data shown are the mean of three independent experiments, and the error bars represent \pm SD. Four different concentrations of UNAG were tested: 25, 100, 250, and 363 μ M. The measurements were taken at 5, 10, 20, and 30 min.

However, we contemplated that the enzyme kinetics data might also be consistent with the need for UNAG to 'unlock' the enzyme for binding of **46**. According to previous reports, recombinantly overexpressed MurA was isolated in the 'closed' UNAM- and PEP-bound form, which persisted throughout the purification procedures (*Figure S1A*).^{22,51,52} It was further reported that increasing concentrations of UNAG

could displace the UNAM, forming a binary complex which can enter the catalytic cycle by additionally binding PEP or partially exist in equilibrium with the 'open' conformational state of the enzyme (*Figure S1B*);^{22,51,52} the latter would then be competent for binding of **46**. UNAG might be bound or not to the MurA complex with **46**, which would not be distinguishable by the enzyme kinetics analysis. Therefore, we decided to use an alternative experimental approach, i.e., non-denaturing ('native') ESI-MS, to analyze the mode of inhibition with respect to UNAG. Native MS preserves the noncovalent interactions between enzymes and their binding partners.⁵³ In addition, denaturing ('non-native') ESI-MS of the protein was also performed to obtain the molecular weight of the ligand-free protein.

The obtained results from the native MS experiments (*Table 6*) reveal that MurA had indeed been expressed in the closed UNAM- and PEP-bound form, showing an equivalent mass to that ternary complex in addition to sodium (*Table 6*, entry 1, and Supporting Information, *Figure S2A*). Upon incubation with UNAG, this complex apparently opened up and the mass of bound UNAG in addition to inorganic phosphate (P_i) was observed (entry 2, and *Figure S2B*). The presence of inorganic phosphate could be explained by the initial enzymatic reaction that would occur when the intrinsically bound PEP molecule is converted with the added UNAG to furnish inorganic phosphate as a by-product. Subsequently, in absence of additional PEP, P_i is not released while the enzyme binds another UNAG, most likely leading to the formation of the observed complex. Two further native MS experiments involved the addition of **46** to the enzyme in both the absence and presence of UNAG. In the absence of UNAG, we again observed the closed enzyme complex with UNAM and PEP (*Table 6* entry 3, and *Figure S2C*). In contrast, when the enzyme was first preincubated with UNAG for 15 minutes prior to addition of **46**, we observed the additional masses

of bound **46**, the enzymatic product P_i as before, and in addition, an acetate ion from the dialysis buffer (entry 4, and *Figure S2D*). This finding led us to reconsider the hypothesis of uncompetitive inhibition of compound **46**, as the mass of the expected enzyme-UNAG-**46** complex was not detected. Retrospectively, the results from the kinetics experiments may be explained by the necessity of the presence of UNAG for unlocking the enzyme structure before the binding of **46** can occur. This means that compound **46** is not simply an uncompetitive MurA inhibitor, but rather a more complex mechanism of action is involved in its binding.

Table 6. Results from non-denaturing (native) ESI-MS on MurA-ligand complexes.

#	Conditions	M_{av} (Da) ^a	ΔM (Da) ^b	Bound ligands	$M_{bound\ ligands}$ (Da)
1	MurA	48423	870	PEP, UNAM, Na ⁺	870
2	MurA + UNAG	48257	704	UNAG, P_i	705
3	MurA + 46	48401	847	PEP, UNAM	847
4	MurA + UNAG + 46	48232	679	46 , P_i , OAc ⁻	679

^a M_{av} is the average detected mass by native MS, ^bThe mass of the ligand-free protein (determined by non-native MS) was 47553 Da.

3.3.3.2.6 Binding Analysis by NMR Spectroscopy

ous attempts to obtain an X-ray co-crystal structure of MurA bound to inhibitor **46** were ultimately unsuccessful (data not shown). This might have resulted from MurA being intrinsically expressed in a closed PEP-UNAM bound form, as it had been reported before⁵¹, and is in agreement with our native MS experiments. This closed ligand-bound conformation is very robust to dilution and does not convert into the open (ligand-free) conformation except in the presence of the enzyme substrate UNAG. Attempts to form crystals of the ligand-free apo enzyme were also

unsuccessful, and therefore, we ultimately could not obtain a co-crystal with **46** bound to MurA. The X-ray crystallography experiments only confirmed that UNAM and PEP were tightly bound to overexpressed MurA, where the crystals corresponded to PDB entry 3SWD (data not shown).⁵¹

Hence, to elucidate the binding mode of inhibitor **46** to MurA in comparison to fosfomicin, we attempted protein-detected NMR spectroscopy in the presence and absence of UNAG, with **46** and fosfomicin. U-¹⁵N-labelled wild type MurA and C115D MurA were expressed in *E. coli*, and ¹⁵N-¹H TROSY (transverse relaxation-optimized spectroscopy) HSQC spectra were recorded with 200 μM protein. The addition of UNAG at 500 μM resulted in significant chemical shift perturbations (CSPs) of a subset of peaks (Supporting Information, *Figure S3*). WT MurA (in the presence of 500 μM UNAG) was incubated with 500 μM fosfomicin or 500 μM compound **46** (WT MurA+UNAG+fosfomicin and WT MurA+UNAG+**46**, *Figure 6*). When comparing the CSPs and peak intensity reductions (arising from binding in a fast or intermediate exchange regime, respectively) of WT MurA+UNAG+fosfomicin with WT MurA+UNAG+**46**, it was noted that a similar subset of peaks was affected by small molecule binding in both cases, indicating binding of both compounds to a similar region of the protein. However, it should be noted that not all peaks affected by fosfomicin are affected by compound **46** and vice versa, suggesting that the binding sites meet in a certain region but do not superimpose.

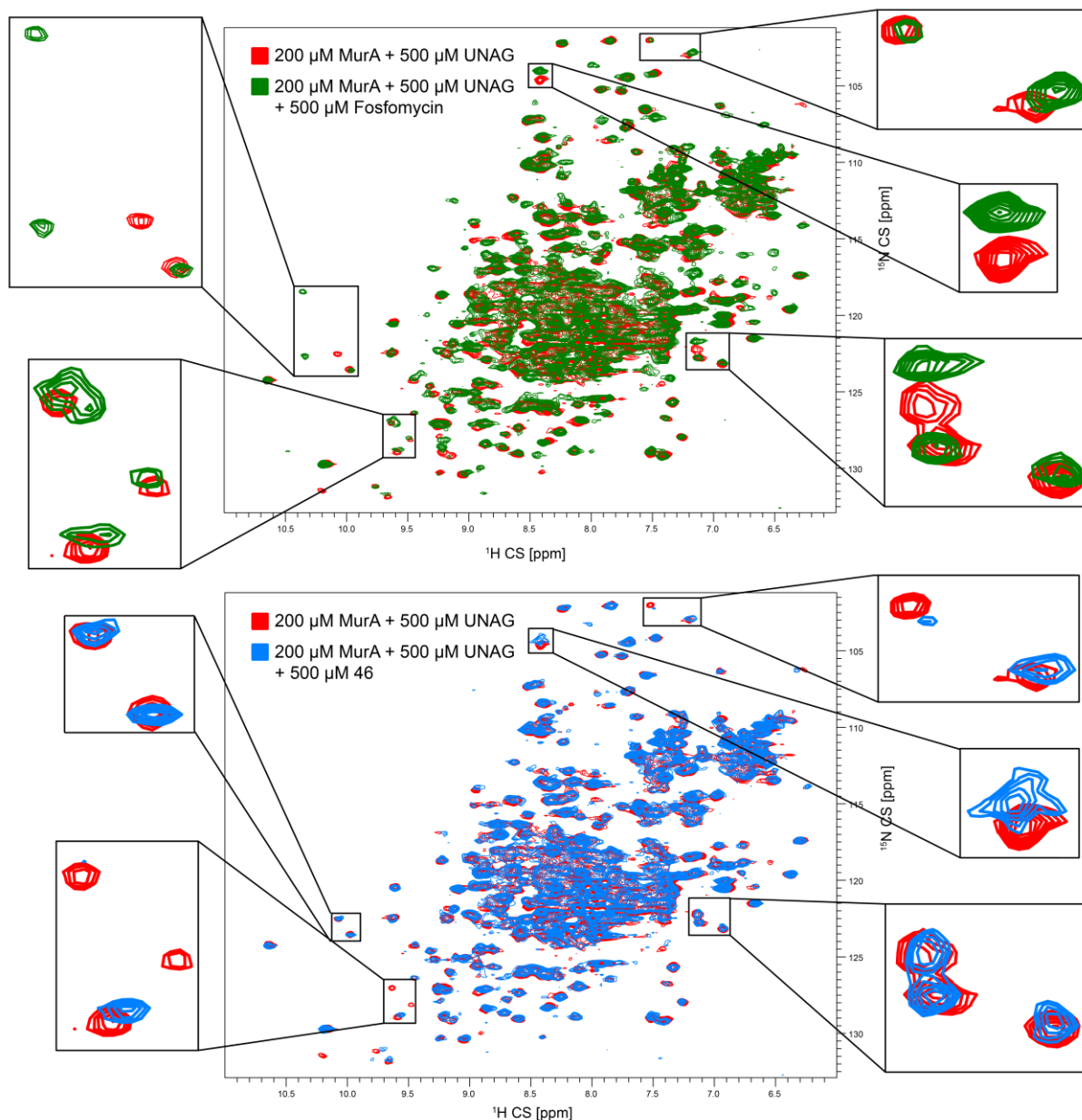


Figure 6. ^{15}N - ^1H TROSY HSQC spectra of WT MurA bound to UNAG (red), overlaid with WT MurA (UNAG-bound) in the presence of fosfomycin (green, top spectrum) or compound **46** (blue, bottom spectrum). Zoom in on selected regions highlights peaks that undergo chemical shift perturbations (CSPs).

When comparing the spectra for WT MurA and C115D MurA in the presence of UNAG (WT MurA+UNAG and C115D MurA+UNAG), the majority of CSPs were found to be identical, except for some differences which identified the peaks representing the region around Cys115 in WT MurA (Supporting Information, *Figure S4*). Additionally, in accordance with the results from enzyme kinetics, X-ray crystallography, and

native MS data, we observed no CSPs caused by **46** in the absence of UNAG (WT MurA+**46**), confirming that specific interaction by this inhibitor with MurA requires the open form of the enzyme (*Figure S5*).

To further investigate the residues involved in the binding of inhibitor **46**, the same set of experiments was repeated with MurA C115D (C115D MurA+UNAG+fosfomycin and C115D MurA+UNAG+**46**, *Figure 7*). Firstly, it was noted that fosfomycin was unable to bind to the C115D mutant. Secondly, compound **46** was still capable of binding MurA C115D (as shown by CSPs and peak intensity reduction, *Figure 7*), indicating that cysteine-115 is not crucial for the binding of compound **46**.

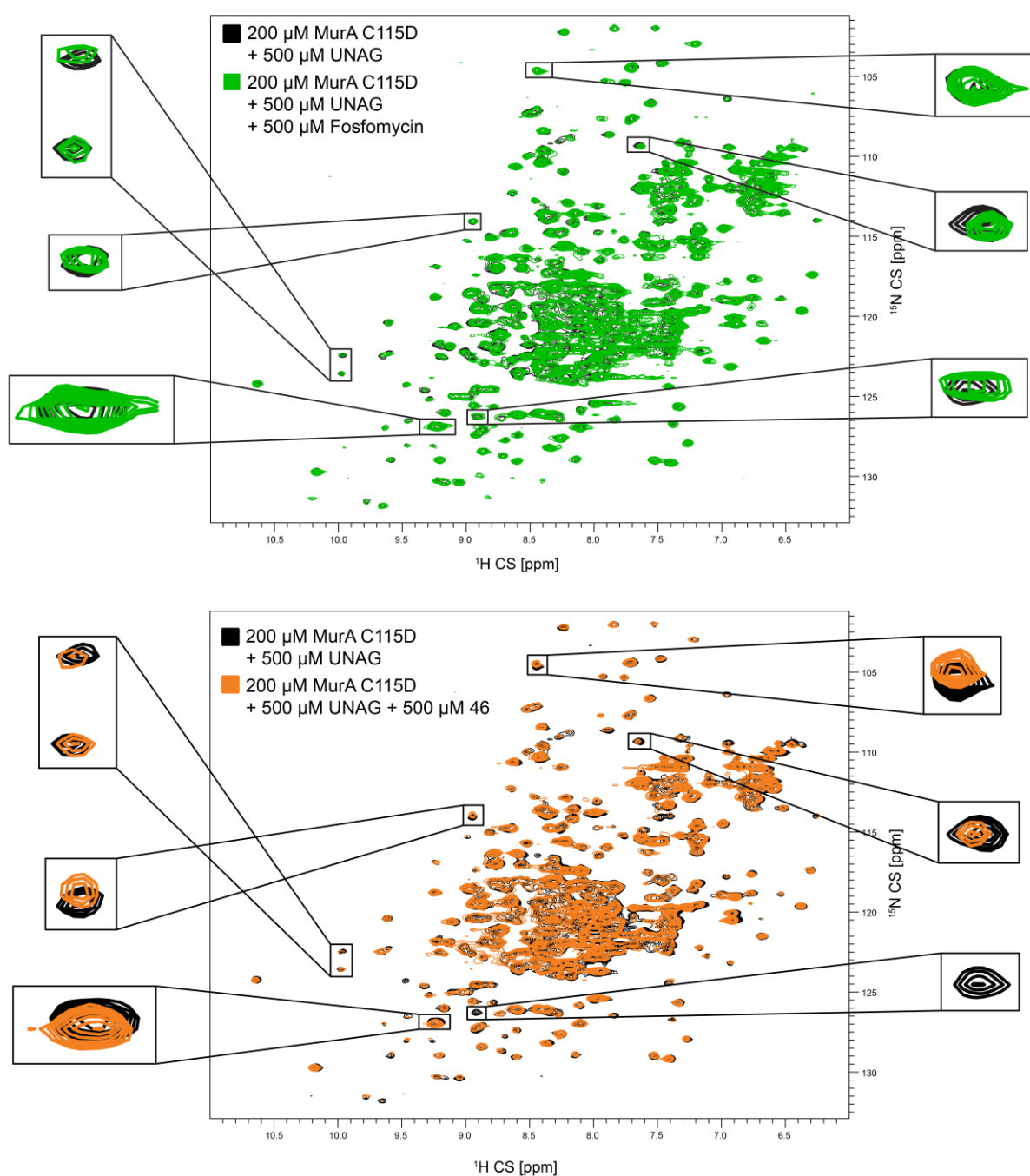


Figure 7. ^{15}N - ^1H TROSY HSQC spectra of MurA C115D bound to UNAG (black), overlaid with MurA C115D (UNAG-bound) in the presence of fosfomycin (green, top spectrum) or compound **46** (orange, bottom spectrum). Zoom in on selected regions highlights peaks that undergo chemical shift perturbations (CSPs).

3.3.3.2.7 Potential Binding Mode of **46** with *E. coli* MurA

Next, we used molecular docking to derive a potential binding mode for **46** that would be in accordance with all experimental data. Our results from the kinetic analysis,

native MS experiments and NMR spectroscopy clearly indicated that the UNAG-bound conformation of MurA is also the form to which **46** binds. Furthermore, as binding of **46** occurred in the absence of UNAG but included a phosphate ion formed from the co-substrate PEP, we reasoned that the binding site of **46** may overlap with that of UNAG but not of PEP. Based on these considerations, we selected an available X-ray co-crystal structure of *E. coli* MurA with UNAG and covalently bound fosfomycin for docking simulations, with the latter serving as a mimic of the PEP-derived phosphate (PDB code: 1UAE),⁵⁴ assuming that the phosphate group of fosfomycin would be coordinated by the same residues. The most plausible binding mode was obtained with the (*S*)-enantiomer of **46** (Figure 8). It largely overlapped with the binding site of UNAG, with the pyrrolidinedione ring occupying the space of the ribose, capturing lysine 160 that normally interacts with the uracil carbonyl. Since the pyrrolidinedione enol tautomer is slightly acidic, the charge-supported interaction with Lys160 might strongly enhance the binding affinity. The proposed binding mode was the only one that explained the clear contribution of the *tert*-butyl ester to the potency (*vide supra*), as only in this pose the *tert*-butyl moiety was in contact with a cluster of hydrophobic side chains, consisting of Val161, Pro289, Val327, and the Lys160 methylene groups, thus acting as a 'plug' closing part of the entry site of the binding pocket (see Figure S1C for further illustration). Interestingly, the terminal 4-chlorophenyl ring was predicted to replace the salt bridge of the UNAG phosphate with Arg120 by a cation- π interaction. This might be a key interaction, explaining why a similar subset of HSQC-NMR CSPs were observed for the binding of **46** and fosfomycin: both inhibitors stabilize the active, open conformation of the enzyme, capturing the large, mobile active site loop via coordination of the key loop residue Arg120 from two sides. This prediction was also consistent with the additive effect of **46** and fosfomycin on the

enzymatic activity that suggested that **46** and fosfomycin can bind simultaneously. Notably, the extended biaryl system at position R² of the general structure was not only important for the interaction with Arg120, but also stabilized the biologically active conformation of the **46** (*S*)-enantiomer by intramolecular CH- π interactions. This conformational pre-organization might reduce the entropic penalty upon binding to the pocket; a largely rigid ligand seems particularly necessary here as the binding site is framed by four flexible loop motifs that must be stabilized. Finally, the outer face of the benzothiazole moiety was positioned in a lipophilic environment that was not filled by UNAG (Supporting Information, *Figure S6*), formed by Pro298, Val327, Phe328, and the methyl group of Thr304. The latter showed hydrophobic interactions with the methyl substituent in the 6-position of the benzothiazole (indicated by a green dashed line in *Figure 8*), potentially explaining the positive impact of this substitution on the potency.

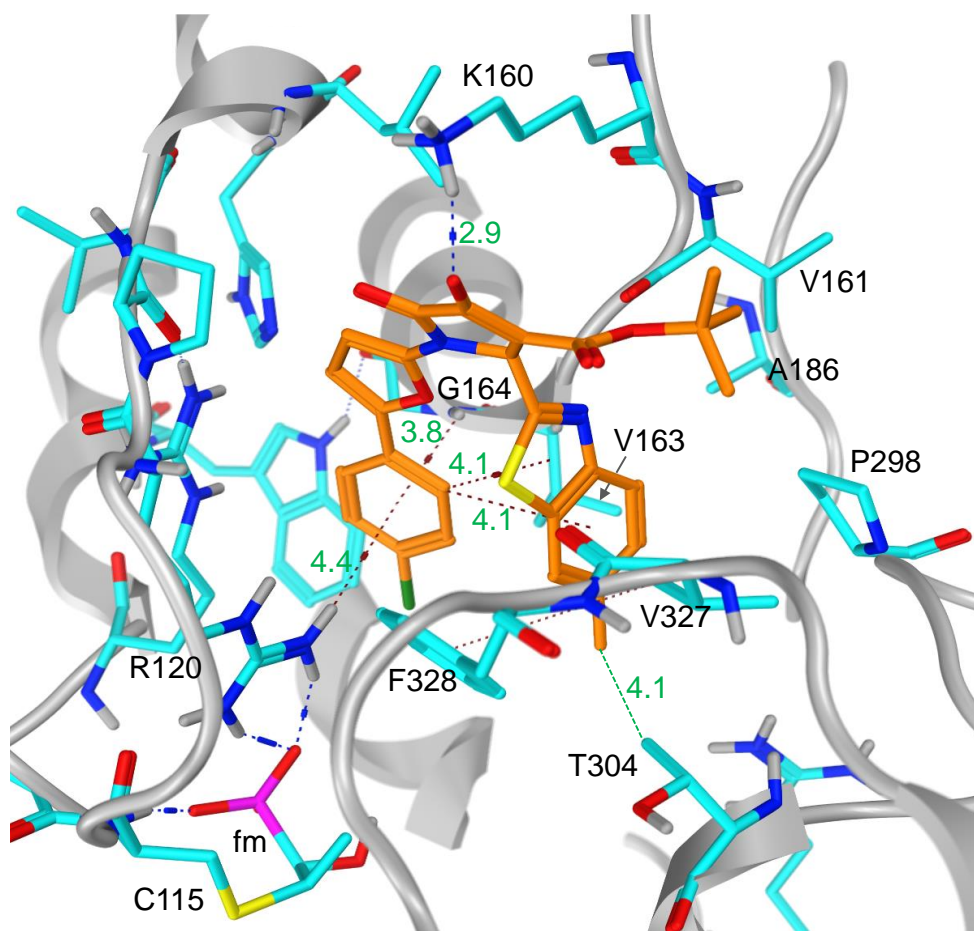


Figure 8. Predicted binding mode (by molecular docking) of **46** ((*S*)-enantiomer) in the X-ray co-crystal structure of UNAG and fosfomycin with MurA from *E. coli* (PDB code: 1UAE).⁵⁴ Inhibitor **46** (orange sticks) was predicted to fill the UNAG binding pocket completely, also including regions not occupied by UNAG. Amino acid residues (cyan) involved in direct or in hydrophobic interactions are labeled. Distances (green numbers) are given in Å; fm: covalently bound fosfomycin; blue dashed lines: H-bonds; brown dashed lines: CH- π and cation- π interactions.

3.3.3.2.8 Compound 46 is Non-cytotoxic to Human Cells

Since the investigated pyrrolidinediones had initially been envisioned as human PKC inhibitors, it was necessary to test their toxicity to human cell lines.⁴⁶ A standard MTT assay revealed that compounds **7** and **46** were non-toxic when applied to HepG2 (human liver carcinoma cell line) and the non-tumor cell line MRC-5 (human lung fibroblasts, *Figure 9*). This highlights the fact that our most potent novel MurA

inhibitors have no significant toxic effect on human cells, in line with their relatively low potency toward PKC.⁴⁶

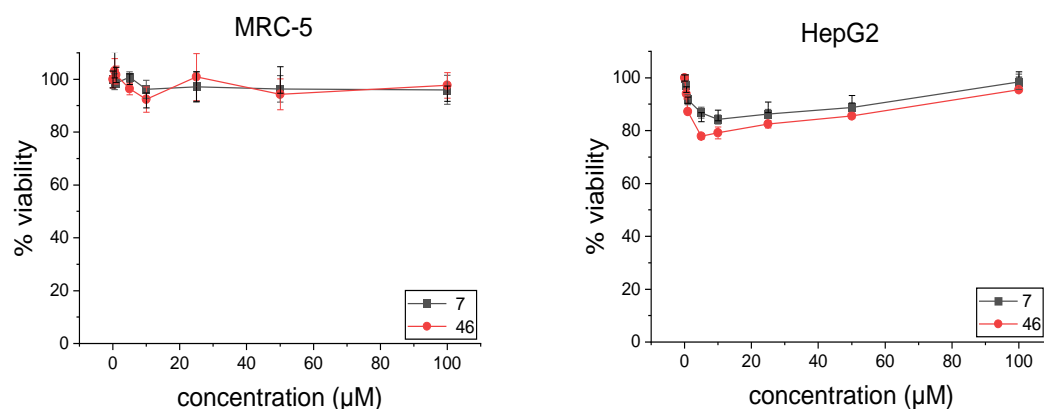


Figure 9. MTT assay result for compounds **7** and **46** indicating no cytotoxicity on both MRC-5 and HepG2 cell lines. The data shown are the mean of three independent experiments, and the error bars represent \pm SD. Eight compound concentrations up to 100 μ M (solubility in medium was verified) were tested and MTT assays were performed after 24 hours.

3.3.3.2.9 Antibacterial Activities

All compounds were tested for their antibacterial activities against *E. coli* Δ tolC as a Gram-negative strain and *S. aureus* Newman as a Gram-positive strain. It was decided to quantify antibacterial activities as IC₉₀ values (i.e., concentrations for 90% growth inhibition) instead of MIC values (i.e., minimal inhibitory concentrations, usually obtained in series of two-fold dilutions) as this would enable a more precise quantification, in particular when moderate activities are also taken into account. Several compounds showed a moderate activity against *S. aureus*, including **46** with an IC₉₀ value of 40 μ M (Supporting Information, Table S1). In contrast, no activity was found against the growth of the *E. coli* Δ tolC strain, which is efflux-deficient due to a deletion in the gene encoding the TolC efflux pump. We hypothesized that the compounds' inactivity against Gram-negative bacteria might be owed to limited

cellular uptake. Due to the high stability of **46**, compound degradation in the bacterial cell could be excluded (*vide infra*).

Polymyxin B nonapeptide (PMBN) is a weak antibacterial agent that lacks bactericidal activity of its own, but is still able to bind to the LPS (lipopolysaccharide) of Gram-negative bacteria and sensitize them to hydrophobic moieties by permeabilizing the outer membrane of the bacteria.^{55,56} PMBN was added in the assays for antibacterial activity to test if the diminished activity of **46** against *E. coli* $\Delta tolC$ was due to limited cellular uptake. It was added in increasing concentrations up to 6 $\mu\text{g}/\text{mL}$ (significantly less than the concentrations often reported).^{55,56} Fosfomycin and ampicillin were included as controls to test their effect as established antibiotics that efficiently pass the outer membrane of *E. coli*. A drastic decrease in the IC_{90} value of **46** was observed that was dependent on the concentration of PMBN, reaching 2.3 μM at 6 $\mu\text{g}/\text{mL}$ of PMBN, a value ca. 3-fold lower than that determined for ampicillin under identical conditions ($\text{IC}_{90} = 6.8 \mu\text{M}$, Supporting Information, *Table S2*). We observed no significant changes in the IC_{90} values of both control antibiotics with increasing concentrations of PMBN, thus confirming that the improvement of the antibacterial activity of **46** was due to its enhanced entry into bacterial cells (*Figure 10*). This experiment also proved that **46** acted efficiently once it reached the interior of the cell. Poor penetration of the bacterial cell membrane might also be responsible for the low activity against *S. aureus* (cf. above). Some congeners that showed lower IC_{90} values at least with *S. aureus* (*Table S1*) seemed to indicate that modification of the ester function (**1**, **37** and **45**) could be crucial to enhance the cellular uptake in future optimization trials with the scaffold.

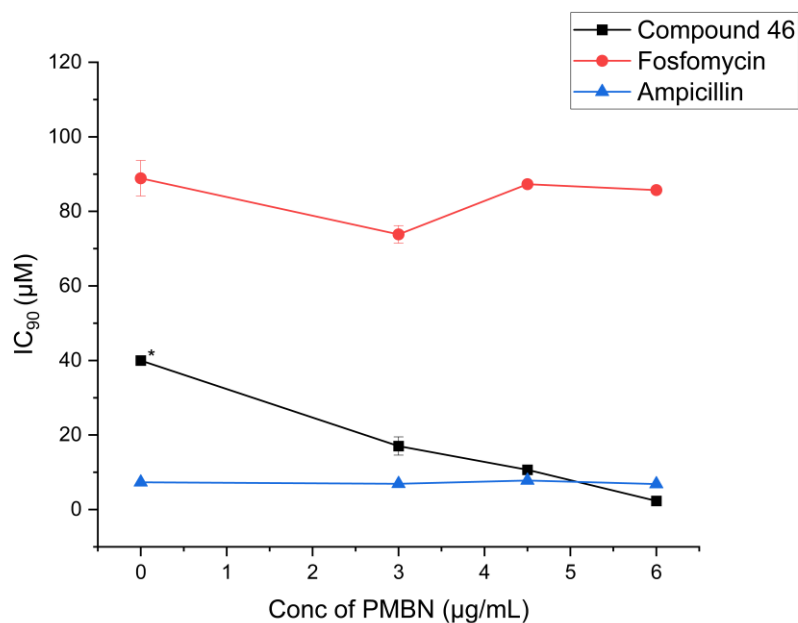


Figure 5. Antibacterial activities (IC₉₀ values) of **46**, fosfomycin, and ampicillin against *E. coli* $\Delta tolC$ in the presence of increasing PMBN concentrations (0, 3, 4.5, and 6 $\mu\text{g/mL}$). The data shown are the mean of two independent experiments, and the error bars represent \pm SD. *IC₉₀ for compound **46** at 0 $\mu\text{g/mL}$ PMBN was >40 μM .

3.3.3.2.10 Stability in Biological Media

The stability of MurA inhibitor **46** was assessed in human S9 liver microsomal fraction. As **46** contains a potentially labile ester function, we also tested the compound's stability in human plasma and in bacterial cell lysate (*E. coli* $\Delta tolC$). Compound **46** did not show any degradation after a two-hour incubation period with human S9 fraction, and neither after four hours in either human plasma or bacterial lysate (Table 7). It thus exhibited a pronounced stability in a variety of biological media.

Table 7. Stability of MurA inhibitor **46** in various biological media.^a

Cmpd	% degradation in S9 fraction ^b	t _{1/2} in S9 fraction (min)	% degradation in human plasma ^c	t _{1/2} in human plasma (min)	% degradation in bacterial lysate ^c	t _{1/2} in bacterial lysate (min)
46	0 ± 8	>120	0 ± 8	>240	0 ± 2%	>240
reference compound ^d	89 ± 10	5.9	100	20	-----	-----

^aThe data shown are the mean of two independent experiments, each performed in duplicates; ^bmeasured after 2 h; ^cmeasured after 4 h; ^dreference compound for the S9 fraction assay was testosterone, and tetracaine was used for the human plasma stability assay.

3.3.4 Conclusions

In this study, we report substituted pyrrolidinediones as a new class of inhibitors of the bacterial enzyme MurA. The overall most potent of these compounds was inhibitor **46** with an IC₅₀ value of 4.5 μM against wild type MurA. Remarkably, **46** inhibited the clinically relevant fosfomycin-resistant MurA mutant C115D with equal potency (IC₅₀ = 4.9 μM). Moreover, it showed an additive effect when tested with fosfomycin, suggesting that with optimized derivatives of **46**, a combination therapy might be conceivable.

The binding of **46** was demonstrated to occur only with the conformationally open form of MurA, unlocked by the presence of the substrate UNAG and rendering the active site accessible. The precise binding mode could not be robustly established due to significant challenges in the crystallography trial. However, based on native MS experiments and the additive inhibition with fosfomycin, it could be inferred that **46** binds in the absence of UNAG but in the presence of fosfomycin or inorganic phosphate. Furthermore, NMR spectroscopic data indicated that the binding of **46** occurs in a region adjacent to or partially overlapping with the region also targeted

by fosfomycin. However, there is no competition for the same binding pocket. The ability of compound **46** to still bind and inhibit the MurA C115D mutant rules out any direct interaction of **46** with the covalent binding partner of fosfomycin, cysteine-115. The reported novel MurA inhibitors were not optimized for uptake into bacterial cells yet, but at least for some compounds we found growth inhibition of *S. aureus* with IC₉₀ values ranging from 18 to 40 μ M. Apart from that, the new class of MurA inhibitors fulfilled other important requirements for antibiotics: It showed no toxicity against human cell lines, as exemplified at least by compounds **7** and **46**. Moreover, Compound **46** was found to be highly stable in human plasma, human liver microsomes (S9 fraction) and bacterial cell lysate. Altogether, we provided evidence that the newly discovered substituted pyrrolidinediones are promising candidates for further development as MurA inhibitors with potential antibacterial activity.

3.3.5 Supporting Information

The Supporting Information can be found in Appendix section **7.6**

Molecular Formula Strings, biological activities and purities (.csv); PDB file of the docking model of **46** with MurA; antibacterial activities of the pyrrolidinediones (Tables S1 and S2); different conformational states of MurA (Figure S1); native MS results (Figure S2); additional ¹⁵N-¹H TROSY HSQC spectra of WT and C115D MurA and overlays (Figures S3-S5); superimposition of the docking model of **46** + UNAG in the co-crystal structure of *E. coli* MurA (Figure S6); UPLC-MS chromatograms, ¹H and ¹³C NMR spectra of representative compounds (Figures S7-S15).

3.3.6 Abbreviations Used

Biph, biphenyl; BME, beta-mercaptoethanol; CC, column chromatography; CSP, chemical shift perturbation; DI-FTICR, direct infusion Fourier transform ion cyclotron

resonance; DMEM, Dulbecco's Modified Eagle Medium; *E. coli*, *Escherichia coli*; GSH, glutathione; IPTG, isopropyl β -D-1-thiogalactopyranoside; LB, lysogeny broth; MeOH, methanol; MTT, 3-(4,5-dimethylthiazol-2-yl)-2,5-diphenyltetrazolium bromide; n.d., not determined; Pa, pascal; PEP, phosphoenolpyruvate; Pi, inorganic phosphate; PMBN, polymyxin B nonapeptide; PVA, polyvinyl alcohol; *S. aureus*, *Staphylococcus aureus*; SD, standard deviation; STEC, shiga toxin-producing *E. coli*; *M. tuberculosis*, *Mycobacterium tuberculosis*; TROSY, Transverse relaxation-optimized spectroscopy; UNAG, UPD-*N*-acetyl glucoseamine; UNAGEP, UPD-*N*-acetyl glucoseamine enolpyruvate; UNAM, UPD-*N*-acetyl muramic acid; vs., versus.

3.3.7 References

- (1) Ventola, C. L. The Antibiotic Resistance Crisis: Part 1: Causes and Threats. *Pharm. Ther.* **2015**, *40* (4), 277–283. <https://doi.org/Article>.
- (2) Gould, I. M.; Bal, A. M.; Gould, I. M.; Bal, A. M. New Antibiotic Agents in the Pipeline and How They Can Help Overcome Microbial Resistance New Antibiotic Agents in the Pipeline and How They Can Help Overcome Microbial Resistance. *Virulence* **2015**, *5594*, 185–191. <https://doi.org/10.4161/viru.22507>.
- (3) Cascioferro, S.; Parrino, B.; Carbone, D.; Pecoraro, C.; Diana, P. Novel Strategies in the War against Antibiotic Resistance. *Future Med. Chem.*, 2021, *13* (6), 529–531. <https://doi.org/10.4155/fmc-2021-0009>.
- (4) Parrino, B.; Carbone, D.; Cirrincione, G.; Diana, P.; Cascioferro, S. Inhibitors of Antibiotic Resistance Mechanisms: Clinical Applications and Future Perspectives. *Future Med. Chem.* 2020, *12* (5), 357–359. <https://doi.org/10.4155/fmc-2019-0326>.
- (5) Sapkota, M.; Marreddy, R. K. R.; Wu, X.; Kumar, M.; Hurdle, J. G. The Early Stage Peptidoglycan Biosynthesis Mur Enzymes Are Antibacterial and Antisporulation Drug Targets for Recurrent *Clostridioides Difficile* Infection. *Anaerobe* **2020**, *61*, 102129. <https://doi.org/10.1016/j.anaerobe.2019.102129>.

- (6) Yang, Y.; Severin, A.; Chopra, R.; Singh, G.; Hu, W.; Keeney, D.; Svenson, K.; Petersen, P. J.; Labthavikul, P.; Shlaes, D. M.; Rasmussen, B. A.; Failli, A. A.; Shumsky, S.; Kutterer, K. M. K.; Gilbert, A.; Mansour, T. S.; Krishnamurthy, G.; Shumsky, J. S. 3, 5-Dioxopyrazolidines, Novel Inhibitors of UDP- N - Acetylenolpyruvylglucosamine Reductase (MurB) with Activity against Gram-Positive Bacteria. *Antimicrob. Agents Chemother.* **2006**, *50* (2), 556–564. <https://doi.org/10.1128/AAC.50.2.556>.
- (7) Bugg, T. D.; Braddick, D.; Dowson, C. G.; Roper, D. I. Bacterial Cell Wall Assembly: Still an Attractive Antibacterial Target. *Trends Biotechnol.* **2011**, *29* (4), 167–173. <https://doi.org/10.1016/j.tibtech.2010.12.006>.
- (8) Reddy, S. G.; Waddell, S. T.; Kuo, D. W.; Wong, K. K.; Pompliano, D. L. Preparative Enzymatic Synthesis and Characterization of the Cytoplasmic Intermediates of Murein Biosynthesis. *J. Am. Chem. Soc.* **1999**, *121* (6), 1175–1178. <https://doi.org/10.1021/ja983850b>.
- (9) el Zoeiby, A.; Sanschagrín, F.; Levesque, R. C. Structure and Function of the Mur Enzymes: Development of Novel Inhibitors. *Mol. Microbiol.* **2003**, *47* (1), 1–12. <https://doi.org/10.1046/j.1365-2958.2003.03289.x>.
- (10) Hrast, M.; Sosič, I.; Šink, R.; Gobec, S. Inhibitors of the Peptidoglycan Biosynthesis Enzymes MurA-F. *Bioorg. Chem.* **2014**, *55*, 2–15. <https://doi.org/10.1016/j.bioorg.2014.03.008>.
- (11) Messaoudi, A.; Zoghlami, M.; Basharat, Z.; Sadfi-Zouaoui, N. Identification of a Potential Inhibitor Targeting MurC Ligase of the Drug Resistant Pseudomonas Aeruginosa Strain through Structure-Based Virtual Screening Approach and In Vitro Assay. *Curr. Pharm. Biotechnol.* **2019**, *20* (14), 1203–1212. <https://doi.org/10.2174/1389201020666190719123133>.
- (12) Kong, K. F.; Schneper, L.; Mathee, K. Beta-Lactam Antibiotics: From Antibiosis to Resistance and Bacteriology. *APMIS.* **2010**, *118* (1), 1–36. <https://doi.org/10.1111/j.1600-0463.2009.02563.x>.
- (13) Gautam, A.; Vyas, R.; Tewari, R. Peptidoglycan Biosynthesis Machinery: A Rich Source of Drug Targets. *Crit. Rev. Biotechnol.* **2011**, *31* (4), 295–336. <https://doi.org/10.3109/07388551.2010.525498>.

- (14) Lovering, A. L.; Safadi, S. S.; Strynadka, N. C. J. Structural Perspective of Peptidoglycan Biosynthesis and Assembly. *Annu. Rev. Biochem.* **2012**, *81* (1), 451–478. <https://doi.org/10.1146/annurev-biochem-061809-112742>.
- (15) Brown, E. D.; Vivas, E. I.; Walsh, C. T.; Kolter, R. MurA (MurZ), the Enzyme That Catalyzes the First Committed Step in Peptidoglycan Biosynthesis, Is Essential in *Escherichia Coli*. *J. Bacteriol.* **1995**, *177* (14), 4194–4197. <https://doi.org/10.1128/jb.177.14.4194-4197.1995>.
- (16) Du, W.; Brown, J. R.; Sylvester, D. R.; Huang, J.; Chalker, A. F.; So, C. Y.; Holmes, D. J.; Payne, D. J.; Wallis, N. G. Two Active Forms of UDP-N-Acetylglucosamine Enolpyruvyl Transferase in Gram-Positive Bacteria. *J. Bacteriol.* **2000**, *182* (15), 4146–4152. <https://doi.org/10.1128/JB.182.15.4146-4152.2000>.
- (17) Kahan, F. M.; Kahan, J. S.; Cassidy, P. J.; Kropp, H. The Mechanism of Action of Fosfomycin (Phosphonomycin). *Ann. N. Y. Acad. Sci.* **1974**, *235* (1), 364–385. <https://doi.org/https://doi.org/10.1111/j.1749-6632.1974.tb43277.x>.
- (18) Falagas, M. E.; Giannopoulou, K. P.; Kokolakis, G. N.; Rafailidis, P. I. Fosfomycin: Use beyond Urinary Tract and Gastrointestinal Infections. *Clin. Infect. Dis.* **2008**, *46* (7), 1069–1077. <https://doi.org/https://doi.org/10.1086/527442>.
- (19) Silver, L. L. Fosfomycin: Mechanism and Resistance. *Cold Spring Harb. Perspect. Med.* **2017**, *7* (2), 1–11. <https://doi.org/10.1101/cshperspect.a025262>.
- (20) Chang, C. M.; Chern, J.; Chen, M. Y.; Huang, K. F.; Chen, C. H.; Yang, Y. L.; Wu, S. H. Avenaciolides: Potential MurA-Targeted Inhibitors against Peptidoglycan Biosynthesis in Methicillin-Resistant *Staphylococcus Aureus* (MRSA). *J. Am. Chem. Soc.* **2015**, *137* (1), 267–275. <https://doi.org/10.1021/ja510375f>.
- (21) Marquardt, J. L.; Brown, E. D.; Walsh, C. T.; Lane, W. S.; Haley, T. M.; Ichikawa, Y.; Wong, C. H.; Walsh, C. T. Kinetics, Stoichiometry, and Identification of the Reactive Thiolate in the Inactivation of UDP-GlcNAc Enolpyruvoyl Transferase by the Antibiotic Fosfomycin. *Biochemistry* **1994**, *33* (35), 10646–10651. <https://doi.org/10.1021/bi00201a011>.
- (22) Wanke, C.; Amrhein, N. Evidence That the Reaction of the UDP-N-acetylglucosamine 1-carboxyvinyltransferase Proceeds through the O-phosphothioketal of Pyruvic Acid Bound to Cys115 of the Enzyme. *Eur. J. Biochem.* **1993**, *218* (3), 861–870. <https://doi.org/10.1111/j.1432-1033.1993.tb18442.x>.

- (23) Suarez, J. E.; Mendoza, M. C. Plasmid-Encoded Fosfomycin Resistance. *Antimicrob. Agents Chemother.* **1991**, *35* (5), 791–795. <https://doi.org/10.1128/AAC.35.5.791>.
- (24) Arca, P.; Reguera, G.; Hardisson, C. Plasmid-Encoded Fosfomycin Resistance in Bacteria Isolated from the Urinary Tract in a Multicentre Survey. *J. Antimicrob. Chemother.* **1997**, *40* (3), 393–399. <https://doi.org/10.1093/jac/40.3.393>.
- (25) Arca, P.; Hardisson, C.; Suarez, J. E. Purification of a Glutathione S-Transferase That Mediates Fosfomycin Resistance in Bacteria. *Antimicrob. Agents Chemother.* **1990**, *34* (5), 844–848. <https://doi.org/10.1128/AAC.34.5.844>.
- (26) Bernat, B. A.; Timothy Laughlin, L.; Armstrong, R. N. Fosfomycin Resistance Protein (FosA) Is a Manganese Metalloglutathione Transferase Related to Glyoxalase I and the Extradiol Dioxygenases. *Biochemistry* **1997**, *36* (11), 3050–3055. <https://doi.org/10.1021/bi963172a>.
- (27) Horii, T.; Kimura, T.; Sato, K.; Shibayama, K.; Ohta, M. Emergence of Fosfomycin-Resistant Isolates of Shiga-like Toxin-Producing Escherichia Coli O26. *Antimicrob. Agents Chemother.* **1999**, *43* (4), 789–793. <https://doi.org/10.1128/aac.43.4.789>.
- (28) Marquardt, J. L.; Siegele, D. A.; Kolter, R.; Walsh, C. T. Cloning and Sequencing of Escherichia Coli MurZ and Purification of Its Product, a UDP-N-Acetylglucosamine Enolpyruvyl Transferase. *J. Bacteriol.* **1992**, *174* (17), 5748–5752. <https://doi.org/10.1128/jb.174.17.5748-5752.1992>.
- (29) De Smet, K. A. L.; Kempell, K. E.; Gallagher, A.; Duncan, K.; Young, D. B. Alteration of a Single Amino Acid Residue Reverses Fosfomycin Resistance of Recombinant MurA from Mycobacterium Tuberculosis. *Microbiology* **1999**, *145* (11), 3177–3184. <https://doi.org/10.1099/00221287-145-11-3177>.
- (30) Kim, D. H.; Lees, W. J.; Kempell, K. E.; Lane, W. S.; Duncan, K.; Walsh, C. T. Characterization of a Cys115 to Asp Substitution in the Escherichia Coli Cell Wall Biosynthetic Enzyme UDP-GlcNAc Enolpyruvyl Transferase (MurA) That Confers Resistance to Inactivation by the Antibiotic Fosfomycin. *Biochemistry* **1996**, *35* (15), 4923–4928. <https://doi.org/10.1021/bi952937w>.
- (31) Mendgen, T.; Scholz, T.; Klein, C. D. Structure-Activity Relationships of Tulipalines, Tuliposides, and Related Compounds as Inhibitors of MurA. *Bioorg.*

- Med. Chem. Lett.* **2010**, *20* (19), 5757–5762.
<https://doi.org/10.1016/j.bmcl.2010.07.139>.
- (32) Bachelier, A.; Mayer, R.; Klein, C. D. Sesquiterpene Lactones Are Potent and Irreversible Inhibitors of the Antibacterial Target Enzyme MurA. *Bioorg. Med. Chem. Lett.* **2006**, *16* (21), 5605–5609.
<https://doi.org/10.1016/j.bmcl.2006.08.021>.
- (33) Steinbach, A.; Scheidig, A. J.; Klein, C. D. The Unusual Binding Mode of Cnicin to the Antibacterial Target Enzyme MurA Revealed by X-Ray Crystallography. *J. Med. Chem.* **2008**, *51* (16), 5143–5147. <https://doi.org/10.1021/jm800609p>.
- (34) Baum, E. Z.; Montenegro, D. A.; Licata, L.; Turchi, I.; Webb, G. C.; Foleno, B. D.; Bush, K.; Turchi, I. Identification and Characterization of New Inhibitors of the Escherichia Coli MurA Enzyme. *Antimicrob. Agents Chemother.* **2001**, *45* (11), 3182–3188. <https://doi.org/10.1128/AAC.45.11.3182-3188.2001>.
- (35) Jin, B. S.; Han, S. G.; Lee, W. K.; Ryoo, S. W.; Lee, S. J.; Suh, S. W.; Yu, Y. G. Inhibitory Mechanism of Novel Inhibitors of UDP-N-Acetylglucosamine Enolpyruvyl Transferase from Haemophilus Influenzae. *J. Microbiol. Biotechnol.* **2009**, *19* (12), 1582–1589. <https://doi.org/10.4014/jmb.0905.05036>.
- (36) Sangshetti, J. N.; Joshi, S. S.; Patil, R. H.; Moloney, M. G.; Shinde, D. B. Mur Ligase Inhibitors as Anti-Bacterials: A Comprehensive Review. *Curr. Pharm. Des.* **2017**, *23* (21), 3164–3196.
<https://doi.org/10.2174/1381612823666170214115048>.
- (37) Baum, E. Z.; Montenegro, D. A.; Licata, L.; Turchi, I.; Webb, G. C.; Foleno, B. D.; Bush, K. Identification and Characterization of New Inhibitors of the Escherichia Coli MurA Enzyme. *Antimicrob. Agents Chemother.* **2001**, *45* (11), 3182–3188. <https://doi.org/10.1128/AAC.45.11.3182-3188.2001>.
- (38) Zoeiby, A. El; Beaumont, M.; Dubuc, E.; Sanschagrín, F.; Voyer, N.; Levesque, R. C. Combinatorial Enzymatic Assay for the Screening of a New Class of Bacterial Cell Wall Inhibitors. *Bioorg. Med. Chem.* **2003**, *11* (7), 1583–1592.
[https://doi.org/10.1016/S0968-0896\(02\)00447-9](https://doi.org/10.1016/S0968-0896(02)00447-9).
- (39) McGivan, J. D.; Chappell, J. B. Avenaciolide: A Specific Inhibitor of Glutamate Transport in Rat Liver Mitochondria. *Biochem. J.* **1970**, *116* (4), 37–38.
<https://doi.org/10.1042/bj1160037Pb>.

- (40) Frisvad, J. C.; Møller, L. L. H.; Larsen, T. O.; Kumar, R.; Arnau, J. Safety of the Fungal Workhorses of Industrial Biotechnology: Update on the Mycotoxin and Secondary Metabolite Potential of *Aspergillus Niger*, *Aspergillus Oryzae*, and *Trichoderma Reesei*. *Appl. Microbiol. Biotechnol.* **2018**, *102* (22), 9481–9515. <https://doi.org/10.1007/s00253-018-9354-1>.
- (41) Varga, J.; Frisvad, J. C.; Samson, R. A. Two New Aflatoxin Producing Species, and an Overview of *Aspergillus* Section *Flavi*. *Stud. Mycol.* **2011**, *69*, 57–80. <https://doi.org/10.3114/sim.2011.69.05>.
- (42) Miller, K.; Dunsmore, C. J.; Leeds, J. A.; Patching, S. G.; Sachdeva, M.; Blake, K. L.; Stubbings, W. J.; Simmons, K. J.; Henderson, P. J. F.; de Los Angeles, J.; Fishwick, C. W. G.; Chopra, I. Benzothioxalone Derivatives as Novel Inhibitors of UDP-N-Acetylglucosamine Enolpyruvyl Transferases (MurA and MurZ). *J. Antimicrob. Chemother.* **2010**, *65* (12), 2566–2573. <https://doi.org/10.1093/jac/dkq349>.
- (43) Gilbert, A. M.; Failli, A.; Shumsky, J.; Yang, Y.; Severin, A.; Singh, G.; Hu, W.; Keeney, D.; Petersen, P. J.; Katz, A. H. Pyrazolidine-3,5-Diones and 5-Hydroxy-1*H*-Pyrazol-3(2*H*)-Ones, Inhibitors of UDP- *N* -Acetylenolpyruvyl Glucosamine Reductase. *J. Med. Chem.* **2006**, *49* (20), 6027–6036. <https://doi.org/10.1021/jm060499t>.
- (44) Kutterer, K. M.; Davis, J. M.; Singh, G.; Yang, Y.; Hu, W.; Severin, A.; Rasmussen, B. A.; Krishnamurthy, G.; Failli, A.; Katz, A. H. 4-Alkyl and 4,4'-Dialkyl 1,2-Bis(4-Chlorophenyl)Pyrazolidine-3,5-Dione Derivatives as New Inhibitors of Bacterial Cell Wall Biosynthesis. *Bioorg. Med. Chem. Lett.* **2005**, *15* (10), 2527–2531. [https://doi.org/S0960-894X\(05\)00364-1](https://doi.org/S0960-894X(05)00364-1) [pii]\r10.1016/j.bmcl.2005.03.058.
- (45) Mokbel, S. A.; Fathalla, R. K.; El-Sharkawy, L. Y.; Abadi, A. H.; Engel, M.; Abdel-Halim, M. Synthesis of Novel 1,2-Diarylpyrazolidin-3-One-Based Compounds and Their Evaluation as Broad Spectrum Antibacterial Agents. *Bioorg. Chem.* **2020**, *99*, 1–12. <https://doi.org/10.1016/j.bioorg.2020.103759>.
- (46) Arencibia, J. M.; Fröhner, W.; Krupa, M.; Pastor-Flores, D.; Merker, P.; Oellerich, T.; Neimanis, S.; Schmithals, C.; Köberle, V.; Süß, E.; Zeuzem, S.; Stark, H.; Piiper, A.; Odadzic, D.; Schulze, J. O.; Biondi, R. M. An Allosteric Inhibitor Scaffold Targeting the PIF-Pocket of Atypical Protein Kinase C Isoforms. *ACS Chem. Biol.* **2017**, *12* (2), 564–573. <https://doi.org/10.1021/acscchembio.6b00827>.

- (47) Schiff, R.; Bertini, C. Synthese Substituierter Bihydrobiketopyrrolcarbonsäureester Mittels Oxalessigester Und Aldehydoaminbasen. *Ber. Dtsch. Chem. Ges.* **1897**, *30* (1), 601–604.
- (48) Merchant, R.; Srtnivasan, V. Heterocyclic Compounds IV: Synthesis and Reactions of Some 2,3-Pyrrolidinedione Derivatives. *Rec. Trav. Chim. Pays Bas* **1962**, *81* (2), 144–155. <https://doi.org/10.1002/recl.19620810209>.
- (49) Lanzetta, P. A.; Alvarez, L. J.; Reinach, P. S.; Candia, O. A. An Improved Assay for Nanomole Amounts of Inorganic Phosphate. *Analytical Biochemistry* **1979**, *100* (1), 95–97. [https://doi.org/10.1016/0003-2697\(79\)90115-5](https://doi.org/10.1016/0003-2697(79)90115-5).
- (50) Stephanopoulos, G. N.; Aristidou, A. A.; Nielsen, J. Regulation of Metabolic Pathways. *Metab. Eng.* **1998**, 147–202. <https://doi.org/10.1016/B978-012666260-3/50006-6>.
- (51) Zhu, J. Y.; Yang, Y.; Han, H.; Betzi, S.; Olesen, S. H.; Marsilio, F.; Schönbrunn, E. Functional Consequence of Covalent Reaction of Phosphoenolpyruvate with UDP-N-Acetylglucosamine 1-Carboxyvinyltransferase (MurA). *J. Biol. Chem.* **2012**, *287* (16), 12657–12667. <https://doi.org/10.1074/jbc.M112.342725>.
- (52) Mizyed, S.; Oddone, A.; Byczynski, B.; Hughes, D. W.; Berti, P. J. UDP-N-Acetylmuramic Acid (UDP-MurNAc) Is a Potent Inhibitor of MurA (Enolpyruvyl-UDP-GlcNAc Synthase). *Biochemistry* **2005**, *44* (10), 4011–4017. <https://doi.org/10.1021/bi047704w>.
- (53) Heck, A. J. R. Native Mass Spectrometry: A Bridge between Interactomics and Structural Biology. *Nat. Methods* **2008**, *5* (11), 927–933. <https://doi.org/10.1038/nmeth.1265>.
- (54) Skarzynski, T.; Mistry, A.; Wonacott, A.; Hutchinson, S. E.; Kelly, V. a; Duncan, K. Structure of UDP-N-Acetylglucosamine Enolpyruvyl Transferase, an Enzyme Essential for the Synthesis of Bacterial Peptidoglycan, Complexed with Substrate UDP-N-Acetylglucosamine and the Drug Fosfomycin. *Structure* **1996**, *4* (12), 1465–1474. [https://doi.org/10.1016/S0969-2126\(96\)00153-0](https://doi.org/10.1016/S0969-2126(96)00153-0).
- (55) Ofek, I.; Cohen, S.; Rahmani, R.; Kabha, K.; Tamarkin, D.; Herzig, Y.; Rubinstein, E. Antibacterial Synergism of Polymyxin B Nonapeptide and Hydrophobic Antibiotics in Experimental Gram-Negative Infections in Mice. *Antimicrob. Agents Chemother.* **1994**, *38* (2), 374–377. <https://doi.org/10.1128/AAC.38.2.374>.

- (56) Tsubery, H.; Ofek, I.; Cohen, S.; Fridkin, M. Structure - Function Studies of Polymyxin B Nonapeptide: Implications to Sensitization of Gram-Negative Bacteria. *J. Med. Chem.* **2000**, *43* (16), 3085–3092. <https://doi.org/10.1021/jm0000057>.
- (57) Jöst, C.; Nitsche, C.; Scholz, T.; Roux, L.; Klein, C. D. Promiscuity and Selectivity in Covalent Enzyme Inhibition: A Systematic Study of Electrophilic Fragments. *J. Med. Chem.* **2014**, *57* (18), 7590–7599. <https://doi.org/10.1021/jm5006918>.
- (58) Vranken, W. F.; Boucher, W.; Stevens, T. J.; Fogh, R. H.; Pajon, A.; Llinas, M.; Ulrich, E. L.; Markley, J. L.; Ionides, J.; Laue, E. D. The CCPN Data Model for NMR Spectroscopy: Development of a Software Pipeline. *Proteins* **2005**, *59* (4), 687–696. <https://doi.org/10.1002/prot.20449>.
- (59) Spork, A. P.; Büschleb, M.; Ries, O.; Wiegmann, D.; Boettcher, S.; Mihalyi, A.; Bugg, T. D. H.; Ducho, C. Lead Structures for New Antibacterials: Stereocontrolled Synthesis of a Bioactive Muraymycin Analogue. *Chem. Eur. J.* **2014**, *20* (47), 15292–15297. <https://doi.org/10.1002/chem.201404775>.
- (60) Gargano, E. M.; Perspicace, E.; Hanke, N.; Carotti, A.; Marchais-Oberwinkler, S.; Hartmann, R. W. Metabolic Stability Optimization and Metabolite Identification of 2,5-Thiophene Amide 17 β -Hydroxysteroid Dehydrogenase Type 2 Inhibitors. *Eur. J. Med. Chem.* **2014**, *87*, 203–219. <https://doi.org/10.1016/j.ejmech.2014.09.061>.

3.4 Targeting the Binding Pocket of the Fluorescent dye 8-Anilino-naphthalene-1-sulfonic acid (ANS) in MurA Holds Potential for the Development of Novel Broad-spectrum Antibiotic Agents

This part of the thesis has been prepared for publication and will be submitted to *Eur. J. Med. Chem.*

The contributions of each author to this chapter are listed below:

Reem K. Fathalla: She performed the initial fluorescence binding assays and was involved in picking the compounds in the screenings. She planned and executed all the biological assays including all the cloning experiments and the enzyme expressions, as well as all the inhibition tests and fluorescence binding assays. She prepared all the corresponding figures in this part and conceived and wrote the text.

Matthias Engel: He was co-responsible for the project design, and practical troubleshooting. He reviewed and edited the work.

Christian Ducho: He was co-responsible for the project design, supervision and administration. He reviewed and edited the work.

3.4.1 Abstract

8-Anilinoanthracene-1-sulfonic acid (ANS) has been extensively used as a fluorescent probe to detect conformational changes of proteins. It has been co-crystallized with several of the proteins it is used to monitor, including the bacterial cell wall synthesis enzyme MurA, which catalyzes the first committed step of peptidoglycan biosynthesis, converting UDP-*N*-acetylglucosamine (UDP-GlcNAc) into enolpyruvyl UDP-GlcNAc. It has been reported before that ANS binds to MurA from *E. cloacae* without inhibiting the enzyme's activity up to a concentration of 1 mM ANS. In this study, we present evidence that ANS inhibits the activity of several isoforms of MurA with IC₅₀ values of 18, 22, and 31 μM against wild-type (WT) *E. coli*, C115D *E. coli*, and *E. cloacae* MurA, respectively. This prompted us to test a larger series of structural analogues of ANS for the inhibition of these MurA enzymes, which led to the discovery of compound **26**. This ANS analogue showed enhanced inhibition of MurA (WT and C115D MurA from *E. coli*, and *E. cloacae* MurA) with IC₅₀ values of 2.7, 10, and 14 μM, respectively. Based on our results, the ANS binding pocket was identified as a novel target site for the development of potential antibiotics.

Keywords: ANS, MurA, peptidoglycan biosynthesis, sulfonic acids, fluorescence binding assay, ligand efficiency.

Abbreviations: ANS, 8-anilinoanthracene-1-sulfonic acid; bp, base pair; DTT, dithiothreitol; *E. cloacae*, *Enterobacter cloacae*; *E. coli*, *Escherichia coli*; EDTA, ethylenediaminetetraacetic acid; GSH, glutathione; kb, kilo base; LB, lysogeny broth; OD, optical density; PDB, protein data bank; PEP, phosphoenolpyruvate; P_i, inorganic phosphate; rpm, rotations per minute; SAR, structure-activity relationship; *S. aureus*, *Staphylococcus aureus*; TAE, Tris-acetate EDTA; UDP-GlcNAc, UDP-*N*-acetylglucosamine; UDP-MurNAc, UDP-*N*-acetylmuramic acid; WT, wild type.

3.4.2 Introduction

The fluorescent dye 8-anilinonaphthalene-1-sulfonic acid (ANS, *Figure 1*) has historically been used as a probe to monitor various proteins, as it shows little to no fluorescence in aqueous environment, but the fluorescence is greatly enhanced with a green-to-blue shift when the compound is bound to proteins [1–3]. ANS is able to bind to the hydrophobic pockets of proteins to detect molten globules, ligand binding, non-polar patches on the surface of proteins, protein aggregation, and general conformational changes [4–10]. Its binding to proteins has been attributed to its ability to form hydrophobic interactions through its anilinonaphthalene core in addition to binding to the cationic side chains of proteins via its sulfonic acid moiety [4,10,11]. The binding affinities are usually low though, with reported K_d values ranging from 37 μM (CDK2) to 83 μM (bovine serum albumin) [12,13]. Nevertheless, several X-ray crystal structures of ANS in complex with a number of proteins are available, such as S100A7 [14], human heart fatty acid binding protein [15], CDK2 [13], and Ppm1p [16], in addition to the reported complex of ANS with the bacterial cell wall synthesis enzyme MurA [3].

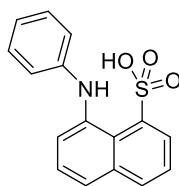


Figure 1. ANS structure

MurA is the first enzyme in the bacterial peptidoglycan biosynthesis pathway. It catalyzes the transfer of an enolpyruvate moiety from phosphoenolpyruvate (PEP) to UDP-*N*-acetylglucosamine (UDP-GlcNAc) (*Figure 2*) [3,17–19]. Heterologously overexpressed MurA is usually isolated in a closed conformation with a PEP molecule

covalently bound to the Cys115 residue and having UDP-*N*-acetylmuramic acid (UDP-MurNAc) non-covalently bound to its active site. UDP-MurNAc is the product of the MurB-catalyzed reaction, i.e., the next step in peptidoglycan biosynthesis after the MurA-mediated transformation [19–24]. This closed conformation is extremely robust to dilution and most commonly used salts in protein purification and crystallization. However, it can be unlocked using the natural MurA substrate UDP-GlcNAc or the side product of the enzymatic reaction, inorganic phosphate (P_i) [20].

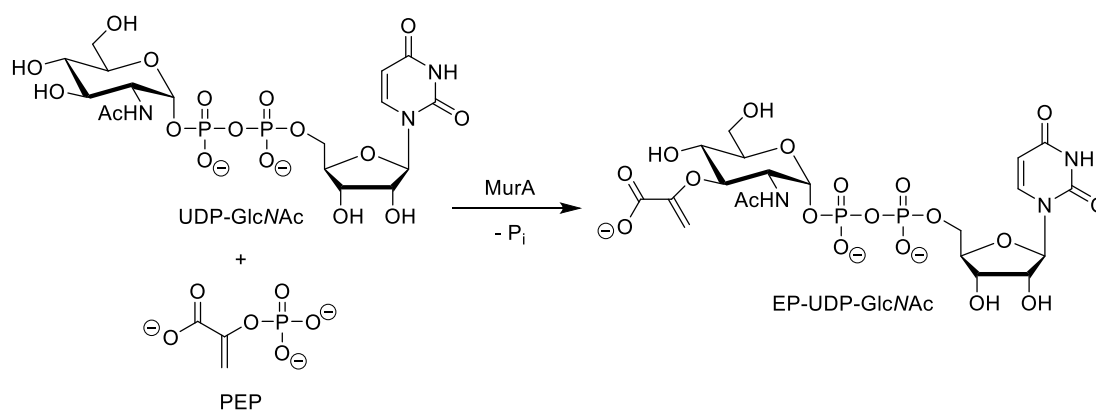


Figure 2. MurA catalytic reaction

Fosfomicin (compound I, *Figure 3*) is the only clinically used antibiotic targeting MurA [25,26]. It inactivates the enzyme by irreversibly binding to the catalytically important Cys115 residue [17,27,28]. However, emerging fosfomicin resistance among clinical isolates from diverse bacterial pathogens has been reported [29–33]. The naturally occurring C115D MurA mutant present in *Mycobacteria* is resistant to inhibition by fosfomicin [22]. Other mechanisms of fosfomicin resistance include decreased uptake [33,34], enzymatic modification of the antibiotic [35,36], and finally, MurA overexpression [37,38]. There is a variety of previously reported MurA inhibitors such as the sesquiterpene lactone derivative cnicin [39,40], aminotetralones [41], benzothioxalone derivatives [42], bromonitrovinylfuran [43],

and avenaciolides [44] (Compounds II-VI, respectively, *Figure 3*). These inhibitors, while often potent towards MurA to a significant extent, show a multitude of limitations that hamper their development into viable drug candidates. These shortcomings include resistance of the C115D MurA mutant (for compounds II-IV) [40-42], non-specific target inhibition and thus cellular toxicity (compounds V and VI) [43,45], and general interaction with thiols in proteins or compounds such as glutathione (GSH) and dithiothreitol (DTT) (compounds IV and V) [42,43].

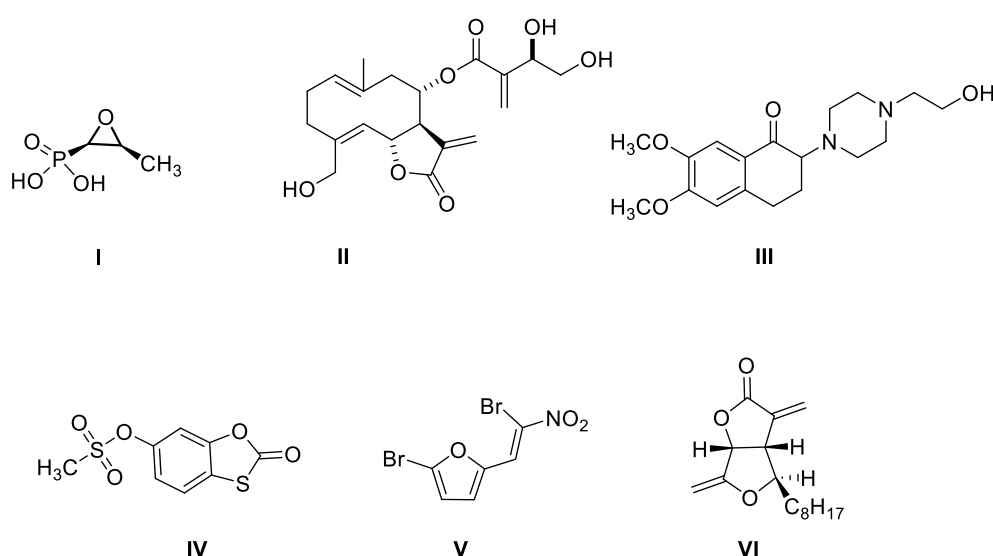


Figure 3. MurA inhibitors

ANS has been used as a fluorescent probe to monitor the conformational changes that occur during binding events of MurA using a corresponding binding assay [24,46,47]. These experiments have been mainly performed using *Enterobacter cloacae* MurA, for which it was reported that ANS did not show any inhibition of the bacterial enzyme up to a 1 mM concentration [47]. An X-ray co-crystal structure of *E. cloacae* MurA bound to ANS is available (PDB code 1EYN), showing that the anilinonaphthalene core is engaged in interactions with Arg91, Pro112, and Gly113, while the sulfonic acid moiety forms an H-bond to Gly113 and captures the active site loop residue Arg120 through a salt bridge (*Figure 4*) [3]. In the enzyme-substrate complex, both Arg91 and

Arg120 interact with the diphosphate bridge of the substrate UDP-GlcNAc [19], and Arg120 has further roles in the catalytic mechanism [20]. We therefore hypothesized that binding of ANS might stabilize an inactive conformation of MurA that would be incapable of substrate binding and catalyzing the enolpyruvate transfer.

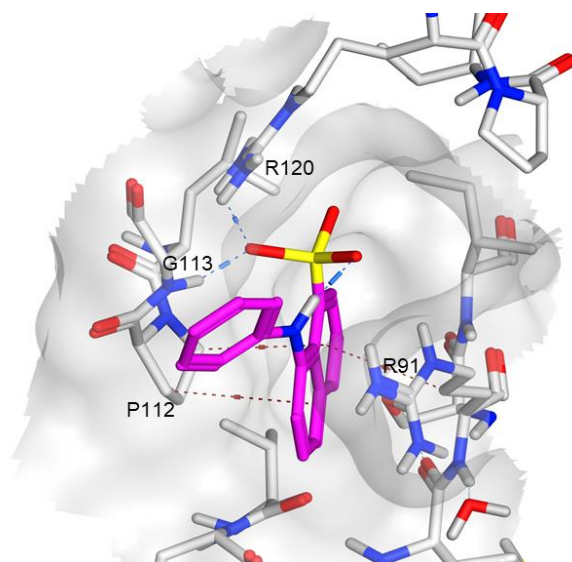


Figure 4. Structural representation of the binding of ANS (violet sticks) to its binding pocket in MurA based on the published cocrystal structure 1EYN [3]. The figure shows CH- π interactions (in brown) between the aminonaphthalene core and the three residues; Arg91, Pro112, and Gly113. It also shows the electrostatic interactions of the sulfonic acid moiety (marked in blue) where it forms a H bond with Gly113, as well as the salt bridge with Arg120

In this work, we report that ANS and some ANS-derived naphthyl sulfonic acids actually showed inhibition of wild type (WT) and C115D *E. coli* MurA, in addition to *E. cloacae* MurA. The small size of these inhibitors affords them remarkable ligand efficiency, and their facile availability allowed us to efficiently explore their structure-activity relationship (SAR).

3.4.3 Results and Discussion

All the initially tested compounds were commercially available, simplified derivatives of ANS lacking the *N*-phenyl group, i.e., in most cases possessing both the sulfonic acid

group and another functionality on the naphthalene ring. We started by studying benzene **1** and naphthalene sulfonic acids **2,3** as well as naphthalene acetic acid **4** in addition to several naphthols **5-9** (*Table 1*). The next step was to explore 1-naphthalene sulfonic acids with an amino group at different positions on the naphthalene ring (**10-14**, *Table 2*). Moreover, replacing the amino group with a hydroxy group was also studied (**15,16**, *Table 2*). Finally, the effect of two sulfonic acid groups on the naphthalene ring in addition to amino and/or hydroxy groups was evaluated (**20-27**, *Table 3*).

3.4.3.1 Biological Evaluation

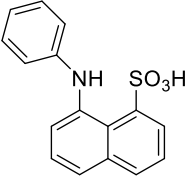
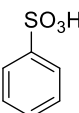
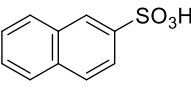
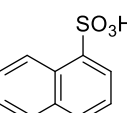
3.4.3.1.1 Initial Compound Selection and MurA Inhibition.

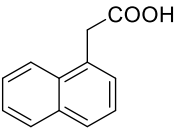
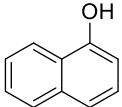
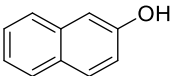
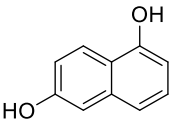
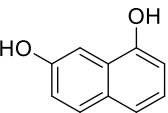
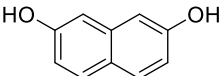
ANS was initially tested as an inhibitor of WT *E. coli*, against which it showed 91% inhibition at 100 μM . It also exhibited 83% and 97% inhibition against C115D *E. coli* and *E. cloacae* MurA, respectively. We initially tested small fragments **1-9** based on the structural features of ANS. They were either substructures of the parent compound, had the acidic functions at different positions, or possessed hydroxyl groups as hydrogen bond donor/acceptor combinations. These selected compounds were also first tested against WT *E. coli* MurA at 100 μM . Subsequently, for compounds showing 30% inhibition or more, the inhibitory potencies against C115D *E. coli* MurA and *E. cloacae* MurA were also measured. IC₅₀ values were determined for compounds showing more than 50% inhibition at 100 μM (*Table 1*).

For this first stage of the SAR study, the sulfonic acid moiety was attached either to a benzene or a naphthalene ring at positions 1 and 2, (compounds **1-3**), revealing only minimal MurA inhibition by such fragments. It might be noteworthy though that the presence of the sulfonic acid at position 1 of the naphthalene ring (compound **3**)

possessed a slightly better activity than the 2-regioisomer (compound **2**). The naphthyl acetic acid derivative (compound **4**) also did not show appreciable MurA inhibition. Naphthols **5-9** showed better MurA inhibition, but the inhibition was still not very strong, thus highlighting the relevance of the sulfonic acid group. Overall, none of the smaller fragments **1-9** retained the activity of ANS, indicating that the combination of all structural motifs of ANS provides its activity.

Table 1. MurA inhibition of a first series of ANS analogues (**1-9**)

Cmpd no.	Structure	<i>E. coli</i> WT MurA		<i>E. coli</i> C115D MurA		<i>E. cloacae</i> MurA	
		% inhibition at 100 μ M	IC ₅₀ \pm SD (μ M)	% inhibition at 100 μ M	IC ₅₀ \pm SD (μ M)	% inhibition at 100 μ M	IC ₅₀ \pm SD (μ M)
ANS		91%	18 \pm 4	83%	22 \pm 8	97%	31 \pm 3
1		0%	n.d.	n.d.	n.d.	n.d.	n.d.
2		5%	n.d.	n.d.	n.d.	n.d.	n.d.
3		17%	n.d.	n.d.	n.d.	n.d.	n.d.

4		13%	n.d.	n.d.	n.d.	n.d.	n.d.
5		34%	n.d.	11%	n.d.	6%	n.d.
6		36%	n.d.	7%	n.d.	3%	n.d.
7		22%	n.d.	n.d.	n.d.	n.d.	n.d.
8		19%	n.d.	n.d.	n.d.	n.d.	n.d.
9		28%	n.d.	n.d.	n.d.	n.d.	n.d.

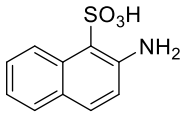
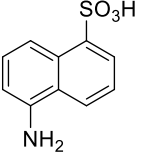
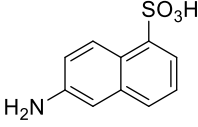
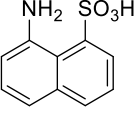
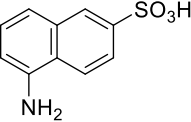
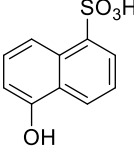
For the next stage of the SAR study, we chose compounds with closer structural resemblance to ANS, having a sulfonic acid group and a hydrogen bond donor (NH₂ or OH) at various positions of the naphthalene rings (*Table 2*). Compounds **10-13** had the sulfonic acid moiety at position 1 of the naphthalene scaffold in addition to an amino group at various positions. They were generally active against *E. cloacae* MurA.

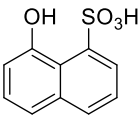
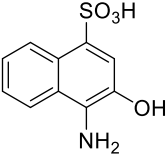
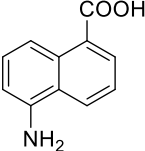
At the same time, only compounds **11** and **13** were reasonably active against both WT and C115D *E. coli* MurA, with **11** (the 5-amino derivative) having an IC₅₀ value of 9.0 μM against WT *E. coli* MurA. Compound **13**, differing from ANS by the missing phenyl unit at the 8-amino group, exhibited only part of the activity of ANS, confirming that that phenyl moiety contributed to the binding affinity, probably by interacting with Arg131 (*Figure 4*).

Thus, **11** was the most potent compound identified so far and was active against all three studied MurA isoforms. When the position of the sulfonic acid group of **11** was formally shifted from 1-sulfonate to 2-sulfonate in **14**, a decrease in *E. coli* MurA inhibition was observed. However, the activity against *E. cloacae* MurA was retained. In compounds **15** and **16**, the 5- and 8-amino groups of compounds **11** and **13**, respectively, were changed to hydroxy groups. This led to significantly decreased activities against all three MurA homologues, with only compound **15** showing some inhibition of WT *E. coli* MurA. Having two hydrogen bond donor moieties in compounds **17** and **18** was not favourable for the inhibitory activities. The added steric bulk or a disadvantageous influence of the positive charge of the benzylic amino group of compound **18** decreased the activity, as it is evident from the comparison with **10**. Replacing the 1-sulfonic acid moiety of compound **13** with a carboxylic group in compound **19** led to a significant loss in potency particularly in the case of both *E. coli* MurA isoforms, clearly indicating that the tetrahedral sulfonic acid group cannot be replaced by the planar carboxylic acid function. This is in full agreement with the

spatial arrangement of the multiple electrostatic interactions of the sulfonic acid group in the ANS-MurA co-crystal structure (*Figure 4*).

Table 2. MurA inhibition of the second series of ANS analogues (**10-19**)

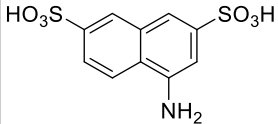
Cmpd no.	Structure	<i>E. coli</i> WT MurA		<i>E. coli</i> C115D MurA		<i>E. cloacae</i> MurA	
		% inhibition at 100 μ M	IC ₅₀ \pm SD (μ M)	% inhibition at 100 μ M	IC ₅₀ \pm SD (μ M)	% inhibition at 100 μ M	IC ₅₀ \pm SD (μ M)
10		48	n.d.	8%	n.d.	64%	49 \pm 5
11		95%	9.0 \pm 0.3	78%	18 \pm 3	95%	31 \pm 2
12		31%	n.d.	48%	n.d.	61%	31 \pm 3
13		66%	44 \pm 10	54%	46 \pm 2	42%	n.d.
14		40%	n.d.	0%	n.d.	66%	27 \pm 3
15		82%	45 \pm 11	48%	n.d.	12%	n.d.

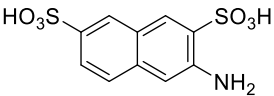
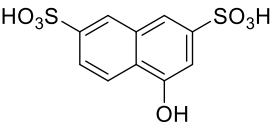
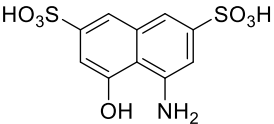
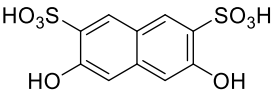
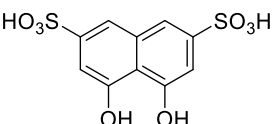
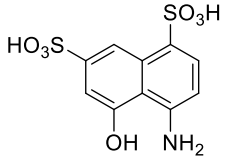
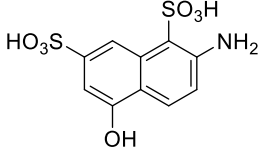
16		38%	n.d.	12%	n.d.	4%	n.d.
17		46%	n.d.	49%	n.d.	33%	n.d.
18		24%	n.d.	n.d.	n.d.	n.d.	n.d.
19		39%	n.d.	48%	n.d.	61%	44 ± 3

Finally, a third stage of SAR studies involved testing of compounds having two sulfonic acid groups in addition to the hydrogen bond-forming moieties. As a first set of according potential MurA inhibitors, 2,7-disulfonic acid derivatives having one or two additional hydrogen bond-forming units were tested (compounds **20-25**). In general, these compounds were strongly active against all studied MurA homologues, indicating a beneficial effect of the extra sulfonic acid group in the structure. An exception to this were the hydroxy derivatives (compounds **22, 24** and **25**) whose decreased activity against *E. cloacae* MurA suggested a limited tolerance of the *E. cloacae* enzyme towards the phenolic hydroxy group as a structural motif. This is particularly evident from **24** and **25**, where the symmetric dihydroxy substitution does not allow placing the hydroxyl in the less detrimental binding orientation. Presumably the higher electron density at the oxygen (relative to the amino nitrogen)

causes electrostatic repulsion with the backbone carbonyl of either Val87 or Lys88 at the bottom of the ANS binding pocket (cf. *Figure 7*), while an H-bond cannot form due to the unsuitable donor angle of the hydroxyl. Consistent with this hypothesis, the addition of an amino group as a second hydrogen bonding motif on the naphthalene ring (compound **23**) restored the inhibition of *E. cloacae* MurA, because the different angle of the amino function would allow H-bond formation with either the Val87 backbone carbonyl or the Ser93 side chain (cf. *Figure 4*), thus positively contributing to the binding affinity. Compounds **26** and **27** had the sulfonic acid moieties at positions 1 and 7 in addition to the presence of both amino and hydroxy groups. In particular for compound **26**, the favourable mixed amino/hydroxy substitution at the naphthalene scaffold was combined with the optimum placement of the second sulfonic acid group, thus furnishing the most potent compound against both C115D *E. coli* and *E. cloacae* MurA and the second most potent inhibitor of WT *E. coli* MurA. The overall resultant SAR for the inhibition of MurA by ANS and its analogues is summarized in *Figure 5*.

Table 3. MurA inhibition of the second series of ANS analogues (**20-27**)

Cmpd no.	Structure	<i>E. coli</i> WT MurA		<i>E. coli</i> C115D MurA		<i>E. cloacae</i> MurA	
		% inhibition at 100 μ M	IC ₅₀ \pm SD (μ M)	% inhibition at 100 μ M	IC ₅₀ \pm SD (μ M)	% inhibition at 100 μ M	IC ₅₀ \pm SD (μ M)
20		96%	9.1 \pm 0.6	5%	n.d.	57%	39 \pm 10

21		94%	5.0 ± 2.4	70%	56 ± 3	81%	33 ± 8
22		82%	51 ± 5	38%	n.d.	22%	n.d.
23		97%	6.2 ± 0.4	88%	33 ± 8	92%	24 ± 2
24		99%	0.95 ± 0.23	87%	31 ± 5	49%	n.d.
25		54%	84 ± 9	56%	85 ± 9	6%	n.d.
26		96%	2.7 ± 0.5	95%	10 ± 2	93%	14 ± 1
27		98%	11 ± 1	84%	26 ± 5	66%	89 ± 6

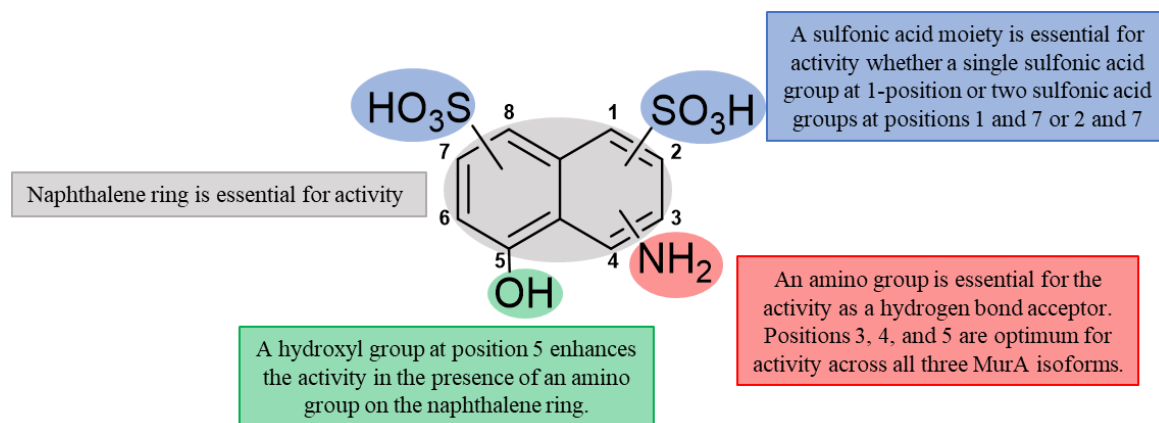


Figure 5. Summary of the SAR of ANS derivatives for the inhibition of MurA

3.4.3.1.2 Antibacterial Activity.

The compounds were tested as inhibitors of the growth of *E. coli* $\Delta tolC$ (an efflux-deficient strain) and *S. aureus* (Newman strain). All the tested compounds, including ANS, did not show any notable growth inhibition at concentrations up to 100 μM . This finding might be attributed to the compounds' inability to enter the bacterial cells resulting from their highly hydrophilic nature with at least one sulfonic acid moiety in the structure.

3.4.3.1.3 Fluorescence-based Binding Assay.

A fluorescence-based binding assay was performed to confirm the binding of ANS and two of its derivatives (compounds **11** and **26**) to both WT *E. coli* and *E. cloacae* MurA (Figure 6). The concentration used for each compound was titrated according to the fluorescence intensity produced from measuring the respective compound alone. ANS had minimal fluorescence on its own, and thus 100 μM was used in the measurements. Compounds **11** and **26** had a fluorescence intensity that was higher than the detection limit of the spectrofluorometer at 100 μM , and therefore, lower concentrations (10 μM and 1 μM for **11** and **26**, respectively) had to be used.

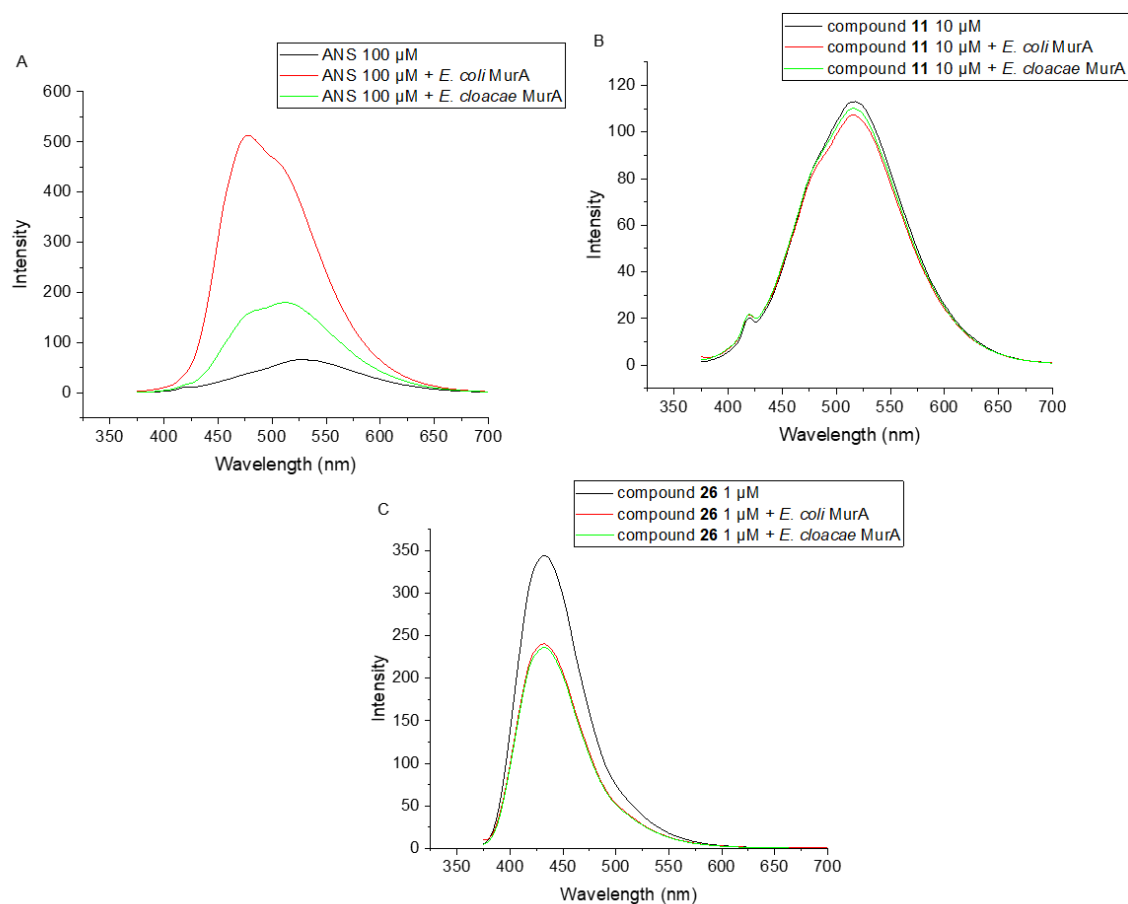


Figure 6. Results from the fluorescence-based binding assay with *E. coli* (red line) and *E. cloacae* MurA (green line) for: **A.** 100 μ M ANS, **B.** 10 μ M compound **11**, **C.** 1 μ M compound **26**

In the absence of MurA, ANS showed weak fluorescence intensity that increased when bound to MurA (Figure 6A). This was in agreement with previously reported results [47]. The increase in ANS fluorescence intensity was significantly higher with *E. coli* MurA than with *E. cloacae* MurA. For compound **11**, no change in fluorescence was observed for the compound in absence and presence of MurA (Figure 6B). However, for compound **26**, a quenching effect on the fluorescence was observed when the compound was bound to both MurA homologues (Figure 6C). While the behavior of compound **26** in the presence of MurA was different to that of ANS, this quenching confirms that a binding event occurs between compound **26** and both WT *E. coli* and *E. cloacae* MurA, respectively.

3.4.3.2 Binding Model of the ANS Derivative Compound **26**

To derive a binding model for our most potent inhibitor **26**, it was straightforward to perform molecular docking to the ANS binding pocket from the X-ray co-crystal structure with *E. cloacae* MurA (PDB entry 1EYN) [3]. Although there was no comparable ANS co-crystal structure with *E. coli* MurA available, it should be noted that all residues lining the ANS binding pocket are strictly conserved between the two species, suggesting that ANS and its derivatives may interact similarly with both MurA homologues.

In our model, binding of compound **26** was mainly driven by electrostatic interactions, particularly by the salt bridges between the sulfonic acid moieties and Arg120 and Arg91, respectively (*Figure 7A*). Thus, the gain of potency observed with most derivatives carrying two sulfonic acid functions (*Table 3*) can be explained by the formation of a second salt bridge, in addition to the one already present with ANS (cf. *Figure 4*). Being exposed to the solvent, the sulfonic acid in position 1 may not only directly interact with Arg120 but also with Arg91 via a bridging water molecule. The predicted H-bonds of the 4-amino- and 5-hydroxy substituents with Ser93 and the Lys88 backbone carbonyl, respectively, are also in agreement with the obtained SAR data, as this mixed tandem motif enhanced the inhibitory potency (compare compound **23** with compound **25**, *Table 3*). Additional contributions to the binding affinity arise from the CH- π interactions between the naphthyl ring and Pro112/Arg91. The superimposition of the docking pose with ANS as bound in the co-crystal structure shows that compound **26** was positioned in an overall similar manner, where the naphthyl ring and the 1-sulfonic acid largely overlap (*Figure S1*). This was not surprising as the binding mode was mainly controlled by the optimal interaction with the arginine residues 91 and 120, both with ANS and **26**. In the case

of ANS, the 8-aminophenyl moiety is marginally engaged in a cation- π interaction with Arg91 (*Figure 4*), while for **26**, Arg91 is captured by the 1-sulfonic acid. Overall, the rather small molecule **26** is densely decorated by substituents that are all involved in interactions with the binding pocket.

Eventually, the binding model as well as the co-crystal structure with ANS indicate that the ANS binding pocket extends into a hydrophobic groove, defined by the residues Val109, Leu111, Pro121, Val122 and Ile94 (*Figure 7B*), thus offering the advantageous possibility to significantly enhance the binding affinity through expansion of the ANS core toward that direction.

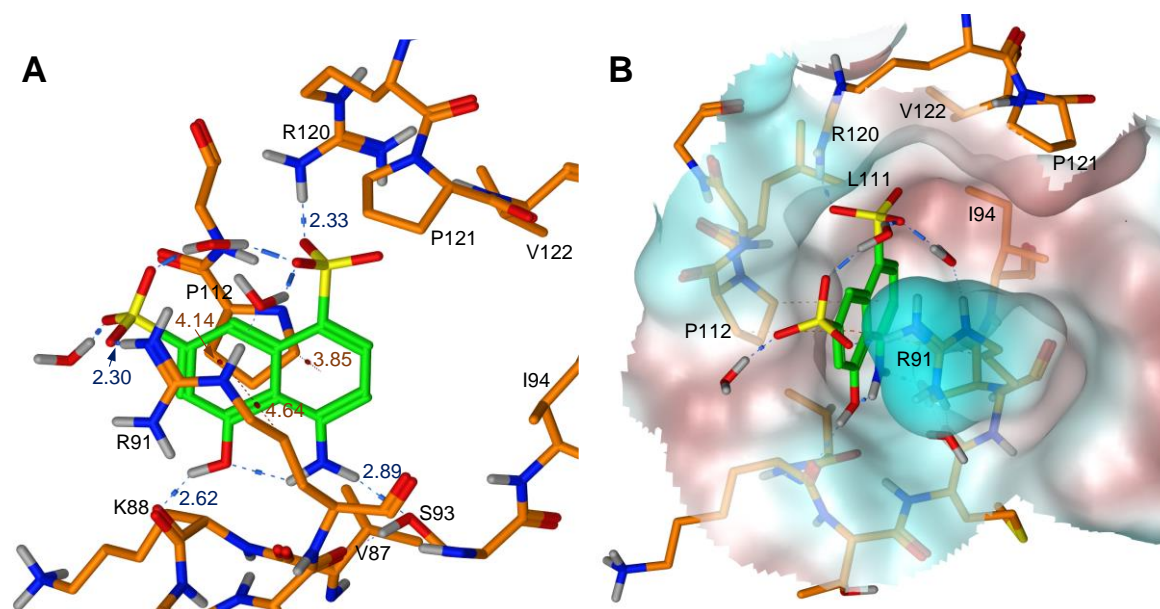


Figure 7. Predicted binding model of **26** in the ANS pocket of *E. cloacae* MurA. Compound **26** (green) was docked in the binding pocket occupied by ANS in the cocrystal structure with MurA, using the PDB coordinates 1EYN [3]. **A.** Side view showing the predicted ionic, H-bond and CH- π interactions. Residues of interacting side chains and of the adjacent hydrophobic cluster are labelled, numbers denote ligand-protein distances in Å. **B.** Top view with transparent Connolly surface encoding hydrophilic (cyan) and lipophilic (brown) areas. The interacting residues and the lipophilic residues within a 5.5 Å radius in the connected hydrophobic groove are labelled. Electrostatic interactions are indicated in blue and CH- π interactions in brown, the protein chain is coloured orange. Some residues are omitted for clarity

3.4.4 Conclusions

In this work, we have proven that the long-used fluorescent chemical probe ANS is actually an inhibitor of the bacterial protein MurA. This is in remarkable contrast to a previous report that had not found inhibitory activity of ANS towards MurA at concentrations up to 1 mM. In our experiments, ANS showed an IC₅₀ value of 17 μ M *in vitro* against WT MurA from *E. coli*. We also report SAR results for a series of ANS-derived naphthalene sulfonic acids that furnished MurA inhibitors with IC₅₀ values in the low micromolar range. They inhibited three different MurA isoforms including the fosfomicin-resistant C115D *E. coli* MurA, in addition to WT *E. coli* MurA and MurA from *E. cloacae*. The most potent overall inhibitor of all three MurA isoforms, compound **26**, had IC₅₀ values of 2.7, 10, and 14 μ M on WT *E. coli*, C115D *E. coli*, and *E. cloacae* MurA, respectively. The docked binding mode of compound **26** shows that it interacts with MurA in a similar manner to ANS, while forming an extra salt bridge interaction with Arg 91, thus increasing its potency against MurA despite it being smaller in size than ANS. These compounds did not inhibit bacterial growth, which may be attributed to poor cellular uptake resulting from their anionic properties. In the future, this issue might be solved by applying prodrug strategies for enhanced membrane permeation. Our work shows that small ligands are able to efficiently inhibit MurA at low micromolar concentrations, as exemplified by compounds **24** and **26**. Thus, the ANS pocket could be classified as a druggable site that offers, besides the basic side chains, several H-bond donor/acceptor moieties, in addition to a yet unexploited adjacent hydrophobic groove lined by the side chains of Val109, Leu111, Pro121, Val122 and Ile94. Thus, it can be speculated that structurally extended ANS derivatives, addressing more of this potential interaction site, might well reach nM potencies. This extension of the parent structure may also help in improving the

derivatives' physicochemical properties, thus facilitating their uptake into bacterial cells. ANS derivatives therefore represent new 'hit' structures for the development of efficient MurA inhibitors with improved antibacterial potencies.

3.4.5 References

- (1) L.S. Chang, E.Y. Wen, J.J. Hung, C.C. Chang, Energy Transfer from Tryptophan Residues of Proteins to 8-Anilino-naphthalene-1-Sulfonate, *J. Protein Chem.* 13 (1994) 635–640. <https://doi.org/10.1007/BF01890462>.
- (2) L. Stryer, The interaction of a naphthalene dye with apomyoglobin and apohemoglobin: A fluorescent probe of non-polar binding sites, *J. Mol. Biol.* 13 (1965) 482–495. [https://doi.org/10.1016/S0022-2836\(65\)80111-5](https://doi.org/10.1016/S0022-2836(65)80111-5).
- (3) E. Schönbrunn, S. Eschenburg, K. Luger, W. Kabsch, N. Amrhein, Structural basis for the interaction of the fluorescence probe 8-anilino-1-naphthalene sulfonate (ANS) with the antibiotic target MurA, *Proc. Natl. Acad. Sci. USA.* 97 (2000) 6345–6349. <https://doi.org/10.1073/pnas.120120397>.
- (4) N. Wang, E.B. Faber, G.I. Georg, Synthesis and Spectral Properties of 8-Anilino-naphthalene-1-sulfonic Acid (ANS) Derivatives Prepared by Microwave-Assisted Copper(0)-Catalyzed Ullmann Reaction, *ACS Omega.* 4 (2019) 18472–18477. <https://doi.org/10.1021/acsomega.9b03002>.
- (5) E. Daniel, G. Weber, Cooperative Effects in Binding by Bovine Serum Albumin. I. The Binding of 1-Anilino-8-naphthalenesulfonate. Fluorimetric Titrations, *Biochemistry.* 5 (1966) 1893–1900. <https://doi.org/10.1021/bi00870a016>.
- (6) Z. Zuo, H. Fan, J. Guo, W. Zhou, L. Li, Kinetics and thermodynamics of 1-anilino-8-naphthalene sulfonate interactions with Urinary Trypsin Inhibitor, *Protein J.* 31 (2012) 585–591. <https://doi.org/10.1007/s10930-012-9443-4>.
- (7) N.D. Younan, J.H. Viles, A Comparison of Three Fluorophores for the Detection of Amyloid Fibers and Prefibrillar Oligomeric Assemblies. ThT (Thioflavin T); ANS (1-Anilino-naphthalene-8-sulfonic Acid); and bisANS (4,4'-Dianilino-1,1'-binaphthyl-5,5'-disulfonic Acid), *Biochemistry.* 54 (2015) 4297–4306. <https://doi.org/10.1021/acs.biochem.5b00309>.
- (8) K. Kakuda, K. ichi Yamaguchi, K. Kuwata, R. Honda, A valine-to-lysine substitution at position 210 induces structural conversion of prion protein into

- a β -sheet rich oligomer, *Biochem. Biophys. Res. Commun.* 506 (2018) 81–86. <https://doi.org/10.1016/j.bbrc.2018.10.075>.
- (9) Y. Goto, A.L. Fink, Conformational States of β -Lactamase: Molten-Globule States at Acidic and Alkaline pH with High Salt, *Biochemistry*. 28 (1989) 945–952. <https://doi.org/10.1021/bi00429a004>.
- (10) D. Matulis, R. Lovrien, 1-Anilino-8-Naphthalene Sulfonate Anion-Protein Binding Depends Primarily on Ion Pair Formation, *Biophys. J.* 74 (1998) 422–429. [https://doi.org/10.1016/S0006-3495\(98\)77799-9](https://doi.org/10.1016/S0006-3495(98)77799-9).
- (11) O.K. Gasyimov, B.J. Glasgow, ANS Fluorescence: Potential to Augment the Identification of the External Binding Sites of Proteins, *Biochim. Biophys. Acta.* 1774 (2007) 403–407.
- (12) D.M. Togashi, A.G. Ryder, A fluorescence analysis of ANS bound to bovine serum albumin: Binding properties revisited by using energy transfer, *J. Fluoresc.* 18 (2008) 519–526. <https://doi.org/10.1007/s10895-007-0294-x>.
- (13) S. Betzi, R. Alam, M. Martin, D.J. Lubbers, H. Han, S.R. Jakkaraj, G.I. Georg, E. Schönbrunn, Discovery of a potential allosteric ligand binding site in CDK2, *ACS Chem. Biol.* 6 (2011) 492–501. <https://doi.org/10.1021/cb100410m>.
- (14) R. León, J.I. Murray, G. Cragg, B. Farnell, N.R. West, T.C.S. Pace, P.H. Watson, C. Bohne, M.J. Boulanger, F. Hof, Identification and characterization of binding sites on S100A7, a participant in cancer and inflammation pathways, *Biochemistry*. 48 (2009) 10591–10600. <https://doi.org/10.1021/bi901330g>.
- (15) M. Hirose, S. Sugiyama, H. Ishida, M. Niiyama, D. Matsuoka, T. Hara, E. Mizohata, S. Murakami, T. Inoue, S. Matsuoka, M. Murata, Structure of the human-heart fatty-acid-binding protein 3 in complex with the fluorescent probe 1-anilino-naphthalene-8-sulphonic acid, *J. Synchrotron Radiat.* 20 (2013) 923–928. <https://doi.org/10.1107/S0909049513021298>.
- (16) M.R. Groves, I.B. Müller, X. Kreplin, J. Müller-Dieckmann, A method for the general identification of protein crystals in crystallization experiments using a noncovalent fluorescent dye, *Acta Crystallogr. D Biol. Crystallogr.* 63 (2007) 526–535. <https://doi.org/10.1107/S0907444906056137>.
- (17) S. Sack, Z. Dauter, C. Wanke, N. Amrhein, E. Mandelkow, E. Schönbrunn, Crystallization and preliminary X-ray diffraction analysis of UDP-N-

- acetylglucosamine enolpyruvyltransferase of *Enterobacter cloacae*, *J. Struct. Biol.* 117 (1996) 73–76. <https://doi.org/10.1006/jsbi.1996.0071>.
- (18) E. Schönbrunn, S. Sack, S. Eschenburg, A. Perrakis, F. Krekel, N. Amrhein, E. Mandelkow, Crystal structure of UDP-N-acetylglucosamine enolpyruvyltransferase, the target of the antibiotic fosfomycin, *Structure*. 4 (1996) 1065–1075. [https://doi.org/10.1016/S0969-2126\(96\)00113-X](https://doi.org/10.1016/S0969-2126(96)00113-X).
- (19) T. Skarzynski, A. Mistry, A. Wonacott, S.E. Hutchinson, V. a Kelly, K. Duncan, Structure of UDP-N-acetylglucosamine enolpyruvyl transferase, an enzyme essential for the synthesis of bacterial peptidoglycan, complexed with substrate UDP-N-acetylglucosamine and the drug fosfomycin, *Structure*. 4 (1996) 1465–74. [https://doi.org/10.1016/S0969-2126\(96\)00153-0](https://doi.org/10.1016/S0969-2126(96)00153-0).
- [(20) J.Y. Zhu, Y. Yang, H. Han, S. Betzi, S.H. Olesen, F. Marsilio, E. Schönbrunn, Functional consequence of covalent reaction of phosphoenolpyruvate with UDP-N-acetylglucosamine 1-carboxyvinyltransferase (MurA), *J. Biol. Chem.* 287 (2012) 12657–12667. <https://doi.org/10.1074/jbc.M112.342725>.
- (21) E.D. Brown, J.L. Marquardt, J.P. Lee, C.T. Walsh, K.S. Anderson, Detection and Characterization of a Phospholactoyl-Enzyme Adduct in the Reaction Catalyzed by UDP-N-acetylglucosamine Enolpyruvoyl Transferase, MurZ, *Biochemistry*. 33 (1994) 10638–10645. <https://doi.org/10.1021/bi00201a010>.
- (22) D.H. Kim, W.J. Lees, K.E. Kempell, W.S. Lane, K. Duncan, C.T. Walsh, Characterization of a Cys115 to Asp substitution in the *Escherichia coli* cell wall biosynthetic enzyme UDP-GlcNAc enolpyruvyl transferase (MurA) that confers resistance to inactivation by the antibiotic fosfomycin, *Biochemistry*. 35 (1996) 4923–4928. <https://doi.org/10.1021/bi952937w>.
- (23) C. Wanke, N. Amrhein, Evidence that the reaction of the UDP-N-acetylglucosamine 1-carboxyvinyltransferase proceeds through the O-phosphothioketal of pyruvic acid bound to Cys115 of the enzyme, *Eur. J. Biochem.* 218 (1993) 861–870. <https://doi.org/10.1111/j.1432-1033.1993.tb18442.x>.
- (24) S. Mized, A. Oddone, B. Byczynski, D.W. Hughes, P.J. Berti, UDP-N-acetylmuramic acid (UDP-MurNAc) is a potent inhibitor of MurA (enolpyruvyl-UDP-GlcNAc synthase), *Biochemistry*. 44 (2005) 4011–4017. <https://doi.org/10.1021/bi047704w>.

- (25) L.L. Silver, Fosfomycin: Mechanism and resistance, *Cold Spring Harb. Perspect. Med.* 7 (2017) 1–11. <https://doi.org/10.1101/cshperspect.a025262>.
- (26) C. Marquès, V. Collin, C. Franceschi, N. Charbonnel, S. Chatellier, C. Forestier, Fosfomycin and *Staphylococcus aureus*: transcriptomic approach to assess effect on biofilm, and fate of unattached cells, *J. Antibiot.* 73 (2020) 91–100. <https://doi.org/10.1038/s41429-019-0256-y>.
- (27) S. Eschenburg, M. Priestman, E. Schönbrunn, Evidence that the fosfomycin target Cys115 in UDP-N-acetylglucosamine Enolpyruvyl Transferase (MurA) is essential for product release, *J. Biol. Chem.* 280 (2005) 3757–3763. <https://doi.org/10.1074/jbc.M411325200>.
- (28) J.L. Marquardt, E.D. Brown, C.T. Walsh, W.S. Lane, T.M. Haley, Y. Ichikawa, C.H. Wong, C.T. Walsh, Kinetics, Stoichiometry, and Identification of the Reactive Thiolate in the Inactivation of UDP-GlcNAc Enolpyruvyl Transferase by the Antibiotic Fosfomycin, *Biochemistry.* 33 (1994) 10646–10651. <https://doi.org/10.1021/bi00201a011>.
- (29) P. Liu, S. Chen, Z. ying Wu, M. Qi, X. yang Li, C. xia Liu, Mechanisms of fosfomycin resistance in clinical isolates of carbapenem-resistant *Klebsiella pneumoniae*, *J Glob. Antimicrob. Resist.* 22 (2020) 238–243. <https://doi.org/10.1016/j.jgar.2019.12.019>.
- (30) A. Sorlozano-Puerto, I. Lopez-Machado, M. Albertuz-Crespo, L.J. Martinez-Gonzalez, J. Gutierrez-Fernandez, Characterization of fosfomycin and nitrofurantoin resistance mechanisms in *Escherichia coli* isolated in clinical urine samples, *Antibiotics.* 9 (2020) 1–19. <https://doi.org/10.3390/antibiotics9090534>.
- (31) Z. Fu, Y. Ma, C. Chen, Y. Guo, F. Hu, Y. Liu, X. Xu, M. Wang, Prevalence of fosfomycin resistance and mutations in *murA*, *glpT*, and *uhpT* in methicillin-resistant *Staphylococcus aureus* strains isolated from blood and cerebrospinal fluid samples, *Front. Microbiol.* 6 (2016) 1–6. <https://doi.org/10.3389/fmicb.2015.01544>.
- (32) K.L. Fillgrove, S. Pakhomova, M.R. Schaab, M.E. Newcomer, R.N. Armstrong, Structure and mechanism of the genomically encoded fosfomycin resistance protein, FosX, from *Listeria monocytogenes*, *Biochemistry.* 46 (2007) 8110–8120. <https://doi.org/10.1021/bi700625p>.

- (33) J.E. Suarez, M.C. Mendoza, Plasmid-encoded fosfomycin resistance, *Antimicrob. Agents Chemother.* 35 (1991) 791–795. <https://doi.org/10.1128/AAC.35.5.791>.
- (34) P. Arca, G. Reguera, C. Hardisson, Plasmid-encoded fosfomycin resistance in bacteria isolated from the urinary tract in a multicentre survey, *J. Antimicrob. Chemother.* 40 (1997) 393–399. <https://doi.org/10.1093/jac/40.3.393>.
- (35) P. Arca, C. Hardisson, J.E. Suarez, Purification of a glutathione S-transferase that mediates fosfomycin resistance in bacteria, *Antimicrob. Agents Chemother.* 34 (1990) 844–848. <https://doi.org/10.1128/AAC.34.5.844>.
- (36) B.A. Bernat, L. Timothy Laughlin, R.N. Armstrong, Fosfomycin resistance protein (FosA) is a manganese metalloglutathione transferase related to glyoxalase I and the extradiol dioxygenases, *Biochemistry.* 36 (1997) 3050–3055. <https://doi.org/10.1021/bi963172a>.
- (37) T. Horii, T. Kimura, K. Sato, K. Shibayama, M. Ohta, Emergence of fosfomycin-resistant isolates of Shiga-like toxin-producing *Escherichia coli* O26, *Antimicrob. Agents Chemother.* 43 (1999) 789–793. <https://doi.org/10.1128/aac.43.4.789>.
- (38) J.L. Marquardt, D.A. Siegele, R. Kolter, C.T. Walsh, Cloning and sequencing of *Escherichia coli* murZ and purification of its product, a UDP-N-acetylglucosamine enolpyruvyl transferase, *J. Bacteriol.* 174 (1992) 5748–5752. <https://doi.org/10.1128/jb.174.17.5748-5752.1992>.
- (39) A. Steinbach, A.J. Scheidig, C.D. Klein, The unusual binding mode of cnicin to the antibacterial target enzyme MurA revealed by X-ray crystallography, *J. Med. Chem.* 51 (2008) 5143–5147. <https://doi.org/10.1021/jm800609p>.
- (40) A. Bachelier, R. Mayer, C.D. Klein, Sesquiterpene lactones are potent and irreversible inhibitors of the antibacterial target enzyme MurA, *Bioorg. Med. Chem. Lett.* 16 (2006) 5605–5609. <https://doi.org/10.1016/j.bmcl.2006.08.021>.
- (41) C.J. Dunsmore, K. Miller, K.L. Blake, S.G. Patching, P.J.F. Henderson, J.A. Garnett, W.J. Stubbings, S.E. v Phillips, D.J. Palestrant, J.D.L. Angeles, J.A. Leeds, I. Chopra, C.W.G. Fishwick, 2-Aminotetralones: Novel inhibitors of MurA and MurZ, *Bioorg. Med. Chem. Lett.* 18 (2008) 1730–1734. <https://doi.org/10.1016/j.bmcl.2008.01.089>.

- (42) K. Miller, C.J. Dunsmore, J.A. Leeds, S.G. Patching, M. Sachdeva, K.L. Blake, W.J. Stubbings, K.J. Simmons, P.J.F. Henderson, J. de Los Angeles, C.W.G. Fishwick, I. Chopra, Benzothioxalone derivatives as novel inhibitors of UDP-N-acetylglucosamine enolpyruvyl transferases (MurA and MurZ), *J. Antimicrob. Chemother.* 65 (2010) 2566–2573. <https://doi.org/10.1093/jac/dkq349>.
- (43) T. Scholz, C.L. Heyl, D. Bernardi, S. Zimmermann, L. Kattner, C.D. Klein, Chemical, biochemical and microbiological properties of a brominated nitrovinylfuran with broad-spectrum antibacterial activity, *Bioorg. Med. Chem.* 21 (2013) 795–804. <https://doi.org/10.1016/j.bmc.2012.11.018>.
- (44) C.M. Chang, J. Chern, M.Y. Chen, K.F. Huang, C.H. Chen, Y.L. Yang, S.H. Wu, Avenaciolides: Potential MurA-targeted inhibitors against peptidoglycan biosynthesis in methicillin-resistant *Staphylococcus aureus* (MRSA), *J. Am. Chem. Soc.* 137 (2015) 267–275. <https://doi.org/10.1021/ja510375f>.
- (45) J.D. McGivan, J.B. Chappell, Avenaciolide: a specific inhibitor of glutamate transport in rat liver mitochondria., *Biochem. J.* 116 (1970) 37–38. <https://doi.org/10.1042/bj1160037Pb>.
- (46) E. Schönbrunn, S. Eschenburg, F. Krekel, K. Luger, N. Amrhein, Role of the loop containing residue 115 in the induced-fit mechanism of the bacterial cell wall biosynthetic enzyme MurA, *Biochemistry.* 39 (2000) 2164–2173. <https://doi.org/10.1021/bi991091j>.
- (47) E. Schönbrunn, D.I. Svergun, N. Amrhein, M.H.J. Koch, Studies on the conformational changes in the bacterial cell wall biosynthetic enzyme UDP-N-acetylglucosamine enolpyruvyltransferase (MurA), *Eur. J. Biochem.* 253 (1998) 406–412. <https://doi.org/10.1046/j.1432-1327.1998.2530406.x>.
- (48) In Silico Bioinformatics Resources, University of Düsseldorf ligation calculator, http://www.insilico.uni-duesseldorf.de/Lig_Input.html.
- (49) R.K. Fathalla, W. Fröhner, C.D. Bader, P.D. Fischer, C. Dahlem, D. Chatterjee, S. Mathea, A.K. Kiemer, H. Arthanari, R. Müller, M. Abdel-Halim, C. Ducho, M. Engel, Identification and Biochemical Characterization of Pyrrolidinediones as Novel Inhibitors of the Bacterial Enzyme MurA, *J. Med. Chem.* (2022) articles ASAP. <https://doi.org/10.1021/acs.jmedchem.2c01275>.
- (50) A.P. Spork, M. Büschleb, O. Ries, D. Wiegmann, S. Boettcher, A. Mihalyi, T.D.H. Bugg, C. Ducho, Lead Structures for New Antibacterials: Stereocontrolled

- Synthesis of a Bioactive Muraymycin Analogue, *Chem. Eur. J.* 20 (2014) 15292–15297. <https://doi.org/10.1002/chem.201404775>.
- (51) A.K. Elhady, M. Abdel-Halim, A.H. Abadi, M. Engel, Development of Selective Clk1 and -4 Inhibitors for Cellular Depletion of Cancer-Relevant Proteins, *J. Med. Chem.* 60 (2017) 5377–5391. <https://doi.org/10.1021/acs.jmedchem.6b01915>.

3.5 Nanoparticle Fraught Liposomes: A Platform for Increased Antibiotic Selectivity in Multidrug Resistant Bacteria

This part of the thesis has been published in *Mol. Pharmaceutics* in 2022.

S. Fangary, M. Abdel-Halim, R. K. Fathalla, R. Hassan, N. Farag, M. Engel, S. Mansour, and S. N. Tammam, *Mol. Pharm.* **2022**, *19*, 3163-3177, DOI: 10.1021/acs.molpharmaceut.2c00258.

The contributions of each author to this chapter are listed below:

Suzan Fangary: She synthesized the nanoparticles, and performed the drug delivery assays for this work. She was involved in the writing of the manuscript.

Mohammad Abdel-Halim: He co-conceived the main idea for the work in this paper. He was involved in the supervision, and in the writing and editing of the manuscript.

Reem K. Fathalla: She synthesized the main reference compound in this publication. She tested the compounds on *S. aureus*, *E. coli* DH5 α and *E. coli* Δ tolC. She performed the MurA and MurB assays for the reference compound and calculated the corresponding IC₅₀ and MIC values. Finally, she was involved in the writing process of the manuscript.

Raghda Hassan: She performed some of the microbiology and *in vivo* experiments for the manuscript.

Noha Farag: She performed some of the microbiology and *in vivo* experiments for the manuscript.

Matthias Engel: He was involved in the supervision and editing of the manuscript.

Samar Mansour: She was involved in the supervision and editing of the manuscript.

Salma N. Tammam: She co-conceived the main idea for this work. She was responsible for the main supervision, administration and writing and editing of the manuscript.

3.5.1 Abstract

Increasing antibiotic concentrations within bacterial cells, whilst reducing them in mammalian ones would ultimately result in an enhancement of antibacterial actions, overcoming of multidrug resistance (MDR), all whilst minimizing toxicity. Nanoparticles (NPs) have been used in numerous occasions to overcome antibiotic resistance, poor drug solubility and stability. However, the concomitant increase in antibiotic concentration in mammalian cells and the resultant toxicity are usually overlooked. Without compromising bacterial cell fusion, large liposomes have been reported to show reduced uptake in mammalian cells. Therefore, in this work, small NP freight liposomes (NP-Lip) were formulated with the aim of increasing NP uptake and antibiotic delivery in bacterial cells but not in mammalian ones. Small poly lactic-co-glycolic acid (PLGA) NPs were therefore loaded with Erythromycin (Er); an antibiotic with low membrane permeability that is susceptible to drug efflux and **3c**; a 5-cyanothiazolyl urea derivative with low solubility and stability. *In vitro* experiments demonstrated that the incorporation of the small NPs into large liposomes resulted in a reduction in NP uptake by HEK293 cells whilst increasing it in Gram-negative bacteria (*E. coli* DH5 α , *E. coli* K12, and *P. aeruginosa*), consequently resulting in an enhancement of antibiotic selectivity by 4 folds towards *E. coli* (both strains) and 8 folds towards *P. aeruginosa*. Ocular administration of NP-Lip in a *P. aeruginosa* keratitis mouse model demonstrated the ability of Er/**3c** loaded NP-Lip to result in a complete recovery. More importantly, in comparison to NPs, the ocular administration of NP-Lip showed a reduction in TNF-alpha and IL-6 levels, implying reduced interaction with mammalian cells *in vivo*. This work therefore clearly demonstrated how tailoring the nano-bio interaction could result in selective drug delivery and a reduction in toxicity.

Keywords

Selective drug delivery; Multidrug resistance; liposomes; nanoparticles; *P. aeruginosa* keratitis; phenyl thiazolyl urea derivatives; carbamate derivatives

3.5.2 Introduction

Bacterial resistance to antibiotics is one of the biggest threats to global health[1]. Antibiotic resistance is more pronounced in Gram-negative bacteria due to their low outer membrane permeability and multidrug efflux pumps[2]. Additionally, the therapeutic use of several experimental compounds that show promising antibacterial properties is hampered by their poor solubility. To that end, therapeutic modalities that could address low drug solubility and assist in overcoming multidrug resistance are highly needed.

Erythromycin (*Er-Figure 1*) is a widely used antibiotic that exerts its antibacterial action through the inhibition of the 50S bacterial ribosome. However, the efficacy of Er against Gram-negative bacteria is limited by its reduced ability to permeate the Gram-negative outer membrane[3] and its susceptibility to extrusion *via* the drug efflux systems[3,4].

Phenyl thiazolyl urea and carbamate derivatives are novel antibacterial agents[6]. These compounds inhibit specific bacterial enzymes altering peptidoglycan biosynthesis ultimately leading to loss of cell shape, integrity, and bacterial death[6]. Among those compounds, **3c** (5-cyanothiazolyl urea derivative-*Figure 1*) is a very interesting candidate. **3c** showed promising antibacterial effects towards a number of Gram-positive drug resistant bacteria including methicillin resistant *Staphylococcus aureus* (MRSA), vancomycin resistant *Enterococcus* (VRE), and penicillin resistant *Streptococcus pneumoniae* (PRSP). Similar to Er, **3c** is less effective against Gram-negative bacteria[6]. In addition, the effectiveness of **3c** is drastically reduced in the

presence of serum due to plasma protein binding given its low polarity ($\log P = 3.44$)[6] and hence its development into a therapeutic compound is at standstill despite its potent antibacterial effects.

Small nanoparticles (NPs) (less than 200 nm) can access the bacterial cytosol *via* different mechanisms than those utilized by free drugs[7]. Since the NPs are not recognized by the drug efflux pumps, they therefore shield the loaded drug along their journey to the cytosol, where it is then released[8–11]. Within this context, the ability of the NPs to shield the loaded drug, would also circumvent its binding to plasma proteins[12] and enable the delivery of hydrophobic drugs into the bacterial cell. Notwithstanding, small NPs usually exhibit higher cellular association than larger ones (1000nm and above)[13,14]. Hence in attempt to overcome bacterial resistance with the use of small NPs, an enhancement of toxicity towards mammalian cells could occur, unless these small NPs were somehow made unavailable for mammalian cell interaction.

Liposomes have been reported to fuse with the bacterial outer membrane, delivering their content into bacterial cells[15]. The extent of fusion in bacterial cells is not affected by liposomal size or lamellarity[16], unlike mammalian cells where the liposome's capacity to fuse with the cell membrane diminishes with the increase in size[17]. Accordingly, in case, if the antibiotics were encapsulated into small NPs that were then loaded into much larger liposomes, an increased drug delivery into bacterial cells but not mammalian ones could be achieved (*Figure 1*).

In this work, in an attempt to address antibacterial drug resistance whilst avoiding toxicity towards mammalian cells, large liposomes fraught with small NPs encapsulating antibiotics were developed and tested against Gram-negative bacteria. To initially determine the reason behind the reduced effectiveness of **3c** towards

Gram-negative bacteria, the anti-bacterial effects of **3c** towards *E. coli* DH5 α and *E. coli* TolC were investigated in the presence and absence of the membrane permeabilizer polymyxin B nonapeptide (PMBN). Subsequently, both Er and **3c** were loaded into small polymeric NPs that were then loaded into larger liposomes. The ability of the developed system to increase antibiotic efficacy towards *E. coli* and *P. aeruginosa* whilst reducing cytotoxicity towards mammalian cells was then assessed *in vitro* and *in vivo* in an ocular *P. aeruginosa* keratitis mouse model.

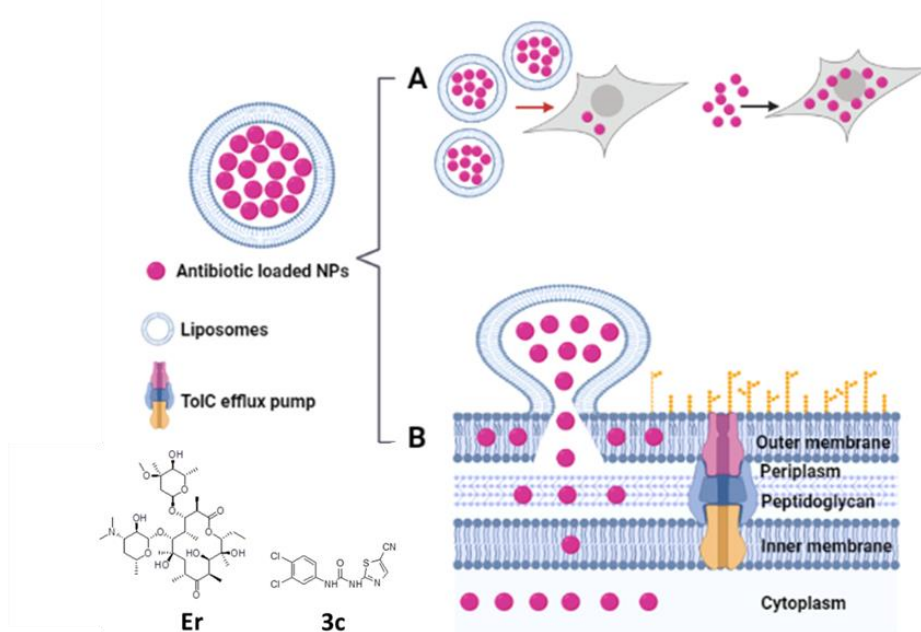


Figure 1. Schematic representation of the ability of the NP fraught liposomes (NP-Lip) to (A) reduce drug delivery in mammalian cells in comparison to small NPs and (B) enable evasion of resistance mechanisms in Gram-negative bacteria. Figure was created using BioRender.com

3.5.3 Methods

3.5.3.1 Assessing the Effectiveness of **3c** against *E. coli* DH5 α and *E. coli* TolC with the Aid of Polymyxin B nonapeptide (PMBN)

Minimum inhibitory concentrations (MIC) were determined for **3c** as described in [18,19]. **3c** was initially dissolved in dimethyl-sulfoxide (DMSO) and subsequently diluted in Luria-Bertani (LB) broth. Increasing concentrations of **3c** (0.39-12.5 $\mu\text{g/ml}$)

were then incubated with bacterial suspensions (10×10^7 CFU/ml), both in the presence and absence of PMBN (6 μ g/ml). Incubation was conducted for 16 hours at 37 °C and 50 rpm. After the incubation, optical density (OD) was measured using a POLARstar Omega Micro plate Reader (BMG LABTECH). MIC₅₀ values were computed by plotting the absorbance values against the concentrations of **3c**. MIC₅₀ values are defined as a concentration that could inhibit 50 % of the growth control. In a similar manner, the OD was determined for *E. coli TolC* upon treatment with increasing concentrations on PMBN as control.

3.5.3.2 Preparation and Characterization of Unloaded Polymeric Nanoparticles-(NPs) and Liposomes-(Lip)

Polymeric NPs were prepared by the emulsion solvent evaporation method[20] using poly-lactic-co-glycolic acid as a polymer (PLGA, ratio 50/50 Mwt:17000 g/mole, Changchun Folioplast Bio-Tech c., Ltd, Changchun, China). PLGA was dissolved in 2 ml of ethyl acetate at a concentration of 1 mg/ml and emulsified in a 10 ml of 1 %(v/v) Tween 80 by continuous stirring at 800 rpm for 10 minutes, followed by sonication at 70% amplitude (70-Watt, 20 kHz) for 5 minutes on ice. NPs were then stirred overnight to allow the evaporation of the organic phase. Finally, NPs were collected and centrifuged at room temperature using 10 kDa Amicon® ultra-4 centrifugal filter units at 32928 rcf for 30 minutes.

Blank liposomes (Lip) were formulated using direct mixing of lipids in aqueous phase[21]. Briefly, 16 mg soybean lecithin (LEC, Lipoid GmbH, Ludwigshafen, Germany) and 2 mg cholesterol (CHOL, Sigma-Aldrich Chemie GmbH, Taufkirchen, Germany) were dispersed directly in 5 ml ultra-pure water and subsequently mixed using a vortex mixer for 2 minutes at 2500 rpm. Liposomes were then collected by centrifugation in a cooling centrifuge adjusted to 10°C at 10752 rcf for 10 minutes.

The Lip pellet was reconstituted to 1 ml using ultra-pure water and used for further investigations.

NP and Lip hydrodynamic diameter (HD) and zeta potential (ZP) were measured using a Malvern Zetasizer Nano ZS90 (Malvern Instruments Ltd, Worcestershire, UK). Three batches were prepared and analyzed in triplicates at 25 °C. Results were expressed as mean \pm standard deviation (SD).

To investigate the stability, Lip and NP-Lip were formulated and stored at 4 °C for 14 days. HD of both Lip and NP-Lip was measured using Malvern Zetasizer at day 1 (directly after the preparation) and after 2, 7, and 14 days.

For morphological analysis, one drop of each formulation was placed on a carbon-coated film 300 mesh copper grid, followed by staining with 1 M uranyl acetate solution. Samples were then examined using JEOL-JEM 1010 Transmission Electron Microscopy (TEM; JEOL Ltd., Tokyo, Japan). NP-Lip morphology was also assessed by LEO Supra 55 Field Emission Scanning Electron Microscopy (SEM; Zeiss, Oberkochen, Germany) after gold sputtering using Anatech Hummer 8.0 sputter system for 2 minutes at 15mA.

3.5.3.3 Encapsulation of NPs in Liposomes

NPs were prepared as detailed previously. Subsequently, 5 ml NPs were purified and concentrated by centrifugation in 10 kDa ultra-centrifuge filter units yielding a NP suspension corresponding to 2 mg/ml in terms of PLGA. The concentrated NPs were then dispersed in 5 ml de-ionized water in which 16 mg LEC and 2 mg CHOL were also dispersed and mixed using a vortex mixer for 2 minutes at 2500 rpm. HD and ZP for NPs in liposomes (NP-Lip) were determined by Malvern Zetasizer. Additionally, NP-Lip morphology was assessed by TEM as detailed earlier and by Nikon Eclipse Ti Confocal Laser Scanning Microscopy using 60 x magnifications (CLSM; Nikon

Cooperation, Tokyo, Japan). For CLSM analysis, rhodamine B (RB, Sigma-Aldrich Chemie GmbH, Taufkirchen, Germany) was incorporated in NPs. Briefly, 250 μ l of (4 mg/ml) RB solution in DMSO were added to 2 ml of 1 mg/ml PLGA solution in ethyl acetate. This organic phase was then emulsified in 10 ml of 1% v/v Tween 80 solution with continuous stirring at 800 rpm for 10 minutes, followed by sonication for 5 minutes on ice. To remove the excess unencapsulated dye, RB-NPs were then centrifuged using 10 kDa Amicon® ultra-4 centrifugal filter units and loaded into liposomes as detailed earlier. However, this time, 2.5 % of liposomes` cholesterol content was replaced with TopFluor Cholesterol (FL-CHOL, Avanti Lipid, Alabama, USA).

To determine NP EE% in NP-Lip, NPs were initially loaded with rhodamine 123 (R123, Sigma-Aldrich Chemie GmbH, Taufkirchen, Germany) in a similar manner to RB. The encapsulated dye was also removed by centrifugation in 10 kDa Amicon® ultra-4 centrifugal filter units. R123 loaded NPs were encapsulated into Lip, after investigating the release of R123 over 24 hours (*Supplementary Figure 1*). To assess the effect of NP concentration on the EE%, 2 different concentrations of PLGA NPs; 0.2 mg/ml and 0.4 mg/ml (final polymer concentration per liposomal preparation) were conducted. The higher NP concentration was obtained by concentrating 10 ml of PLGA NPs in the centrifugation filter units to 0.5 ml so that a total of 2 mg PLGA (0.4 mg/ml) are incorporated in the liposomes. To separate unencapsulated NPs from those encapsulated in liposomes, NP loaded liposomes were then centrifuged at 10 °C, 10752 rcf for 10 minutes. The centrifugation conditions (speed and duration) were validated to ensure that only NP-Lip would pellet and not unencapsulated R123 loaded NPs (*Supplementary Table 1*). Supernatants were then used to determine the concentration of unencapsulated R123-NPs by fluorometry at the

excitation/emission wavelength λ 485/535 nm. The experiment was conducted in triplicates and results were expressed as mean EE% \pm SDNPs drug loading and EE% determination

NPs were loaded with either Er (Arcos Organics, Geel, Belgium) or **3c**. The synthesis of **3c** was accomplished via one step according to Francisco *et al.*[6]. Drug loaded NPs were prepared as mentioned in **section 3.5.3.2**. However, in this case, drugs were dissolved in the polymeric organic phase. NPs were prepared using increasing drug concentrations (1 and 2 mg/ml for Er and 0.25, 0.5, and 1 mg/ml for **3c**). Drug loaded NP morphology was examined by TEM.

To quantify the unencapsulated drug, drug loaded NPs were centrifuged in centrifugal filter units, the concentration of unencapsulated drugs in the NP flow through was determined using an in-house developed ultra-high performance liquid chromatography-tandem mass spectrometer (UHPLC-MS/MS) method using diphenhydramine as internal standard. Method details and validation are provided in the Supplementary information file. Analyses were acquired on a Waters ACQUITY Xevo TQD system, which consisted of ACQUITY UPLC H-Class system and XevoTQD triple-quadrupole tandem mass spectrometer with an electrospray ionization (ESI) interface (Waters Corp., Milford, USA). ACQUITY UPLC BEH C18 50 mm \times 2.1 mm column (particle size, 1.7 μ m) was used to separate analytes (Waters, Wexford, Ireland). System operation and data acquisition were controlled using MassLynx 4.1 software (Waters, Milford, USA). All data were processed with the TargetLynx quantification program (Waters, Milford, USA). The concentration of encapsulated drug was determined indirectly from the unencapsulated one[22].

3.5.3.4 *In vitro* Cell Viability Assessment

3.5.3.4.1 Cytotoxicity Evaluation- HEK293 Cells

The cytotoxicity of the formulations was evaluated by using 3-(4, 5-Dimethyl-2-thiazolyl)-2,5-diphenyltetrazolium bromide assay (MTT, SERVA Electrophoresis GmbH, Heidelberg, Germany). HEK293 cells were seeded in 96 well plates at a density of 2×10^4 cells/well and allowed to adhere overnight. Cells were then treated with increasing concentrations of blank unloaded NPs, NP-Lip, Er-NPs, Er-NP-Lip, **3c**-NPs, **3c**-NP-Lip, and free Er and free Er + unloaded NP-Lip as detailed in *Supplementary Table 2*. As a control, cells were also treated with increasing concentrations of Tween 80 exposed to same purification steps as blank unloaded NPs. Cell treatment with free **3c** was not possible, given the drug's low solubility. Cells were incubated with formulations for 24 hours. Subsequently, cell culture media were aspirated and cells were washed with phosphate buffered saline (PBS) and cell viability was determined using MTT assay as detailed in [23]. The results were expressed as mean viability (%) and SD relative to untreated cells. Cell viability was also determined following HEK293 cell treatment with unloaded NPs and NP-Lip (10 and 100 $\mu\text{g}/\text{ml}$ in terms of PLGA concentration). However, in this case, the incubation time was instead 2 hours. Relative Inhibitory concentrations resulting in 50% loss in viability (IC_{50}) were computed.

3.5.3.4.2 NPs & NP-Lip Cellular Association

HEK293 cells were primarily seeded in a 96 well plate at a density of 2×10^4 cells/well and allowed to adhere overnight. Next, media were aspirated and the cells were then treated with 10 $\mu\text{g}/\text{ml}$ of both R123-NPs and R123-NP-Lip in terms of PLGA concentration. After 2 hours, the NPs/NP-Lip containing media were aspirated. Wells were washed twice with PBS and the concentration of associated particles was

determined by fluorometry using a plate reader set to excitation/emission wavelength λ 485/535 nm. NP and NP-Lip calibration curves were constructed and used to compute the associated concentration of NP and NP-Lip, respectively[24].

3.5.3.5 *In vitro* Antimicrobial Susceptibility Testing towards Gram-negative Bacteria

Gram-negative bacteria; *P. aeruginosa*, *E. coli* K12, and *E. coli* DH5 α were purchased from American Type Culture Collection (ATCC, Manassas, USA). The bacteria were streaked onto Müller-Hinton Agar (MHA) plates then the plates were incubated for 18-24 hours at 37 °C. For each isolate, a single colony from the plate was transferred into 20 ml Müller-Hinton broth (MHB) medium and incubated overnight at 37 °C at 120 rpm in shaking incubator. The bacterial suspension to be used as the inoculum was diluted to produce a bacterial cell suspension of 10×10^5 CFU/ml[25,26]. Er and **3c** were dissolved in DMSO (7 mg/ml of Er & 2.5 mg/ml of **3c**), followed by preparing serial dilution of free drugs in MHB. Bacterial cells were treated with increasing concentrations of blank NP-Lip, Er-NP-Lip, **3c**-NP-Lip, Er and **3c**. Concentrations tested are detailed in *Supplementary Table 3*. For this experiment, sterility control wells of (MHB), negative (-ve) control wells of (MHB, and drugs/formulations solutions), and growth control wells of (MHB, and inoculum) or (MHB, inoculum, and DMSO in the case of free drugs' MTT) were included. All tested drugs/formulations were sterilized under UV for 30 minutes. In a 96 well plate, 50 μ l of drugs/formulations solutions were added, followed by the addition of 10×10^5 CFU/ml bacterial cell suspensions (50 μ l). The plates were incubated for 16-24 hours at 37 °C in aerobic conditions. Subsequently, (0.3 mg/ml) MTT solution was added to every single well and the 96-well plates were incubated for 2 hours at 37 °C. After 2 hours incubation with MTT solution, the produced formazan crystals were solubilized

using DMSO. The absorbance values were determined using a Wallac plate reader at a wavelength of λ 595 nm[27]. The results were reported as mean \pm SD calculated for each concentration. The % cell viability per well was calculated as follows:

$$\% \text{ Cell viability} = \frac{(\text{Absorbance of treated wells} - \text{Absorbance of -ve control wells})}{\text{Absorbance of growth control wells}} \times 100$$

3.5.3.6 *In vitro* Antimicrobial Susceptibility of *P. aeruginosa*

P. aeruginosa induced keratitis was developed as detailed in[27]. Briefly, *P. aeruginosa* was grown in MHB overnight at 37°C, and was then centrifuged at 7,000 g for 5 minutes. The cell pellet was washed and resuspended in 0.9 % sterile saline. Calibrated turbidity measurement was conducted at λ = 600 nm to adjust bacterial concentration to 10^6 CFU/10 μ l.

Swiss albino mice were purchased from the National Research Center (NRC), Cairo, Egypt and housed under pathogen-free conditions at the animal facility of German University in Cairo. For model optimization, three (1 mm) scratches were made in both eyes of the infected mice group using a sterile 25-gauge needle. A 10 μ l aliquot containing 1×10^6 cells of *P. aeruginosa* was applied to the corneal surface. Both eyes were examined at 1, 2, 3, 4, 5, 7, 24, 48, 72 hours and 6 days post-infection to grade the infection according to clinical score as detailed in[27]. Briefly, eyes received score between 0 to +4; where 0 = clear or slight corneal opacity, partially covering the pupil; +1 = slight opacity fully covering the anterior segment; +2 = dense opacity, partially or fully covering the pupil; +3 = dense opacity covering the entire anterior segment; and +4 = corneal perforation or phthisis bulbi (i.e., shrunken eye).

To evaluate NP-Lip, mice were initially divided into 2 groups: the first group served as the healthy control whereas *P. aeruginosa* keratitis was induced in the second group. Twenty-four hours after inoculation, the infected group was further divided

into 7 groups (n=8). Animals with *P. aeruginosa* keratitis received either free Er, NPs, NP-Lip, Er-NPs, Er-NP-Lip, **3c**-NP-Lip, or the same volume of sterile saline.

Animals received a twice daily topical application of 200 µg of free Er, Er-NPs, and Er-NP-Lip directly to the infected cornea and 100 µg in the case of **3c**-NP-Lip, or the same dose of unloaded NPs and NP-Lips (160 µg of PLGA) for four days. After the last dose, the mice were sacrificed and eyeballs from 6 animals per group were harvested and homogenized in 0.9 % sterile saline using a Dounce homogenizer to yield a homogenate (0.0234 g/ml), which was then cultured on MHA plates, followed by incubation for 24 hours at 37 °C. CFUs were counted and expressed in terms of Log viability ± SD[28].

For histopathological investigations, eyes were harvested and fixed in 10% formal saline for 24 hours. Eyes were subsequently washed using tap water, followed by dehydration using serial dilutions of alcohol (methyl, ethyl, and absolute ethyl). Specimens were cleared in xylene and embedded in paraffin at 56°C in hot air oven for 24 hours. Paraffin bees wax tissue blocks were prepared for sectioning at 4 µm thickness by a sledge microtome. The obtained tissue sections were collected on glass slides, deparaffinized, stained by hematoxylin and eosin stain, and examined by histopathologist who was blinded to study groups[29].

Eyeballs were harvested from healthy uninfected animals that have been treated with unloaded NPs and Lip.

To evaluate the inflammatory potential of NPs and NP-Lips, healthy animals received a twice daily topical application of unloaded NPs and NP-Lips (160 µg of PLGA) for four days. Eyes homogenates (0.0234 g/ml) were then used for the quantification of TNF-alpha and interleukin (IL-6) by Enzyme-Linked Immunosorbent (ELISA) assay

as per manufacturer's instructions (BioSource IL-6; MBS824703 and TNF-alpha; MBS825075).

3.5.3.7 Statistical Analysis

Statistical analysis tests were performed using Graph-Pad InStat software. Unpaired t-test and one-way analysis of variance test (ANOVA) tests were performed. Levels of statistical significance are demonstrated as *P<0.05 considered significant, **P<0.01 considered very significant, and ***P<0.001 considered extremely significant.

3.5.4 Results and Discussion

3.5.4.1 Introduction Assessing the Effectiveness of **3c** against *E. coli* DH5 α and *E. coli* TolC with the Aid of Polymyxin B (PMBN)

E. coli TolC is a mutant *E. coli* strain which lacks AcrAB-TolC multidrug efflux pump gene[30]. When **3c** was used in the treatment of *E. coli* TolC, a much lower MIC₅₀ was observed in comparison to the *E. coli* DH5 α , which bears the TolC multidrug efflux system (*Figure 2A*), indicating that drug efflux is one of the reasons for reduced effectiveness of **3c** towards Gram-negative bacteria. Reduced permeability is also another reason. PMBN is a lipopeptide with bactericidal effects[31]. PMBN exerts its effect *via* a detergent-like mechanism of action, in which it interacts with lipopolysaccharide (LPS) of the outer membrane of Gram-negative bacteria increasing its permeability[31]. When PMBN was used in a combination with **3c**, further reduction in MIC₅₀ was observed for both *E. coli* DH5 α and *E. coli* TolC (*Figure 2A*). At the same concentrations, PMBN on its own did not result in reduction in bacterial cell viability (*Figure 2B*). It could therefore be speculated that similar to Er, **3c** shows reduced effectiveness against Gram-negative bacteria due to its low outer membrane permeability and susceptibility to drug efflux. However, for further

confirmation the measurement of intra-bacterial concentration of **3c** would be insightful.

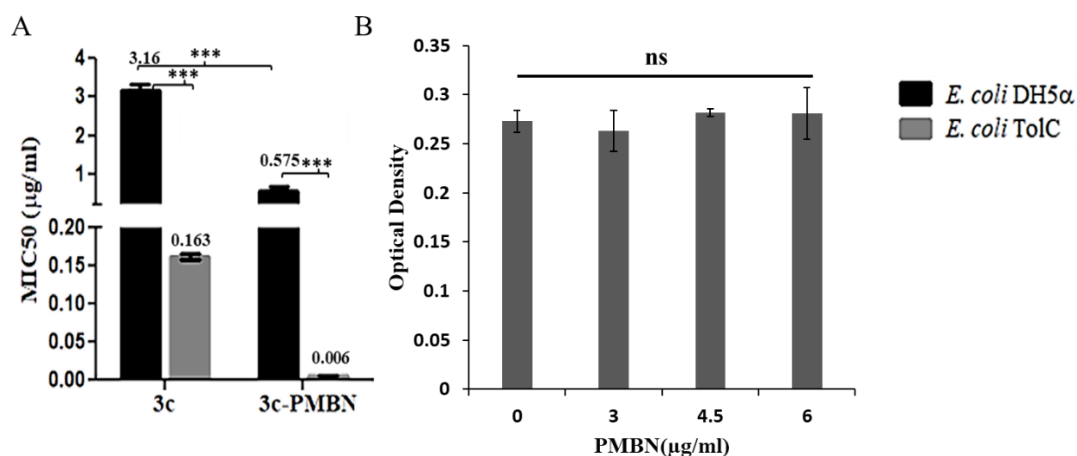


Figure 2. (A) Activity of **3c** and **3c-PMBN** against *E. coli* DH5 α and *E. coli* TolC. (B) The effect of PMBN on *E. coli* TolC viability. Statistical analysis was performed by GraphPad InStat software using one-way ANOVA, where *P < 0.05, **P < 0.01, and ***P < 0.001

3.5.4.2 Preparation and Characterization of NP, Lip and NP-Lip

Literature includes ample evidence on the ability of small NPs (less than 200 nm) to diffuse through the complex structure of Gram-negative bacteria and combat drug resistance[8,32–34]. A possible reason is that the smaller size offers a larger surface area, resulting in increased interaction with bacterial cells[33,35]. However, the same would apply to mammalian cells. Small NPs (less than 200 nm) are also known to achieve higher association with mammalian cells[13,14]. This association is reduced with the increase in NP size[36]. In fact, particles larger than 1µm seem to show very limited uptake in non-phagocytic mammalian cells[37,38]. This inverse relation between particle size and uptake is less significant with bacterial cells[16], particularly with liposomes. Liposomes have been reported to fuse with bacterial membranes, releasing their content into the membranes or the interior of the bacterial cells[15,39,40]. For such reasons, here small PLGA NPs were initially prepared. The NPs showed a small HD corresponding to 83 ± 1 nm with polydispersity

index (PDI) of 0.205 ± 0.011 and a ZP of -33 ± 0.6 mV (*Table 1*). The obtained particles were spherical and unaggregated as indicated by TEM (*Figure 3A*). Large Lip were then formulated by the direct dispersion of lipids in water[21], where Lip HD corresponded to 1304 ± 8 nm and ZP corresponded to -13.3 ± 0.6 mV (*Table 1*). More importantly, Lip showed uni-lamellar structures (*Figure 3B*). This unilamellarity would guarantee the release of the NPs into the bacterial cell upon fusion of the Lip with the bacterial membrane as indicated in *Figure 1*.

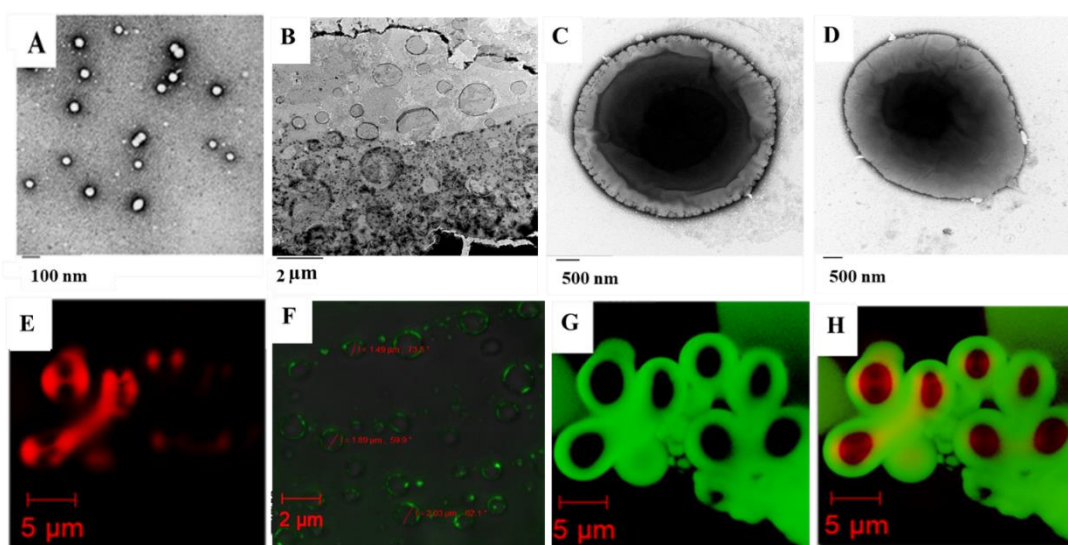


Figure 3. TEM images of **(A)** NPs, **(B)** blank Lip, **(C and D)** NPs in Lip & CLSM images of **(E)** Red NPs due to RB content, **(F and G)** liposomes, liposomal bi-layer appeared green due to green FL-CHOL content and **(H)** overlaying of green **(G)** and red filters **(E)** indicating the incorporation of NPs in the liposomal core

It is noteworthy that by utilizing the same lipid composition, liposome formulation using the thin-film hydration method was also attempted (Supplementary information file). However, the obtained liposomes had a small HD (201 ± 10 nm), which was expected given that sonication was employed. The latter was necessary to yield uni-lamellar vesicles from the multi-lamellar ones that are produced following hydration of the lipid film[41]. Alternatively, the use of extruders with large pore size

could have yielded larger liposomes. In addition to the liposome structure, we speculated that the vortex agitation method would result in a higher EE% of NPs. In the thin-film hydration method, the aqueous NP suspension would be used in the hydration of the lipid film and hence the NPs would be expected to diffuse across the already formed bi-layers to make their way into the vesicle core. This approach has been indeed successful for a number of NPs[42–47] (*Supplementary Table 4*). However, these NPs were mostly small inorganic NPs with diameters below 20 nm and the final liposome size ranging from 5-20 folds larger. When larger PLGA NPs (342 nm) were encapsulated, the final liposomal size was slightly larger (364 nm) indicating that a single particle was coated with the lipid bi-layer, as opposed to multiple NPs being encapsulated within the aqueous core. Here, in the vortex agitation method, liposomes formed were approximately 40 folds larger in diameter, indicating the encapsulation of several NPs with the aqueous core. The latter was confirmed by CLSM images (*Figure 3E, G and H*) that clearly show the incorporation of NPs into the liposomal core. In CLSM images, NPs appear red as a function of the loaded RB, whereas the liposomal bi-layers appear green due to their TopFluor Cholesterol content (FL-CHOL). The encapsulation of NPs into the liposomes has however resulted in an increase in Lip HD, where NP-Lip showed a HD of 4646 ± 3 nm and a ZP of -20 ± 5 mV (*Table 1*). The latter was confirmed by TEM images of NP-Lip (*Figure 3C and D*) and by SEM (*Supplementary Figure 3*). The EE% was also rather high when NP-Lips were prepared using 0.2 and 0.4 mg/ml PLGA NPs, where both concentrations resulted in an EE% of $98.4\% \pm 0.04$ and $98\% \pm 0.06$, respectively (*Table 1*). Accordingly, further work was conducted with liposomes prepared with the higher NP concentration (0.4 mg/ml), particularly since no increase in size was observed with the higher concentration. It is important to note that the EE% was

calculated for encapsulated NPs presented in the form of PLGA content, where it was assumed that the total amount of PLGA utilized in NP formulation successfully formed NPs. Notwithstanding, determination of the actual NP yield would be insightful.

Figure 4A shows comparative results of HD of Lip and NP-Lip upon storage for 14 days. Interestingly, Lip HD did not change over a period of 14 days. However, NP-Lip showed non-significant decrease in HD upon storage for 7 days, a significant reduction in the HD was observed after 14 days, possibly indicating the release of the loaded NPs. To confirm the latter, NP-Lips were stored for longer duration (5 weeks), following which particle size distribution was assessed by Malvern Zetasizer before and after centrifugation at 10752 rcf, 10°C for 10 minutes to separate Lip or NP-Lip from released NPs. *Figure 4B* shows the size distribution chart before centrifugation, showing two populations, the smaller one (approximately 100 nm) which represents released NPs, and the larger one representing NP-Lip. After centrifugation (*Figure 4C*), the peak intensity of the smaller population is reduced relative to the larger population. It could be hence speculated that the reduction of NP-Lip size seen with time was due to NP release. This release is only significant following storage for 14 days. Notwithstanding, CLSM assessment of the NP-Lip in which the NPs were loaded with a fluorophore would provide further confirmation.

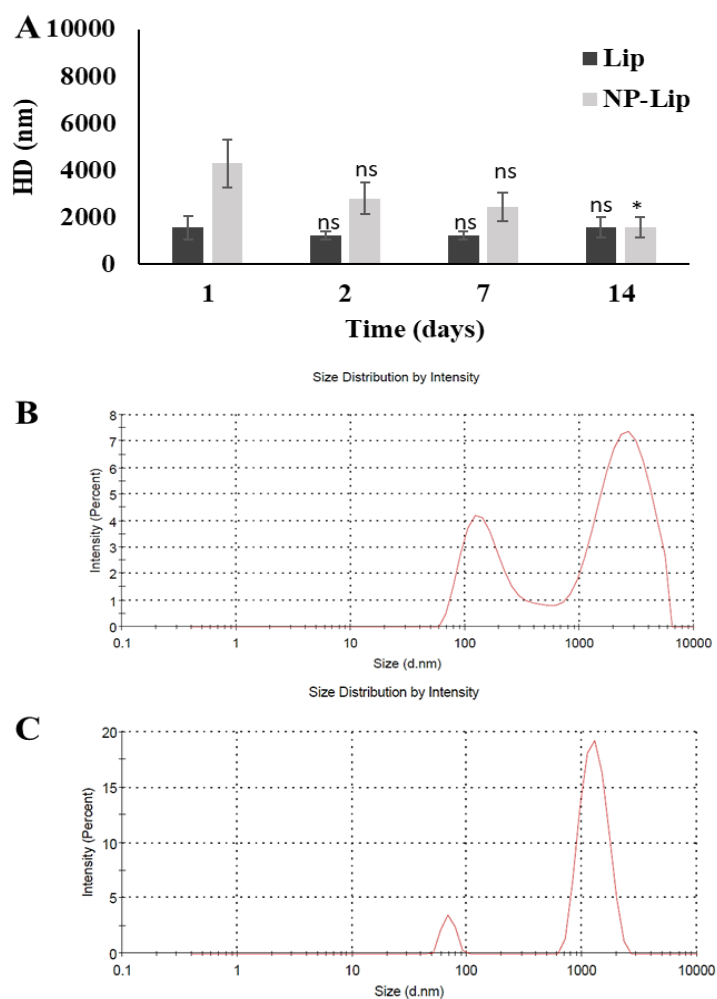


Figure 4. (A) HD of Lip and NP-Lip over a period of 14 days. Statistical analysis was performed by GraphPad InStat software using one-way ANOVA, where * $P < 0.05$, ** $P < 0.01$, and *** $P < 0.001$ relative to HD recorded at day 1. Size distribution charts obtained by Malvern Zetasizer for NP-Lip upon storage for 5 weeks before centrifugation **(B)**, and after centrifugation **(C)** at 10752 rcf, 10°C for 10 minutes to separate Lip or NP-Lip from released NPs

While liposomal antibiotic formulations have been shown to result in an enhancement of the antibacterial activity[40] in comparison to unencapsulated antibiotics, here the formulation of liposomes that directly incorporate Er and **3c** without prior incorporation in NPs were not intended. This is because the selected drugs are extremely hydrophobic[6,48]. Accordingly, upon fusion of the liposomes with bacterial outer membrane, the free drugs will be released into the periplasmic

space[39,49] and as a consequence captured by the efflux system and pumped out of the bacterial cell. In contrast, upon loading into NPs, the NPs can shield and deliver the antibiotics deep into the cytoplasm away from the efflux system.

In PLGA NPs, the encapsulated drug concentration corresponded to $250 \mu\text{g/ml} \pm 0.04$ and $50 \mu\text{g/ml} \pm 4.62$ for Er and **3c**, respectively, when NPs were formulated using 1 and 0.25 mg/ml of Er and **3c**, respectively. At these concentrations, NPs maintained their small size ($92 \pm 8 \text{ nm}$ and $64 \pm 3 \text{ nm}$ for Er-NPs and **3c**-NPs, respectively) (*Table 1*) and their morphology (*Supplementary Figure 4*). The use of higher drug concentrations resulted in an increase in particle size and aggregation. This possibly is due to the saturation of the polymer with the loaded drug. The latter becomes rather obvious when considering drug loading. For one mg of PLGA, an approximate amount of 1.25 mg of Er or 0.25 mg of **3c** were loaded. We have previously observed similar high loading efficiencies[22] and in that case, further increase in loaded drug concentration also resulted in aggregation. It is important to note that the centrifugation filter units utilized in the separation of free drugs from encapsulated drugs for EE% determination have been validated and it was confirmed that drugs are not retained within the filter unit (see Supplementary information file). *Table 1* summarizes the characterization of NPs, Lip and NP-Lip.

Table 1. Characterization of different nanocarriers under study.

	HD (nm) \pm SD	ZP (mV) \pm SD	EE% \pm SD	Drug: Polymer and/or lipids *
PLGA NPs	$83 \pm 1 \text{ nm}$	$-33 \pm 0.6 \text{ mV}$	-	-
Lip	$1304 \pm 8 \text{ nm}$	$-13.3 \pm 0.6 \text{ mV}$	-	-
3c-NPs	$64 \pm 3 \text{ nm}$	$-33 \pm 4 \text{ mV}$	$20\% \pm 4.62$	0.25 : 1
Er-NPs	$92 \pm 8 \text{ nm}$	$-21 \pm 3 \text{ mV}$	$25\% \pm 0.043$	1.25 : 1
NP-Lip	$4646 \pm 3 \text{ nm}$	$-20 \pm 5 \text{ mV}$	$98\% \pm 0.06^+$	-
3c-NP-Lip	$3683 \pm 12 \text{ nm}$	$-20 \pm 10 \text{ mV}$	$\approx 19.6\%^{\#}$	0.024:1

Er-NP-Lip	5130 ± 9 nm	-18±6 mV	≈ 24.5%#	0.125:1
------------------	-------------	----------	----------	---------

*Loaded drug : polymer and or lipid ratio expressed as weight: weight -*In terms of NPs - #calculated as percentage from total drug added during NP preparation

3.5.4.3 *In vitro* Cell Viability Assessment

As a polymer, PLGA is generally regarded as safe (GRAS)[50]. However, when formulated into NPs in some cases toxicity is observed[51]. Literature includes numerous examples in which cell treatment with PLGA NPs did not reveal significant losses in cell viability[52–54] and other cases in which cytotoxicity was observed[51]. It is worth noting that smaller particles (less than 100 nm) are usually more toxic than larger ones (more than 200 nm)[55]. In this work, PLGA NPs showed significant loss in viability in HEK293 cells, even at very low concentrations (*Figure 5A*). This cytotoxicity was greatly reduced upon encapsulation of NPs into Lip (*Figure 5B*). Two possible reasons might explain the difference in cytotoxicity observed. The first reason is the difference in extent of uptake between small NPs and the much larger Lips. In case NPs show much higher uptake, then it would be reasonable to show higher toxicity. For such reason, the extent of NP and NP-Lip uptake was compared. Following two hours incubation with HEK293 cells, the associated concentration corresponded to $0.4 \pm 0.06 \mu\text{g/ml}$ for NPs, while that for NP-Lip was undetectable (below $0.1 \mu\text{g/ml}$). Further confirmation of NP uptake by Confocal Laser Scanning Electron Microscopy (CLSM) would be insightful. It is noteworthy that the uptake experiment was conducted following two hours incubation only, since at this point significant cell death has not yet occurred (*Supplementary Figure 5*).

In addition to the higher uptake, another plausible reason is the residual Tween 80 content. In case the centrifugation filter units used were not able to eliminate all the excess Tween 80 in NPs, this residual surfactant would be expected to show toxicity

towards HEK293 cells. As indicated earlier larger PLGA NPs (more than 200 nm) usually show minimal *in vitro* cytotoxicity, at least when compared to their smaller counterparts (less than 200 nm)[52–54]. It is possible that the difference in toxicity is attributed to the higher uptake observed with smaller NPs[36], notwithstanding, the NP purification process might also contribute to that difference. It is important to note that due to their large size, larger NPs could be easily sedimented by centrifugation resulting in efficient purification of surfactant micelles that cannot pellet down at the same speed. However, since the NPs prepared here do not sediment even after centrifugation for prolonged times at high speed, their purification and concentration were conducted in centrifugation filter units. Residual tween 80 remains within the filter units even with membranes of high molecular weight cut-off (up to 1000 kDa), resulting in an increase in cytotoxicity. To demonstrate the latter, HEK293 cells were treated with solutions of Tween 80 that were exposed to the same purification steps as the plain NPs. This solution was then diluted with cell culture medium in an identical manner to NP suspension. When cells were incubated with Tween 80 in an amount that corresponds to 100 µg/ml NPs and above, a significant difference in HEK293 cell viability was not observed, indicating that at these concentrations the toxicity imparted was attributed to the free surfactant (*Figure 5A*). Surprisingly, at lower concentrations (10 and 50 µg/ml), NPs were more cytotoxic than free Tween 80. The latter was not expected, since when Tween 80 was used for the formulation of NPs, Tween 80 tails were incorporated within the PLGA matrix[56], making these molecules less available for HEK293 cell permeabilization and cell death[56]. It might be speculated that at lower concentrations, the toxicity imparted was a function of the NPs, while the toxicity observed with the higher amounts of NPs was attributed to increased amounts of free Tween 80. However, when NPs were

encapsulated into the liposomes, the Lip could be easily purified by centrifugation given their large size (approx. 4 μ m), enabling their separation from the Tween 80 micelles. Since Tween 80 has been reported to show bacteriostatic effects[57] and since NP-Lip showed reduced uptake and cytotoxicity in mammalian cells as exemplified here in HEK293 cells, it was decided to take an advantage of Tween 80 bacteriostatic effect and to reduce NP cytotoxicity towards HEK293 cells through their incorporation into liposomes without further attempts at NP purification. Similar results were observed with Er-NPs (*Figure 5C*) and **3c**-NPs (*Figure 5D*) when compared to Er-NP-Lip (*Figure 5E*) and **3c**-NP-Lip (*Figure 5F*). It is also worth noting that NP-Lip resulted in a reduction in Er toxicity (*Supplementary Figure 6A*). When HEK293 cells were however treated with free Er in combination with unloaded drug-free NP-Lip, higher losses in viability were observed (*Supplementary Figure 6B*) relative to those seen when HEK293 cells were treated with Er-NP-Lip, hence indicating that the encapsulation of Er into NP-Lip increases its safety towards HEK293 cells.

It is interesting to note that HEK293 cell viability was higher upon treatment with Er-NP-Lip in comparison to the corresponding unloaded formulation. While the exact underlying reason is yet to be determined. Desaki *et al.* demonstrated that Er treatment resulted in anti-inflammatory effects through the inhibition of the transcriptional factors including activator protein-1 (AP-1) and nuclear factor- κ B (NF- κ B) ultimately resulting in the reduction of the expression of interleukin-8 (IL-8) in human bronchial epithelial cells[58]. In addition, Takizawa *et al.* found that Er has been resulted in a dose-dependent reduction in interleukin-6 (IL-6) in human bronchial epithelial cells[59]. In both cases, the concentrations of Er tested were much lower than those tested here. In the case of Er-NP-Lip, the low cell association might

have resulted in a very low concentration of intracellular Er that resulted in similar results. To confirm this hypothesis, further investigations are however required.

The IC₅₀ values of Er, Er-NP-Lip, and **3c**-NP-Lip were corresponded to 808 ± 50.17, 1616 ± 59.55, and 155 ± 10.66 µg/ml, respectively in terms of drug concentration. Treatment of HEK293 cells with the free **3c** and the calculation of IC₅₀ for **3c** was not possible due to the drug's low solubility.

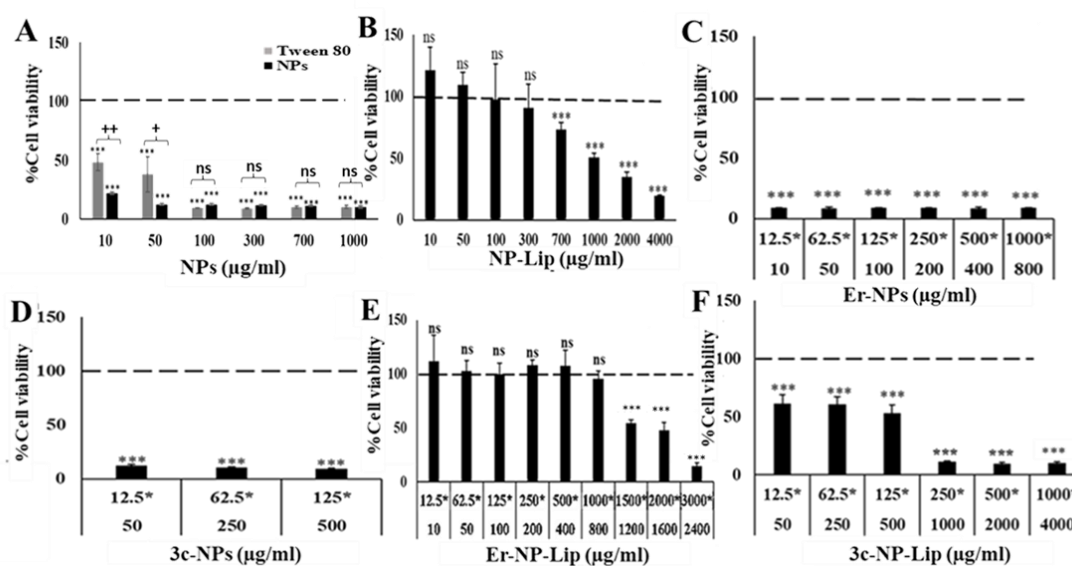


Figure 5: Percentage of HEK293 cell viability when treated with (A) NPs or the correspondent amount of Tween 80 (B) NP-Lip, (C) Er-NPs, (D) **3c**-NPs, (E) Er-NP-Lip, and (F) **3c**-NP-Lip for 24 hours. Concentrations in terms of drugs (Er or **3c**) are demonstrated with asterisks (*). Concentrations in terms of PLGA are expressed without asterisks (*)

3.5.4.4 *In vitro* Antimicrobial Susceptibility Testing towards Gram-negative Bacteria

Liposomes have been previously used to enhance the antimicrobial activity of certain drugs[60,61] Liposomal formulations of tobramycin, gentamicin, and amikacin reduced MICs towards a number of drug resistance strains of *Burkholderia cenocepacia* in comparison to free drugs[15]. In these cases, liposomal formulations were sufficient because the bacterial resistance (towards these drugs) was mainly the result of their inability to permeate the bacterial membrane and not their efflux via

efflux pumps[62]. In case, that these drugs were also subjected to drug efflux, then their release into the periplasm by the liposomes would not have been sufficient and an additive mechanism should be integrated to combat both resistance mechanisms. Within this context, literature includes examples of cases where the use of liposomes has been complemented with other mechanisms to account for drug efflux. For instance, drug efflux and low outer membrane permeability are the major mechanisms for bacterial resistance to fluoroquinolone antibiotics[63–65]. Fan *et al.* formulated levofloxacin loaded liposomes linked with short antimicrobial peptide (S-thanatin (Ts)) to combat the resistance of different clinical isolates of *Klebsiella pneumoniae*. Ts functions by altering of the electrical potential of the membrane, hence affecting the activity of the drug efflux pumps[66]. The authors reported that levofloxacin loaded liposomes were of lower efficacy in comparison to those modified with Ts[66]. In other cases, liposomes were loaded with very high drug concentrations to saturate the efflux pumps, allowing for the remaining drug molecules to reach their intracellular target[67].

NPs access the cytosol *via* different mechanisms than that utilized by free drugs[7]. Since the NPs themselves are not recognized by the drug efflux pumps, they are able to shield the drug along their journey to the cytosol, where the drug is then released away from the efflux pumps[8–11]. *Figure 6* shows the antibacterial effect of (A) Er, (B) Er-NP-Lip, (C) **3c**, (D) **3c**-NP-Lip towards *E. coli* DH5 α , *E. coli* K12, and *P. aeruginosa* when compared to untreated control cells. Both free drugs and drug loaded NP-Lip have resulted in reduction in bacterial cell viability. However, encapsulation of the drugs into NP-Lip seems to enhance their antibacterial effects. The latter is obvious by the reduction in MIC₅₀ values computed for free drugs and those loaded in NP-Lip (*Figure 6E* and *F*). It is worth noting, that in the case of **3c**, the

highest concentration tested (30 $\mu\text{g/ml}$) was not able to result in a viability loss lower than 50% in *P. aeruginosa*, and hence a MIC₅₀ value was not computed. The latter was however possible with 3c-NP-Lip, where a MIC₅₀ of 26 $\mu\text{g/ml}$ was obtained. It is worth noting that the results obtained are attributed to the encapsulated drugs, as opposed to drugs that have been released in cell culture/bacterial medium. The latter is based on results indicating minimum drug release from NP-Lip in cell culture and bacterial medium over a 24-hour period (*Supplementary Figure 7*).

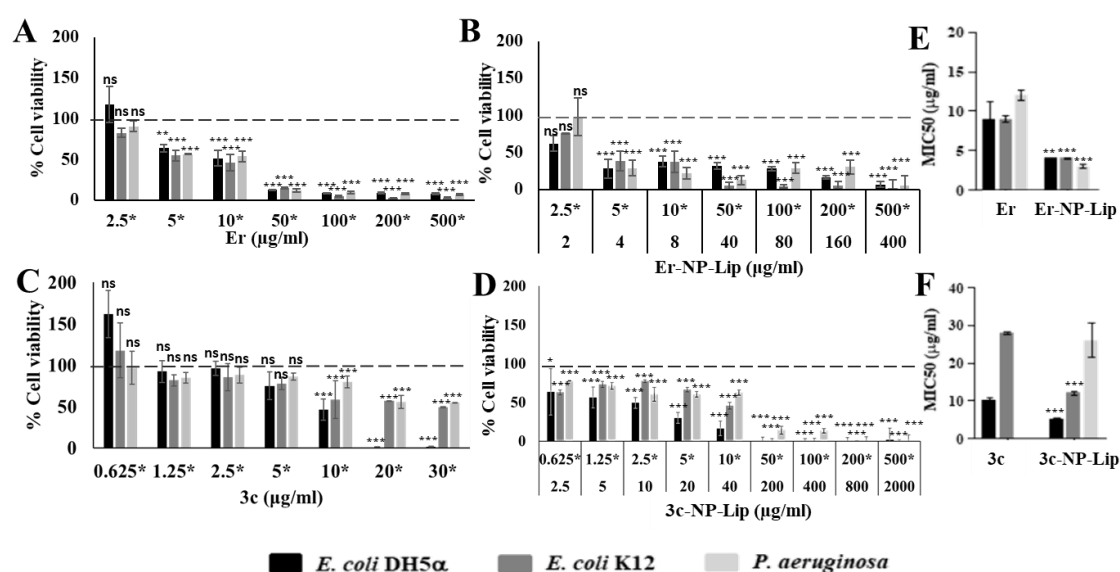


Figure 6: Percentage of Gram-negative bacteria viability when treated with (A) Er, (B) Er-NP-Lip, (C) 3c, (D) 3c-NP-Lip after 24 hours. Concentrations expressed in terms of drugs (Er or 3c) are demonstrated with an asterisk (*), while the concentrations expressed in terms of PLGA concentrations are expressed without an asterisk (*). MIC₅₀ upon treatment with (E) Er and Er- NP-Lip, (F) 3c and 3c-NP-Lip in terms of drug concentration. Statistical analysis was performed by GraphPad InStat software using one-way Anova, where *P < 0.05, **P < 0.01, and ***P < 0.001 relative to untreated control cells in A, B, C, and D and relative to free drug in E and F

Er was directly loaded into liposomes (*Supplementary information file*) and its ability to reduce cell viability of *E. coli* DH5 α , *E. coli* K12, and *P. aeruginosa* was assessed. *Supplementary Figure 8* shows that liposomes were less efficient than NP-Lip. The

latter indicated that Lips most probably release the drugs into the periplasmic space where they lie prey to drug efflux pumps. Within this context, TEM images of bacterial cells treated with Lip, NPs and NP-Lip would be rather insightful.

Interestingly, drug-less NP-Lip also showed an antibacterial effect. *Figure 7* shows the losses in bacterial viability upon treatment with unloaded NP-Lip in the same concentration range as those used in Er-NP-Lip (*Figure 7A*) and **3c**-NP-Lip (*Figure 7B*). In fact, unloaded NP-Lip showed a MIC₅₀ value (in terms of PLGA concentration) corresponding to 120 ± 10.08 , 66 ± 1.64 , and 249 ± 47.61 $\mu\text{g/ml}$ for *E. coli* DH5 α , *E. coli* K12, and *P. aeruginosa*. Tween 80 exhibits bacteriostatic effects[57], we therefore speculate that antibacterial effects of the blank formulations are due to the Tween 80 content. Experiments conducted with PLGA NPs incorporated in liposomes in which the NPs were formulated using other surfactants are however necessary for confirmation. Notwithstanding, literature includes other examples in which other nanostructures have resulted in a bacteriostatic effect in the absence of drugs[68–76]. Reasons for the antibacterial effects include; permeabilization of bacterial membranes[68,69], binding to DNA and inhibition of bacterial replication[70,76] and interference with electron transport chain[70,72]. With disregard to the reason behind the antibacterial effects of the unloaded NP-Lip, it is important to note that for both drug loaded and unloaded NP-Lip, MIC₅₀ values towards *E. coli* DH5 α , *E. coli* K12, and *P. aeruginosa* were much lower than those obtained in HEK293 cells. *Figure 7C* presents a comparison between the IC₅₀ values of Er, Er-NP-Lip, **3c**-NP-Lip towards HEK293 cells, *E. coli* DH5 α , *E. coli* K12, and *P. aeruginosa*. It becomes very obvious that the 50% inhibitory concentration of free Er was lowered by the drug loading towards bacterial cells, while it was significantly increased towards HEK293 cells meaning that drug loaded formulation enabled minimal association to human cells and maximum

interaction with bacterial cells in comparison to Er. A similar comparison between **3c** and **3c**-NP-Lip was not possible, due to the poor solubility of **3c**. Notwithstanding, it is important to highlight that NP-Lips have made the administration of **3c** possible that was not possible in its free form.

It is reasonable to debate that Er in its free form was already less toxic towards HEK293 cells in comparison to bacterial cells, which questions the need for encapsulation in NP-Lip. *Figure 7D* shows the selectivity index (SI) for free Er and Er-NP-Lip taking into account the MIC₅₀ against *E. coli* DH5 α , *E. coli* K12, *P. aeruginosa* and the IC₅₀ on HEK293 cells ($SI=IC_{50}/MIC_{50}$)[51]. *Figure 7D* reveals that while free Er showed IC₅₀ values that were 90 folds higher than its MIC₅₀ value in *E. coli* (both strains), Er-NP-Lip showed 404 folds difference indicating that the formulation improves Er effectiveness while maintaining its safety towards human cell by 4 folds. For *P. aeruginosa*, while free Er showed IC₅₀ value that was 67 folds higher than its MIC₅₀ value, Er-NP-Lip showed 539 folds difference (8 folds) meaning that Er liposomal formulation was able to increase the selectivity of the free Er towards bacteria in addition to enhancement its safety profile. This indicates that encapsulation of Er in NP-Lip can allow treatment with much higher concentration than in the free form. This is in addition to the ability of the formulation in enhancing the drug's pharmacokinetic profile and enable drug targeting[77].

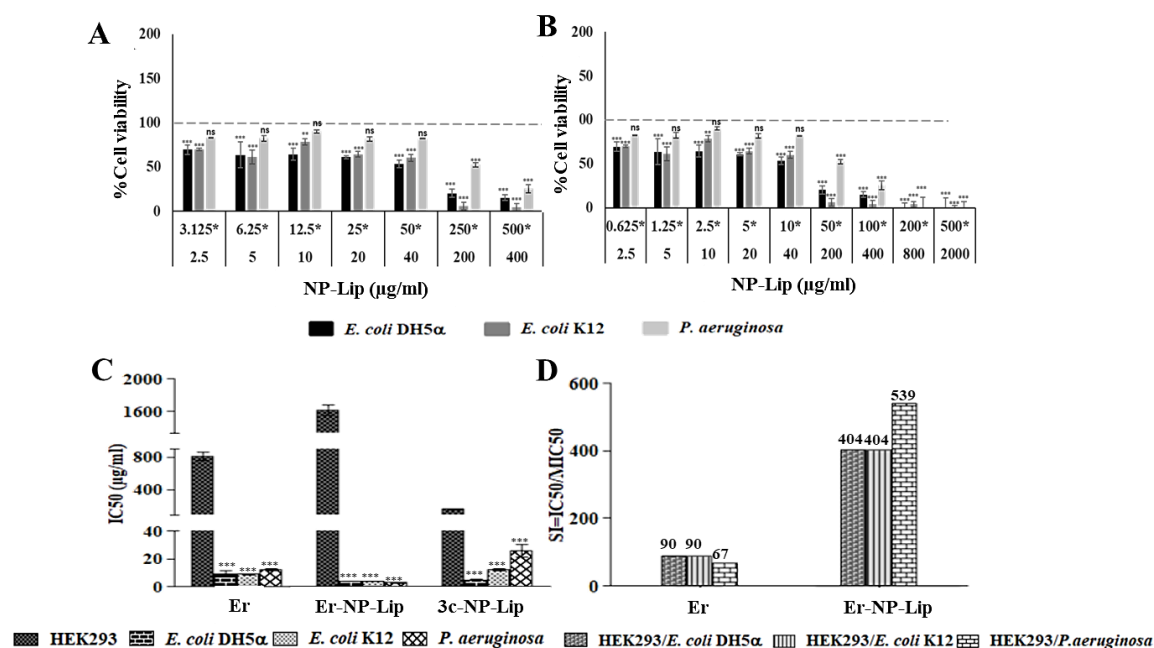


Figure 7: Percentage of Gram-negative bacteria viability when treated with unloaded NP-Lip for 24 hours at the same concentrations of (A) Er-NP-Lip, (*) corresponds to concentrations expressed in terms of Er, (B) 3c-NP-Lip, (*) corresponds to concentrations expressed in terms of 3c. (C) IC₅₀ values of Er, Er-NP-Lip, 3c-NP-Lip on HEK293 cells and *E. coli* DH5α, *E. coli* K12, and *P. aeruginosa*. and (D) Selectivity indexes (SI=IC₅₀/MIC₅₀) of free Er and Er -NP-Lip. Statistical analysis was performed by GraphPad InStat software using one-way ANOVA, where *P < 0.05, **P < 0.01, and ***P < 0.001 relative to untreated control bacterial cells in (A, B) and relative to HEK293 cells in (C)

3.5.4.5 *In vivo* Antimicrobial Susceptibility of *P. aeruginosa*

On an *in vitro* level, NP-Lips have addressed the low solubility of 3c enabling cell treatment with higher concentrations than those allowed by the free drug. In addition, NP-Lips increased the selectivity index of Er. However, how would NP-Lip perform *in vivo*? It is initially necessary to acknowledge that due to the liposomes' large size, their phagocytosis following intravenous administration is very likely[78–80]. The latter is not entirely undesirable. In fact, circulating phagocytes are summoned to the infection site[81] and may therefore act as Trojan horses, delivering the drugs to the site of infection[82]. An alternative application is their local administration, such into the eye. For treatment of ophthalmic conditions, the topical route is the easiest and is the

most frequently used. However, the blink reflex and the rapid renewal of the lachrymal fluid, eliminates most of the drugs administered topically[83]. The latter indicates the need to increase drug residence time in the eye. Bacterial keratitis is a major cause of ocular morbidity. *P. aeruginosa* keratitis is a destructive disease of the cornea and is the major cause of the contact lens-related ulcerative keratitis[84]. The disease is characterized by a rapid inflammatory response accompanied by suppurative coagulative necrosis, that often leads to irreversible damage of the corneal architecture, leading to vision loss[85]. Bacterial keratitis is currently controlled by topical administration of antibiotics[85]. However, the constant emergence of antibiotic resistant bacteria poses a serious challenge for effective management[85], additionally low drug concentrations in the eye and low ocular residence time also contribute to the ineffectiveness of therapy[86]. Hence, treatment modalities that could overcome antibiotic MDR and increase residence time in the eye are highly needed. These modalities should also enable increased interaction of the drug with the target[87]. In case of *P. aeruginosa* keratitis, the target is *P. aeruginosa* residing in the pre-corneal space. To determine whether NP-Lip would address the aforementioned points, a *P. aeruginosa* induced keratitis mouse model was developed as detailed in[27]. Model optimization and validation are detailed in the Supplementary information file (*Supplementary Figure 9*). Animals were treated twice daily with topical eye drops of either free Er, Er-NPs, or Er-NP-Lip at a dose of 200 µg of Er. This dose was selected based on previous reports employing macrolide antibiotics in the topical therapy of keratitis[88]. Animals were also treated with an equivalent amount of blank NPs and NP-Lip. Treatment with free **3c** was not possible due the drug's limited solubility. Treatment with **3c**-NP-Lip was however possible in which animals received a dose equivalent to 100 µg. Since to date to the best of our

knowledge, this trial represents the first attempt to administer **3c** *in vivo*, a reference dose was not available, here a dose of 100 µg was selected since this dose was delivered by the same amount of NP-Lip used for the administration of Er and was hence considered as a pilot attempt.

Figure 8A shows the reduction in *P. aeruginosa* viability following treatment for 4 days. Er, Er-NPs, Er-NP-Lip and **3c**-NP-Lip all result in strong antibacterial effects. However, histopathological and clinical investigations of the eyes in *Figure 8B-P* show that while Er-NPs, Er-NP-Lip and **3c**-NP-Lip were able to reverse the histopathological changes that have occurred in the infected eyes, Er treated eyes still showed clear signs of inflammation. The latter indicates the superior antibacterial effects exerted by both NPs and NP-Lip which could be attributed to their ability to reduce MDR and/or increase drug residence time in the eye. While the former has been clearly demonstrated by the *in vitro* results reported herein, the latter would be demonstrated by animal trials, considering dosing regimens with less frequent treatments and/or a reduced dose. These trials would also be necessary to demonstrate whether from an anti-bacterial standpoint Er-NP-Lip are superior to Er-NPs.

Two interesting observations have also been made, the first is that **3c**-NP-Lip showed better antibacterial effects than Er-NP-Lip (*Figure 8A*), even at a much lower drug dose. While a direct comparison of the antibiotic efficacy is not intended, the results clearly show how the ability of NPs to address poor drug solubility might in fact be the solution to numerous drugs with very promising portfolios, but their clinical benefit has not been yet reaped due to their poor solubility and *in vivo* stability. The second is that blank NPs and NP-Lip showed a similar antibacterial effect to drug

loaded ones. The latter would enable antibiotic free antibacterial therapy, which might also address the bacterial resistance dilemma.

If NPs and NP-Lips are both effective, does this indicate that the encapsulation of NPs in liposomes is not necessary? *Figure 9* shows the expression levels of TNF-alpha and IL-6 in eyes obtained from healthy mice. Treatment with plain PLGA NPs causes ocular inflammation showing significant elevation of TNF-alpha and IL-6 compared to healthy control group. The encapsulation of NPs in Lip reduced the expression of both cytokines. In fact, treatment with PLGA NPs has been reported to result in an increase of TNF- α production by macrophages[89]. Interestingly, this increases with an increase in particle size, since macrophages are more efficient in the uptake of larger NPs, even those larger than 5-6 μm [89]. Since in this experiment healthy animals were utilized, one could speculate that the excessive production of TNF-alpha and IL-6 observed with NPs was not attributed to uptake by ocular phagocytes, since NP-Lip would show higher uptake[89], but by alternative cells. Retinal pigment epithelial (RPE) forms part of the blood-retina barrier cells. These cells are potent producers of inflammatory cytokines and hence play an important role in the pathogenesis of ocular inflammation[90], and the production of inflammatory cytokines[90]. NP uptake by the RPE following topical application has been reported[91] and seems to diminish with the increase in NP size[92]. The latter is underpinned by the numerous attempts of drug delivery to the RPE that have utilized small NPs (less than 200 nm)[91,93-95] and by the complexity of the corneal barriers. The cornea consists of five layers: the epithelium, the Bowman's layer, the stroma, the Descemet's membrane, and the endothelium, each of different composition and blocks different types of molecules according to their lipophilicity. This would indeed indicate why NP-Lip showed lower inflammatory cytokine production than the much

smaller NPs. Since here drug delivery to the RPE is not required, given the extracellular nature of the infection[28], the use of NP-Lip is probably more suited to the cause.

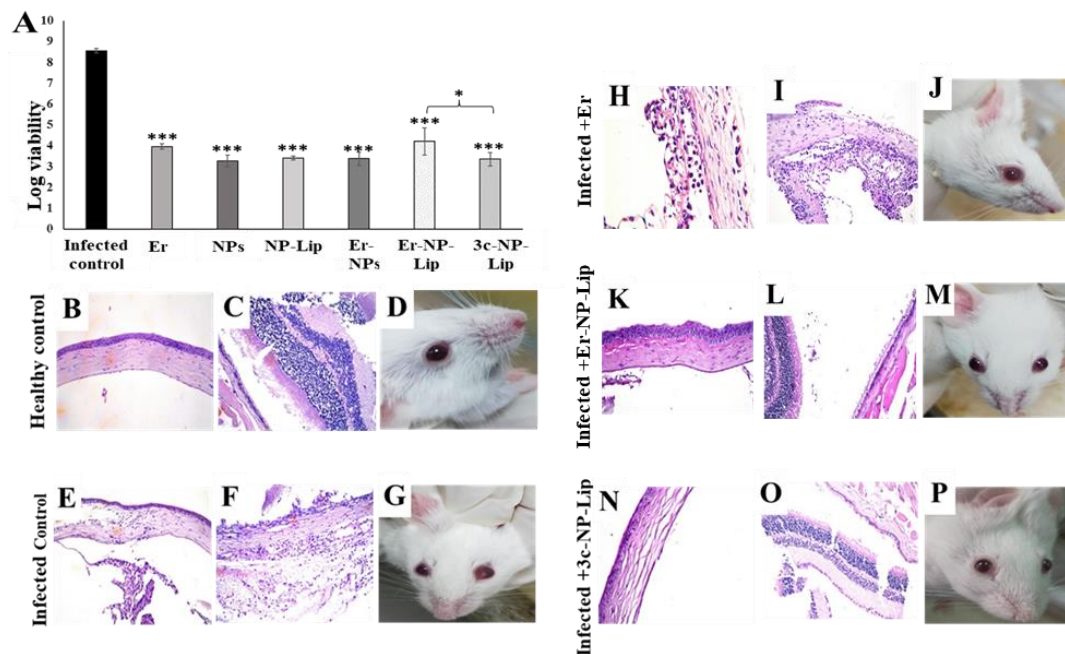


Figure 8: (A) Log viability of *P. aeruginosa* upon treatment with free Er, NPs, NP-Lip, Er-NP, Er-NP-Lip and 3c-NP-Lip. Statistical analysis was performed by GraphPad InStat software using one-way ANOVA, where * $P < 0.05$, ** $P < 0.01$, and *** $P < 0.001$ relative to infected untreated control cells. Histological and clinical examination of mouse eyes from healthy controls (B-D) showing (B) normal histological structure of the cornea (C) retina, choroid and sclera and (D) normal appearance of eyes with no signs of inflammation nor corneal opacity. Infected controls (E-G) showing (E) inflammatory cell infiltration in the stroma of cornea is observed and (F) sclera infiltration by leucocytic inflammatory cells with (G) eyes showing clear corneal opacity. Infected animal receiving Er (H-J) showing (H) edema with focal inflammatory cell infiltration in the stroma of sclera (I) and iris (J) with no corneal opacity. Infected animals treated with Er-NP-Lip (K-M) and 3c-NP-Lip (N-P) show normal histological structures in the cornea, iris, retina choroid and sclera, with eyes showing no signs of inflammation or opacity

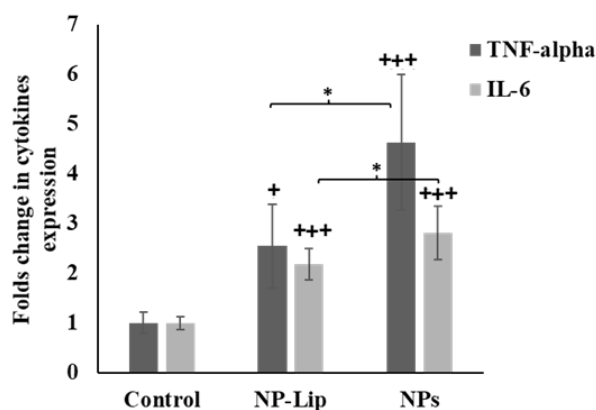


Figure 9: Folds change in TNF-alpha and IL-6 expression relative to the untreated control upon treatment with unloaded NP-Lip and NPs. Statistical analysis was performed by GraphPad InStat software using one-way ANOVA, where *P < 0.05, **P < 0.01, and ***P < 0.001. Asterisks expressed with (+) represent statistics relative to untreated control

3.5.5 Conclusion

In this work, small NPs have been successfully loaded into larger liposomes (NP-Lip), with the main aim of delivering antibiotics into Gram-negative bacteria whilst minimizing the concomitant increased drug allocation in human cells. In comparison to small NPs, NP-Lip have indeed resulted in a reduction in association to HEK293 cells and increased one in *E. coli* DH5 α , *E. coli* K12, and *P. aeruginosa*. More specifically, Er-NP-Lip has resulted in an enhancement of antibiotic selectivity by 4 folds towards *E. coli* DH5 α and *E. coli* K12 and 8 folds towards *P. aeruginosa*. This significant reduction in cytotoxicity towards mammalian cells through the NP-Lip encapsulation, would allow the administration of higher doses of the antibiotics, thus greatly enhancing their therapeutic effect. Additionally, blank drugless NP-Lip showed a potent selective antibacterial effect. This toxicity towards bacteria was not observed in HEK293 cells due to the selective particle uptake. Ocular administration of NP-Lip in a *P. aeruginosa* keratitis mouse model demonstrated the ability of both unloaded NP-Lip and those loaded with Er and **3c** to result in a complete recovery, with drug

loaded NP-Lips showing a superior ability in the reduction of the infection associated with inflammation relative to free Er. It is important to note that in the conducted trials, the available therapeutic window was probably not fully exploited, thus preventing the additional antibiotic effect of the drugs from becoming evident. In this context, treatment with alternative dosing regimens would be insightful. More importantly NP-Lip enabled the *in vivo* administration of **3c**, a promising antibiotic whose therapeutic potential has not been realized due to its poor solubility and stability. On a final note, this work demonstrated how tailoring the nano-bio interaction could result in selective drug delivery and a reduction in unwanted off-target effects.

3.5.6 References

- (1) Ventola, C.L. The antibiotic resistance crisis: part 1: causes and threats. *P T* **2015**, *40*, 277–83.
- (2) Masi, M.; Réfregiers, M.; Pos, K.M.; Pagès, J.-M. Mechanisms of envelope permeability and antibiotic influx and efflux in Gram-negative bacteria. *Nat. Microbiol.* **2017**, *2*, 17001, doi:10.1038/nmicrobiol.2017.1.
- (3) Ofek, I.; Cohen, S.; Rahmani, R.; Kabha, K.; Tamarkin, D.; Herzig, Y.; Rubinstein, E. Antibacterial synergism of polymyxin B nonapeptide and hydrophobic antibiotics in experimental gram-negative infections in mice. *Antimicrob. Agents Chemother.* **1994**, *38*, 374–377, doi:10.1128/AAC.38.2.374.
- (4) Chollet, R.; Chevalier, J.; Bryskier, A.; Pagès, J.-M. The AcrAB-TolC Pump Is Involved in Macrolide Resistance but Not in Telithromycin Efflux in *Enterobacter aerogenes* and *Escherichia coli*. *Antimicrob. Agents Chemother.* **2004**, *48*, 3621–3624, doi:10.1128/AAC.48.9.3621-3624.2004.
- (5) Li, X.-Z.; Zhang, L.; Poole, K. Interplay between the MexA-MexB-OprM multidrug efflux system and the outer membrane barrier in the multiple antibiotic resistance of *Pseudomonas aeruginosa*. *J. Antimicrob. Chemother.* **2000**, *45*, 433–436, doi:10.1093/jac/45.4.433.

- (6) Francisco, G.D.; Li, Z.; Albright, J.D.; Eudy, N.H.; Katz, A.H.; Petersen, P.J.; Labthavikul, P.; Singh, G.; Yang, Y.; Rasmussen, B.A.; *et al.* Phenyl thiazolyl urea and carbamate derivatives as new inhibitors of bacterial cell-wall biosynthesis. *Bioorg. Med. Chem. Lett.* **2004**, *14*, 235–238, doi:10.1016/j.bmcl.2003.09.082.
- (7) Kumar, A.; Pandey, A.K.; Singh, S.S.; Shanker, R.; Dhawan, A. Cellular uptake and mutagenic potential of metal oxide nanoparticles in bacterial cells. *Chemosphere* **2011**, *83*, 1124–1132, doi:10.1016/j.chemosphere.2011.01.025.
- (8) Wang, L.; Hu, C.; Shao, L. The antimicrobial activity of nanoparticles: present situation and prospects for the future. *Int. J. Nanomedicine* **2017**, *Volume 12*, 1227–1249, doi:10.2147/IJN.S121956.
- (9) Tammam, S.N. Lipid Based Nanoparticles as Inherent Reversing Agents of Multidrug Resistance in Cancer. *Curr. Pharm. Des.* **2018**, *23*, 6714–6729, doi:10.2174/1381612823666171122104738.
- (10) Vauthier, C. Drug delivery to resistant tumors: the potential of poly(alkyl cyanoacrylate) nanoparticles. *J. Control. Release* **2003**, *93*, 151–160, doi:10.1016/j.jconrel.2003.08.005.
- (11) Cuvier, C.; Roblot-Treupel, L.; Millot, J.M.; Lizard, G.; Chevillard, S.; Manfait, M.; Couvreur, P.; Poupon, M.F. Doxorubicin-loaded nanospheres bypass tumor cell multidrug resistance. *Biochem. Pharmacol.* **1992**, *44*, 509–517, doi:10.1016/0006-2952(92)90443-M.
- (12) Zhang, R.X.; Li, J.; Zhang, T.; Amini, M.A.; He, C.; Lu, B.; Ahmed, T.; Lip, H.; Rauth, A.M.; Wu, X.Y. Importance of integrating nanotechnology with pharmacology and physiology for innovative drug delivery and therapy – an illustration with firsthand examples. *Acta Pharmacol. Sin.* **2018**, *39*, 825–844, doi:10.1038/aps.2018.33.
- (13) Wei, W.-H.; Dong, X.-M.; Liu, C.-G. In Vitro Investigation of Self-Assembled Nanoparticles Based on Hyaluronic Acid-Deoxycholic Acid Conjugates for Controlled Release Doxorubicin: Effect of Degree of Substitution of Deoxycholic Acid. *Int. J. Mol. Sci.* **2015**, *16*, 7195–7209, doi:10.3390/ijms16047195.
- (14) Shang, L.; Nienhaus, K.; Nienhaus, G. Engineered nanoparticles interacting with cells: size matters. *J. Nanobiotechnology* **2014**, *12*, 5, doi:10.1186/1477-3155-12-5.

- (15) Halwani, M.; Mugabe, C.; Azghani, A.O.; Lafrenie, R.M.; Kumar, A.; Omri, A. Bactericidal efficacy of liposomal aminoglycosides against Burkholderia cenocepacia. *J. Antimicrob. Chemother.* **2007**, *60*, 760–769, doi:10.1093/jac/dkm289.
- (16) Ma, Y.; Wang, Z.; Khalil, H.; Wang, R.; Lu, T.; Zhao, W.; Zhang, Y.; Chen, T.; Chen, J. Fusion between fluid liposomes and intact bacteria: study of driving parameters and in vitro bactericidal efficacy. *Int. J. Nanomedicine* **2016**, *Volume 11*, 4025–4036, doi:10.2147/IJN.S55807.
- (17) Markin, V. S., & Kozlov, M. M. (1984). Theory of membrane fusion. Adhesion-condensation mechanism. *Biophysics*, *29*(2), 265-270.
- (18) Zgoda, J.R.; Porter, J.R. A Convenient Microdilution Method for Screening Natural Products Against Bacteria and Fungi. *Pharm. Biol.* **2001**, *39*, 221–225, doi:10.1076/phbi.39.3.221.5934.
- (19) Spork, A.P.; Büschleb, M.; Ries, O.; Wiegmann, D.; Boettcher, S.; Mihalyi, A.; Bugg, T.D.H.; Ducho, C. Lead Structures for New Antibacterials: Stereocontrolled Synthesis of a Bioactive Muraymycin Analogue. *Chem. - A Eur. J.* **2014**, *20*, 15292–15297, doi:10.1002/chem.201404775.
- (20) Kızılbey, K. Optimization of Rutin-Loaded PLGA Nanoparticles Synthesized by Single-Emulsion Solvent Evaporation Method. *ACS Omega* **2019**, *4*, 555–562, doi:10.1021/acsomega.8b02767.
- (21) Valle, M.J.; Navarro, A. Liposomes Prepared in Absence of Organic Solvents: Sonication Versus Lipid Film Hydration Method. *Curr. Pharm. Anal.* **2015**, *11*, 86–91, doi:10.2174/1573412910666141114221935.
- (22) El-Safy, S.; Tammam, S.N.; Abdel-Halim, M.; Ali, M.E.; Youshia, J.; Shetab Boushehri, M.A.; Lamprecht, A.; Mansour, S. Collagenase loaded chitosan nanoparticles for digestion of the collagenous scar in liver fibrosis: The effect of chitosan intrinsic collagen binding on the success of targeting. *Eur. J. Pharm. Biopharm.* **2020**, *148*, 54–66, doi:10.1016/j.ejpb.2020.01.003.
- (23) Lorscheidt, S.; Shetab Boushehri, M.A.; Klaschik, S.; Lamprecht, A. Sub-cytotoxic doses of pharmaceutical silica nanoparticles show significant impact on the proteome of HepG2 cells. *J. Control. Release* **2019**, *306*, 1–14, doi:10.1016/j.jconrel.2019.05.033.

- (24) Azzam, M.; El Safy, S.; Abdelgelil, S.A.; Weiskirchen, R.; Asimakopoulou, A.; de Lorenzi, F.; Lammers, T.; Mansour, S.; Tammam, S. Targeting Activated Hepatic Stellate Cells Using Collagen-Binding Chitosan Nanoparticles for siRNA Delivery to Fibrotic Livers. *Pharmaceutics* **2020**, *12*, 590, doi:10.3390/pharmaceutics12060590.
- (25) Ungaro, F.; D'Angelo, I.; Coletta, C.; d'Emmanuele di Villa Bianca, R.; Sorrentino, R.; Perfetto, B.; Tufano, M.A.; Miro, A.; La Rotonda, M.I.; Quaglia, F. Dry powders based on PLGA nanoparticles for pulmonary delivery of antibiotics: Modulation of encapsulation efficiency, release rate and lung deposition pattern by hydrophilic polymers. *J. Control. Release* **2012**, *157*, 149–159, doi:10.1016/j.jconrel.2011.08.010.
- (26) Determination of minimum inhibitory concentrations (MICs) of antibacterial agents by broth dilution. *Clin. Microbiol. Infect.* **2003**, *9*, ix–xv, doi:10.1046/j.1469-0691.2003.00790.x.
- (27) Fukuda, K.; Ishida, W.; Uchiyama, J.; Rashel, M.; Kato, S.; Morita, T.; Muraoka, A.; Sumi, T.; Matsuzaki, S.; Daibata, M.; *et al.* Pseudomonas aeruginosa Keratitis in Mice: Effects of Topical Bacteriophage KPP12 Administration. *PLoS One* **2012**, *7*, e47742, doi:10.1371/journal.pone.0047742.
- (28) Amorena, B.; Gracia, E.; Monzón, M.; Leiva, J.; Oteiza, C.; Pérez, M.; Alabart, J.-L.; Hernández-Yago, J. Antibiotic susceptibility assay for Staphylococcus aureus in biofilms developed in vitro. *J. Antimicrob. Chemother.* **1999**, *44*, 43–55, doi:10.1093/jac/44.1.43.
- (29) Bancroft, J.D.; Stevens, A. and Turner, D.R. (1996). Theory and practice of histological techniques. Fourth ed. Churchill Livingstone, New York, London, San Francisco, Tokyo.
- (30) Mokbel, S.A.; Fathalla, R.K.; El-Sharkawy, L.Y.; Abadi, A.H.; Engel, M.; Abdel-Halim, M. Synthesis of novel 1,2-diarylpyrazolidin-3-one-based compounds and their evaluation as broad spectrum antibacterial agents. *Bioorg. Chem.* **2020**, *99*, 103759, doi:10.1016/j.bioorg.2020.103759.
- (31) Zavascki, A.P.; Goldani, L.Z.; Li, J.; Nation, R.L. Polymyxin B for the treatment of multidrug-resistant pathogens: a critical review. *J. Antimicrob. Chemother.* **2007**, *60*, 1206–1215, doi:10.1093/jac/dkm357.

- (32) Kumar, A.; Pandey, A.K.; Singh, S.S.; Shanker, R.; Dhawan, A. A flow cytometric method to assess nanoparticle uptake in bacteria. *Cytom. Part A* **2011**, n/a-n/a, doi:10.1002/cyto.a.21085.
- (33) Preparation and evaluation of chitosan-tripolyphosphate nanoparticles suspension as an antibacterial agent. *J. Appl. Pharm. Sci.* **2018**, *8*, 147–156, doi:10.7324/JAPS.2018.81217.
- (34) Lu, Z.; Rong, K.; Li, J.; Yang, H.; Chen, R. Size-dependent antibacterial activities of silver nanoparticles against oral anaerobic pathogenic bacteria. *J. Mater. Sci. Mater. Med.* **2013**, *24*, 1465–1471, doi:10.1007/s10856-013-4894-5.
- (35) Guo, L.; Wang, H.; Wang, Y.; Liu, F.; Feng, L. Organic Polymer Nanoparticles with Primary Ammonium Salt as Potent Antibacterial Nanomaterials. *ACS Appl. Mater. Interfaces* **2020**, *12*, 21254–21262, doi:10.1021/acsami.9b19921.
- (36) Oh, E.; Delehanty, J.B.; Sapsford, K.E.; Susumu, K.; Goswami, R.; Blanco-Canosa, J.B.; Dawson, P.E.; Granek, J.; Shoff, M.; Zhang, Q.; *et al.* Cellular Uptake and Fate of PEGylated Gold Nanoparticles Is Dependent on Both Cell-Penetration Peptides and Particle Size. *ACS Nano* **2011**, *5*, 6434–6448, doi:10.1021/nn201624c.
- (37) Prabha, S.; Arya, G.; Chandra, R.; Ahmed, B.; Nimesh, S. Effect of size on biological properties of nanoparticles employed in gene delivery. *Artif. Cells, Nanomedicine, Biotechnol.* **2016**, *44*, 83–91, doi:10.3109/21691401.2014.913054.
- (38) Markin, V. S.; Kozlov, M. M. Theory of Membrane Fusion. Adhesion-Condensation Mechanism. *Biophysics (Oxf)*. 1984, *29* (2), 265–270.
- (39) Zhang, L.; Pornpattananangkul, D.; Hu, C.-M.; Huang, C.-M. Development of Nanoparticles for Antimicrobial Drug Delivery. *Curr. Med. Chem.* **2010**, *17*, 585–594, doi:10.2174/092986710790416290.
- (40) Mugabe, C.; Halwani, M.; Azghani, A.O.; Lafrenie, R.M.; Omri, A. Mechanism of Enhanced Activity of Liposome-Entrapped Aminoglycosides against Resistant Strains of *Pseudomonas aeruginosa*. *Antimicrob. Agents Chemother.* **2006**, *50*, 2016–2022, doi:10.1128/AAC.01547-05.
- (41) Tammam, S.N.; Lamprecht, A. Nanostructures in Drug Delivery. In *Pharmaceutical Nanotechnology: Innovation and Production*; Wiley-VCH Verlag GmbH & Co. KGaA: Weinheim, Germany, 2016; pp. 101–134.

- (42) Martina, M.-S.; Fortin, J.-P.; Ménager, C.; Clément, O.; Barratt, G.; Grabielle-Madelmont, C.; Gazeau, F.; Cabuil, V.; Lesieur, S. Generation of Superparamagnetic Liposomes Revealed as Highly Efficient MRI Contrast Agents for in Vivo Imaging. *J. Am. Chem. Soc.* **2005**, *127*, 10676–10685, doi:10.1021/ja0516460.
- (43) Wang, H.; Zhao, P.; Su, W.; Wang, S.; Liao, Z.; Niu, R.; Chang, J. PLGA/polymeric liposome for targeted drug and gene co-delivery. *Biomaterials* **2010**, *31*, 8741–8748, doi:10.1016/j.biomaterials.2010.07.082.
- (44) Benyettou, F.; Chebbi, I.; Motte, L.; Seksek, O. Magnetoliposome for alendronate delivery. *J. Mater. Chem.* **2011**, *21*, 4813, doi:10.1039/c1jm00060h.
- (45) Prassl, R.; Frascione; Diwooky; Almer; Opriessnig; Vonach; Gradauer; Leitinger; Mangge; Stollberger Ultrasmall superparamagnetic iron oxide (USPIO)-based liposomes as magnetic resonance imaging probes. *Int. J. Nanomedicine* **2012**, 2349, doi:10.2147/IJN.S30617.
- (46) Kulshrestha, P.; Gogoi, M.; Bahadur, D.; Banerjee, R. In vitro application of paclitaxel loaded magnetoliposomes for combined chemotherapy and hyperthermia. *Colloids Surfaces B Biointerfaces* **2012**, *96*, 1–7, doi:10.1016/j.colsurfb.2012.02.029.
- (47) Giri, J.; Guha Thakurta, S.; Bellare, J.; Kumar Nigam, A.; Bahadur, D. Preparation and characterization of phospholipid stabilized uniform sized magnetite nanoparticles. *J. Magn. Magn. Mater.* **2005**, *293*, 62–68, doi:10.1016/j.jmmm.2005.01.044.
- (48) Bryskier, A.; Bergogne-Bérézin, E. Macrolides. In *Antimicrobial Agents*; ASM Press: Washington, DC, USA, 2014; pp. 475–526.
- (49) *Nanotechnology Applied To Pharmaceutical Technology*; Rai, M., Alves dos Santos, C., Eds.; Springer International Publishing: Cham, 2017; ISBN 978-3-319-70298-8.
- (50) Han, F.Y.; Thurecht, K.J.; Whittaker, A.K.; Smith, M.T. Bioerodable PLGA-Based Microparticles for Producing Sustained-Release Drug Formulations and Strategies for Improving Drug Loading. *Front. Pharmacol.* **2016**, *7*, doi:10.3389/fphar.2016.00185.
- (51) Ibrahim, W.N.; Muizzuddin Bin Mohd Rosli, L.; Doolaanea, A.A. Formulation, Cellular Uptake and Cytotoxicity of Thymoquinone-Loaded PLGA Nanoparticles

- in Malignant Melanoma Cancer Cells. *Int. J. Nanomedicine* **2020**, Volume 15, 8059–8074, doi:10.2147/IJN.S269340.
- (52) Xiong, S.; George, S.; Yu, H.; Damoiseaux, R.; France, B.; Ng, K.W.; Loo, J.S.-C. Size influences the cytotoxicity of poly (lactic-co-glycolic acid) (PLGA) and titanium dioxide (TiO₂) nanoparticles. *Arch. Toxicol.* **2013**, *87*, 1075–1086, doi:10.1007/s00204-012-0938-8.
- (53) Semete, B.; Booysen, L.; Lemmer, Y.; Kalombo, L.; Katata, L.; Verschoor, J.; Swai, H.S. In vivo evaluation of the biodistribution and safety of PLGA nanoparticles as drug delivery systems. *Nanomedicine Nanotechnology, Biol. Med.* **2010**, *6*, 662–671, doi:10.1016/j.nano.2010.02.002.
- (54) Basarkar, A.; Devineni, D.; Palaniappan, R.; Singh, J. Preparation, characterization, cytotoxicity and transfection efficiency of poly(dl-lactide-co-glycolide) and poly(dl-lactic acid) cationic nanoparticles for controlled delivery of plasmid DNA. *Int. J. Pharm.* **2007**, *343*, 247–254, doi:10.1016/j.ijpharm.2007.05.023.
- (55) Chiu, H.I.; Samad, N.A.; Fang, L.; Lim, V. Cytotoxicity of targeted PLGA nanoparticles: a systematic review. *RSC Adv.* **2021**, *11*, 9433–9449, doi:10.1039/D1RA00074H.
- (56) Ahmad, W.; Shetab Boushehri, M.A.; Lamprecht, A. Polymeric matrix hydrophobicity governs saponin packing-density on nanoparticle surface and the subsequent biological interactions. *J. Colloid Interface Sci.* **2021**, *596*, 500–513, doi:10.1016/j.jcis.2021.03.027.
- (57) Rose, M.J.; Aron, S.A.; Janicki, B.W. Effect of Various Nonionic Surfactants on Growth of *Escherichia coli*. *J. Bacteriol.* **1966**, *91*, 1863–1868, doi:10.1128/jb.91.5.1863-1868.1966.
- (58) Desaki, M.; Takizawa, H.; Ohtoshi, T.; Kasama, T.; Kobayashi, K.; Sunazuka, T.; Omura, S.; Yamamoto, K.; Ito, K. Erythromycin Suppresses Nuclear Factor- κ B and Activator Protein-1 Activation in Human Bronchial Epithelial Cells. *Biochem. Biophys. Res. Commun.* **2000**, *267*, 124–128, doi:10.1006/bbrc.1999.1917.
- (59) Takizawa, H.; Desaki, M.; Ohtoshi, T.; Kikutani, T.; Okazaki, H.; Sato, M.; Akiyama, N.; Shoji, S.; Hiramatsu, K.; Ito, K. Erythromycin Suppresses Interleukin 6 Expression by Human Bronchial Epithelial Cells: A Potential Mechanism of Its

- Anti-inflammatory Action. *Biochem. Biophys. Res. Commun.* **1995**, *210*, 781–786, doi:10.1006/bbrc.1995.1727.
- (60) Torres, I.M.S.; Bento, E.B.; Almeida, L. da C.; Sá, L.Z.C.M. de; Lima, E.M. Preparation, characterization and in vitro antimicrobial activity of liposomal ceftazidime and cefepime against *Pseudomonas aeruginosa* strains. *Brazilian J. Microbiol.* **2012**, *43*, 984–992, doi:10.1590/S1517-83822012000300020.
- (61) Gao, W.; Hu, C.-M.J.; Fang, R.H.; Zhang, L. Liposome-like nanostructures for drug delivery. *J. Mater. Chem. B* **2013**, *1*, 6569, doi:10.1039/c3tb21238f.
- (62) Kotra, L.P.; Haddad, J.; Mobashery, S. Aminoglycosides: Perspectives on Mechanisms of Action and Resistance and Strategies to Counter Resistance. *Antimicrob. Agents Chemother.* **2000**, *44*, 3249–3256, doi:10.1128/AAC.44.12.3249-3256.2000.
- (63) Nikaido, H. Molecular Basis of Bacterial Outer Membrane Permeability Revisited. *Microbiol. Mol. Biol. Rev.* **2003**, *67*, 593–656, doi:10.1128/MMBR.67.4.593-656.2003.
- (64) Srikumar, R.; Kon, T.; Gotoh, N.; Poole, K. Expression of *Pseudomonas aeruginosa* Multidrug Efflux Pumps MexA-MexB-OprM and MexC-MexD-OprJ in a Multidrug-Sensitive *Escherichia coli* Strain. *Antimicrob. Agents Chemother.* **1998**, *42*, 65–71, doi:10.1128/AAC.42.1.65.
- (65) Srinivasan, V.B.; Singh, B.B.; Priyadarshi, N.; Chauhan, N.K.; Rajamohan, G. Role of Novel Multidrug Efflux Pump Involved in Drug Resistance in *Klebsiella pneumoniae*. *PLoS One* **2014**, *9*, e96288, doi:10.1371/journal.pone.0096288.
- (66) Fan, X.; Fan, J.; Wang, X.; Wu, P.; Wu, G. S-thanatol functionalized liposome potentially targeting on *Klebsiella pneumoniae* and its application in sepsis mouse model. *Front. Pharmacol.* **2015**, *6*, doi:10.3389/fphar.2015.00249.
- (67) Furneri, P.M.; Fresta, M.; Puglisi, G.; Tempera, G. Ofloxacin-Loaded Liposomes: In Vitro Activity and Drug Accumulation in Bacteria. *Antimicrob. Agents Chemother.* **2000**, *44*, 2458–2464, doi:10.1128/AAC.44.9.2458-2464.2000.
- (68) Rabea, E.I.; Badawy, M.E.-T.; Stevens, C. V.; Smagghe, G.; Steurbaut, W. Chitosan as Antimicrobial Agent: Applications and Mode of Action. *Biomacromolecules* **2003**, *4*, 1457–1465, doi:10.1021/bm034130m.

- (69) Al-Adham, I.S.I.; Khalil, E.; Al-Hmoud, N.D.; Kierans, M.; Collier, P.J. Microemulsions are membrane-active, antimicrobial, self-preserving systems. *J. Appl. Microbiol.* **2000**, *89*, 32–39, doi:10.1046/j.1365-2672.2000.01078.x.
- (70) Ouda Sahar, M. Some Nanoparticles Effects on Proteus sp. and Klebsiella Sp. Isolated from Water. *Am. J. Infect. Dis. Microbiol.* **2014**, *2*, 4–10, doi:10.12691/ajidm-2-1-2.
- (71) Franci, G.; Falanga, A.; Galdiero, S.; Palomba, L.; Rai, M.; Morelli, G.; Galdiero, M. Silver Nanoparticles as Potential Antibacterial Agents. *Molecules* **2015**, *20*, 8856–8874, doi:10.3390/molecules20058856.
- (72) Morones, J.R.; Elechiguerra, J.L.; Camacho, A.; Holt, K.; Kouri, J.B.; Ramírez, J.T.; Yacaman, M.J. The bactericidal effect of silver nanoparticles. *Nanotechnology* **2005**, *16*, 2346–2353, doi:10.1088/0957-4484/16/10/059.
- (73) Gil-Tomás, J.; Tubby, S.; Parkin, I.P.; Narband, N.; Dekker, L.; Nair, S.P.; Wilson, M.; Street, C. Lethal photosensitisation of Staphylococcus aureus using a toluidine blue O–tiopronin–gold nanoparticle conjugate. *J. Mater. Chem.* **2007**, *17*, 3739, doi:10.1039/b706615e.
- (74) Pissuwan, D.; Cortie, C.H.; Valenzuela, S.M.; Cortie, M.B. Functionalised gold nanoparticles for controlling pathogenic bacteria. *Trends Biotechnol.* **2010**, *28*, 207–213, doi:10.1016/j.tibtech.2009.12.004.
- (75) Perni, S.; Piccirillo, C.; Pratten, J.; Prokopovich, P.; Chrzanowski, W.; Parkin, I.P.; Wilson, M. The antimicrobial properties of light-activated polymers containing methylene blue and gold nanoparticles. *Biomaterials* **2009**, *30*, 89–93, doi:10.1016/j.biomaterials.2008.09.020.
- (76) Rai, A.; Prabhune, A.; Perry, C.C. Antibiotic mediated synthesis of gold nanoparticles with potent antimicrobial activity and their application in antimicrobial coatings. *J. Mater. Chem.* **2010**, *20*, 6789, doi:10.1039/c0jm00817f.
- (77) Abdifetah, O.; Na-Bangchang, K. Pharmacokinetic studies of nanoparticles as a delivery system for conventional drugs and herb-derived compounds for cancer therapy: a systematic review. *Int. J. Nanomedicine* **2019**, *Volume 14*, 5659–5677, doi:10.2147/IJN.S213229.

- (78) Tammam, S.N.; Azzazy, H.M.E.; Lamprecht, A. Biodegradable Particulate Carrier Formulation and Tuning for Targeted Drug Delivery. *J. Biomed. Nanotechnol.* **2015**, *11*, 555–577, doi:10.1166/jbn.2015.2017.
- (79) Kutscher, H.L.; Chao, P.; Deshmukh, M.; Singh, Y.; Hu, P.; Joseph, L.B.; Reimer, D.C.; Stein, S.; Laskin, D.L.; Sinko, P.J. Threshold size for optimal passive pulmonary targeting and retention of rigid microparticles in rats. *J. Control. Release* **2010**, *143*, 31–37, doi:10.1016/j.jconrel.2009.12.019.
- (80) Champion, J.A.; Walker, A.; Mitragotri, S. Role of Particle Size in Phagocytosis of Polymeric Microspheres. *Pharm. Res.* **2008**, *25*, 1815–1821, doi:10.1007/s11095-008-9562-y.
- (81) Murray, P.J.; Wynn, T.A. Protective and pathogenic functions of macrophage subsets. *Nat. Rev. Immunol.* **2011**, *11*, 723–737, doi:10.1038/nri3073.
- (82) Prior, S.; Gander, B.; Blarer, N.; Merkle, H.P.; Subirá, M.L.; Irache, J.M.; Gamazo, C. In vitro phagocytosis and monocyte-macrophage activation with poly(lactide) and poly(lactide-co-glycolide) microspheres. *Eur. J. Pharm. Sci.* **2002**, *15*, 197–207, doi:10.1016/S0928-0987(01)00218-4.
- (83) *Nanostructured Biomaterials for Overcoming Biological Barriers*; Alonso, M.J., Csaba, N.S., Eds.; Drug Discovery; Royal Society of Chemistry: Cambridge, 2012; ISBN 978-1-84973-363-2.
- (84) Mahin Samadi, P.; Gerami, P.; Elmi, A.; Khanaki, K.; Faezi, S. Pseudomonas aeruginosa keratitis: passive immunotherapy with antibodies raised against divalent flagellin. *Iran. J. Basic Med. Sci.* **2019**, *22*, 58–64, doi:10.22038/ijbms.2018.31499.7643.
- (85) Suryawanshi, A.; Cao, Z.; Thitiprasert, T.; Zaidi, T.S.; Panjwani, N. Galectin-1-Mediated Suppression of Pseudomonas aeruginosa -Induced Corneal Immunopathology. *J. Immunol.* **2013**, *190*, 6397–6409, doi:10.4049/jimmunol.1203501.
- (86) Ghafoorianfar, S.; Ghorani-Azam, A.; Mohajeri, S.A.; Farzin, D. Efficiency of nanoparticles for treatment of ocular infections: Systematic literature review. *J. Drug Deliv. Sci. Technol.* **2020**, *57*, 101765, doi:10.1016/j.jddst.2020.101765.
- (87) Pontillo, A.R.N.; Detsi, A. Nanoparticles for ocular drug delivery: modified and non-modified chitosan as a promising biocompatible carrier. *Nanomedicine* **2019**, *14*, 1889–1909, doi:10.2217/nnm-2019-0040.

- (88) Chandra, N.S.; Torres, M.F.; Winthrop, K.L.; Bruckner, D.A.; Heidemann, D.G.; Calvet, H.M.; Yakrus, M.; Mondino, B.J.; Holland, G.N. Cluster of Mycobacterium Chelonae keratitis cases following laser in-situ keratomileusis. *Am. J. Ophthalmol.* **2001**, *132*, 819–830, doi:10.1016/S0002-9394(01)01267-3.
- (89) Nicolete, R.; Santos, D.F. dos; Faccioli, L.H. The uptake of PLGA micro or nanoparticles by macrophages provokes distinct in vitro inflammatory response. *Int. Immunopharmacol.* **2011**, *11*, 1557–1563, doi:10.1016/j.intimp.2011.05.014.
- (90) Holtkamp; Van Rossem; DE Vos; Willekens; Peek; Kijlstra Polarized secretion of IL-6 and IL-8 by human retinal pigment epithelial cells. *Clin. Exp. Immunol.* **1998**, *112*, 34–43, doi:10.1046/j.1365-2249.1998.00560.x.
- (91) Lajunen, T.; Hisazumi, K.; Kanazawa, T.; Okada, H.; Seta, Y.; Yliperttula, M.; Urtti, A.; Takashima, Y. Topical drug delivery to retinal pigment epithelium with microfluidizer produced small liposomes. *Eur. J. Pharm. Sci.* **2014**, *62*, 23–32, doi:10.1016/j.ejps.2014.04.018.
- (92) Karakoçak, B.B.; Raliya, R.; Davis, J.T.; Chavalmane, S.; Wang, W.-N.; Ravi, N.; Biswas, P. Biocompatibility of gold nanoparticles in retinal pigment epithelial cell line. *Toxicol. Vitr.* **2016**, *37*, 61–69, doi:10.1016/j.tiv.2016.08.013.
- (93) Chittasupho, C.; Posritong, P.; Ariyawong, P. Stability, Cytotoxicity, and Retinal Pigment Epithelial Cell Binding of Hyaluronic Acid-Coated PLGA Nanoparticles Encapsulating Lutein. *AAPS PharmSciTech* **2019**, *20*, 4, doi:10.1208/s12249-018-1256-0.
- (94) Aukunuru, J. V; Ayalasonmayajula, S.P.; Kompella, U.B. Nanoparticle formulation enhances the delivery and activity of a vascular endothelial growth factor antisense oligonucleotide in human retinal pigment epithelial cells. *J. Pharm. Pharmacol.* **2010**, *55*, 1199–1206, doi:10.1211/0022357021701.
- (95) Tasharrofi, N.; Kouhkan, F.; Soleimani, M.; Soheili, Z.-S.; Atyabi, F.; Akbari Javar, H.; Abedin Dorkoosh, F. Efficient gene delivery to primary human retinal pigment epithelial cells: The innate and acquired properties of vectors. *Int. J. Pharm.* **2017**, *518*, 66–79, doi:10.1016/j.ijpharm.2016.12.048.

4. Conclusions and Outlook

With the increasing incidence of bacterial resistance, it is necessary to develop new antibacterial agents acting on previously unexploited targets. Bacterial cell wall synthesis is an attractive target for antibacterial drug discovery, as it is absent in mammalian cells and is necessary for bacterial cell survival. While the late steps of this process are some of the oldest antibacterial drug targets (such as penicillin targeting the transpeptidation step of cell wall synthesis), the earlier steps are underutilized as drug targets. The Mur family of enzymes are attractive potential targets for antibacterial drug development. These enzymes convert the precursor UDP-GlcNAc into UDP-MurNAc pentapeptide through a series of reactions catalyzed by the six members of the family, MurA to MurF.

Fosfomycin is the only clinically used drug targeting a member of the Mur family, MurA. Other previously reported inhibitors in literature suffer from several problems hampering their development as potential antibacterial agents, such as limited potency, inactivity on bacterial cells, inactivity on enzyme mutants, off-target inhibition and potential toxicity to mammalian cells.

We aimed to discover new classes of Mur inhibitors, specifically MurA and MurB inhibitors. First, several pyrazolidinones were synthesized and tested on both MurA and MurB. We next decided to focus more on MurA inhibitors, so a series of pyrrolidinediones were investigated for their MurA inhibition and for their activity on the fosfomycin-resistant C115D MurA mutant. Their binding to MurA was studied in terms of Michaelis-Menten kinetics. Then, native MS and protein NMR techniques were also applied. Afterwards, based on fluorescence binding assays performed with the pyrrolidinediones in addition to the fluorescent probe ANS, we decided to study

the binding and inhibitory potential of ANS to MurA, in addition to testing several simplified ANS derivatives for their inhibition of several subtypes of MurA, namely the WT and C115D *E. coli* MurA as well as *E. cloacae* MurA. Lastly, we decided to revisit a previously published phenyl thiazolyl urea dual MurA/MurB inhibitor. We attempted to improve its entry into bacterial cells without increasing its toxicity to mammalian cells by encapsulating it in nanoparticle-fraught liposomes.

4.1 Synthesis of Novel 1,2-Diarylpyrazolidin-3-one-based Compounds and their Evaluation as Broad Spectrum Antibacterial Agents

The 3,5-pyrazolidinediones are an important class of Mur inhibitors that have been extensively reported to mainly inhibit MurB in addition to MurA.^{138,141,268} While these pyrazolidinediones are able to inhibit the growth of Gram-positive bacteria, they were inactive on Gram-negative pathogens. They were also inactive in the presence of 4% bovine serum albumin (BSA), indicating high lipophilicity and high protein binding. In the study reported in chapter 3.2, a new class of pyrazolidinone derivatives lacking the 5-carbonyl group was developed following the screening of an in-house compound library. This change in structure disrupted the coplanarity of the bis-aryl-pyrazolidine-3,5-dione core, which was interesting to investigate (*Figure 4.1*). This screening revealed that compound **D** had the best antibacterial properties, and it was therefore selected for further development.

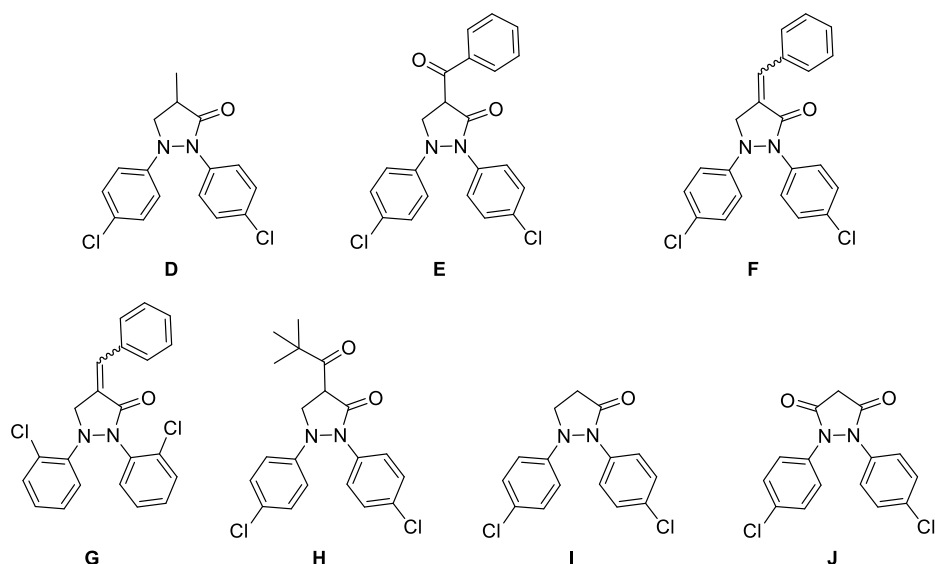
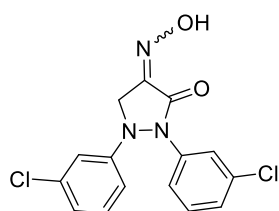


Figure 4.1. Initial list of screened compounds

A series of diaryl pyrazolidinone analogues was synthesized with the most active derivative, compound **24** (Figure 4.2), showing good activity against both Gram-positive and Gram-negative bacteria as well as moderate *in vitro* activity against MurA and MurB enzymes. It was postulated that the oxime group helped retain the structure's MurB activity, in addition to enhancing the anti-MurA activity. Compound **24** also showed low toxicity against human HepG2 cells with an $LD_{50} > 50 \mu\text{g/mL}$.



24

MurA IC_{50} : 88.1 μM
 MurB IC_{50} : 79.5 μM
E. coli ΔtolC MIC: 4 $\mu\text{g/mL}$
B. subtilis MIC: 10 $\mu\text{g/mL}$
S. aureus MIC: 4 $\mu\text{g/mL}$

Figure 4.2. Pyrazolidinone oxime derivative **24**

While the pyrazolidinone derivatives showed a broad-spectrum activity against Gram-negative and Gram-positive bacteria, their specific antibacterial target was not fully verified as their moderate inhibition against MurA and MurB enzymes does not

conclusively explain their more potent antibacterial effect. Exploring the additional target of these compounds will help pinpoint the exact cause of their potent antibacterial effect. This will also help in further improving the potency of the compounds by optimizing their inhibition to their target. They however represent a step forward in the search for potent broad-spectrum antibacterial agents that can help fight the growing bacterial resistance problem.

4.2 Identification and Biochemical Characterization of Pyrrolidinediones as Novel Inhibitors of the Bacterial Enzyme MurA

Pyrrolidinediones were first synthesized as atypical PKC inhibitors. However, they were found to be moderately active to completely inactive against this human enzyme.²⁶⁹ Their structural similarity to the reported pyrazolidinediones prompted their testing as MurA inhibitors. Another advantage for these structures was that their inhibition mode should not involve the catalytically important Cys115 residue, which offers chances to target the fosfomycin-resistant C115D mutant.¹⁹⁴ An initial screening of structurally diverse pyrrolidinedione derivatives revealed that the biaryl-substituted derivatives showed the highest MurA inhibition with an equipotent effect to the established MurA inhibitor fosfomycin. Different analogues were then tested changing the substituents in each round to reveal the optimal substitution pattern for inhibition. The most potent compound in these SAR studies was compound **46** which had a *t*-butyl ester and an extended aryl side chain (*Figure 4.3*).

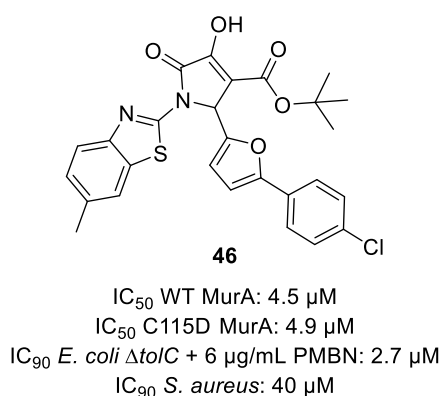


Figure 4.3. Structure and biological activity of compound **46**

Compound **46** was tested on *E. coli* MurA (both the WT and the C115D mutant) and it was equally active on both isoforms. It was also revealed to bind reversibly to MurA and to have an additive effect to fosfomycin in the enzymatic assay. The specific binding mode of the compound was investigated first using Michaelis-Menten enzyme kinetics where it gave inconclusive results that suggested an uncompetitive inhibition pattern, hinting towards inhibition of the UDP-GlcNAc-bound form of the enzyme. This hypothesis was further tested through native MS analysis and protein NMR experiments with the enzyme and compound **46** in presence and absence of UDP-GlcNAc. These tests revealed that in agreement with previous findings, MurA is expressed in a closed complex bound to the MurB product UDP-MurNAc and PEP and is (in this state) unable to bind to compound **46**.²⁰⁰ However, this complex could be opened using UDP-GlcNAc, and was then able to bind to **46**.²⁰⁰

Stability testing of compound **46** revealed it to be stable for two hours in human S9 fraction and four hours in human plasma and bacterial cell lysate. Toxicity screening on human HepG2 and MRC-5 cells showed that **46** was non-toxic to both cancer and non-cancer cell lines. Finally, testing **46** on *E. coli* Δ*tolC* in presence of the cell membrane permeabilizer PMBN revealed that once the compound enters the

bacterial cell, it is highly active with an IC_{90} value of 2.7 μ M. Its effect on the Gram-positive *S. aureus* was less pronounced with an IC_{90} value of 40 μ M.

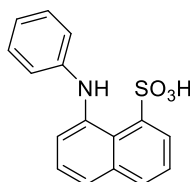
Looking forward, improving the pharmacological properties of these compounds is highly desirable. This will allow a wider range of assays that were hampered by the poor solubility of many members of this class of compounds. Achieving this can be through classical SAR studies, exploring a wider range of side chains on the core pyrrolidinedione ring system that would keep the lipophilicity requirement for the potency yet improve the overall solubility. Increasing their entry into bacterial cells is also a main goal for the future, as it was verified that using the membrane permeabilizer PMBN greatly improved their antibacterial effect against Gram-negative bacteria. Another method to increase their bacterial cell penetration, is to use pharmaceutical technology methods such as inclusion into nanoparticles or using nanoparticle-loaded liposomes to encapsulate the compounds.

These results show that pyrrolidinediones are very promising candidates for the inhibition of MurA, escaping the C115D mutation. They show potential when co-administered with fosfomycin. Their metabolic stability and apparent lack of toxicity to human cells add to their value as a potential antibacterial drug candidates.

4.3 Targeting the Binding Pocket of the Fluorescent Dye 8-Anilinonaphthalene 1-sulfonic acid (ANS) in MurA Holds Potential for the Development of Novel Broad-spectrum Antibiotic Agents

ANS was widely used to track the conformational changes of various proteins as mentioned in section 1.7. It has been established to bind to MurA, acting as a fluorescent probe for various binding events. It was co-crystallized with MurA (PDB

code: 1EYN). However, it was reported to lack any inhibitory effect on *E. cloacae* MurA in concentrations up to 1 mM.^{199,204} However, in our studies, we discovered that ANS was able to inhibit *E. cloacae* MurA as well as *E. coli* MurA, both the WT and the C115D subtypes (Figure 4.4).



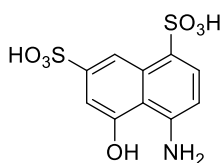
ANS

E. coli WT MurA IC₅₀: 17.7 μM
E. coli C115D MurA IC₅₀: 22 μM
E. cloacae MurA IC₅₀: 31 μM

Figure 4.4. Structure and biological activity of ANS

This prompted the testing of further ANS derivatives with simplified structures, mainly lacking the *N*-phenyl group. These commercially available inhibitors were tested first on WT *E. coli* MurA. Then the most potent derivatives were further tested on the *E. coli* C115D mutant and *E. cloacae* MurA. The screening revealed that the optimal structure for the ANS derivatives included the presence of a naphthalene core in addition to at least one sulfonic acid moiety. A hydrogen bond acceptor, namely, an amino group, was also necessary for the activity.

The most potent of these ANS derivatives was compound **26** which was potent on all three tested subtypes of MurA (Figure 4.5). Unfortunately, these compounds were inactive when tested on both Gram-negative and Gram-positive bacterial cells. This inactivity could be attributed to their high polarity and uptake-hampering negative charge from the sulfonic acid moiety in their structure.

**26**

E. coli WT MurA IC₅₀: 2.7 μM
E. coli C115D MurA IC₅₀: 10 μM
E. cloacae MurA IC₅₀: 13.7 μM

Figure 4.5. ANS derivative 26

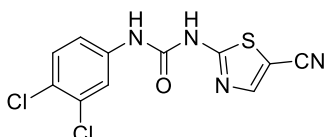
Further SAR studies would greatly benefit this class of compounds, as it could help in greatly improving their antibacterial effect. Converting the sulfonic acid groups into sulfonamide groups could significantly improve their penetration into bacterial cells by eliminating the negative charge and decreasing their overall polarity. The small size of these derivatives facilitates the exploration of further side chain patterns for increasing the potency of these compounds both on MurA and on bacterial cells.

This work shows that rather small fragment-like ANS derivatives were able to inhibit the three studied MurA isoforms with high ligand efficiency and represents a step forward en route to finding a viable MurA inhibitor as a candidate for drug discovery efforts.

4.4 Nanoparticle Fraught Liposomes: A Platform for Increased Antibiotic Selectivity in Multidrug Resistant Bacteria

Problems with bacterial cell uptake of antibacterial agents often limit their potency. This is evident in the case of erythromycin, a protein synthesis inhibitor and an established antibiotic, whose efficacy in Gram-negative bacteria is hampered by poor uptake and susceptibility to efflux pumps.^{270,271} Another example of decreased uptake limiting the use of a potent antibacterial agent is the phenyl cyanothiazolyl urea derivative **3c** (Figure 4.6).¹⁶⁸ Phenyl thiazolyl urea derivatives were reported by

Francisco *et al.* and act as potent dual inhibitors of both MurA and MurB enzymes. They have a promising antibacterial effect against Gram-positive bacteria, but are less potent against Gram-negative bacteria. However, due to their high lipophilicity, they show high plasma protein binding which greatly reduces their antibacterial action in presence of serum.¹⁶⁸



MurA %inhib. at 80 μM : 29.3%
 MurB IC_{50} : 27.9 μM
 MIC *E. coli* DH5 α : 20 μM
 MIC *E. coli* DH5 α + PMBN: 2.5 μM
 MIC *E. coli* ΔtolC : 1.25 μM
 MIC *E. coli* ΔtolC + PMBN: 0.625 μM
 MIC *S. aureus*: 1.25 μM

Figure 4.6. Biological activity of compound **3c**

A suggested solution to improve the bacterial cell uptake of both aforementioned agents is encapsulating them in small nanoparticles (NPs) which use a different mechanism for their uptake than free drugs and are not recognized by bacterial efflux pumps.^{272,273} A disadvantage for the use of small NPs is their increased uptake into mammalian cells which can enhance the toxicity of their cargo.²⁷⁴ In order to overcome this, these small NPs were loaded into specifically designed large liposomes, which preserve their ability to bind to the bacterial outer membranes releasing their contents into the cells.²⁷⁵ Their large size, however, prevents their binding to mammalian membranes which decreases their toxicity.²⁷⁶ The developed system was tested on *E. coli* DH5 α and K12 in addition to *P. aeruginosa*, both *in vitro* and *in vivo* in an ocular keratitis mouse model.

The NP-loaded liposomes (NP-Lip) were able to minimize the human cell uptake and associated toxicity, as demonstrated by the decreased association of the NP-Lip to

human HEK293 cells. An increased uptake into Gram-negative bacteria such as *E. coli* DH5 α and K12 in addition to *P. aeruginosa* was also observed (Figure 4.7).

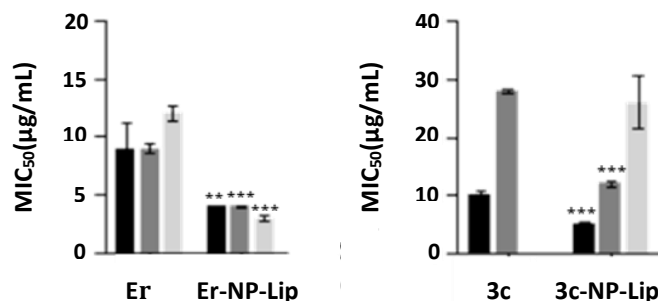


Figure 4.7. Antibacterial activities of Erythromycin and compound **3c** with and without the NP-Lip formulation

In vivo studies of the NP-Lip in a *P. aeruginosa* keratitis mouse model demonstrated the superior ability of the drug-loaded NP-Lips to decrease infection and inflammation relative to the unloaded NP-Lips. This NP-Lip approach therefore facilitated the *in vivo* use of compound **3c**, despite its solubility issues and plasma protein binding capabilities. This shows that tailoring the biomolecular interactions could result in selective drug delivery and a reduction in unwanted off-target effects, and would be a very beneficial tool in improving the antibacterial efficacy of promising antibacterial drug candidates that are hampered by poor pharmacological properties.

5. Experimental Section

5.1 Experimental Methodology of Chapter 3.3

The numbering of compounds in this chapter follows the numbering in chapter 3.3.

The references for this section are included in section 3.3.7.

5.1.1 General Chemical and Analytical Methods

Solvents and reagents were obtained from commercial suppliers and used as received. NMR spectra were recorded using the Bruker Avance™ NMR spectrometer. ¹H NMR spectra were measured at 500 MHz and ¹³C NMR spectra at 126 MHz. All ¹³C NMR spectra are ¹H-decoupled. All spectra were recorded at room temperature and were referenced internally to solvent residual signals wherever possible. Chemical shifts (δ) are quoted in ppm and coupling constants (J) are reported in Hz.

All final compounds had a percentage purity of at least 95%, and this could be verified using UPLC coupled with mass spectrometry. Mass spectra (UPLC-ESI-MS) were obtained utilizing Waters ACQUITY Xevo TQD framework, which consisted of an ACQUITY UPLC H-Class system and Xevo™ TQD triple-quadrupole tandem mass spectrometer with an electrospray ionization (ESI) interface (Waters Corp., Milford, MA, USA). Acquity BEH C18 50 mm × 2.1 mm column (particle size, 1.7 μ m) was utilized to separate analytes (Waters). The solvent system consisted of water containing 0.1% formic acid (A) and 0.1% formic acid in acetonitrile (B). HPLC-technique: flow rate 400 μ L/min. The percentage of B started at an initial of 5% and maintained for 0.5 minute, then increased up to 100% during 4 min, kept at 100% for 2 min, and flushed back to 5% in 1 min. The MS scan was carried out at the accompanying conditions: capillary voltage 3.5 kV, cone voltage 20V, radio frequency

(RF) lens voltage 2.5V, source temperature 150 °C and desolvation gas temperature 500 °C. Nitrogen was used as the desolvation and cone gas at a flow rate of 1000 and 20 L/h, respectively. System operation and data acquisition were controlled using Mass Lynx 4.1 software (Waters).

High-resolution mass spectra were recorded on a Thermo Fisher Scientific Q Exactive Orbitrap mass spectrometer equipped with a heated ESI source and a quadrupole-orbitrap coupled mass detector and an Ultimate3000 HPLC Thermo Fisher Scientific. The MS detection was carried out at a spray voltage of 3.8 kV, a nitrogen sheath gas pressure of 4.0×10^5 Pa, an auxiliary gas pressure of 1.0×10^5 Pa and a capillary temperature of 300°C. All samples were injected by autosampler with an injection volume of 15 µL. A RP Nucleoshell Phenyle-hexyle® (50-2, 3.0µm) column by Macherey-Nagel GmbH was used as a stationary phase. The solvent system consisted of formic acid 0.1% (A) and acetonitrile with formic acid 0.1% (B) with a flow rate of 700 mL/min. The percentage of B started at an initial of 5%, was kept at 5% for 1.0 min, then rapidly increased up to 100 % during 0.2 min, then kept at 100% until 2.8 min and flushed back to the initial 5 %. Samples were desalinated by the use of a switch valve. The first 1.1 min of each run were directed to waste, to avoid a pollution of the ion source. Xcalibur software was used for data acquisition and plotting.

5.1.2 General Procedure for Synthesis of the Compounds

A mixture of amine (1.0 eq; 1.54mmol) and aldehyde (1.1 eq; 1.69 mmol) was dissolved in 4 ml ethanol and 1 ml of acetic acid over molecular sieve, generating a pH around 5 which supports the formation of imines. The reaction was stirred for 30 min at 80°C. Then, the 3,4-dioxo butanoate derivative (1.1 eq; 1.69 mmol) was added followed by an additional heating time at reflux temperature for 24-48 h. The mixture was cooled down, added to diethyl ether and the corresponding precipitate was

suction filtered, washed with water, and diethyl ether. After drying, the residue was dissolved in DCM and washed first with 1N HCl and then with saturated NaCl solution. The combined organic extracts were dried over MgSO₄ and concentrated under reduced pressure. The resulting solid was recrystallized from diethylether/MeOH or purified by column chromatography (CC) using silica gel as a stationary phase with 10% MeOH in DCM as the eluent, getting the desired compounds in acceptable yields ranging from 10% - 80%

5.1.3 Analysis Results for the Compounds

Ethyl 1-(6-chlorobenzo[d]thiazol-2-yl)-2-(4-chlorophenyl)-4-hydroxy-5-oxo-2,5-dihydro-1H-pyrrole-3-carboxylate (1). The compound was synthesized according to the general procedure and was recrystallized from diethylether/MeOH to give an offwhite solid; yield: 409 mg (91%); ¹H-NMR (500 MHz, DMSO-d₆) [δ ppm]: 7.76 (s, 1H), 12.36 (s, 1H), 8.15 (d, *J* = 2.1 Hz, 1H), 7.62 (d, *J* = 8.7 Hz, 1H), 7.44 (d, *J* = 8.5 Hz, 2H), 7.41 (dd, *J* = 8.7, 2.1 Hz, 1H), 7.34 (d, *J* = 8.5 Hz, 2H), 6.05 (s, 1H), 4.12 – 3.98 (m, 2H), 1.10 (t, *J* = 7.1 Hz, 3H); ¹³C-NMR (125 MHz, DMSO-d₆) [δ ppm]: 164.68, 161.56, 155.33, 151.32, 147.00, 135.52, 132.95, 132.49, 129.80, 128.29, 128.12, 126.75, 122.38, 121.66, 114.34, 60.86, 60.09, 13.91; ESI-MS [M-H]⁻: 447.0; HRMS-ESI: *m/z* calcd. for C₂₀H₁₄Cl₂N₂O₄S [M + H]⁺: 449.0124, found: 449.0105. HPLC purity: 100%

Ethyl 1-(5-chlorobenzo[d]oxazol-2-yl)-2-(4-chlorophenyl)-4-hydroxy-5-oxo-2,5-dihydro-1H-pyrrole-3-carboxylate (2). The compound was synthesized according to the general procedure and was recrystallized from diethylether/MeOH to give a white solid; yield: 321 mg (74%); ¹H NMR (500 MHz, DMSO) δ 12.28 (s, 1H), 7.68 (d, *J* = 8.7 Hz, 1H), 7.67 (d, *J* = 2.1 Hz, 1H), 7.44 (d, *J* = 8.6 Hz, 2H), 7.36 (d, *J* = 8.6 Hz, 2H), 7.32 (dd, *J* = 8.7, 2.2 Hz, 1H), 5.94 (s, 1H), 4.12 – 3.98 (m, 2H), 1.09 (t, *J* = 7.1

Hz, 3H); ^{13}C NMR (126 MHz, DMSO) δ 162.97, 161.49, 154.00, 151.17, 146.79, 141.11, 135.18, 132.82, 129.73, 129.16, 128.29, 124.13, 118.45, 113.81, 111.74, 60.12, 59.99, 13.89; ESI-MS $[\text{M}-\text{H}]^-$: 431.1; HRMS-ESI: m/z calcd. for $\text{C}_{20}\text{H}_{14}\text{Cl}_2\text{N}_2\text{O}_5$ $[\text{M} + \text{H}]^+$: 433.0353 found: 433.0355. HPLC purity: 100%

Ethyl 1-([1,1'-biphenyl]-4-yl)-4-hydroxy-5-oxo-2-phenyl-2,5-dihydro-1H-pyrrole-3-carboxylate (3). The compound was synthesized according to the general procedure and was purified using CC (10% MeOH in DCM) to give a light yellow solid; yield: 70 mg (35%); ^1H NMR (500 MHz, DMSO) δ 11.76 (s, 1H), 7.69 (d, $J = 8.7$ Hz, 2H), 7.63 – 7.56 (m, $J = 7.9, 4.2$ Hz, 4H), 7.41 (t, $J = 7.7$ Hz, 2H), 7.35 – 7.27 (m, $J = 13.9, 7.3$ Hz, 3H), 7.24 (t, $J = 7.6$ Hz, 2H), 7.17 (t, $J = 7.2$ Hz, 1H), 6.12 (s, 1H), 4.11 – 3.96 (m, 2H), 1.09 (t, $J = 7.1$ Hz, 3H); ^{13}C NMR (126 MHz, DMSO) δ 164.04, 161.91, 152.52, 139.11, 136.80, 136.55, 135.65, 128.87, 128.25, 127.93, 127.73, 127.37, 126.79, 126.42, 122.65, 112.27, 60.47, 59.66, 13.97; ESI-MS $[\text{M}-\text{H}]^-$: 398.2; HRMS-ESI: m/z calcd. for $\text{C}_{25}\text{H}_{21}\text{NO}_4$ $[\text{M} + \text{H}]^+$: 400.1543 found: 400.1545. HPLC purity: 100%

Ethyl 1,2-bis(4-chlorophenyl)-4-hydroxy-5-oxo-2,5-dihydro-1H-pyrrole-3-carboxylate (4). The compound was synthesized according to the general procedure and was purified using CC (10% MeOH in DCM) to give light yellow crystals; yield: 243 mg (31%); ^1H NMR (500 MHz, DMSO) δ 11.84 (s, 1H), 7.61 (d, $J = 9.0$ Hz, 2H), 7.36 (d, $J = 9.0$ Hz, 2H), 7.33 – 7.25 (m, 4H), 6.10 (s, 1H), 4.12 – 3.94 (m, 2H), 1.09 (t, $J = 7.1$ Hz, 3H); ^{13}C NMR (126 MHz, DMSO) δ 164.09, 161.92, 152.95, 135.62, 135.06, 132.51, 129.74, 129.49, 128.73, 128.33, 124.01, 111.66, 59.77, 14.04; ESI-MS $[\text{M}-\text{H}]^-$: 390.1; HRMS-ESI: m/z calcd. for $\text{C}_{19}\text{H}_{15}\text{Cl}_2\text{NO}_4$ $[\text{M} + \text{H}]^+$: 392.0451 found: 392.0453. HPLC purity: 100%

Ethyl 2-([1,1'-biphenyl]-4-yl)-4-hydroxy-5-oxo-1-phenyl-2,5-dihydro-1H-pyrrole-3-carboxylate (5). The compound was synthesized according to the general

procedure and was recrystallized from diethylether/MeOH to give a light yellow solid; yield: 360 mg (45%); $^1\text{H-NMR}$ (500 MHz, DMSO) δ 11.78 (s, 1H), 7.63 (d, $J = 7.6$ Hz, 2H), 7.58 (d, $J = 7.2$ Hz, 2H), 7.53 (d, $J = 8.4$ Hz, 2H), 7.40 (t, $J = 7.7$ Hz, 2H), 7.37 – 7.27 (m, 5H), 7.09 (t, $J = 7.4$ Hz, 1H), 6.14 (s, 1H), 4.12 – 3.97 (m, 2H), 1.10 (t, $J = 7.1$ Hz, 3H); $^{13}\text{C-NMR}$ (126 MHz, DMSO) δ 164.08, 162.03, 152.83, 139.52, 139.38, 136.31, 135.84, 128.88, 128.71, 128.33, 127.47, 126.53, 126.44, 125.29, 122.37, 111.85, 60.15, 59.67, 14.01; ESI-MS $[\text{M-H}]^-$: 398.2; HRMS-ESI: m/z calcd. for $\text{C}_{25}\text{H}_{21}\text{NO}_4$ $[\text{M} + \text{H}]^+$: 400.1543 found: 400.1525. HPLC purity: 97%

Ethyl 2-([1,1'-biphenyl]-4-yl)-1-(4-chlorobenzyl)-4-hydroxy-5-oxo-2,5-dihydro-1H-pyrrole-3-carboxylate (6). The compound was synthesized according to the general procedure and was purified using CC (10% MeOH in DCM) to give a white solid; yield: 82 mg (18%); $^1\text{H NMR}$ (500 MHz, DMSO) δ 11.79 (s, 1H), 7.65 (dd, $J = 8.3, 1.2$ Hz, 2H), 7.61 (d, $J = 8.4$ Hz, 2H), 7.46 (t, $J = 7.7$ Hz, 2H), 7.37 (dt, $J = 3.5, 1.5$ Hz, 1H), 7.34 (d, $J = 8.5$ Hz, 2H), 7.20 (d, $J = 8.3$ Hz, 2H), 7.11 (d, $J = 8.5$ Hz, 2H), 5.07 (s, 1H), 4.78 (d, $J = 15.5$ Hz, 1H), 4.05 – 3.90 (m, 2H), 3.79 (d, $J = 15.6$ Hz, 1H), 1.04 (t, $J = 7.1$ Hz, 3H); $^{13}\text{C NMR}$ (126 MHz, DMSO) δ 164.91, 161.95, 153.67, 140.11, 139.58, 135.61, 135.06, 131.95, 129.58, 128.95, 128.50, 128.32, 127.57, 126.86, 126.65, 111.57, 60.03, 59.52, 43.26, 13.97; ESI-MS $[\text{M-H}]^-$: 446.2; HRMS-ESI: m/z calcd. for $\text{C}_{26}\text{H}_{22}\text{ClNO}_4$ $[\text{M} + \text{H}]^+$: 448.1310 found: 448.1295. HPLC purity: 100%

Ethyl 2-([1,1'-biphenyl]-4-yl)-1-(6-chlorobenzo[d]thiazol-2-yl)-4-hydroxy-5-oxo-2,5-dihydro-1H-pyrrole-3-carboxylate (7). The compound was synthesized according to the general procedure and was recrystallized from diethylether/MeOH to give a white solid; yield: 156 mg (96%); $^1\text{H NMR}$ (500 MHz, DMSO) δ 12.29 (s, 1H), 8.17 – 8.13 (m, 1H), 7.64 (d, $J = 8.7$ Hz, 1H), 7.63 – 7.59 (m, 4H), 7.48 (d, $J = 8.4$ Hz, 2H), 7.44 – 7.38 (m, 1H), 7.35 – 7.31 (m, 1H), 6.11 (s, 1H), 4.14 – 3.99 (m, 2H), 1.12 (t, $J =$

7.1 Hz, 3H); ^{13}C NMR (126 MHz, DMSO) δ 164.77, 161.63, 155.40, 150.97, 147.07, 139.75, 139.45, 135.45, 132.99, 128.89, 128.37, 128.27, 127.51, 126.73, 126.57, 126.40, 122.41, 121.65, 114.87, 61.23, 60.11, 13.92; ESI-MS [M-H] $^-$: 489.1; HRMS-ESI: m/z calcd. for $\text{C}_{26}\text{H}_{19}\text{ClN}_2\text{O}_4\text{S}$ [M + H] $^+$: 491.0827 found: 491.0811. HPLC purity: 100%

Ethyl 1-(benzo[d]thiazol-2-yl)-4-hydroxy-5-oxo-2-phenyl-2,5-dihydro-1H-pyrrole-3-carboxylate (8). The compound was synthesized according to the general procedure and was recrystallized from diethylether/MeOH to give a white solid; yield: 135 mg (71%); ^1H NMR (500 MHz, DMSO) δ 12.19 (s, 1H), 8.04 – 7.90 (m, 1H), 7.67 – 7.56 (m, 1H), 7.41 – 7.36 (m, 1H), 7.33 – 7.26 (m, $J = 7.7, 6.1, 3.0$ Hz, 1H), 7.24 – 7.20 (m, 1H), 6.08 (s, 1H), 4.12 – 3.98 (m, 2H), 1.09 (t, $J = 7.1$ Hz, 3H); ^{13}C NMR (126 MHz, DMSO) δ 164.60, 161.61, 154.48, 151.05, 148.19, 136.39, 131.29, 128.09, 127.98, 127.71, 126.32, 124.18, 121.90, 121.20, 114.82, 61.46, 60.00, 13.88; ESI-MS [M-H] $^-$: 379.1; HRMS-ESI: m/z calcd. for $\text{C}_{20}\text{H}_{16}\text{N}_2\text{O}_4\text{S}$ [M + H] $^+$: 381.0904 found: 381.0886. HPLC purity: 100%

Ethyl 4-hydroxy-1-(4-methylbenzo[d]thiazol-2-yl)-5-oxo-2-phenyl-2,5-dihydro-1H-pyrrole-3-carboxylate (9). The compound was synthesized according to the general procedure and was recrystallized from diethylether/MeOH to give a white solid; yield: 110 mg (56%); ^1H NMR (500 MHz, DMSO) δ 12.21 (s, 1H), 7.84 – 7.68 (m, $J = 8.4, 4.0$ Hz, 1H), 7.42 (d, $J = 7.1$ Hz, 2H), 7.29 (t, $J = 7.5$ Hz, 2H), 7.25 – 7.21 (m, $J = 7.4, 3.9, 1.3$ Hz, 1H), 7.20 – 7.15 (m, 2H), 6.05 (s, 1H), 4.10 – 3.97 (m, 2H), 2.45 (s, 3H), 1.06 (t, $J = 7.1$ Hz, 3H); ^{13}C NMR (126 MHz, DMSO) δ 164.33, 161.64, 153.22, 151.39, 147.30, 136.51, 130.95, 130.54, 128.15, 127.98, 127.89, 126.64, 124.15, 119.21, 114.42, 61.66, 59.95, 17.37, 13.87; ESI-MS [M-H] $^-$: 393.1; HRMS-ESI: m/z calcd. for $\text{C}_{21}\text{H}_{18}\text{N}_2\text{O}_4\text{S}$ [M + H] $^+$: 395.106 found: 395.1041. HPLC purity: 100%

Ethyl 4-hydroxy-1-(6-methylbenzo[d]thiazol-2-yl)-5-oxo-2-phenyl-2,5-dihydro-1H-pyrrole-3-carboxylate (10). The compound was synthesized according to the general procedure and was recrystallized from diethylether/MeOH to give a light yellow solid; yield: 151 mg (77%); ^1H NMR (500 MHz, DMSO) δ 12.17 (s, 1H), 7.83 – 7.68 (m, 1H), 7.52 (d, J = 8.3 Hz, 1H), 7.37 (d, J = 7.1 Hz, 2H), 7.28 (t, J = 7.5 Hz, 2H), 7.25 – 7.17 (m, 2H), 6.05 (s, 1H), 4.10 – 3.98 (m, 2H), 2.37 (s, 3H), 1.09 (t, J = 7.1 Hz, 3H); ^{13}C NMR (126 MHz, DMSO) δ 164.46, 161.62, 153.63, 151.08, 146.21, 136.44, 133.76, 131.44, 128.08, 127.97, 127.71, 127.66, 121.42, 120.85, 114.73, 61.44, 59.99, 20.96, 13.89; ESI-MS $[\text{M}-\text{H}]^-$: 393.1; HRMS-ESI: m/z calcd. for $\text{C}_{21}\text{H}_{18}\text{N}_2\text{O}_4\text{S}$ $[\text{M} + \text{H}]^+$: 395.1060 found: 395.1041. HPLC purity: 100%

Ethyl 1-(4-chlorobenzo[d]thiazol-2-yl)-4-hydroxy-5-oxo-2-phenyl-2,5-dihydro-1H-pyrrole-3-carboxylate (11). The compound was synthesized according to the general procedure and was recrystallized from diethylether/MeOH to give a white solid; yield: 152 mg (73%); ^1H NMR (500 MHz, DMSO) δ 12.27 (s, 1H), 7.96 (dd, J = 8.0, 1.0 Hz, 1H), 7.49 (dd, J = 7.8, 1.0 Hz, 1H), 7.44 (d, J = 7.1 Hz, 2H), 7.33 – 7.26 (m, J = 7.9, 3.2, 1.8 Hz, 3H), 7.26 – 7.20 (m, 1H), 6.07 (s, 1H), 4.11 – 3.97 (m, 2H), 1.06 (t, J = 7.1 Hz, 3H); ^{13}C NMR (126 MHz, DMSO) δ 164.69, 161.60, 155.16, 151.25, 145.12, 136.13, 132.88, 128.25, 128.09, 127.94, 126.37, 125.05, 121.03, 114.70, 61.63, 59.98, 13.85; ESI-MS $[\text{M}-\text{H}]^-$: 413.0; HRMS-ESI: m/z calcd. for $\text{C}_{20}\text{H}_{15}\text{ClN}_2\text{O}_4\text{S}$ $[\text{M} + \text{H}]^+$: 415.0514 found: 415.0494. HPLC purity: 100%

Ethyl 1-(6-chlorobenzo[d]thiazol-2-yl)-4-hydroxy-5-oxo-2-phenyl-2,5-dihydro-1H-pyrrole-3-carboxylate (12). The compound was synthesized according to the general procedure and was recrystallized from diethylether/MeOH to give a white solid; yield: 162 mg (78%); ^1H NMR (500 MHz, DMSO) δ 12.24 (s, 1H), 8.13 (d, J = 2.2 Hz, 1H), 7.61 (d, J = 8.7 Hz, 1H), 7.42 – 7.36 (m, 3H), 7.29 (t, J = 7.4 Hz, 2H), 7.25 – 7.19

(m, 1H), 6.05 (s, 1H), 4.13 – 3.97 (m, 2H), 1.08 (t, $J = 7.1$ Hz, 3H); ^{13}C NMR (126 MHz, DMSO) δ 164.75, 161.58, 155.32, 150.94, 147.06, 136.23, 132.96, 128.23, 128.10, 128.04, 127.74, 126.70, 122.37, 121.62, 114.95, 61.52, 60.03, 13.87; ESI-MS [M-H] $^-$: 413.0; HRMS-ESI: m/z calcd. for $\text{C}_{20}\text{H}_{15}\text{ClN}_2\text{O}_4\text{S}$ [M + H] $^+$: 415.0514 found: 415.0493. HPLC purity: 100%

Ethyl 4-hydroxy-5-oxo-1-(6-phenoxybenzo[*d*]thiazol-2-yl)-2-phenyl-2,5-dihydro-1*H*-pyrrole-3-carboxylate (13). The compound was synthesized according to the general procedure and was recrystallized from diethylether/MeOH to give a light yellow solid; yield: 174 mg (74%); ^1H NMR (500 MHz, DMSO) δ 12.20 (s, 1H), 7.70 (d, $J = 2.6$ Hz, 1H), 7.65 – 7.62 (m, 1H), 7.40 – 7.33 (m, 4H), 7.29 (t, $J = 7.4$ Hz, 2H), 7.25 – 7.19 (m, 1H), 7.14 – 7.09 (m, 1H), 7.06 (dd, $J = 8.8, 2.5$ Hz, 1H), 7.00 – 6.96 (m, 2H), 6.06 (s, 1H), 4.11 – 3.98 (m, 2H), 1.09 (t, $J = 7.1$ Hz, 3H); ^{13}C NMR (126 MHz, DMSO) δ 164.52, 161.61, 157.27, 154.10, 152.99, 151.09, 144.62, 136.38, 132.82, 130.01, 128.10, 128.00, 127.72, 123.25, 122.28, 118.62, 118.07, 114.73, 112.14, 61.44, 60.00, 13.89; ESI-MS [M-H] $^-$: 471.2; HRMS-ESI: m/z calcd. for $\text{C}_{26}\text{H}_{20}\text{N}_2\text{O}_5\text{S}$: 471.1166 found: 471.1150. HPLC purity: 100%

Ethyl 4-hydroxy-5-oxo-2-phenyl-1-(4,5,6,7-tetrahydrobenzo[*d*]thiazol-2-yl)-2,5-dihydro-1*H*-pyrrole-3-carboxylate (14). The compound was synthesized according to the general procedure and was recrystallized from diethylether/MeOH to give a light yellow solid; yield: 40 mg (40%); ^1H NMR (500 MHz, DMSO) δ 12.05 (s, 1H), 7.31 – 7.14 (m, 5H), 5.90 (s, 1H), 4.09 – 3.95 (m, 2H), 2.68 – 2.51 (m, $J = 30.3, 13.5$ Hz, 3H), 2.31 (d, $J = 17.0$ Hz, 1H), 1.69 (d, $J = 3.3$ Hz, 4H), 1.06 (t, $J = 7.1$ Hz, 3H); ^{13}C NMR (126 MHz, DMSO) δ 163.28, 161.65, 151.51, 151.40, 144.62, 136.53, 128.01, 127.88, 127.63, 122.86, 113.81, 60.93, 59.86, 26.05, 22.63, 22.37, 22.26, 13.87; ESI-

MS [M-H]⁻: 383.1; HRMS-ESI: m/z calcd. for C₂₀H₂₀N₂O₄S [M + H]⁺: 385.1217 found: 385.1197. HPLC purity: 97%

Ethyl 4-hydroxy-1-(naphtho[1,2-*d*]thiazol-2-yl)-5-oxo-2-phenyl-2,5-dihydro-1H-pyrrole-3-carboxylate (15). The compound was synthesized according to the general procedure and was recrystallized from diethylether/MeOH to give a yellow solid; yield: 160 mg (74%); ¹H NMR (500 MHz, DMSO) δ 12.23 (s, 1H), 8.45 – 8.35 (m, 1H), 8.05 (d, *J* = 8.7 Hz, 1H), 7.99 (d, *J* = 8.1 Hz, 1H), 7.81 (d, *J* = 8.6 Hz, 1H), 7.65 (ddd, *J* = 8.2, 7.0, 1.2 Hz, 1H), 7.57 (ddd, *J* = 8.2, 7.0, 1.3 Hz, 1H), 7.52 (dd, *J* = 8.3, 1.1 Hz, 2H), 7.32 (t, *J* = 7.7 Hz, 2H), 7.24 – 7.16 (m, 1H), 6.16 (s, 1H), 4.16 – 3.96 (m, 2H), 1.09 (t, *J* = 7.1 Hz, 3H); ¹³C NMR (126 MHz, DMSO) δ 164.25, 161.68, 154.27, 151.40, 144.10, 136.60, 131.65, 128.15, 128.09, 128.02, 127.29, 126.90, 126.74, 126.03, 124.50, 122.84, 119.47, 114.52, 61.76, 59.99, 13.90.; ESI-MS [M-H]⁻: 429.1; HRMS-ESI: m/z calcd. for C₂₄H₁₈N₂O₄S [M + H]⁺: 431.106 found: 431.104. HPLC purity: 100%

Ethyl 2-([1,1'-biphenyl]-4-yl)-1-(benzo[*d*]thiazol-2-yl)-4-hydroxy-5-oxo-2,5-dihydro-1H-pyrrole-3-carboxylate (16). The compound was synthesized according to the general procedure and was recrystallized from diethylether/MeOH to give a white solid; yield: 93 mg (62%); ¹H NMR (500 MHz, DMSO) δ 12.24 (s, 1H), 8.00 (ddd, *J* = 7.9, 1.2, 0.5 Hz, 1H), 7.68 – 7.64 (m, 1H), 7.63 – 7.59 (m, 4H), 7.48 (d, *J* = 8.4 Hz, 2H), 7.42 (t, *J* = 7.0 Hz, 1H), 7.40 – 7.36 (m, 1H), 7.35 – 7.28 (m, *J* = 9.1, 8.3, 4.8, 1.2 Hz, 2H), 6.14 (s, 1H), 4.14 – 4.01 (m, 2H), 1.12 (t, *J* = 7.1 Hz, 3H); ¹³C NMR (126 MHz, DMSO) δ 164.63, 161.68, 154.55, 151.09, 148.20, 139.71, 139.48, 135.62, 131.31, 128.88, 128.34, 127.50, 126.57, 126.39, 126.36, 124.21, 121.94, 121.25, 114.69, 61.17, 60.09, 13.93; ESI-MS [M-H]⁻: 455.2; HRMS-ESI: m/z calcd. for C₂₆H₂₀N₂O₄S [M + H]⁺: 457.1217 found: 457.1196. HPLC purity: 100%

Ethyl 2-([1,1'-biphenyl]-4-yl)-1-(6-bromobenzo[*d*]thiazol-2-yl)-4-hydroxy-5-oxo-2,5-dihydro-1*H*-pyrrole-3-carboxylate (17). The compound was synthesized according to the general procedure and was recrystallized from diethylether/MeOH to give a beige solid; yield: 158 mg (89%); ¹H NMR (500 MHz, DMSO) δ 12.29 (s, 1H), 8.29 – 8.26 (m, 1H), 7.62 (d, *J* = 1.3 Hz, 1H), 7.61 – 7.57 (m, 1H), 7.52 (dd, *J* = 8.7, 2.1 Hz, 1H), 7.48 (d, *J* = 8.4 Hz, 2H), 7.42 (t, *J* = 7.7 Hz, 2H), 7.37 – 7.29 (m, 1H), 6.11 (s, 1H), 4.13 – 4.01 (m, 2H), 1.12 (t, *J* = 7.1 Hz, 3H); ¹³C NMR (126 MHz, DMSO) δ 164.78, 161.64, 155.36, 150.98, 147.36, 139.74, 139.45, 135.45, 133.46, 129.42, 128.89, 128.37, 127.51, 126.57, 126.39, 124.49, 122.80, 116.18, 114.88, 61.23, 60.11, 13.92; ESI-MS [M-H]⁻: 533.0; HRMS-ESI: *m/z* calcd. for C₂₆H₁₉BrN₂O₄S [M + H]⁺: 535.0322 found: 535.0306. HPLC purity: 100%

Ethyl 2-([1,1'-biphenyl]-4-yl)-4-hydroxy-5-oxo-1-(6-(trifluoromethyl)benzo[*d*]thiazol-2-yl)-2,5-dihydro-1*H*-pyrrole-3-carboxylate (18). The compound was synthesized according to the general procedure and was recrystallized from diethylether/MeOH to give a white solid; yield: 113 mg (65%); ¹H NMR (500 MHz, DMSO) δ 12.33 (s, 1H), 8.52 (dd, *J* = 1.1, 0.6 Hz, 1H), 7.82 (d, *J* = 8.5 Hz, 1H), 7.68 (dd, *J* = 8.7, 1.7 Hz, 1H), 7.63 – 7.58 (m, 4H), 7.50 (d, *J* = 8.4 Hz, 2H), 7.42 (t, *J* = 7.7 Hz, 2H), 7.35 – 7.30 (m, 1H), 6.15 (s, 1H), 4.15 – 3.99 (m, 2H), 1.12 (t, *J* = 7.1 Hz, 3H); ¹³C NMR (126 MHz, DMSO) δ 165.02, 161.63, 157.68, 150.92, 150.85, 139.78, 139.45, 135.37, 131.92, 128.89, 128.41, 127.52, 126.57, 126.41, 124.37 (q, ¹*J*_{C-F} = 272.1 Hz), 124.32 (q, ²*J*_{C-F} = 32.0 Hz), 123.17, 121.68, 120.14, 115.06, 61.32, 60.15, 13.91; ESI-MS [M-H]⁻: 523.2; HRMS-ESI: *m/z* calcd. for C₂₇H₁₉F₃N₂O₄S [M + H]⁺: 525.109 found: 525.1075. HPLC purity: 99%

Ethyl 2-([1,1'-biphenyl]-4-yl)-4-hydroxy-1-(6-methylbenzo[*d*]thiazol-2-yl)-5-oxo-2,5-dihydro-1*H*-pyrrole-3-carboxylate (19). The compound was synthesized

according to the general procedure and was recrystallized from diethylether/MeOH to give a light yellow solid; yield: 129 mg (83%); ^1H NMR (500 MHz, DMSO) δ 12.24 (s, 1H), 7.78 (s, 1H), 7.64 – 7.57 (m, $J = 11.6, 4.6$ Hz, 4H), 7.54 (d, $J = 8.3$ Hz, 1H), 7.46 (d, $J = 8.3$ Hz, 2H), 7.42 (t, $J = 7.7$ Hz, 2H), 7.33 (t, $J = 7.3$ Hz, 1H), 7.20 (dd, $J = 8.5, 1.4$ Hz, 1H), 6.10 (s, 1H), 4.13 – 4.02 (m, 2H), 2.37 (s, 3H), 1.12 (t, $J = 7.1$ Hz, 3H); ^{13}C NMR (126 MHz, DMSO) δ 164.48, 161.67, 153.70, 151.11, 146.21, 139.68, 139.48, 135.66, 133.79, 131.47, 128.88, 128.31, 127.68, 127.49, 126.57, 126.37, 121.44, 120.88, 114.60, 61.14, 60.06, 20.95, 13.92; ESI-MS $[\text{M}-\text{H}]^-$: 469.2; HRMS-ESI: m/z calcd. for $\text{C}_{27}\text{H}_{22}\text{N}_2\text{O}_4\text{S}$ $[\text{M} + \text{H}]^+$: 471.1373 found: 471.1358. HPLC purity: 100%

Ethyl 2-([1,1'-biphenyl]-4-yl)-4-hydroxy-1-(6-methoxybenzo[*d*]thiazol-2-yl)-5-oxo-2,5-dihydro-1*H*-pyrrole-3-carboxylate (20). The compound was synthesized according to the general procedure and was recrystallized from diethylether/MeOH to give a yellow solid; yield: 128 mg (80%); ^1H NMR (500 MHz, DMSO) δ 12.20 (s, 1H), 7.62 (d, $J = 1.3$ Hz, 1H), 7.60 – 7.58 (m, 1H), 7.55 (d, $J = 8.9$ Hz, 1H), 7.46 (d, $J = 8.4$ Hz, 2H), 7.42 (t, $J = 7.7$ Hz, 2H), 7.37 – 7.29 (m, 1H), 6.98 (dd, $J = 8.9, 2.6$ Hz, 1H), 6.09 (s, 1H), 4.13 – 4.00 (m, 2H), 3.77 (s, 3H), 1.12 (t, $J = 7.1$ Hz, 3H); ^{13}C NMR (126 MHz, DMSO) δ 164.36, 161.69, 156.50, 152.54, 151.20, 142.36, 139.68, 139.48, 135.69, 132.74, 128.88, 128.30, 127.49, 126.57, 126.38, 121.87, 115.08, 114.43, 104.91, 61.09, 60.04, 55.62, 13.93; ESI-MS $[\text{M}-\text{H}]^-$: 485.2; HRMS-ESI: m/z calcd. for $\text{C}_{27}\text{H}_{22}\text{N}_2\text{O}_5\text{S}$ $[\text{M} + \text{H}]^+$: 487.1322 found: 487.1306. HPLC purity: 100%

Ethyl 2-([1,1'-biphenyl]-4-yl)-1-(4-chlorobenzo[*d*]thiazol-2-yl)-4-hydroxy-5-oxo-2,5-dihydro-1*H*-pyrrole-3-carboxylate (21). The compound was synthesized according to the general procedure and was purified using CC (10% MeOH in DCM) to give a white solid; yield: 117 mg (48%); ^1H NMR (500 MHz, DMSO) δ 12.31 (s, 1H), 7.97 (dd, $J = 8.0, 1.0$ Hz, 1H), 7.64 – 7.58 (m, 4H), 7.54 (d, $J = 8.5$ Hz, 2H), 7.49 (dd, $J =$

7.8, 1.0 Hz, 1H), 7.42 (t, $J = 7.7$ Hz, 2H), 7.36 – 7.31 (m, 1H), 7.29 (t, $J = 7.9$ Hz, 1H), 6.12 (s, 1H), 4.17 – 3.98 (m, 2H), 1.10 (t, $J = 7.1$ Hz, 3H); ^{13}C NMR (126 MHz, DMSO) δ 164.71, 161.66, 155.23, 151.28, 145.14, 139.80, 139.49, 135.36, 132.91, 128.90, 127.51, 126.59, 126.41, 126.22, 125.08, 121.06, 114.60, 61.35, 60.07, 13.90; ESI-MS [M-H] $^-$: 489.1; HRMS-ESI: m/z calcd. for $\text{C}_{26}\text{H}_{19}\text{ClN}_2\text{O}_4\text{S}$ [M + H] $^+$: 491.0827 found: 491.0812. HPLC purity: 100%

Ethyl 2-([1,1'-biphenyl]-4-yl)-4-hydroxy-1-(4-methoxybenzo[d]thiazol-2-yl)-5-oxo-2,5-dihydro-1H-pyrrole-3-carboxylate (22). The compound was synthesized according to the general procedure and was recrystallized from diethylether/MeOH to give a beige solid; yield: 102 mg (42%); ^1H NMR (500 MHz, DMSO) δ 12.25 (s, 1H), 7.63 – 7.58 (m, 4H), 7.55 (dd, $J = 8.0, 0.9$ Hz, 1H), 7.47 (d, $J = 8.4$ Hz, 2H), 7.42 (t, $J = 7.7$ Hz, 2H), 7.36 – 7.30 (m, 1H), 7.24 (t, $J = 8.0$ Hz, 1H), 6.95 (dd, $J = 8.1, 0.9$ Hz, 1H), 6.14 (s, 1H), 4.13 – 4.01 (m, 2H), 3.86 (s, 3H), 1.13 (t, $J = 7.1$ Hz, 3H); ^{13}C NMR (126 MHz, DMSO) δ 164.52, 161.69, 152.75, 152.08, 151.26, 139.69, 139.48, 138.23, 135.66, 132.99, 128.88, 128.33, 127.49, 126.58, 126.34, 125.28, 114.50, 113.87, 109.31, 61.08, 60.05, 56.55, 13.93; ESI-MS [M-H] $^-$: 485.2; HRMS-ESI: m/z calcd. for $\text{C}_{27}\text{H}_{22}\text{N}_2\text{O}_5\text{S}$ [M + H] $^+$: 487.1322 found: 487.1306. HPLC purity: 95%

Ethyl 2-([1,1'-biphenyl]-4-yl)-1-(4,6-difluorobenzo[d]thiazol-2-yl)-4-hydroxy-5-oxo-2,5-dihydro-1H-pyrrole-3-carboxylate (23). The compound was synthesized according to the general procedure and was recrystallized from diethylether/MeOH to give a white solid; yield: 130 mg (80%); ^1H NMR (500 MHz, DMSO) δ 12.34 (s, 3H), 7.90 – 7.73 (m, 4H), 7.64 – 7.58 (m, $J = 8.4, 4.1, 1.6$ Hz, 16H), 7.48 (d, $J = 8.4$ Hz, 8H), 7.42 (t, $J = 7.7$ Hz, 8H), 7.36 – 7.30 (m, 8H), 6.11 (s, 4H), 4.13 – 4.01 (m, 8H), 1.11 (t, $J = 7.1$ Hz, 12H); ^{13}C NMR (126 MHz, DMSO) δ 164.81, 161.60, 158.36 (dd, $^1J_{\text{C-F}} = 242.9, ^3J_{\text{C-F}} = 10.5$ Hz), 154.90, 153.40 (dd, $^1J_{\text{C-F}} = 255.4, ^3J_{\text{C-F}} = 13.6$

Hz), 150.94, 139.79, 139.41, 135.28, 134.55 (dd, $^3J_{C-F} = 13.5$, $^3J_{C-F} = 4.9$ Hz), 133.69 (dd, $^2J_{C-F} = 13.0$, $^4J_{C-F} = 2.1$ Hz), 128.89, 128.46, 127.52, 126.57, 126.37, 114.93, 104.74 (dd, $^2J_{C-F} = 26.9$, $^4J_{C-F} = 3.7$ Hz), 102.32 (dd, $^2J_{C-F} = 28.7$, $^2J_{C-F} = 21.6$ Hz), 61.25, 60.12, 13.90; ESI-MS [M-H]⁻: 491.1; HRMS-ESI: m/z calcd. for C₂₆H₁₈F₂N₂O₄S [M + H]⁺: 493.1028 found: 493.1014. HPLC purity: 100%

Ethyl 2-([1,1'-biphenyl]-4-yl)-1-(5,6-dimethylbenzo[d]thiazol-2-yl)-4-hydroxy-5-oxo-2,5-dihydro-1H-pyrrole-3-carboxylate (24). The compound was synthesized according to the general procedure and was recrystallized from diethylether/MeOH to give a white solid; yield: 151 mg (94%); ¹H NMR (500 MHz, DMSO) δ 12.23 (s, 1H), 7.71 (s, 1H), 7.63 – 7.57 (m, 4H), 7.47 – 7.44 (m, 3H), 7.42 (t, $J = 7.7$ Hz, 2H), 7.35 – 7.30 (m, 1H), 6.09 (s, 1H), 4.14 – 4.00 (m, 2H), 2.26 (s, 3H), 2.25 (s, 3H), 1.12 (t, $J = 7.1$ Hz, 3H); ¹³C NMR (126 MHz, DMSO) δ 164.38, 161.70, 153.60, 151.19, 146.78, 139.65, 139.49, 135.73, 135.17, 133.20, 128.89, 128.64, 128.30, 127.49, 126.57, 126.35, 121.57, 121.54, 114.43, 61.14, 60.04, 54.90, 19.54, 13.93; ESI-MS [M-H]⁻: 483.2; HRMS-ESI: m/z calcd. for C₂₈H₂₄N₂O₄S [M + H]⁺: 485.1530 found: 485.1514. HPLC purity: 100%

Ethyl 4-hydroxy-2-(4-hydroxyphenyl)-1-(6-methylbenzo[d]thiazol-2-yl)-5-oxo-2,5-dihydro-1H-pyrrole-3-carboxylate (25). The compound was synthesized according to the general procedure and was purified using CC (10% MeOH in DCM) to give a yellow solid; yield: 48 mg (23%); ¹H NMR (500 MHz, DMSO) δ 9.15 (s, 1H), 7.77 – 7.60 (m, 1H), 7.51 (d, $J = 8.3$ Hz, 1H), 7.23 – 7.13 (m, 1H), 7.08 (d, $J = 8.6$ Hz, 2H), 6.58 (d, $J = 8.6$ Hz, 2H), 5.77 (s, 1H), 3.92 – 3.82 (m, 2H), 2.37 (s, 3H), 1.02 (t, $J = 7.1$ Hz, 3H); ¹³C NMR (126 MHz, DMSO) δ 169.26, 164.84, 164.56, 156.01, 154.55, 146.62, 132.97, 131.56, 131.47, 128.42, 127.25, 121.18, 120.51, 114.17, 101.76, 60.31, 57.23, 20.93,

14.41; ESI-MS [M-H]⁻: 409.1; HRMS-ESI: m/z calcd. for C₂₁H₁₈N₂O₅S [M + H]⁺: 411.1009 found: 411.0991. HPLC purity: 99%

Ethyl 2-(furan-2-yl)-4-hydroxy-1-(6-methylbenzo[d]thiazol-2-yl)-5-oxo-2,5-dihydro-1H-pyrrole-3-carboxylate (26). The compound was synthesized according to the general procedure and was recrystallized from diethylether/MeOH to give a light brown solid; yield: 129 mg (67%); ¹H NMR (500 MHz, DMSO) δ 12.32 (s, 1H), 7.83 – 7.74 (m, 1H), 7.64 (d, *J* = 8.3 Hz, 1H), 7.51 (dd, *J* = 1.8, 0.7 Hz, 1H), 7.25 (ddd, *J* = 8.4, 1.8, 0.6 Hz, 1H), 6.65 (dd, *J* = 3.3, 0.7 Hz, 1H), 6.39 (dd, *J* = 3.3, 1.8 Hz, 1H), 6.23 (s, 1H), 4.20 – 4.03 (m, 2H), 2.40 (s, 3H), 1.14 (t, *J* = 7.1 Hz, 3H); ¹³C NMR (126 MHz, DMSO) δ 164.06, 161.52, 153.59, 151.44, 147.96, 146.25, 142.40, 133.85, 131.43, 127.74, 121.46, 120.92, 111.61, 110.75, 110.38, 60.00, 55.19, 20.99, 13.97; ESI-MS [M-H]⁻: 383.0; HRMS-ESI: m/z calcd. for C₁₉H₁₆N₂O₅S [M + H]⁺: 385.0853 found: 385.0835. HPLC purity: 95%

Ethyl 4-hydroxy-1-(6-methylbenzo[d]thiazol-2-yl)-5-oxo-2-(thiophen-2-yl)-2,5-dihydro-1H-pyrrole-3-carboxylate (27). The compound was synthesized according to the general procedure and was recrystallized from diethylether/MeOH to give a light yellow solid; yield: 110 mg (55%); ¹H NMR (500 MHz, DMSO) δ 12.36 (s, 1H), 7.82 – 7.79 (m, 1H), 7.66 (d, *J* = 8.3 Hz, 1H), 7.44 – 7.37 (m, 1H), 7.35 – 7.31 (m, 1H), 7.28 – 7.22 (m, *J* = 8.4, 1.7, 0.6 Hz, 1H), 6.94 (dd, *J* = 5.1, 3.6 Hz, 1H), 6.41 (s, 1H), 4.17 – 4.05 (m, 2H), 2.40 (s, 3H), 1.13 (t, *J* = 7.1 Hz, 3H); ¹³C NMR (126 MHz, DMSO) δ 163.79, 161.56, 153.52, 151.05, 146.22, 139.58, 133.88, 131.51, 128.35, 127.76, 126.72, 125.73, 121.49, 120.94, 114.33, 60.08, 56.69, 20.99, 13.95; ESI-MS [M-H]⁻: 399.0; HRMS-ESI: m/z calcd. for C₁₉H₁₆N₂O₄S₂ [M + H]⁺: 401.0624 found: 401.0606. HPLC purity: 100%

Ethyl 4-hydroxy-1-(6-methylbenzo[d]thiazol-2-yl)-5-oxo-2-(pyridin-3-yl)-2,5-dihydro-1H-pyrrole-3-carboxylate (28). The compound was synthesized according to the general procedure and was recrystallized from diethylether/MeOH to give a white solid; yield: 62 mg (31%); ^1H NMR (500 MHz, DMSO) δ 12.56 (s, 1H), 8.74 (s, 1H), 8.43 (s, 1H), 7.78 (s, 1H), 7.73 (d, $J = 7.2$ Hz, 1H), 7.52 (d, $J = 7.5$ Hz, 1H), 7.29 (s, 1H), 7.20 (d, $J = 8.5$ Hz, 1H), 6.09 (s, 1H), 4.04 (dd, $J = 18.9, 7.7$ Hz, 2H), 2.37 (s, 3H), 1.07 (t, $J = 6.2$ Hz, 3H); ^{13}C NMR (126 MHz, DMSO) δ 164.46, 161.62, 161.33, 154.43, 153.69, 150.23, 148.89, 146.09, 134.51, 133.81, 132.73, 131.38, 127.71, 123.37, 121.46, 120.82, 59.97, 59.32, 20.96, 13.91; ESI-MS $[\text{M}-\text{H}]^-$: 394.1; HRMS-ESI: m/z calcd. for $\text{C}_{20}\text{H}_{17}\text{N}_3\text{O}_4\text{S}$ $[\text{M} + \text{H}]^+$: 396.1013 found: 396.0996. HPLC purity: 100%

Ethyl 4-hydroxy-1-(6-methylbenzo[d]thiazol-2-yl)-2-(naphthalen-2-yl)-5-oxo-2,5-dihydro-1H-pyrrole-3-carboxylate (29). The compound was synthesized according to the general procedure and was recrystallized from diethylether/MeOH to give a white solid; yield: 45 mg (56%); ^1H NMR (500 MHz, DMSO) δ 12.25 (s, 1H), 8.00 (s, 1H), 7.97 – 7.91 (m, $J = 6.3, 3.2$ Hz, 1H), 7.86 – 7.80 (m, 2H), 7.78 – 7.73 (m, 1H), 7.51 – 7.43 (m, 4H), 7.15 (dd, $J = 8.4, 1.2$ Hz, 1H), 6.23 (s, 1H), 4.06 – 3.96 (m, 2H), 2.34 (s, 3H), 1.06 (t, $J = 7.1$ Hz, 3H); ^{13}C NMR (126 MHz, DMSO) δ 164.53, 161.68, 153.71, 151.25, 146.13, 133.96, 133.74, 132.64, 132.61, 131.40, 127.81, 127.63, 127.59, 127.45, 127.22, 126.16, 125.20, 121.41, 120.81, 114.58, 61.62, 60.00, 20.93, 13.88; ESI-MS $[\text{M}-\text{H}]^-$: 443.1; HRMS-ESI: m/z calcd. for $\text{C}_{25}\text{H}_{20}\text{N}_2\text{O}_4\text{S}$ $[\text{M} + \text{H}]^+$: 445.1217 found: 445.1197. HPLC purity: 100%

Ethyl 4-hydroxy-2-(6-hydroxynaphthalen-2-yl)-1-(6-methylbenzo[d]thiazol-2-yl)-5-oxo-2,5-dihydro-1H-pyrrole-3-carboxylate (30). The compound was synthesized according to the general procedure and was purified using CC (10% MeOH in DCM) to give a light red solid; yield: 48 mg (21%); ^1H NMR (500 MHz, DMSO)

δ 12.17 (s, 1H), 9.71 (s, 1H), 7.84 (d, $J = 1.5$ Hz, 1H), 7.78 – 7.76 (m, 1H), 7.76 – 7.74 (m, 1H), 7.57 (d, $J = 8.6$ Hz, 1H), 7.48 (d, $J = 8.3$ Hz, 1H), 7.31 (dd, $J = 8.6, 1.8$ Hz, 1H), 7.19 – 7.14 (m, $J = 8.4, 1.7, 0.5$ Hz, 1H), 7.07 – 7.01 (m, 2H), 6.16 (s, 1H), 4.07 – 3.96 (m, 2H), 2.35 (d, $J = 9.9$ Hz, 3H), 1.06 (t, $J = 7.1$ Hz, 3H); ^{13}C NMR (126 MHz, DMSO) δ 164.54, 161.72, 155.60, 153.68, 151.02, 146.20, 134.29, 133.72, 131.42, 130.29, 129.39, 127.63, 127.26, 127.08, 125.83, 125.34, 121.40, 120.83, 118.77, 114.78, 108.44, 61.65, 59.99, 20.94, 13.91; ESI-MS [M-H] $^-$: 459.1; HRMS-ESI: m/z calcd. for $\text{C}_{25}\text{H}_{20}\text{N}_2\text{O}_5\text{S}$ [M + H] $^+$: 461.1166 found: 461.1143. HPLC purity: 97%

Ethyl 4-hydroxy-1-(6-methylbenzo[*d*]thiazol-2-yl)-2-(naphthalen-1-yl)-5-oxo-2,5-dihydro-1*H*-pyrrole-3-carboxylate (31). The compound was synthesized according to the general procedure and was recrystallized from diethylether/MeOH to give a beige solid; yield: 152 mg (68%); ^1H NMR (500 MHz, DMSO) δ 12.18 (s, 1H), 8.70 (d, $J = 8.6$ Hz, 1H), 7.90 (d, $J = 8.0$ Hz, 1H), 7.78 (d, $J = 8.1$ Hz, 1H), 7.75 – 7.68 (m, 2H), 7.58 (t, $J = 7.2$ Hz, 1H), 7.33 (t, $J = 7.7$ Hz, 1H), 7.20 (dd, $J = 7.3, 1.0$ Hz, 1H), 7.09 (s, 1H), 7.06 (dd, $J = 8.4, 1.3$ Hz, 1H), 7.02 (d, $J = 8.3$ Hz, 1H), 3.87 – 3.75 (m, 2H), 2.31 (s, 3H), 0.67 (t, $J = 7.1$ Hz, 3H); ^{13}C NMR (126 MHz, DMSO) δ 164.81, 161.64, 153.57, 151.36, 145.99, 133.65, 133.49, 133.27, 132.40, 131.45, 128.33, 128.10, 127.50, 125.51, 125.39, 125.08, 122.22, 121.39, 120.52, 116.05, 59.70, 55.76, 20.91, 13.38; ESI-MS [M-H] $^-$: 443.2; HRMS-ESI: m/z calcd. for $\text{C}_{25}\text{H}_{20}\text{N}_2\text{O}_4\text{S}$ [M + H] $^+$: 445.1217 found: 445.1201. HPLC purity: 100%

Ethyl 4-hydroxy-2-(4-methoxynaphthalen-1-yl)-1-(6-methylbenzo[*d*]thiazol-2-yl)-5-oxo-2,5-dihydro-1*H*-pyrrole-3-carboxylate (32). The compound was synthesized according to the general procedure and was recrystallized from diethylether/MeOH to give a yellow solid; yield: 150 mg (63%); ^1H NMR (500 MHz, DMSO) δ 12.09 (s, 1H), 8.65 (d, $J = 9.0$ Hz, 1H), 8.16 (dd, $J = 8.5, 0.9$ Hz, 1H), 7.82 – 7.69

(m, 2H), 7.60 – 7.49 (m, 1H), 7.10 (d, $J = 8.2$ Hz, 1H), 7.06 (dd, $J = 8.5, 1.4$ Hz, 1H), 7.02 (d, $J = 8.3$ Hz, 1H), 6.99 (s, 1H), 6.79 (d, $J = 8.3$ Hz, 1H), 3.88 – 3.79 (m, 5H), 2.31 (s, 3H), 0.71 (t, $J = 7.1$ Hz, 3H); ^{13}C -NMR (126 MHz, DMSO) δ 164.87, 161.76, 154.51, 153.56, 151.11, 146.08, 133.65, 133.24, 131.49, 127.53, 125.86, 125.09, 124.88, 124.72, 122.80, 121.43, 121.40, 120.56, 116.10, 103.81, 59.76, 55.72, 55.43, 20.95, 13.50; ESI-MS [M-H] $^-$: 473.1; HRMS-ESI: m/z calcd. for $\text{C}_{26}\text{H}_{22}\text{N}_2\text{O}_5\text{S}$ [M + H] $^+$: 475.1322 found: 475.1306. HPLC purity: 97%

Ethyl 2-(benzo[d]thiazol-2-yl)-4-hydroxy-1-(6-methylbenzo[d]thiazol-2-yl)-5-oxo-2,5-dihydro-1H-pyrrole-3-carboxylate (33). The compound was synthesized according to the general procedure and was recrystallized from diethylether/MeOH to give a yellow solid; yield: 167 mg (74%); ^1H -NMR (500 MHz, DMSO) δ 12.70 (s, 1H), 8.10 – 8.07 (m, 1H), 7.94 – 7.91 (m, 1H), 7.80 – 7.79 (m, 1H), 7.54 (d, $J = 8.3$ Hz, 1H), 7.43 (dtd, $J = 16.4, 7.2, 1.4$ Hz, 2H), 7.20 (dd, $J = 8.5, 1.4$ Hz, 1H), 6.59 (s, 1H), 4.17 – 4.03 (m, 2H), 2.36 (s, 3H), 1.12 (t, $J = 7.1$ Hz, 3H); ^{13}C -NMR (126 MHz, DMSO) δ 167.04, 164.20, 161.46, 153.73, 151.98, 151.69, 145.86, 134.88, 133.99, 131.43, 127.83, 126.19, 125.54, 122.91, 122.26, 121.58, 120.81, 112.61, 60.26, 58.61, 20.94, 13.94; ESI-MS [M-H] $^-$: 450.1; HRMS-ESI: m/z calcd. for $\text{C}_{22}\text{H}_{17}\text{N}_3\text{O}_4\text{S}_2$ [M + H] $^+$: 452.0733 found: 452.0713. HPLC purity: 96%

Ethyl 2-([1,1'-biphenyl]-2-yl)-4-hydroxy-1-(6-methylbenzo[d]thiazol-2-yl)-5-oxo-2,5-dihydro-1H-pyrrole-3-carboxylate (34). The compound was synthesized according to the general procedure and was recrystallized from diethylether/MeOH to give a white solid; yield: 115 mg (49%); ^1H NMR (500 MHz, DMSO) δ 12.10 (s, 1H), 8.04 (d, $J = 7.2$ Hz, 2H), 7.75 – 7.71 (m, 1H), 7.57 (t, $J = 7.6$ Hz, 2H), 7.52 (d, $J = 8.3$ Hz, 1H), 7.42 (t, $J = 7.4$ Hz, 1H), 7.31 – 7.17 (m, 4H), 7.06 (dd, $J = 7.8, 1.0$ Hz, 1H), 6.27 (s, 1H), 4.16 – 4.05 (m, 2H), 2.36 (s, 3H), 1.09 (t, $J = 7.1$ Hz, 3H); ^{13}C NMR (126 MHz,

DMSO) δ 164.53, 162.16, 153.41, 151.97, 146.05, 143.51, 141.25, 133.69, 133.30, 131.57, 130.71, 130.37, 128.02, 127.79, 127.63, 127.49, 126.89, 124.56, 121.36, 120.52, 114.95, 60.10, 57.66, 20.99, 14.06; ESI-MS [M-H]⁻: 469.1; HRMS-ESI: m/z calcd. for C₂₇H₂₂N₂O₄S [M + H]⁺: 471.1373 found: 471.1358. HPLC purity: 100%

Ethyl 2-(4-(6-chloropyridazin-3-yl)phenyl)-4-hydroxy-1-(6-methylbenzo[d]thiazol-2-yl)-5-oxo-2,5-dihydro-1H-pyrrole-3-carboxylate

(35). The compound was synthesized according to the general procedure and was recrystallized from diethylether/MeOH to give light yellow crystals; yield: 140 mg (55%); ¹H-NMR (500 MHz, DMSO) δ 12.32 (s, 1H), 8.28 (d, J = 9.1 Hz, 1H), 8.07 (d, J = 8.4 Hz, 2H), 7.97 (d, J = 9.1 Hz, 1H), 7.78 (s, 1H), 7.59 (d, J = 8.4 Hz, 2H), 7.52 (d, J = 8.3 Hz, 1H), 7.19 (dd, J = 8.4, 1.3 Hz, 1H), 6.15 (s, 1H), 4.13 – 4.01 (m, 2H), 2.36 (s, 3H), 1.12 (t, J = 7.1 Hz, 3H); ¹³C-NMR (126 MHz, DMSO) δ 164.49, 161.64, 157.78, 155.21, 153.69, 151.45, 146.13, 139.16, 134.35, 133.79, 131.42, 129.17, 128.54, 127.68, 127.53, 126.82, 121.46, 120.86, 114.14, 61.09, 60.08, 20.94, 13.93; ESI-MS [M-H]⁻: 505.2; HRMS-ESI: m/z calcd. for C₂₅H₁₉ClN₄O₄S [M + H]⁺: 507.0888 found: 507.0868. HPLC purity: 100%

Ethyl 4-hydroxy-1-(6-methylbenzo[d]thiazol-2-yl)-5-oxo-2-(5-phenylfuran-2-yl)-2,5-dihydro-1H-pyrrole-3-carboxylate (36). The compound was synthesized according to the general procedure and was purified using CC (10% MeOH in DCM) to give a yellow solid; yield: 60 mg (26%); ¹H-NMR (500 MHz, DMSO-d₆) [δ ppm]: 7.91 (s, 1H), 7.74 (d, J = 8.14 Hz, 1H), 7.68 (m, 2H), 7.48 (m, 2H), 7.34 (m, 2H), 6.97 (d, J = 3.40 Hz, 1H), 6.84 (d, J = 3.50 Hz, 1H), 6.41 (s, 1H), 4.22 (m, 2H), 2.50 (s, 3H), 1.25 (t, J = 7.16 Hz, 3H); ¹³C-NMR (126 MHz, DMSO-d₆) [δ ppm]: 164.04, 161.59, 153.69, 152.11, 151.59, 148.12, 146.22, 133.84, 131.44, 129.96, 128.85, 127.73, 123.18, 121.45, 120.89, 112.21, 111.40, 106.83, 60.02, 55.37, 20.95, 13.96; ESI-MS [M-H]⁻:

459.1; HRMS-ESI: m/z calcd. for $C_{25}H_{20}N_2O_5S$ $[M + H]^+$: 461.1166 found: 461.1144.

HPLC purity: 100%

Ethyl 4-hydroxy-1-(6-methylbenzo[d]thiazol-2-yl)-5-oxo-2-(thiophen-2-yl)-2,5-dihydro-1H-pyrrole-3-carboxylate (37). The compound was synthesized according to the general procedure and was recrystallized from diethylether/MeOH to give a beige solid; yield: 144 mg (58%); 1H -NMR (500 MHz, DMSO- d_6) [δ ppm]: 7.76 (s, 1H), 7.64 (d, $J=8.19$ Hz, 1H), 7.36 (m, 1H), 7.30 (m, 1H), 7.22 (m, 1H), 6.91 (m, 1H), 6.37 (s, 1H), 4.10 (q, $J=7.14$ Hz, 2H), 2.36 (s, 3H), 1.04 (t, $J=7.07$ Hz, 3H); ^{13}C -NMR (125 MHz, DMSO- d_6) [δ ppm]: 163.48, 161.53, 146.18, 133.87, 131.47, 128.33, 127.73, 126.70, 125.69, 121.45, 60.05, 56.65, 20.96, 13.93; ESI-MS $[M-H]^-$: 493.60; HRMS-ESI: m/z calcd. for $C_{25}H_{19}ClN_2O_5S$ $[M + H]^+$: 495.0776 found: 495.0757. HPLC purity: 100%

Ethyl 2-(5-(2-chloro-4-(trifluoromethyl)phenyl)furan-2-yl)-4-hydroxy-1-(6-methyl benzo[d]thiazol-2-yl)-5-oxo-2,5-dihydro-1H-pyrrole-3-carboxylate (38). The compound was synthesized according to the general procedure and was recrystallized from diethylether/MeOH to give a beige solid; yield: 168 mg (57%); 1H NMR (500 MHz, DMSO) δ 12.47 (s, 1H), 7.89 (d, $J=8.2$ Hz, 2H), 7.81 – 7.78 (m, $J=6.5$, 1.6, 0.6 Hz, 2H), 7.64 (d, $J=8.3$ Hz, 1H), 7.26 – 7.21 (m, 2H), 6.86 (d, $J=3.6$ Hz, 1H), 6.34 (s, 1H), 4.23 – 4.03 (m, 2H), 2.38 (s, 3H), 1.12 (t, $J=7.1$ Hz, 3H); ^{13}C NMR (126 MHz, DMSO) δ 164.02, 161.58, 153.77, 151.83, 150.24, 147.17, 146.20, 133.91, 131.61, 131.47, 129.18, 128.51 (q, $^2J_{C-F}=32.9$ Hz), 128.10, 127.81, 127.69 (q, $^3J_{C-F}=3.8$ Hz), 124.50 (q, $^3J_{C-F}=3.5$ Hz), 123.22 (q, $^1J_{C-F}=272.4$ Hz), 121.50, 120.94, 114.17, 112.32, 111.12, 60.11, 55.19, 20.98, 13.99; ESI-MS $[M-H]^-$: 561.1; HRMS-ESI: m/z calcd. for $C_{26}H_{18}ClF_3N_2O_5S$ $[M + H]^+$: 563.065 found: 563.0632. HPLC purity: 100%

Ethyl 4-hydroxy-1-(6-methylbenzo[*d*]thiazol-2-yl)-5-oxo-2-(4-phenylthiophen-2-yl)-2,5-dihydro-1*H*-pyrrole-3-carboxylate (39). The compound was synthesized according to the general procedure and was recrystallized from diethylether/MeOH to give a beige solid; yield: 149 mg (63%); ¹H NMR (500 MHz, DMSO) δ 12.31 (s, 1H), 7.80 – 7.78 (m, 1H), 7.77 – 7.75 (m, 1H), 7.70 (d, *J* = 1.4 Hz, 1H), 7.67 (d, *J* = 8.3 Hz, 1H), 7.65 (dd, *J* = 8.4, 1.2 Hz, 2H), 7.38 (t, *J* = 7.7 Hz, 2H), 7.29 – 7.22 (m, 2H), 6.39 (s, 1H), 4.18 – 4.04 (m, 2H), 2.38 (s, 3H), 1.13 (t, *J* = 7.1 Hz, 3H); ¹³C NMR (126 MHz, DMSO) δ 164.69, 162.11, 153.77, 146.27, 141.84, 140.38, 134.90, 133.76, 131.52, 129.08, 128.89, 127.73, 127.13, 126.77, 126.09, 125.75, 121.46, 120.86, 120.31, 59.61, 56.72, 20.99, 14.10; ESI-MS [M-H]⁻: 475.1; HRMS-ESI: *m/z* calcd. for C₂₅H₂₀N₂O₄S₂ [M + H]⁺: 477.0937 found: 477.0922. HPLC purity: 95%

Ethyl 4-hydroxy-1-(6-methylbenzo[*d*]thiazol-2-yl)-5-oxo-2-(2-(thiophen-2-yl)phenyl)-2,5-dihydro-1*H*-pyrrole-3-carboxylate (40). The compound was synthesized according to the general procedure and was recrystallized from diethylether/MeOH to give an offwhite solid; yield: 177 mg (74%); ¹H NMR (500 MHz, DMSO) δ 12.13 (s, 1H), 7.84 (dd, *J* = 3.5, 1.2 Hz, 1H), 7.74 – 7.72 (m, 1H), 7.70 (dd, *J* = 5.1, 1.2 Hz, 1H), 7.51 (d, *J* = 8.3 Hz, 1H), 7.40 (dd, *J* = 7.7, 1.3 Hz, 1H), 7.27 (td, *J* = 7.5, 1.4 Hz, 1H), 7.24 – 7.15 (m, 3H), 7.08 (dd, *J* = 7.9, 1.3 Hz, 1H), 6.54 (s, 1H), 4.16 – 4.00 (m, 2H), 2.35 (s, 3H), 1.04 (t, *J* = 7.1 Hz, 3H); ¹³C NMR (126 MHz, DMSO) δ 164.47, 162.01, 153.35, 152.16, 146.09, 142.17, 136.32, 134.46, 133.67, 131.54, 131.09, 128.02, 127.97, 127.95, 127.53, 127.11, 126.60, 124.94, 121.38, 120.67, 114.80, 59.99, 57.40, 20.98, 14.01; ESI-MS [M-H]⁻: 475.1; HRMS-ESI: *m/z* calcd. for C₂₅H₂₀N₂O₄S₂ [M + H]⁺: 477.0937 found: 477.0922. HPLC purity: 99%

***tert*-butyl 4-hydroxy-1-(4-methylbenzo[*d*]thiazol-2-yl)-5-oxo-2-phenyl-2,5-dihydro-1*H*-pyrrole-3-carboxylate (41).** The compound was synthesized

according to the general procedure and was purified using CC (10% MeOH in DCM) to give a light yellow solid; yield: 60 mg (28%); ^1H NMR (500 MHz, DMSO) δ 11.98 (s, 1H), 7.78 – 7.75 (m, 1H), 7.42 (d, J = 7.1 Hz, 2H), 7.31 (t, J = 7.5 Hz, 2H), 7.28 – 7.22 (m, 1H), 7.22 – 7.16 (m, 2H), 5.97 (s, 1H), 2.46 (s, 3H), 1.23 (s, 9H); ^{13}C NMR (126 MHz, DMSO) δ 164.28, 161.04, 153.30, 151.48, 147.32, 136.57, 130.96, 130.51, 128.41, 128.00, 127.77, 126.63, 124.11, 119.19, 115.86, 80.74, 61.77, 27.53, 17.42; ESI-MS [$\text{M}-\text{H}$] $^-$: 421.1; HRMS-ESI: m/z calcd. for $\text{C}_{23}\text{H}_{22}\text{N}_2\text{O}_4\text{S}$ [$\text{M} + \text{H}$] $^+$: 423.1373 found: 423.1357. HPLC purity: 100%

***tert*-butyl 4-hydroxy-1-(6-methylbenzo[*d*]thiazol-2-yl)-5-oxo-2-phenyl-2,5-dihydro-1*H*-pyrrole-3-carboxylate (42).** The compound was synthesized according to the general procedure and was recrystallized from diethylether/MeOH to give a light yellow solid; yield: 363 mg (86%); ^1H NMR (500 MHz, DMSO) δ 12.13 (s, 1H), 7.92 – 7.88 (m, 1H), 7.66 (d, J = 8.3 Hz, 1H), 7.53 – 7.48 (m, 2H), 7.44 (t, J = 7.5 Hz, 2H), 7.39 – 7.35 (m, 1H), 7.33 (dd, J = 8.3, 1.7 Hz, 1H), 6.11 (s, 1H), 2.50 (s, 3H), 1.38 (s, 9H); ^{13}C NMR (126 MHz, DMSO) δ 164.54, 161.05, 153.70, 151.45, 146.21, 136.59, 133.66, 131.42, 127.96, 127.94, 127.92, 127.61, 121.39, 120.78, 115.80, 80.68, 61.48, 27.55, 20.94; ESI-MS [$\text{M}-\text{H}$] $^-$: 421.1; HRMS-ESI: m/z calcd. for $\text{C}_{23}\text{H}_{22}\text{N}_2\text{O}_4\text{S}$ [$\text{M} + \text{H}$] $^+$: 423.1373 found: 423.1376. HPLC purity: 100%

***tert*-butyl 1-(6-chlorobenzo[*d*]thiazol-2-yl)-4-hydroxy-5-oxo-2-phenyl-2,5-dihydro-1*H*-pyrrole-3-carboxylate (43).** The compound was synthesized according to the general procedure and was recrystallized from diethylether/MeOH to give a light yellow solid; yield: 137 mg (62%); ^1H NMR (500 MHz, DMSO) δ 12.00 (s, 1H), 8.15 – 8.10 (m, 1H), 7.66 – 7.58 (m, 1H), 7.43 – 7.36 (m, 3H), 7.31 (t, J = 7.4 Hz, 2H), 7.27 – 7.22 (m, 1H), 5.98 (s, 1H), 1.25 (s, 9H); ^{13}C NMR (126 MHz, DMSO) δ 164.18, 160.44, 154.87, 150.45, 146.57, 135.74, 132.46, 127.67, 127.55, 127.50, 127.48,

126.17, 121.81, 121.10, 115.94, 80.39, 61.10, 27.03; ESI-MS [M-H]⁻: 441.1; HRMS-ESI: m/z calcd. for C₂₂H₁₉ClN₂O₄S [M + H]⁺: 443.0827 found: 443.0809. HPLC purity: 100%

2-hydroxyethyl **2-(5-(4-chlorophenyl)furan-2-yl)-4-hydroxy-1-(6-methylbenzo[d]thiazol-2-yl)-5-oxo-2,5-dihydro-1H-pyrrole-3-carboxylate**

(44). The compound was synthesized according to the general procedure and was recrystallized from diethylether/MeOH to give an orange solid; yield: 85 mg (45%); ¹H NMR (500 MHz, DMSO) δ 12.45 (s, 1H), 7.80 (s, 1H), 7.63 (d, J = 8.3 Hz, 1H), 7.57 (d, J = 8.6 Hz, 2H), 7.43 (d, J = 8.6 Hz, 2H), 7.24 (dd, J = 8.4, 1.2 Hz, 1H), 6.91 (d, J = 3.4 Hz, 1H), 6.77 (d, J = 3.4 Hz, 1H), 6.34 (s, 1H), 4.09 (dtd, J = 16.3, 11.1, 5.1 Hz, 2H), 3.55 (t, J = 5.5 Hz, 2H), 2.38 (s, 3H); ¹³C NMR (126 MHz, DMSO) δ 164.07, 161.67, 153.76, 151.70, 151.07, 148.52, 146.25, 133.96, 131.85, 131.50, 128.99, 128.86, 127.84, 124.95, 121.55, 120.95, 112.53, 111.33, 107.75, 65.86, 58.83, 55.38, 21.03; ESI-MS [M-H]⁻: 509.1; HRMS-ESI: m/z calcd. for C₂₅H₁₉ClN₂O₆S [M + H]⁺: 511.0725 found: 511.0704. HPLC purity: 95%

Methyl **2-(5-(4-chlorophenyl)furan-2-yl)-4-hydroxy-1-(6-methylbenzo[d]thiazol-2-yl)-5-oxo-2,5-dihydro-1H-pyrrole-3-carboxylate**

(45). The compound was synthesized according to the general procedure and was purified using CC (10% MeOH in DCM) to give a beige solid; yield: 64 mg (27%); ¹H NMR (500 MHz, DMSO) δ 12.42 (s, 1H), 7.82 – 7.77 (m, J = 0.7 Hz, 1H), 7.64 (d, J = 8.3 Hz, 1H), 7.58 (d, J = 8.7 Hz, 2H), 7.44 (d, J = 8.7 Hz, 2H), 7.25 (dd, J = 8.6, 1.4 Hz, 1H), 6.91 (d, J = 3.4 Hz, 1H), 6.75 (d, J = 3.5 Hz, 1H), 6.29 (s, 1H), 3.68 (s, 3H), 2.39 (s, 3H); ¹³C NMR (126 MHz, DMSO) δ 164.06, 162.14, 153.68, 151.56, 151.10, 148.47, 146.22, 133.92, 131.86, 131.45, 128.98, 128.82, 127.81, 124.94, 121.51, 120.95, 112.52, 111.04, 107.73, 55.33, 51.54, 21.00; ESI-MS [M-H]⁻: 479.0; HRMS-ESI: m/z calcd. for C₂₄H₁₇ClN₂O₅S [M + H]⁺: 481.0619 found: 481.0603. HPLC purity: 100%

tert-butyl 2-(5-(4-chlorophenyl)furan-2-yl)-4-hydroxy-1-(6-methylbenzo[d]thiazol-2-yl)-5-oxo-2,5-dihydro-1H-pyrrole-3-carboxylate

(46). The compound was synthesized according to the general procedure and was recrystallized from diethylether/MeOH to give an orange solid; yield: 600 mg (52%); ^1H NMR (500 MHz, DMSO) δ 12.16 (s, 1H), 7.81 – 7.77 (m, 1H), 7.64 (d, J = 8.3 Hz, 1H), 7.61 (d, J = 8.7 Hz, 2H), 7.45 (d, J = 8.8 Hz, 2H), 7.28 – 7.21 (m, 1H), 6.95 (d, J = 3.4 Hz, 1H), 6.76 (d, J = 3.5 Hz, 1H), 6.23 (s, 1H), 2.38 (s, 3H), 1.30 (s, 9H); ^{13}C NMR (126 MHz, DMSO) δ 164.01, 160.93, 153.80, 151.66, 150.98, 148.94, 146.24, 133.84, 131.84, 131.47, 128.98, 128.85, 127.76, 124.90, 121.48, 120.91, 112.76, 112.48, 107.61, 80.85, 55.39, 27.60, 21.00; ESI-MS $[\text{M}-\text{H}]^-$: 521.1; HRMS-ESI: m/z calcd. for $\text{C}_{27}\text{H}_{23}\text{ClN}_2\text{O}_5\text{S}$ $[\text{M} + \text{H}]^+$: 523.1089 found: 523.1073. HPLC purity: 100%

5.1.4 Biological Evaluation

5.1.4.1 Protein Expression

WT *E. coli* K12 and the C115D mutant MurA were overexpressed as His-tag fusion proteins in *E. coli* BL21 cells. The pAB3 and pAB4 expression plasmids for the WT and C115D mutant MurA respectively were a generous gift from Prof. Dr. Christian Klein, Universität Heidelberg.⁵⁷ The transformed cells were grown at 37°C in LB medium (supplemented with 50 $\mu\text{g}/\text{mL}$ kanamycin) in an INFORS HT Unitron shaking incubator at 180 rpm until a cell density (OD_{600 nm}) of 0.8 was reached (Thermo Fisher Scientific Genesys 10 UV/Vis spectrophotometer). The protein expression was then induced by the addition of 1 mM isopropyl β -D-1-thiogalactopyranoside (IPTG) with continued shaking for 2 hours at 37°C. The cells were harvested by centrifugation at 4000 rpm, 4°C for 30 minutes. The resulting cell pellets were frozen overnight at -80°C to aid in cell lysis and maximize protein yield. The cell pellets were suspended in a lysis buffer consisting of 20 mM Tris-HCl (pH 8), 250 mM NaCl, 5 mM

imidazole and a protease inhibitor cocktail tablet (Roche, cOmplete). They were then sonicated on ice for 10 minutes. The supernatants were obtained following centrifugation at 4000 rpm for 30 minutes at 4°C, and loaded onto a Ni²⁺-NTA agarose column (Qiagen) equilibrated with lysis buffer. Several washing steps were performed using a wash buffer containing 20 mM Tris-HCl (pH 8), 250 mM NaCl, and 20 mM imidazole, and the His-tagged proteins were eluted using 750 mM imidazole added to the lysis buffer. To eliminate the excess imidazole, the resulting protein was dialyzed at 4°C against a buffer containing 20 mM Tris-HCl (pH 8.0), 150 mM NaCl, 1mM 1,4-dithio-D-threitol (DTT), protease inhibitor cocktail and 10% glycerol. The resulting protein concentrations were 5 µg/µL for the wild type MurA, and 0.74 µg/µL for the C115D mutant, as determined by the Thermo Fisher Scientific NanoDrop 2000. The proteins were then aliquoted, flash frozen in liquid nitrogen, and stored at -80 °C. The protein used for native MS was cleaned up using ammonium acetate solution instead of Tris buffer with the same additives in the purification steps. The final dialysis step was performed in an ammonium acetate solution (pH 7.5) with 1 mM DTT and 0.5 mM NaCl. The resulting protein had a concentration of 6.91 µg/µL.

5.1.4.2 MurA Assay

The assay was performed in 96 well plates (Greiner bio-one, F-bottom clear) in a final volume of 100 µL. 1.25 µg, WT MurA was pre-incubated with 150 µM UNAG for 15 minutes at rt. Then the corresponding inhibitors (or DMSO as a control) were added and further incubated for 15 minutes at room temperature (total DMSO concentration was 2%). A master mix consisting of 150 µM PEP, 2 mM Dithiothreitol (DTT) and 25 mM Tris-HCl (pH 7.5) (final concentrations) was then added and the mixture incubated at 37°C for 30 min. For the C115D MurA, the initial UNAG preincubation step was skipped, and the protein was directly preincubated with the inhibitors, while

150 μM UNAG was added to the master mix. The reaction was stopped by the addition of 100 μL of a solution containing malachite green (0.045 % (w/v) in a 1 % PVA solution) and sodium molybdate (4.8% (w/v) in 5 N HCl) at a ratio of 3:1. After 5 min, the absorbance at 625 nm was measured using a BMG LABTECH POLARstar Omega Microplate Reader. The background absorbance (same reaction without addition of MurA) was subtracted from the measured absorbance values. The reaction was prepared in triplicates and IC_{50} values were determined using at least 8 concentrations of the inhibitors. The data were fitted to a dose-response curve using OriginPro 2020.

5.1.4.3 MurB Expression and Assay

Mur B was expressed, its substrate UNAGEP was synthesized and the MurB inhibition assay was performed according to the procedure detailed in Mokbel *et al.*⁴⁵

5.1.4.4 Evaluation of the Reversibility of Inhibition

The experiment was done by incubating enzyme and test compound in an initial concentrated solution, followed by dilution and measurement of the enzymatic activity. For the diluted experiment, the initial concentrated solution, 30 μg MurA was preincubated with 400 μM UNAG for 15 minutes. 2 μL of 0.25 mM inhibitor was added in a final volume of 50 μL . The mixture was further incubated for 15 minutes, and 2 μL of said mixture was added to a master mix containing 150 μM UNAG, 150 μM PEP, 2 mM Dithiothreitol (DTT) and 25 mM Tris-HCl (pH 7.5) (final concentrations) in a final volume of 100 μL . For comparison with the concentrated conditions, an extra 1 μL of 1 mM inhibitor was added to reach the initial inhibitor concentration. The assay was then continued in the same way as the regular MurA enzymatic assay.

As an additional control, the composition of the diluted assay solution was directly

pipetted, and the regular MurA assay procedure was applied with the final inhibitor concentration of 200 nM.

5.1.4.5 Examination of the Synergism between Compound 46 and Fosfomycin

The MurA assay procedure mentioned above was applied using a final concentration of 2 μ M for both the fosfomycin and **46** maintaining a DMSO concentration of 2% in the total assay volume.

5.1.4.6 Enzyme Kinetics Properties

Reactions were performed in deep well plates (Eppendorf, Deepwell 96/2000 μ L, Standard) in a final volume of 550 μ L; 4 total experiments were done at different concentrations of compound **46** (0, 0.5X, 0.625X and 0.75X IC_{50}). For each experiment 4 concentrations of UNAG were used; 25, 100, 250 and 363 μ M. 100 μ L aliquots from the deep well plates were taken at 5, 10, 20 and 30 minutes and the absorbance was measured after the addition of the malachite green/sodium molybdate mixture (3:1). The same procedure as for the enzymatic assay was applied, except that the UNAG was used to start the reaction. The absorbance vs. time for each UNAG concentration was plotted and the slope for each line was used in a Lineweaver-Burk plot, where the reciprocal of the slope (representing $1/V_0$) was plotted against $1/UNAG$ concentration (representing $1/S$) for each compound **46** concentration. The assay was performed in triplicates and the results were plotted using OriginPro 2020.

5.1.4.7 Native MS

The samples were prepared in the ammonium acetate containing dialysis buffer (see under "protein expression") at a 20 μ M protein concentration, then the substrates were then added. The final volume of each sample was 100 μ L. Native protein DFTICR measurements were performed in positive ionization mode on a Bruker Solarix

XR 7T equipped with the Bruker ESI source. The mass spectrometer was externally calibrated to a mass accuracy below 1 ppm, before injecting the samples with the preinstalled syringe pump at 2 μ l/min flowrate. Source and mass analyzer parameters were set as follows: dry gas flow rate 4 L/min at 200 °C, capillary voltage -4000 V, collision RF amplitude 1700 Vpp, Q1 mass 1000 and sweep excitation power 23%. 32 scans were performed accumulating for 500 ms using a total m/z range from 150-5000. The data size was set to 512k.

The acquired spectra were analyzed with the Bruker Data Analysis software using the implemented charge-state-ruler and deconvoluted by using the Maximum Entropy algorithm (Spectrum Square Associates, Inc.).

5.1.4.8 Protein X-ray Co-crystallography

The recombinantly produced MurA protein (45 mg/mL) was combined with compound 46 (1 mM) in order to form the enzyme:inhibitor complex. No major precipitation was observed upon mixing. Crystallization drops were set up using the coarse screens HCS3, HIN3, JCSG7 and LFS6 (all purchased from Molecular Dimensions). The drops were prepared in 3-well crystallization plates (Swissci) by mixing the protein solution with the precipitant solutions in the ratios 2:3, 1:2 and 1:3 to a final volume of 300 nL. The plates were incubated at 4°C or 20°C, respectively.

Crystals appeared in a multitude of crystallization conditions. About 50 crystals were probed by collecting X-ray data and analyzing the datasets with the SLS automated data processing (adp) pipeline. 2 crystal forms were identified, corresponding to the PDB entries 1EJC and 3SWD,⁵¹ respectively. In both crystal forms, no electron density for compound 46 was observed.

5.1.4.9 Expression and Purification of U-¹⁵N MurA and U-¹⁵N C115D MurA

Modified M9 minimal medium was prepared as follows: 6 g Na₂HPO₄, 3 g KH₂PO₄ and 0.5 g NaCl were dissolved in 1 L of double deionized water and autoclaved. Then, kanamycin was added to a final concentration of 35 µg/mL, as well as sterile filtered solutions of MgSO₄ (final concentration = 2.5 mM), CaCl₂ (final concentration = 0.1 mM), 4 g D-Glucose, 1 g ¹⁵NH₄Cl and 100 µL of a 10,000x vitamin mix (5 g riboflavin, 5 g niacinamide, 5 g pyridoxine monohydrate and 5 g thiamine dissolved in ethanol)

10 mL LB media per liter large culture supplemented with kanamycin at a concentration of 50 µg/mL was inoculated with 1-5 colonies from MurA or C115D MurA producing *E. coli* BL21 cells LB agar plates and incubated in a shaking incubator (INFORS HT Unitron shaking incubator) at 37 °C overnight. The following morning, 1 L of the modified M9 media described above was inoculated with 10 mL of the overnight culture. The bacteria were grown in a shaking incubator at 37 °C to an OD₆₀₀ of ~ 0.4, after which the temperature was dropped to 20 °C. Protein expression was induced at an OD₆₀₀ of 0.7-0.9 with isopropyl β-D-1-thiogalactopyranosid (IPTG) at a final concentration of 0.5 mM and grown at 20 °C overnight. The next day, the bacteria were harvested by centrifugation at 6,000 x g for 15 min and the cell pellets were either stored at -80 °C or immediately prepared for purification.

Bacterial cell pellets were resuspended in ~ 25 mL resuspension buffer (50 mM Tris-HCl, pH 8.0, 150 mM NaCl, 10 mM imidazole, 2 mM β-mercaptoethanole [BME], 1 cOmplete™ Protease Inhibitor Cocktail tablet) per liter culture. Resuspended cells were then lysed by sonication (30 % amplitude, 5 min sonication time, 2 s on pulse, 4

s off pulse). Cell lysates were pelleted by centrifugation at 30,000 x g for 40 min at 4 °C. Cleared lysates were incubated with ~ 3 mL Ni-NTA agarose resin, preequilibrated with wash buffer (50 mM Tris-HCl, pH = 8.0, 150 mM NaCl, 10 mM imidazole, 2 mM BME) per liter culture for 2-16 h at 4 °C. The resin was washed with wash buffer until 10 µL of eluent no longer stained blue with 50 µL of Bradford reagent (Coomassie blue G-250). Bound protein was eluted with elution buffer (50 mM Tris-HCl, pH = 8.0, 150 mM NaCl, 350 mM imidazole, 2 mM BME). After elution, the protein was dialyzed overnight against 4 L of dialysis buffer (50 mM Tris-HCl, pH = 7.5, 1 mM ethylenediaminetetraacetic acid [EDTA] and 2 mM dithiothreitol [DTT]). Dialyzed protein was concentrated to ~ 5 mL and subjected to size exclusion chromatography using a Superdex 200 increase 10/300 GL column preequilibrated with MurA NMR buffer (50 mM sodium phosphate, pH = 7.0, 1 mM EDTA, 2 mM DTT).

5.1.4.10 Protein NMR Experiments

¹⁵N-¹H-HSQC spectra were recorded on a Bruker Avance III 800 MHz spectrometer with a TXO-style cryogenically cooled probe. ¹⁵N-labelled WT or C115D MurA was concentrated to a final concentration of 200 µM in a MurA NMR buffer supplemented with 5% D₂O. A reference spectrum was recorded at 298 K by addition of DMSO to a final concentration of 2%. Additional ¹⁵N-¹H-HSQC spectra were recorded after the addition of UNAG and **46** or fosfomycin, as well as **46** or fosfomycin alone, each to a final concentration of 500 µM. NMR experiments were processed with nmrPipe and analyzed using the ccpNMR software (version 2.4.1).⁵⁸

5.1.4.11 Cytotoxicity Evaluation

20,000 MRC-5 (human lung fibroblasts) and 25,000 HepG2 (human liver cancer) cells were seeded into 96 well plates. On the next day, the cells were treated with the compounds (dissolved in DMSO) for 24 h. After treatment, their viability was determined by an MTT assay: the supernatants were replaced by 0.5 mg/ml MTT (3-(4,5-dimethylthiazole-2-yl)-2,5 diphenyltetrazolium bromide, Sigma-Aldrich #M5655) in DMEM (Dulbecco's Modified Eagle Medium). After incubation, the cells were lysed in DMSO, and the absorbance was measured at 560 nm using a Promega GloMax microplate reader.

5.1.4.12 Antibacterial Testing and IC₉₀ Determination

IC₉₀ values for *E. coli* $\Delta tolC$, and *S. aureus* (Newman strain) were determined for all compounds with a maximal DMSO concentration of 1% as previously described.⁵⁹ Final compound concentrations prepared from serial dilutions ranged from 1.25 to 40 μ M. The ODs were determined after addition of the compounds and again after incubation for 16 h at 37 °C and 50 rpm in 96 well plates using a POLARstar Omega Microplate Reader (BMG LABTECH). The indicated IC₉₀ values are means of two independent determinations. They are defined as the lowest concentration of compounds that reduced the OD₆₀₀ by ≥ 90 % and were determined from the inhibition curves. Experiments were made at least two times and the standard deviation was less than 20 % (most cases: < 15 %). LB broth was used for *E. coli*, and Müller Hinton medium was used for *S. aureus*.

For the PMBN experiments, PMBN was dissolved in dd H₂O at a concentration of 5 mg/mL. An appropriate amount of PMBN (final concentration in the plates was either 3, 4.5, or 6 μ g/mL) was added to the diluted bacterial solution right before adding to the plates containing the compounds. The plates were incubated and measured as

mentioned previously. ODs for the plates containing PMBN were compared to the ones without PMBN and no decrease in bacterial viability was observed.

5.1.4.13 Stability in Biological Media

Stability in human S9 fraction, and human plasma was performed as described by Spork *et. al* and Gargano *et. al.*^{59,60} For the stability in bacterial lysate, an overnight liquid culture was prepared by inoculating 10 mL LB medium with one colony of *E. coli* $\Delta tolC$. The culture was shaken over night at 37°C and 180 rpm in a shaking incubator (INFORS HT Unitron shaking incubator). The following day, 250 mL LB were inoculated with 1 mL of the overnight culture and grown to an OD of 0.6 (Thermo Fisher Scientific Genesys 10 UV/Vis spectrophotometer). The cells were recovered by centrifugation at 4°C, and 5000 rpm in a Sorval/SLA1500 centrifuge. The cell pellet was then resuspended in 10 mL of 0.05 M Na phosphate buffer supplemented with 1mM MgCl₂ and one protease inhibitor cocktail tablet (Roche, cOmplete). The cells were lysed by sonication for ten 15 sec cycles, at 80% power, then centrifuged at 4000 rpm for 30 minutes at 4°C to obtain the bacterial lysate as the supernatant, which was then aliquoted and flash frozen in liquid N₂ and stored at -80°C.

The stability assay was carried out in duplicates, in separate caps for different incubation periods, solutions containing 10 μ M of the test compound in addition to the prepared bacterial lysate at 30 μ L total volume were incubated at 37 °C. Incubations were stopped by the addition of an ice-cold 1.5 μ M solution of diphenhydramine (internal standard for HPLC-MS analysis) in acetonitrile (double volume of initial incubation mixture for a 1 μ M final concentration). The obtained samples were mixed for 10 min and then centrifuged (13300 rpm for 5 min). The supernatants were analyzed by high-resolution MS on a Thermo Fisher Scientific Q

Exactive Orbitrap mass spectrometer with ESI ionization mode coupled with an Ultimate 3000 HPLC system by Thermo Fisher Scientific, equipped with a Thermo Accucore phenyl-X column (2.1 μm , 3 \times 100 mm). Quantifications (max. 333 nM test compound and 1 μM diphenhydramine as internal standard) were based on a previously recorded calibration curve for the respective test compound (final concentrations: 10-500 nM).

5.2 Experimental Methodology of Chapter 3.4

The numbering of compounds in this chapter follows the numbering in chapter 3.4.

The references for this section are included in section 3.4.5.

5.2.1 Chemistry

The compounds were all purchased from Sigma Aldrich, Alfa aesar, BLD pharm, Carbosynth, Fluorochem, TCI, abcr, and AK scientific and used as received. (CAS numbers for the compounds are listed in Table S1, Supporting Information). The identity and purity of some selected relevant compounds was confirmed using LC-MS analysis (*Figures S2, S3 and S4*, Supporting Information, section 7.7).

5.2.2 Biological Evaluation

5.2.2.1 Cloning of the *E. cloacae murA* Insert into an Expression Plasmid

The *E. cloacae murA* insert was obtained in a pEX-A258 vector from Eurofins Scientific (Supporting Information, *Figure S5*, section 7.7). The expression vector pGEX-4T-1 was obtained as a part of the pGEX-4T-1-3xMyc-ERK2-K52R plasmid from Addgene. Both plasmids were double digested using 1 μL each, NcoI and NotI restriction enzymes, and 5 μL NEBuffer r3.1, all from New England Biolabs. 1 μg of each plasmid was digested in a reaction with 50 μL final volume, and the mixture was incubated at

37 °C for 2 h. The resultant bands were purified using gel electrophoresis with a 1% agarose gel in 1X TAE buffer (0.4 M Tris acetate and 0.01 M EDTA). The samples were prepared as follows: for the reference, 2 µL peqGOLD 1 kb DNA ladder was used in addition to 23 µL water and 5 µL 6X DNA loading dye (consisting of 25 mg bromothymol blue, 6 mL glycerol and 4 mL 5X TAE buffer). As for the cut plasmids, to each 50 µL reaction, 10 µL 6X DNA loading dye was added. The samples were run at 100 V, and the gel was then incubated in 600 mL 1X TAE buffer and 30 µL ethidium bromide for 30 min and then de-stained for 10 min in water. Bands of the correct size for the MurA insert and expression vector were cut (1291 bp and 5050 bp, respectively (Supporting Information Figure S2)). The DNA was extracted using the Macherey Nagel NucleoSpin Gel and PCR Clean-up kit, with resultant concentrations being 7.8 ng/µL for the *E. cloacae* MurA insert and 13.5 ng/µL for the pGEX-4T1 vector.

The insert and the vector were ligated together with a ratio of 60 ng of the expression vector to 46 ng of the insert, according to the *in silico* University of Duesseldorf ligation calculator [47]. 1 µL T4 DNA ligase from New England Biolabs, 2 µL 10X ligase buffer and water were added to a final volume of 20 µL. The reaction was incubated at rt for 4 h and the ligated plasmid was used to transform chemically competent C41 *E. coli* BL21 cells.

5.2.2.2 Transformation for Overexpression of MurA

The bacterial transformation protocol started with thawing competent C41 *E. coli* BL21 cells from Sigma Aldrich (catalogue number: CMC0017) on ice, then 50 ng plasmid DNA was added, and the cells were incubated on ice for 30 min. The *E. coli* MurA WT and C115D mutant plasmids were obtained as previously described [49] and the *E. cloacae* MurA expression plasmid was generated as described above. The

cells were then heat-shocked for 1 min at 42 °C and were again stored on ice for 2 min. Subsequently, 500 mL LB medium was added to the cells and they were incubated at 37 °C shaking at 180 rpm for 1 h in an INFORS HT Unitron shaking incubator. The cells were then plated on LB plates with 50 µg/mL ampicillin and incubated at 37 °C overnight. Plasmids were extracted from the produced cultures using the GenElute HP Plasmid Miniprep kit from Sigma Aldrich (catalogue number: PLN70). The purified plasmids were first checked by double-digestion using NcoI and NotI and applied to a 1% agarose gel (*vide supra*). The two bands with the correct masses of the insert and vector were observed (Fig. S7, Supporting Information). They were then confirmed to have the correct sequence using DNA sequencing analysis by Azenta Life Sciences Inc., USA (predefined Sanger sequencing using 3GEX and 5GEX primers).

5.2.2.3 Protein Expression and Purification

E. cloacae MurA was overexpressed as GST-tag fusion protein in *E. coli* BL21 cells. The transformed cells were grown at 37 °C in LB medium (supplemented with 50 µg/mL ampicillin) in the shaking incubator until a cell density (OD 600 nm) of 0.8 was reached (Thermo Fisher Scientific Genesys 10uv spectrophotometer). The protein expression was then induced by the addition of 1 mM isopropyl β-D-1-thiogalactopyranoside (IPTG) with continued shaking at 37 °C for 2 h. The cells were harvested by centrifugation at 4000 rpm and 4 °C for 30 min. The resultant cell pellet was frozen at -80 °C overnight to support cell lysis and maximize protein yield. The cell pellet was suspended in 10 mL lysis buffer consisting of 125 mM Tris-HCl (pH 7.5), 150 mM NaCl, 1 mM 1,4-dithio-d-threitol (DTT), 1 mM EDTA, 1 mg/mL lysozyme from chicken egg white, 0.5% Igepal (v/v), and a protease inhibitor cocktail tablet (Roche, cOmplete). They were then sonicated on ice for 10 min. The supernatant was obtained following centrifugation at 4000 rpm at 4 °C for 30 min and then loaded onto

PureCube Glutathione agarose beads and incubated at 4 °C for 1 h in an end-to-end shaker for optimum binding. The beads were applied to disposable 5 mL polypropylene columns (Thermo Scientific) and three washing steps were performed using a wash buffer containing 125 mM Tris-HCl (pH 7.5), 150 mM NaCl, 1 mM DTT and 1 mM EDTA. The GST-tagged protein was eluted using 125 mM Tris-HCl (pH 7.5), 150 mM NaCl, 1 mM DTT, in addition to 50 mM reduced glutathione. The resultant protein was dialyzed at 4 °C against a buffer containing 20 mM Tris-HCl (pH 7.5), 150 mM NaCl, 1 mM DTT, protease inhibitor cocktail and 10% glycerol. The resultant protein concentration was 1.4 µg/µL as determined using a Thermo Fisher Scientific NanoDrop 2000. The protein was then aliquoted, flash-frozen in liquid nitrogen, and stored at -80 °C.

5.2.2.4 Antibacterial Activities

Growth inhibition for *E. coli* $\Delta tolC$, and *S. aureus* (Newman strain) was investigated for all compounds with a maximal DMSO concentration of 1% as previously described [50]. Final compound concentrations prepared from serial dilutions ranged from 3.125 to 100 µM. OD values were determined at 600 nm after addition of the compounds and again after incubation at 37 °C and 50 rpm for 16 h in 96-well plates using a POLARstar Omega Microplate Reader (BMG LABTECH). Experiments were made at least twice. LB broth was used for *E. coli*, and Müller Hinton medium was used for *S. aureus*.

5.2.2.5 Fluorescence Binding Assay

Fluorescence spectra were measured at rt and recorded on a FP-8300 JASCO spectrometer (wavelength accuracy ± 1.5 nm) using quartz glass cuvettes (precision cuvettes made of quartz glass Model FP-1004, JASCO parts center). The measurements were conducted in a buffer consisting of 50 mM phosphate buffer (pH

6.9) with 1 mM DTT. The fluorescence was measured at an excitation wavelength of 366 nm and the emission spectra were recorded between 375 nm and 700 nm. The concentrations of both WT *E. coli* and *E. cloacae* MurA were 140 $\mu\text{g/mL}$. The concentrations of ANS and compounds **11** and **26** were 100, 10 and 1 μM , respectively. The spectra were recorded 5 min after addition of the ligand.

5.2.3 Molecular Modelling and Docking

The molecular modelling and docking studies were performed using MOE 2010 as previously described in El Hady *et. al.*[51].

6. References

- (1) S. Sengupta, M. K. Chattopadhyay, H. P. Grossart; The Multifaceted Roles of Antibiotics and Antibiotic Resistance in Nature; *Front. Microbiol.* **2013**, *4*, 1–13.
- (2) M. Hutchings, A. Truman, B. Wilkinson; Antibiotics: Past, Present and Future; *Curr. Opin. Microbiol.* **2019**, *51*, 72–80.
- (3) C. L. Ventola; The Antibiotic Resistance Crisis: Part 1: Causes and Threats; *Pharm. Ther.* **2015**, *40*, 277–283.
- (4) S. A. Waksman; The Role of Antibiotics in Nature; *Perspect. Biol. Med.* **1961**, *4*, 271–286.
- (5) A. Fleming; On the Antibacterial Action of Cultures of a *Penicillium*, with Special Reference to Their Use in the Isolation of *B. Influenzæ*; *Br. J. Exp. Pathol.* **1929**, *10*, 226–236.
- (6) A. C. Pawlowski, J. W. Johnson, G. D. Wright; Evolving Medicinal Chemistry Strategies in Antibiotic Discovery; *Curr. Opin. Biotechnol.* **2016**, *42*, 108–117.
- (7) E. D. Brown, G. D. Wright; Antibacterial Drug Discovery in the Resistance Era; *Nature* **2016**, *529*, 336–343.
- (8) C. Walsh; Where Will New Antibiotics Come From? *Nat. Rev. Microbiol.* **2003**, *1*, 65–70.
- (9) H. Brötz-Oesterhelt, P. Sass; Postgenomic Strategies in Antibacterial Drug Discovery; *Future Microbiol.* **2010**, *5*, 1553–1579.
- (10) U. Theuretzbacher; Future Antibiotics Scenarios: Is the Tide Starting to Turn? *Int. J. Antimicrob. Agents* **2009**, *34*, 15–20.
- (11) K. Bush; Improving Known Classes of Antibiotics: An Optimistic Approach for the Future; *Curr. Opin. Pharmacol.* **2012**, *12*, 527–534.
- (12) L. L. Silver; Challenges of Antibacterial Discovery; *Clin. Microbiol. Rev.* **2011**, *24*, 71–109.
- (13) M. S. Morehead, C. Scarbrough; Emergence of Global Antibiotic Resistance; *Prim. Care – Clin. Off. Pract.* **2018**, *45*, 467–484.
- (14) B. D. Lushniak; Antibiotic Resistance: A Public Health Crisis; *Public Health Rep.* **2014**, *129*, 314–316.

- (15) J. Davies; Origins and Evolution of Antibiotic Resistance; *Microbiologia* **1996**, 74, 9–16.
- (16) K. Poole; Mechanisms of Bacterial Biocide and Antibiotic Resistance; *J. Appl. Microbiol.* **2002**, 92, 55S-64S.
- (17) M. N. Alekshun, S. B. Levy; Molecular Mechanisms of Antibacterial Multidrug Resistance; *Cell*, **2007**, 128, 1037–1050.
- (18) WHO. Prioritization of Pathogens to Guide Discovery, Research and Development of New Antibiotics for Drug-Resistant Bacterial Infections, Including Tuberculosis; **2017**, <https://www.who.int/publications/i/item/WHO-EMP-IAU-2017.12>
- (19) L. B. Rice; Federal Funding for the Study of Antimicrobial Resistance in Nosocomial Pathogens: No ESKAPE; *J. Infect. Dis.* **2008**, 197, 1079–1081.
- (20) D. M. P. de Oliveira, B. M. Forde, T. J. Kidd, P. N. A. Harris, M. A. Schembri, S. A. Beatson, D. L. Paterson, M. J. Walker; Antimicrobial Resistance in ESKAPE Pathogens; *Clin. Microbiol. Rev.* **2020**, 33, 1–19.
- (21) R. J. Fair, Y. Tor; Antibiotics and Bacterial Resistance in the 21st Century; *Perspect. Med. Chem.* **2014**, 6, 25–64.
- (22) A. Shariati, M. Dadashi, M. T. Moghadam, A. van Belkum, S. Yaslianifard, D. Darban-Sarokhalil; Global Prevalence and Distribution of Vancomycin Resistant, Vancomycin Intermediate and Heterogeneously Vancomycin Intermediate *Staphylococcus Aureus* Clinical Isolates: A Systematic Review and Meta-Analysis; *Sci. Rep.* **2020**, 10, 12689.
- (23) WHO. *Global Tuberculosis Report 2021*; **2021**, <https://www.who.int/teams/global-tuberculosis-programme/tb-reports/global-tuberculosis-report-2021>
- (24) H. K. Doh, J. K. Hee, S. K. Park, S. J. Kong, S. K. Young, T. H. Kim, K. K. Eun, M. L. Ki, S. L. Sung, S. P. Jae, W. J. Koh, C. H. Lee, Y. K. Ji, S. S. Tae; Treatment Outcomes and Long-Term Survival in Patients with Extensively Drug-Resistant Tuberculosis; *Am. J. Resp. Care Med.* **2008**, 178, 1075–1082.
- (25) S. E. Dorman, R. E. Chaisson; From Magic Bullets Back to the Magic Mountain: The Rise of Extensively Drug-Resistant Tuberculosis; *Nat. Med.* **2007**, 13, 295–298.

- (26) M. Morar, G. D. Wright; The Genomic Enzymology of Antibiotic Resistance; *Annu. Rev. Genet.* **2010**, *44*, 25–51.
- (27) G. A. Pankey, L. D. Sabath; Clinical Relevance of Bacteriostatic versus Bactericidal Mechanisms of Action in the Treatment of Gram-Positive Bacterial Infections; *Clin. Infect. Dis.* **2004**, *38*, 864–870.
- (28) J. Nemeth, G. Oesch, S. P. Kuster; Bacteriostatic versus Bactericidal Antibiotics for Patients with Serious Bacterial Infections: Systematic Review and Meta-Analysis; *J. Antimicrob. Chemother.* **2015**, *70*, 382–395.
- (29) E. L. Miller; The Penicillins: A Review and Update; *J. Midwifery Women's Health* **2002**, *47*, 426–434.
- (30) H. Brötz-Oesterhelt, N. A. Brunner; How Many Modes of Action Should an Antibiotic Have? *Curr. Opin. Pharmacol.* **2008**, *8*, 564–573.
- (31) O. A. Abraham, V. M. Rosa, S. S. Marco Antonio, G. Claudia, M. E. María del Rosario; Review of Antibiotic and Non-Antibiotic Properties of Beta-Lactam Molecules; *Antiinflamm. Antiallergy Agents Med. Chem.* **2016**, *15*, 3–14.
- (32) M. S. Butler, K. A. Hansford, M. A. T. Blaskovich, R. Halai, M. A. Cooper; Glycopeptide Antibiotics: Back to the Future; *J. Antibiot.* **2014**, *67*, 631–644.
- (33) H. K. Kang, Y. Park; Glycopeptide Antibiotics: Structure and Mechanisms of Action; *J. Bacteriol. Virol.* **2015**, *45*, 67–78.
- (34) F. Schlünzen, R. Zarivach, J. Jörg Harms, A. Bashan, A. Tocilj, R. Albrecht, A. Yonath, F. Franceschi; Structural Basis for the Interaction of Antibiotics with the Peptidyl Transferase Centre in Eubacteria; *Nature* **2001**, *413*, 814–821.
- (35) S. Arenz, D. N. Wilson; Bacterial Protein Synthesis as a Target for Antibiotic Inhibition; *Cold Spring Harb. Perspect. Med.* **2016**, *6*, a025361.
- (36) P. M. Hawkey; Mechanisms of Quinolone Action and Microbial Response; *J. Antimicrob. Chemother.* **2003**, *51*, 29–35.
- (37) R. J. Henry; The Mode of Action of Sulfonamides; *Bacteriol. Rev.* **1943**, *7*, 175–262.
- (38) R. Gleckman, N. Blagg, D. W. Joubert; Trimethoprim: Mechanisms of Action, Antimicrobial Activity, Bacterial Resistance, Pharmacokinetics, Adverse Reactions, and Therapeutic Indications; *Pharmacotherapy* **1981**, *1*, 14–19.

- (39) P. H. Nakhate, V. K. Yadav, A. N. Pathak; Correspondence: A Review on Daptomycin; the First US-FDA Approved Lipopeptide Antibiotics; *J. Sci. Innov.* **2013**, *2*, 970–980.
- (40) A. P. Zavascki, L. Z. Goldani, J. Li, R. L. Nation; Polymyxin B for the Treatment of Multidrug-Resistant Pathogens: A Critical Review; *J. Antimicrob. Chemother.* **2007**, *60*, 1206–1215.
- (41) M. J. Trimble, P.; Mlynářčik, M. Kolář, R. E. W. Hancock; Polymyxin: Alternative Mechanisms of Action and Resistance; *Cold Spring Harb. Perspect. Med.* **2016**, *6*, 1–22.
- (42) D. Scheffers, M. Pinho; Bacterial Cell Wall Synthesis: New Insights from Localization Studies; *Microbiol. Mol. Biol. Rev.* **2005**, *69*, 585–607.
- (43) A. L. Koch; The Exoskeleton of Bacterial Cells (the Sacculus): Still a Highly Attractive Target for Antibacterial Agents That Will Last for a Long Time; *Crit. Rev. Microbiol.* **2000**, *26*, 1–35.
- (44) A. L. Lovering, S. S. Safadi, N. C. J. Strynadka; Structural Perspective of Peptidoglycan Biosynthesis and Assembly; *Annu. Rev. Biochem.* **2012**, *81*, 451–478.
- (45) P. Schumann; Peptidoglycan Structure; *Methods Microbiol.* **2011**, *38*, 101–129.
- (46) S. Sobhanifar, D. T. King, N. C. J. Strynadka; Fortifying the Wall: Synthesis, Regulation and Degradation of Bacterial Peptidoglycan; *Curr. Opin. Struct. Biol.* **2013**, *23*, 695–703.
- (47) D. W. Green; The Bacterial Cell Wall as a Source of Antibacterial Targets; *Expert Opin. Therap. Targets* **2002**, *6*, 1–20.
- (48) J. B. Ward; Biosynthesis of Peptidoglycan: Points of Attack by Wall Inhibitors; *Pharmacol. Ther.* **1984**, *25*, 327–369.
- (49) T. J. Beveridge; Ultrastructure, Chemistry, and Function of the Bacterial Wall; *Int. Rev. Cytol.* **1981**, *72*, 229–317.
- (50) A. El Zoeiby, F. Sanschagrín, P. C. Havugimana, A. Garnier, R. C. Levesque; In Vitro Reconstruction of the Biosynthetic Pathway of Peptidoglycan Cytoplasmic Precursor in *Pseudomonas Aeruginosa*; *FEMS Microbiol. Lett.* **2001**, *201*, 229–235.
- (51) D. Mengin-Lecreulx, B. Flouret, J. van Heijenoort; Cytoplasmic Steps of Peptidoglycan Synthesis in *Escherichia Coli*; *J. Bacteriol.* **1982**, *151*, 1109–1117.

- (52) P. Sarkar, V. Yarlagadda, C. Ghosh, J. A. Haldar; Review on Cell Wall Synthesis Inhibitors with an Emphasis on Glycopeptide Antibiotics; *MedChemComm* **2017**, 516–533.
- (53) H. Barreteau, A. Kovač, A. Boniface, M. Sova, S. Gobec, D. Blanot; Cytoplasmic Steps of Peptidoglycan Biosynthesis; *FEMS Microbiol. Rev.* **2008**, *32*, 168–207.
- (54) B. Badet, P. Vermoote, P. Yves Haumont, F. Lederer, F. Le Goffic; Glucosamine Synthetase from *Escherichia Coli*: Purification, Properties, and Glutamine-Utilizing Site Location; *Biochemistry* **1987**, *26*, 1940–1948.
- (55) A. Teplyakov, G. Obmolova, M. A. Badet-Denisot, B. Badet, I. Polikarpov; Involvement of the C Terminus in Intramolecular Nitrogen Channeling in Glucosamine 6-Phosphate Synthase: Evidence from a 1.6 Å Crystal Structure of the Isomerase Domain; *Structure* **1998**, *6*, 1047–1055.
- (56) L. Jolly, P. Ferrari, D. Blanot, J. van Heijenoort, F. Fassy, D. Mengin-Lecreulx; Reaction Mechanism of Phosphoglucosamine Mutase from *Escherichia Coli*; *Eur. J. Biochem.* **1999**, *262*, 202–210.
- (57) D. Mengin Lecreulx, J. van Heijenoort; Copurification of Glucosamine-1-Phosphate Acetyltransferase and *N*-Acetylglucosamine-1-Phosphate Uridyltransferase Activities of *Escherichia Coli*: Characterization of the GlmU Gene Product as a Bifunctional Enzyme Catalyzing Two Subsequent Steps in the Pathway for UDP-*N*-Acetylglucosamine Synthesis; *J. Bacteriol.* **1994**, *176*, 5788–5795.
- (58) C. Rani, I. Khan; A. UDP-GlcNAc Pathway: Potential Target for Inhibitor Discovery against *M. Tuberculosis*; *Eur. J. Pharm. Sci.* **2016**, 62–70.
- (59) A. El Zoeiby, F. Sanschagrín, R. C. Levesque; Structure and Function of the Mur Enzymes: Development of Novel Inhibitors; *Mol. Microbiol.* **2003**, *47*, 1–12.
- (60) M. Hrast, I. Sosič, R. Šink, S. Gobec; Inhibitors of the Peptidoglycan Biosynthesis Enzymes MurA-F; *Bioorg. Chem.* **2014**, *55*, 2–15.
- (61) H. Hao, G. Cheng, M. Dai, Q. Wu, Z. Yuan; Inhibitors Targeting on Cell Wall Biosynthesis Pathway of MRSA; *Mol. Biosyst.* **2012**, *8*, 2828.
- (62) L. M. Mihalovits, G. G. Ferenczy, G. M. Keserü; Catalytic Mechanism and Covalent Inhibition of UDP-*N*-Acetylglucosamine Enolpyruvyl Transferase (MurA): Implications to the Design of Novel Antibacterials; *J. Chem. Inf. Model.* **2019**, *59*, 5161–5173.

- (63) T. Skarzynski, A. Mistry, A. Wonacott, S. E.; Hutchinson, V. A. Kelly, K. Duncan; Structure of UDP-*N*-Acetylglucosamine Enolpyruvyl Transferase, an Enzyme Essential for the Synthesis of Bacterial Peptidoglycan, Complexed with Substrate UDP-*N*-Acetylglucosamine and the Drug Fosfomycin; *Structure* **1996**, *4*, 1465–1474.
- (64) K. L. Constantine, L. Mueller, V. Goldfarb, M. Wittekind, W. J. Metzler, J. Yanchunas Jr., J. G. Robertson, M. F. Malley, M. S. Friedrichs, B. T. Farmer 2nd; Characterization of NADP⁺ Binding to Perdeuterated MurB: Backbone Atom NMR Assignments and Chemical-Shift Changes; *J. Mol. Biol.* **1997**, *267*, 1223–1246.
- (65) T. E. Benson, C. T. Walsh, J. M. Hogle; The Structure of the Substrate-Free Form of MurB, an Essential Enzyme for the Synthesis of Bacterial Cell Walls; *Structure* **1996**, *4*, 47–54.
- (66) A. Perdih, M. Hrast, H. Barreteau, S. Gobec, G. Wolber, T. Solmajer; Benzene-1,3-Dicarboxylic Acid 2,5-Dimethylpyrrole Derivatives as Multiple Inhibitors of Bacterial Mur Ligases (MurC-MurF); *Bioorg. Med. Chem.* **2014**, *22*, 4124–4134.
- (67) C. A. Smith; Structure, Function and Dynamics in the Mur Family of Bacterial Cell Wall Ligases; *J. Mol. Biol.* **2006**, *362*, 640–655.
- (68) P. LeMagueres, H. Im, J. Ebalunode, U. Strych, M. J. Benedik, J. M. Briggs, H.; Kohn, K. L. Krause; The 1.9 Å Crystal Structure of Alanine Racemase from *Mycobacterium Tuberculosis* Contains a Conserved Entryway into the Active Site; *Biochemistry* **2005**, *44*, 1471–1481.
- (69) J. P. Shaw, G. A. Petsko, D. Ringe; Determination of the Structure of Alanine Racemase from *Bacillus Stearothermophilus* at 1.9-Å Resolution; *Biochemistry* **1997**, *36*, 1329–1342.
- (70) C. Fan, P. C. Moews, C. T. Walsh, J. R. Knox; Vancomycin Resistance Structure of D-Alanine D-Alanine Ligase at 2.3 Å Resolution; *Science* **1994**, *266*, 439–443.
- (71) A. Bouhss, A. E. Trunkfield, T. D. H. Bugg, D. Mengin-Lecreulx; The Biosynthesis of Peptidoglycan Lipid-Linked Intermediates; *FEMS Microbiol. Rev.* **2008**, *32*, 208–233.
- (72) B. C. Chung, J. Zhao, R. A. Gillespie, D. Y. Kwon, Z. Guan, J. Hong, P. Zhou, S. Y. Lee; Crystal Structure of MraY, an Essential Membrane Enzyme for Bacterial Cell Wall Synthesis; *Science* **2013**, *341*, 1012–1016.

- (73) T. den Blaauwen, J. M. Andreu, O. Monasterio; Bacterial Cell Division Proteins as Antibiotic Targets; *Bioorg. Chem.* **2014**, *55*, 27–38.
- (74) A. E. Trunkfield, S. S. Gurcha, G. S. Besra, T. D. H. Bugg; Inhibition of *Escherichia Coli* Glycosyltransferase MurG and *Mycobacterium Tuberculosis* Gal Transferase by Uridine-Linked Transition State Mimics; *Bioorg. Med. Chem.* **2010**, *18*, 2651–2663.
- (75) A. A. Branstrom, S. Midha, C. B. Longley, K. Han, E. R. Baizman, H. R. Axelrod; Assay for Identification of Inhibitors for Bacterial MraY Translocase or MurG Transferase; *Anal. Biochem.* **2000**, *280*, 315–319.
- (76) J. van Heijenoort; Recent Advances in the Formation of the Bacterial Peptidoglycan Monomer Unit. *Nat. Prod. Rep.* **2001**, *18*, 503–519.
- (77) D. Münch, H. G. Sahl; Structural Variations of the Cell Wall Precursor Lipid II in Gram-Positive Bacteria - Impact on Binding and Efficacy of Antimicrobial Peptides; *Biochim. Biophys. Acta Biomembr.* **2015**, *1848*, 3062–3071.
- (78) S. S. Hegde, T. E. Shrader; FemABX Family Members Are Novel Nonribosomal Peptidyltransferases and Important Pathogen-Specific Drug Targets; *J. Biol. Chem.* **2001**, *276*, 6998–7003.
- (79) T. Schneider, M. M. Senn, B. Berger-Bächi, A. Tossi, H. G. Sahl, I. Wiedemann; In Vitro Assembly of a Complete, Pentaglycine Interpeptide Bridge Containing Cell Wall Precursor (Lipid II-Gly5) of *Staphylococcus Aureus*; *Mol. Microbiol.* **2004**, *53*, 675–685.
- (80) T. A. Figueiredo, R. G. Sobral, A. M. Ludovice, J. M. F. de Almeida, N. K. Bui, W. Vollmer, H. de Lencastre, A. Tomasz; Identification of Genetic Determinants and Enzymes Involved with the Amidation of Glutamic Acid Residues in the Peptidoglycan of *Staphylococcus Aureus*; *PLoS Pathog.* **2012**, *8*, 1–13.
- (81) W. Vollmer, D. Blanot, M. A. de Pedro; Peptidoglycan Structure and Architecture; *FEMS Microbiol. Rev.* **2008**, *32*, 149–167.
- (82) S. Ha, D. Walker, Y.; Shi, S. Walker; The 1.9 Å Crystal Structure of *Escherichia Coli* MurG, a Membrane-Associated Glycosyltransferase Involved in Peptidoglycan Biosynthesis; *Protein Sci.* **2000**, *9*, 1045–1052.
- (83) N. Ruiz; Lipid Flippases for Bacterial Peptidoglycan Biosynthesis; *Lipid Insights* **2015**, *8*, 21–31.

- (84) N. Ruiz; Filling Holes in Peptidoglycan Biogenesis of *Escherichia Coli*; *Curr. Opin. Microbiol.* **2016**, *34*, 1–6.
- (85) Ruiz, N. Bioinformatics Identification of MurJ (MviN) as the Peptidoglycan Lipid II Flippase in *Escherichia Coli*. *Proc. Natl. Acad. Sci. U.S.A.* **2008**, *105*, 15553–15557.
- (86) T. Mohammadi, V. van Dam, R.; Sijbrandi, T. Vernet, A. Zapun, A. Bouhss, M. Diepeveen-De Bruin, M. Nguyen-Distéche, B. de Kruijff, E. Breukink; Identification of FtsW as a Transporter of Lipid-Linked Cell Wall Precursors across the Membrane; *EMBO J.* **2011**, *30*, 1425–1432.
- (87) A. Taguchi, M. A. Welsh, L. S. Marmont, W. Lee, M. Sjodt, A. C. Kruse, D.; Kahne, T. G. Bernhardt, S. Walker; FtsW Is a Peptidoglycan Polymerase That Is Functional Only in Complex with Its Cognate Penicillin-Binding Protein; *Nat. Microbiol.* **2019**, *4*, 587–594.
- (88) L. T. Sham, E. K. Butler, M. D. Lebar, D. Kahne, T. G. Bernhardt, N. Ruiz; MurJ Is the Flippase of Lipid-Linked Precursors for Peptidoglycan Biogenesis; *Science* **2014**, *345*, 220–222.
- (89) S. Kumar, F. A. Rubino, A. G. Mendoza, N. Ruiz; The Bacterial Lipid II Flippase MurJ Functions by an Alternating-Access Mechanism; *J. Biol. Chem.* **2019**, *294*, 981–990.
- (90) C. Goffin, J. M. Ghuysen; Multimodular Penicillin-Binding Proteins: An Enigmatic Family of Orthologs and Paralogs; *Microbiol. Mol. Biol. Rev.* **1998**, *62*, 1079–1093.
- (91) B. C. Chung, E. H. Mashalidis, T. Tanino, M. Kim, A. Matsuda, J. Hong, S. Ichikawa, S. Y. Lee; Structural Insights into Inhibition of Lipid I Production in Bacterial Cell Wall Synthesis; *Nature* **2016**, *533*, 557–560.
- (92) E. Sauvage, F. Kerff, M. Terrak, J. A. Ayala, P. Charlier; The Penicillin-Binding Proteins: Structure and Role in Peptidoglycan Biosynthesis; *FEMS Microbiol. Rev.* **2008**, *32*, 234–258.
- (93) A. Gautam, R. Vyas, R. Tewari; Peptidoglycan Biosynthesis Machinery: A Rich Source of Drug Targets. *Crit. Rev. Biotechnol.* **2011**, *31*, 295–336.
- (94) J. L. Strominger, D. I. Tipper, P. D. Madison; Bacterial Cell Wall Synthesis and Structure in Relation to the Mechanism of Action of Penicillins and Other Antibacterial Agents; *Am. J. Med.* **1965**, *39*, 708–721.

- (95) V. Sukhithasri, N. Nisha, L. Biswas, V. Anil Kumar, R. Biswas; Innate Immune Recognition of Microbial Cell Wall Components and Microbial Strategies to Evade Such Recognitions; *Microbiol. Res.* **2013**, *168*, 396–406.
- (96) M. H. Laaberki, J. Pfeffer, A. J. Clarke, J. Dworkin; O-Acetylation of Peptidoglycan Is Required for Proper Cell Separation and S-Layer Anchoring in *Bacillus Anthracis*; *J. Biol. Chem.* **2011**, *286*, 5278–5288.
- (97) J. B. Raymond, S. Mahapatra, D. C. Crick, M. S. Pavelka; Identification of the NamH Gene, Encoding the Hydroxylase Responsible for the N-Glycolylation of the Mycobacterial Peptidoglycan. *J. Biol. Chem.* **2005**, *280*, 326–333.
- (98) A. Benachour, R. Ladjouzi, A. le Jeune, L. Hébert, S. Thorpe, P. Courtin, M. P. Chapot-Chartier, T. K. Prajsnar, S. J. Foster, S. Mesnage; The Lysozyme-Induced Peptidoglycan N-Acetylglucosamine Deacetylase Pgda (EF1843) Is Required for Enterococcus Faecalis Virulence; *J. Bacteriol.* **2012**, *194*, 6066–6073.
- (99) J. G. Swoboda, J. Campbell, T. C. Meredith, S. Walker; Wall Teichoic Acid Function, Biosynthesis, and Inhibition; *ChemBioChem* **2010**, *11*, 35–45.
- (100) D. Münch, T. Roemer, S. H. Lee, M. Engeser, H. G. Sahl, T. Schneider; Identification and *in Vitro* Analysis of the GatD/MurT Enzyme-Complex Catalyzing Lipid II Amidation in *Staphylococcus Aureus*; *PLoS Pathog.* **2012**, *8*, 1–11.
- (101) E. Bernard, T. Rolain, P. Courtin, P. Hols, M. P. Chapot-Chartier; Identification of the Amidotransferase AsnB1 as Being Responsible for Meso-Diaminopimelic Acid Amidation in *Lactobacillus Plantarum* Peptidoglycan; *J. Bacteriol.* **2011**, *193*, 6323–6330.
- (102) S. E. Girardin, L. H. Travassos, M. Hervé, D. Blanot, I. G. Boneca, D. J. Philpott, P. J. Sansonetti, D. Mengin-Lecreulx, Peptidoglycan Molecular Requirements Allowing Detection by Nod1 and Nod2; *J. Biol. Chem.* **2003**, *278*, 41702–41708.
- (103) T. J. Lupoli, H. Tsukamoto, E. H. Doud, T. S. A. Wang, S. Walker, D. Kahne; Transpeptidase-Mediated Incorporation of D-Amino Acids into Bacterial Peptidoglycan; *J. Am. Chem. Soc.* **2011**, *133*, 10748–10751.
- (104) F. Cava, M. A. de Pedro, H. Lam, B. M. Davis, M. K. Waldor; Distinct Pathways for Modification of the Bacterial Cell Wall by Non-Canonical D-Amino Acids; *EMBO J.* **2011**, *30*, 3442–3453.

- (105) S. Mizyed, A. Oddone, B. Byczynski, D. W. Hughes, P. J. Berti; UDP-*N*-Acetylmuramic Acid (UDP-MurNAc) Is a Potent Inhibitor of MurA (Enolpyruvyl-UDP-GlcNAc Synthase); *Biochemistry* **2005**, *44*, 4011–4017.
- (106) D. Mengin-Lecreulx, J. van Heijenoort; Effect of Growth Conditions on Peptidoglycan Content and Cytoplasmic Steps of Its Biosynthesis in *Escherichia Coli*; *J. Bacteriol.* **1985**, *163*, 208–212.
- (107) E. E. Ishigurot, W. D. Ramey; Involvement of the RelA Gene Product and Feedback Inhibition in the Regulation of UDP-*N*-Acetylmuramyl-Peptide Synthesis in *Escherichia Coli*; *J. Bacteriol.* **1978**, 766–774.
- (108) E. J. J. Lugtenberg, L. de Haas-Menger, W. H. M. Ruyters; Murein Synthesis and Identification of Cell Wall Precursors of Temperature-Sensitive Lysis Mutants of *Escherichia Coli*; *J. Bacteriol.* **1972**, *109*, 326–335.
- (109) T. D. Bugg, D. Braddick, C. G. Dowson, D. I. Roper; Bacterial Cell Wall Assembly: Still an Attractive Antibacterial Target; *Trends Biotechnol.* **2011**, *29*, 167–173.
- (110) M. W. Chen, B. Lohkamp, R. Schnell, J. Lescar, G. Schneider; Substrate Channel Flexibility in *Pseudomonas Aeruginosa* MurB Accommodates Two Distinct Substrates; *PLoS One* **2013**, *8*, 1–10.
- (111) T. E. Benson, C. T. Walsh, J. M. Hogle; X-Ray Crystal Structures of the S229A Mutant and Wild-Type MurB in the Presence of the Substrate Enolpyruvyl-UDP-*N*-Acetylglucosamine at 1.8-Å Resolution; *Biochemistry* **1997**, *36*, 806–811.
- (112) T. S. Mansour, C. E. Caufield, B. Rasmussen, R. Chopra, G. Krishnamurthy, K. M. Morris, K. Svenson, J. Bard, C. Smeltzer, S. Naughton, S. Antane, Y. Yang, A. Severin, D. Quagliato, P. J. Petersen, G. Singh; Naphthyl Tetronic Acids as Multi-Target Inhibitors of Bacterial Peptidoglycan Biosynthesis; *ChemMedChem* **2007**, *2*, 1414–1417.
- (113) T. Deva, E. N. Baker, C. J. Squire, C. A. Smith; Structure of *Escherichia Coli* UDP-*N*-Acetylmuramoyl:L-Alanine Ligase (MurC); *Acta Crystallogr. D* **2006**, *62*, 1466–1474.
- (114) G. Spraggon, R. Schwarzenbacher, A. Kreuzsch, C. C. Lee, P. Abdubek, E. Ambing, T. Biorac, L. S. Brinen, J. M. Canaves, J. Cambell, H. J. Chiu, X. Dai, A. M. Deacon, M. DiDonato, M. A. Elsliger, S. Eshagi, R. Floyd, A. Godzik, C. Grittini, S. K. Grzechnik, E. Hampton, L.; Jaroszewski, C.; Karlak, H. E.; Klock, E.; Koesema, J. S.; Kovarik, P. Kuhn, I. Levin, D. McMullan, T. M. McPhillips, M. D. Miller, A.

- Morse, K. Moy, J. Ouyang, R. Page, K. Quijano, A. Robb, R. C. Stevens, H. van den Bedem, J. Velasquez, J. Vincent, F. von Delft, X. Wang, B. West, G. Wolf, Q. Xu, K. O. Hodgson, J. Wooley, S. A. Lesley, I. A. Wilson; Crystal Structure of an UDP-*N*-Acetylmuramate-Alanine Ligase MurC (TM0231) from *Thermotoga Maritima* at 2.3 Å Resolution; *Proteins: Struct. Funct. Genet.* **2004**, *55*, 1078–1081.
- (115) C. D. Mol, A. Brooun, D. R. Dougan, M. T. Hilgers, L. W. Tari, R. A. Wijnands, M. W. Knuth, D. E. McRee, R. V. Swanson; Crystal Structures of Active Fully Assembled Substrate- and Product-Bound Complexes of UDP-*N*-Acetylmuramic Acid:L-Alanine Ligase (MurC) from *Haemophilus Influenzae*; *J. Bacteriol.* **2003**, *185*, 4152–4162.
- (116) M. Kotnik, J. Humljan, C. Contreras-Martel, M. Oblak, K. Kristan, M. Hervé, D. Blanot, U. Urleb, S. Gobec, A. Dessen, T. Solmajer; Structural and Functional Characterization of Enantiomeric Glutamic Acid Derivatives as Potential Transition State Analogue Inhibitors of MurD Ligase; *J. Mol. Biol.* **2007**, *370*, 107–115.
- (117) N. Zidar, T. Tomašić, R. Šink, A. Kovač, D. Patin, D. Blanot, C. Contreras-Martel, A. Dessen, M. M. Premru, A. Zega, S. Gobec, L. P. Mašič, D. Kikelj; New 5-Benzylidenethiazolidin-4-One Inhibitors of Bacterial MurD Ligase: Design, Synthesis, Crystal Structures, and Biological Evaluation; *Eur. J. Med. Chem.* **2011**, *46*, 5512–5523.
- (118) N. Zidar, T. Tomašić, R. Šink, V. Rupnik, A. Kovač, S. Turk, D. Patin, D. Blanot, C. Contreras Martel, A. Dessen, M. M. Premru, A. Zega, S. Gobec, L. P. Mašič, D. Kikelj; Discovery of Novel 5-Benzylidenerhodanine and 5-Benzylidenethiazolidine-2, 4-Dione Inhibitors of MurD Ligase; *J. Med. Chem.* **2010**, *53*, 6584–6594.
- (119) I. Sosič, H. Barreateau, M. Simčič, R. Šink, J. Cesar, A. Zega, S. G. Grdadolnik, C. Contreras-Martel, A. Dessen, A. Amoroso, B. Joris, D. Blanot, S. Gobec; Second-Generation Sulfonamide Inhibitors of D-Glutamic Acid-Adding Enzyme: Activity Optimisation with Conformationally Rigid Analogues of D-Glutamic Acid. *Eur. J. Med. Chem.* **2011**, *46*, 2880–2894.
- (120) J. Humljan, M. Kotnik, C. Contreras-Martel, D. Blanot, U. Urleb, A. Dessen, T. Šolmajer, S. Gobec; Novel Naphthalene-*N*-Sulfonyl-D-Glutamic Acid Derivatives

- as Inhibitors of MurD, a Key Peptidoglycan Biosynthesis Enzyme; *J. Med. Chem.* **2008**, *51*, 7486–7494.
- (121) E. Gordon, B. Flouret, L. Chantalat, J. van Heijenoort, D. Mengin-Lecreulx, O. Dideberg; Crystal Structure of UDP-*N*-Acetylmuramoyl-L-Alanyl-D-Glutamate: Meso-Diaminopimelate Ligase from *Escherichia Coli*; *J. Biol. Chem.* **2001**, *276*, 10999–11006.
- (122) C. Basavannacharya, P. R. Moody, T. Munshi, N. Cronin, N. H. Keep, S. Bhakta; Essential Residues for the Enzyme Activity of ATP-Dependent MurE Ligase from *Mycobacterium Tuberculosis*; *Protein Cell* **2010**, *1*, 1011–1022.
- (123) K. M. Ruane, A. J. Lloyd, V. Fülöp, C. G. Dowson, H. Barreteau, A. Boniface, S. Dementin, D. Blanot, D. Mengin-Lecreulx, S. Gobec, A. Dessen, D. I. Roper; Specificity Determinants for Lysine Incorporation in *Staphylococcus Aureus* Peptidoglycan as Revealed by the Structure of a MurE Enzyme Ternary Complex; *J. Biol. Chem.* **2013**, *288*, 33439–33448.
- (124) S. Favini-Stabile, C. Contreras-Martel, N. Thielens, A. Dessen; MreB and MurG as Scaffolds for the Cytoplasmic Steps of Peptidoglycan Biosynthesis; *Environ. Microbiol.* **2013**, *15*, 3218–3228.
- (125) Y. Yan, S. Munshi, B. Leiting, M. S. Anderson, J. Chrzas, Z. Chen; Crystal Structure of *Escherichia Coli* UDPMurNAc-Tripeptide D-Alanyl-D-Alanine-Adding Enzyme (MurF) at 2.3 Å Resolution; *J. Mol. Biol.* **2000**, *304*, 435–445.
- (126) S. S. Cha, Y. J. An, C. S. Jeong, J. H. Yu, K. M. Chung; ATP-Binding Mode Including a Carbamoylated Lysine and Two Mg²⁺ Ions, and Substrate-Binding Mode in *Acinetobacter Baumannii* MurF; *Biochem. Biophys. Res. Commun.* **2014**, *450*, 1045–1050.
- (127) M. Hrast, S. Turk, I. Sosič, D. Knez, C. P. Randall, H. Barreteau, C. Contreras-Martel, A. Dessen, A. J. O'Neill, D. Mengin-Lecreulx, D. Blanot, S. Gobec; Structure-Activity Relationships of New Cyanothiophene Inhibitors of the Essential Peptidoglycan Biosynthesis Enzyme MurF; *Eur. J. Med. Chem.* **2013**, *66*, 32–45.
- (128) K. L. Longenecker, G. F. Stamper, P. J. Hajduk, E. H. Fry, C. G. Jakob, J. E. Harlan, R. Edalji, D. M. Bartley, K. A. Walter, L. R. Solomon, T. F. Holzman, Y. G. Gu, C. G. Lerner, B. A. Beutel, V. S. Stoll; Structure of MurF from *Streptococcus*

- Pneumoniae* Co-Crystallized with a Small Molecule Inhibitor Exhibits Interdomain Closure; *Protein Sci.* **2005**, *14*, 3039–3047.
- (129) S. Turk, A. Kovač, A. Boniface, J. M. Bostock, I. Chopra, D. Blanot, S. Gobec; Discovery of New Inhibitors of the Bacterial Peptidoglycan Biosynthesis Enzymes MurD and MurF by Structure-Based Virtual Screening; *Bioorg. Med. Chem.* **2009**, *17*, 1884–1889.
- (130) P. A. Lanzetta, L. J. Alvarez, P. S. Reinach, O. A. Candia; An Improved Assay for Nanomole Amounts of Inorganic Phosphate; *Anal. Biochem.* **1979**, *100*, 95–97.
- (131) A. Keeley, P. Ábrányi-Balogh, M. Hrast, T. Imre, J. Ilaš, S. Gobec, G. M. Keserű; Heterocyclic Electrophiles as New MurA Inhibitors; *Arch. Pharm.* **2018**, *351*, e1800184.
- (132) S. G. Carter, D. W. Karl; Inorganic Phosphate Assay with Malachite Green: An Improvement and Evaluation; *J. of Biochem. Biophys. Methods* **1982**, *7*, 7–13.
- (133) C. J. Andres, J. J. Bronson, S. V. D'Andrea, M. S. Deshpande, P. J. Falk, K. A. Grant-Young, W. E. Harte, H. T. Ho, P. F. Misco, J. G. Robertson, D. Stock, Y. Sun, A. W. Walsh; 4-Thiazolidinones: Novel Inhibitors of the Bacterial Enzyme MurB; *Bioorg. Med. Chem. Lett.* **2000**, *10*, 715–717.
- (134) H. J. Dai, C. N. Parker, J. J. Bao; Characterization and Inhibition Study of MurA Enzyme by Capillary Electrophoresis; *J. Chromatogr. B* **2002**, *766*, 123–132.
- (135) A. D. Napper, S. Sivendran; Miniaturized High-Throughput Fluorescent Assay for Conversion of NAD(P)H to NAD(P); *Curr. Protoc. Chem. Biol.* **2009**, *3*, 1–25.
- (136) G. Deng, R. F. Gu, S. Marmor, S. L. Fisher, H. Jahic, G. Sanyal; Development of an LC-MS Based Enzyme Activity Assay for MurC: Application to Evaluation of Inhibitors and Kinetic Analysis. *J. Pharm. Biomed. Anal.* **2004**, *35*, 817–828.
- (137) J. S. Anderson, M. Matsushashi, M. A. Haskin, J. L. Strominger; Biosynthesis of the Peptidoglycan of Bacterial Cell Walls; *J. Biol. Chem.* **1967**, *242*, 3180–3190.
- (138) Y. Yang, A. Severin, R. Chopra, G. Singh, W. Hu, D. Keeney, K. Svenson, P. J. Petersen, P. Labthavikul, D. M. Shlaes, B. A. Rasmussen, A. A. Failli, S. Shumsky, K. M. K. Kutterer, A. Gilbert, T. S. Mansour, G. Krishnamurthy, J. S. Shumsky; 3,5-Dioxypyrazolidines, Novel Inhibitors of UDP-*N*-Acetylenolpyruvyl glucosamine Reductase (MurB) with Activity against Gram-Positive Bacteria; *Antimicrob. Agents Chemother.* **2006**, *50*, 556–564.

- (139) F. M. Kahan, J. S. Kahan, P. J. Cassidy, H. Kropp; The Mechanism of Action of Fosfomycin (Phosphonomycin); *Ann. N. Y. Acad. Sci.* **1974**, *235*, 364–385.
- (140) J. J. Bronson, K. L. DenBleyker, P. J. Falk, R. A. Mate, H. T. Ho, M. J. Pucci, L. B. Snyder; Discovery of the First Antibacterial Small Molecule Inhibitors of MurB; *Bioorg. Med. Chem. Lett.* **2003**, *13*, 873–875.
- (141) K. M. Kutterer, J. M. Davis, G. Singh, Y. Yang, W. Hu, A. Severin, B. Rasmussen, A. Krishnamurthy, G. Failli, A. Katz; a H. 4-Alkyl and 4,4'-Dialkyl 1,2-Bis(4-Chlorophenyl) Pyrazolidine-3,5-Dione Derivatives as New Inhibitors of Bacterial Cell Wall Biosynthesis; *Bioorg. Med. Chem. Lett.* **2005**, *15*, 2527–2531.
- (142) F. Reck, S. Marmor, S. Fisher, M. A. Wuonola; Inhibitors of the Bacterial Cell Wall Biosynthesis Enzyme MurC; *Bioorg. Med. Chem. Lett.* **2001**, *11*, 1451–1454.
- (143) S. Marmor, C. P. Petersen, F. Reck, W. Yang, N. Gao, S. L. Fisher; Biochemical Characterization of a Phosphinate Inhibitor of *Escherichia Coli* MurC; *Biochemistry* **2001**, *40*, 12207–12214.
- (144) M. M. Sim, S. B. Ng, A. D. Buss, S. C. Crasta, K. L. Goh, S. K. Lee; Benzylidene Rhodanines as Novel Inhibitors of UDP-*N*-Acetylmuramate/L-Alanine Ligase; *Bioorg. Med. Chem. Lett.* **2002**, *12*, 697–699.
- (145) R. Šink, A. Kovač, T. Tomašić, V. Rupnik, A. Boniface, J. Bostock, I. Chopra, D. Blanot, L. P. Mašič, S. Gobec, A. Zega; Synthesis and Biological Evaluation of *N*-Acyhydrazones as Inhibitors of MurC and MurD Ligases; *ChemMedChem* **2008**, *3*, 1362–1370.
- (146) D. E. Ehmman, J. E. Demeritt, K. G. Hull, S. L. Fisher; Biochemical Characterization of an Inhibitor of *Escherichia Coli* UDP-*N*-Acetylmuramyl-L-Alanine Ligase; *Biochim. Biophys. Acta - Proteins Proteom.* **2004**, *1698*, 167–174.
- (147) R. Frlan, A. Kovač, D. Blanot, S. Gobec, S. Pečar, A. Obreza; Design and Synthesis of Novel *N*-Benzylidenesulfonohydrazide Inhibitors of MurC and MurD as Potential Antibacterial Agents; *Molecules* **2008**, *13*, 11–30.
- (148) S. Antane, C. E. Caufield, W. Hu, D. Keeney, P. Labthavikul, K. Morris, S. M. Naughton, P. J. Petersen, B. A. Rasmussen, G. Singh, Y. Yang; Pulvinones as Bacterial Cell Wall Biosynthesis Inhibitors; *Bioorg. Med. Chem. Lett.* **2006**, *16*, 176–180.

- (149) M. E. Tanner, S. Vaganay, J. van Heijenoort, D. Blanot; Phosphinate Inhibitors of the D-Glutamic Acid-Adding Enzyme of Peptidoglycan Biosynthesis. *J. Org. Chem.* **1996**, *61*, 1756–1760.
- (150) L. D. Gegnas, S. T. Waddell, R. M. Chabin, S. Reddy, K. K. Wong; Inhibitors of the Bacterial Cell Wall Biosynthesis Enzyme Mur D; *Bioorg. Med. Chem. Lett.* **1998**, *8*, 1643–1648.
- (151) J. R. Horton, J. M. Bostock, I. Chopra, L. Hesse, S. E. V Phillips, D. J. Adams, A. P. Johnson, C. W. G. Fishwick; Macrocyclic Inhibitors of the Bacterial Cell Wall Biosynthesis Enzyme Mur D; *Bioorg. Med. Chem. Lett.* **2003**, *13*, 1557–1560.
- (152) T. Tomašić, N. Zidar, V. Rupnik, A. Kovač, D. Blanot, S. Gobec, D. Kikelj, L. P. Mašič; Synthesis and Biological Evaluation of New Glutamic Acid-Based Inhibitors of MurD Ligase; *Bioorg. Med. Chem. Lett.* **2009**, *19*, 153–157.
- (153) T. Tomašić, A. Kovač, M. Simčič, D. Blanot, S. G. Grdadolnik, S. Gobec, D. Kikelj, L. P. Mašič; Novel 2-Thioxothiazolidin-4-One Inhibitors of Bacterial MurD Ligase Targeting D-Glu- and Diphosphate-Binding Sites; *Eur. J. Med. Chem.* **2011**, *46*, 3964–3975.
- (154) T. Tomašić, N. Zidar, R. Šink, A. Kovač, D. Blanot, C. Contreras-Martel, A. Dessen, M. Müller-Premru, A. Zega, S. Gobec, D. Kikelj, L. P. Mašič; Structure-Based Design of a New Series of D-Glutamic Acid Based Inhibitors of Bacterial UDP-N-Acetylmuramoyl-L-Alanine: D-Glutamate Ligase (MurD); *J. Med. Chem.* **2011**, *54*, 4600–4610.
- (155) T. Bratkovič, M. Lunder, U. Urleb, B. Štrukelj; Peptide Inhibitors of MurD and MurE, Essential Enzymes of Bacterial Cell Wall Biosynthesis; *J. Basic Microbiol.* **2008**, *48*, 202–206.
- (156) B. Zeng, K. K. Wong, D. L. Pompliano, S. Reddy, M. E. A. Tanner; Phosphinate Inhibitor of the Meso-Diaminopimelic Acid-Adding Enzyme (MurE) of Peptidoglycan Biosynthesis; *J. Org. Chem.* **1998**, *63*, 10081–10086.
- (157) J. Humljan, M. Kotnik, A. Boniface, T. Šolmajer, U. Urleb, D. Blanot, S. Gobec; A New Approach towards Peptidosulfonamides: Synthesis of Potential Inhibitors of Bacterial Peptidoglycan Biosynthesis Enzymes MurD and MurE; *Tetrahedron* **2006**, *62*, 10980–10988.
- (158) J. D. Guzman, A. Gupta, D. Evangelopoulos, C. Basavannacharya, L. C. Pabon, E. A. Plazas, D. R. Muñoz, W. A. Delgado, L. E. Cuca, W. Ribon, S. Gibbons, S. Bhakta;

- Anti-Tubercular Screening of Natural Products from Colombian Plants: 3-Methoxynordomesticine, an Inhibitor of MurE Ligase of *Mycobacterium Tuberculosis*; *J. Antimicrob. Chemother.* **2010**, *65*, 2101–2107.
- (159) W. K. P. Shiu, J. P. Malkinson, M. M. Rahman, J. Curry, P. Stapleton, M. Gunaratnam, S. Neidle, S. Mushtaq, M. Warner, D. M. Livermore, D. Evangelopoulos, C. Basavannacharya, S. Bhakta, B. D. Schindler, S. M. Seo, D. Coleman, G. W. Kaatz, S. Gibbons; A New Plant-Derived Antibacterial Is an Inhibitor of Efflux Pumps in *Staphylococcus Aureus*; *Int. J. Antimicrob. Agents* **2013**, *42*, 513–518.
- (160) C. Paradis-Bleau, A. Lloyd, F. Sanschagrín, H. Maaroufi, T. Clarke, A. Blewett, C. Dowson, D. I. Roper, T. D. Bugg, R. C. Levesque; *Pseudomonas Aeruginosa* MurE Amide Ligase: Enzyme Kinetics and Peptide Inhibitor; *Biochem. J.* **2009**, *421*, 263–272.
- (161) K. M. Comess, M. E. Schurdak, M. J. Voorbach, M. Coen, J. D. Trumbull, H. Yang, L. Gao, H. Tang, X. Cheng, C. G. Lerner, J. O. McCall, D. J. Burns, B. A. Beutel; An Ultraefficient Affinity-Based High-throughout Screening Process: Application to Bacterial Cell Wall Biosynthesis Enzyme MurF; *J. Biomol. Screen.* **2006**, *11*, 743–754.
- (162) G. F. Stamper, K. L. Longenecker, E. H. Fry, C. G. Jakob, A. S. Florjancic, Y. G. Gu, D. D. Anderson, C. S. Cooper, T. Zhang, R. F. Clark, Y. Cia, C. L. Black-Schaefer, J. O. McCall, C. G. Lerner, P. J. Hajduk, B. A. Beutel, V. S. Stoll; Structure-Based Optimization of MurF Inhibitors. *Chem. Biol. Drug Des.* **2006**, *67*, 58–65.
- (163) M. Hrast, M. Anderluh, D. Knez, C. P. Randall, H. Barreteau, A. J. O'Neill, D. Blanot, S. Gobec; Design, Synthesis and Evaluation of Second Generation MurF Inhibitors Based on a Cyanothiophene Scaffold; *Eur. J. Med. Chem.* **2014**, *73*, 83–96.
- (164) E. Z. Baum, S. M. Crespo-Carbone, D. Abbanat, B. Foleno, A. Maden, R. Goldschmidt, K. Bush; Utility of Muropeptide Ligase for Identification of Inhibitors of the Cell Wall Biosynthesis Enzyme MurF; *Antimicrob. Agents Chemother.* **2006**, *50*, 230–236.
- (165) E. Z. Baum, S. M. Crespo-Carbone, A. Klinger, B. D. Foleno, I. Turchi, M. Macielag, K. Bush; A MurF Inhibitor That Disrupts Cell Wall Biosynthesis in *Escherichia Coli*; *Antimicrob. Agents Chemother.* **2007**, *51*, 4420–4426.

- (166) E. Z. Baum, S. M. Crespo-Carbone, B. D. Foleno, L. D. Simon, J. Guillemont, M. Macielag, K. Bush; MurF Inhibitors with Antibacterial Activity: Effect on Muropeptide Levels; *Antimicrob. Agents Chemother.* **2009**, *53*, 3240–3247.
- (167) D. J. Miller, S. M. Hammond, D. Anderluzzi, T. D. H. Bugg; Aminoalkylphosphinate Inhibitors of D-Ala-D-Ala Adding Enzyme; *J. Chem. Soc., Perkin trans. 1* **1998**, *1*, 131–142
- (168) G. D. Francisco, Z. Li, J. D. Albright, N. H. Eudy, A. H. Katz, P. J. Petersen, P. Labthavikul, G. Singh, Y. Yang, B. A. Rasmussen, Y. I. Lin, T. S. Mansour; Phenyl Thiazolyl Urea and Carbamate Derivatives as New Inhibitors of Bacterial Cell-Wall Biosynthesis; *Bioorg. Med. Chem. Lett.* **2004**, *14*, 235–238.
- (169) A. Perdih, A. Kovač, G. Wolber, D. Blanot, S. Gobec, T. Solmajer; Discovery of Novel Benzene 1,3-Dicarboxylic Acid Inhibitors of Bacterial MurD and MurE Ligases by Structure-Based Virtual Screening Approach; *Bioorg. Med. Chem. Lett.* **2009**, *19*, 2668–2673.
- (170) M. Sova, A. Kovač, S. Turk, M. Hrast, D. Blanot, S. Gobec; Phosphorylated Hydroxyethylamines as Novel Inhibitors of the Bacterial Cell Wall Biosynthesis Enzymes MurC to MurF; *Bioorg. Chem.* **2009**, *37*, 217–222.
- (171) Z. Li, G. D. Francisco, W. Hu, P. Labthavikul, P. J. Petersen, A. Severin, G. Singh, Y. Yang, B. A. Rasmussen, Y. I. Lin, J. S. Skotnicki, T. S. Mansour; 2-Phenyl-5,6-Dihydro-2H-Thieno[3,2-c]Pyrazol-3-ol Derivatives as New Inhibitors of Bacterial Cell Wall Biosynthesis; *Bioorg. Med. Chem. Lett.* **2003**, *13*, 2591–2594.
- (172) T. Tomašić, N. Zidar, A. Kovač, S. Turk, M. Simčič, D. Blanot, M. Müller-Premru, M. Filipič, S. G. Grdadolnik, A. Zega, M. Anderluh, S. Gobec, D. Kikelj, L. P. Mašič; 5-Benzylidenethiazolidin-4-Ones as Multitarget Inhibitors of Bacterial Mur Ligases; *ChemMedChem* **2010**, *5*, 286–295.
- (173) Y. G. Gu, A. S. Iorjancic, R. F. Clark, T. Zhang, C. S. Cooper, D. D. Anderson, C. G. Lerner, J. O. McCall, Y. Cai, C. L. Black-Schaefer, G. F. Stamper, P. J. Hajduk, B. A. Beutel; Structure-Activity Relationships of Novel Potent MurF Inhibitors; *Bioorg. Med. Chem. Lett.* **2004**, *14*, 267–270.
- (174) J. B. Baell, G. A. Holloway, J. B. Baell; New Substructure Filters for Removal of Pan Assay Interference Compounds (PAINS) from Screening Libraries and for Their Exclusion in Bioassays; *J. Med. Chem.* **2010**, *53*, 2719–2740.

- (175) W. J. Lees, C. T. Walsh; Analysis of the Enol Ether Transfer Catalyzed by UDP-GlcNAc Enolpyruvyl Transferase Using (E)-and (Z)-Isomers of Phosphoenolbutyrate: Stereochemical, Partitioning, and Isotope Effect Studies; *J. Am. Chem. Soc.* **1995**, *117*, 7329–7337.
- (176) T. Skarzynski, D. H. Kim, W. J. Lees, C. T. Walsh, K. Duncan; Stereochemical Course of Enzymatic Enolpyruvyl Transfer and Catalytic Conformation of the Active Site Revealed by the Crystal Structure of the Fluorinated Analogue of the Reaction Tetrahedral Intermediate Bound to the Active Site of the C115A Mutant of MurA; *Biochemistry* **1998**, *37*, 2572–2577.
- (177) C. Wanke, R. Falchetto, N. Amrhein; The UDP-N-Acetylglucosamine 1-Carboxyvinyl-Transferase of *Enterobacter Cloacae* Molecular Cloning, Sequencing of the Gene and Overexpression of the Enzyme; *FEBS Lett.* **1992**, *301*, 271–276.
- (178) B. Byczynski, S. Mized, P. J. Berti; Nonenzymatic Breakdown of the Tetrahedral (α -Carboxyketal Phosphate) Intermediates of MurA and AroA, Two Carboxyvinyl Transferases. Protonation of Different Functional Groups Controls the Rate and Fate of Breakdown; *J. Am. Chem. Soc.* **2003**, *125*, 12541–12550.
- (179) S. Eschenburg, M. A. Priestman, F. A. Abdul-Latif, C. Delachaume, F. Fassy, E. Schönbrunn; A Novel Inhibitor That Suspends the Induced Fit Mechanism of UDP-N-Acetylglucosamine Enolpyruvyl Transferase (MurA); *J. Biol. Chem.* **2005**, *280*, 14070–14075.
- (180) E. Schönbrunn, S. Eschenburg, W. A. Shuttleworth, J. V. Schloss, N. Amrhein, J. N. S. Evans, W. Kabsch; Interaction of the Herbicide Glyphosate with Its Target Enzyme 5-Enolpyruvylshikimate 3-Phosphate Synthase in Atomic Detail; *Proc. Natl. Acad. Sci. U.S.A.* **2001**, *98*, 1376–1380.
- (181) S. Eschenburg, W. Kabsch, M. L. Healy, E. Schonbrunn; A New View of the Mechanisms of UDP-N-Acetylglucosamine Enolpyruvyl Transferase (MurA) and 5-Enolpyruvylshikimate-3-Phosphate Synthase (AroA) Derived from X-Ray Structures of Their Tetrahedral Reaction Intermediate States; *J. Biol. Chem.* **2003**, *278*, 49215–49222.

- (182) Y. C. Sun, Y. Li, H. Zhang, H. Q. Yan, D. N. Dowling, Y. P. Wang; Reconstitution of the Enzyme AroA and Its Glyphosate Tolerance by Fragment Complementation; *FEBS Lett.* **2006**, *580*, 1521–1527.
- (183) L. L. Silver; Fosfomycin: Mechanism and Resistance; *Cold Spring Harb. Perspect. Med.* **2017**, *7*, 1–11.
- (184) M. F. Alibhai, W. C. Stallings; Closing down on Glyphosate Inhibition-with a New Structure for Drug Discovery; *Proc. Natl. Acad. Sci. U.S.A.* **2001**, *98*, 2944–2946.
- (185) Y. Cao, Q. Peng, S. Li, Z. Deng, J. Gao; The Intriguing Biology and Chemistry of Fosfomycin: The Only Marketed Phosphonate Antibiotic; *RSC Adv.* **2019**, *9*, 42204–42218.
- (186) D. Raina, C. Kumar, V. Kumar, I. A. Khan, S. Saran; Potential Inhibitors Targeting Escherichia Coli UDP-N-Acetylglucosamine Enolpyruvyl Transferase (MurA): An Overview; *Indian J. Microbiol.* **2022**, 11–22.
- (187) E. Schönbrunn, S. Sack, S. Eschenburg, A. Perrakis, F. Krekel, N. Amrhein, E. Mandelkow; Crystal Structure of UDP-N-Acetylglucosamine Enolpyruvyltransferase, the Target of the Antibiotic Fosfomycin; *Structure* **1996**, *4*, 1065–1075.
- (188) A. Gautam, P. Rishi, R. Tewari; UDP-N-Acetylglucosamine Enolpyruvyl Transferase as a Potential Target for Antibacterial Chemotherapy: Recent Developments; *Appl. Microbiol. Biotechnol.* **2011**, 211–225.
- (189) C. D. Klein, A. Bachelier; Molecular Modeling and Bioinformatical Analysis of the Antibacterial Target Enzyme MurA from a Drug Design Perspective; *J. Comput. Aided Mol. Des.* **2006**, *20*, 621–628.
- (190) S. G. Jackson, F. Zhang, P. Chindemi, M. S. Junop, P. J. Berti; Evidence of Kinetic Control of Ligand Binding and Staged Product Release in MurA (Enolpyruvyl UDP-GlcNAc Synthase)-Catalyzed Reactions; *Biochemistry* **2009**, *48*, 11715–11723.
- (191) S. Eschenburg, E. Schönbrunn; Comparative X-Ray Analysis of the Un-Liganded Fosfomycin-Target MurA; *Proteins* **2000**, *40*, 290–298.
- (192) E. Schönbrunn, S. Eschenburg, F. Krekel, K. Luger, N. Amrhein; Role of the Loop Containing Residue 115 in the Induced-Fit Mechanism of the Bacterial Cell Wall Biosynthetic Enzyme MurA; *Biochemistry* **2000**, *39*, 2164–2173.

- (193) C. Wanke, N. Amrhein; Evidence That the Reaction of the UDP-N-acetylglucosamine 1-carboxyvinyltransferase Proceeds through the *O*-phosphothioketal of Pyruvic Acid Bound to Cys115 of the Enzyme; *Eur. J. Biochem.* **1993**, *218*, 861–870.
- (194) D. H. Kim, W. J. Lees, K. E. Kempell, W. S. Lane, K. Duncan, C. T. Walsh; Characterization of a Cys115 to Asp Substitution in the *Escherichia Coli* Cell Wall Biosynthetic Enzyme UDP-GlcNAc Enolpyruvyl Transferase (MurA) That Confers Resistance to Inactivation by the Antibiotic Fosfomycin; *Biochemistry* **1996**, *35*, 4923–4928.
- (195) K. A. L. de Smet, K. E. Kempell, A. Gallagher, K. Duncan, D. B. Young; Alteration of a Single Amino Acid Residue Reverses Fosfomycin Resistance of Recombinant MurA from *Mycobacterium Tuberculosis*; *Microbiology* **1999**, *145*, 3177–3184.
- (196) E. D. Brown, J. L. Marquardt, J. P. Lee, C. T. Walsh, K. S. Anderson; Detection and Characterization of a Phospholactoyl-Enzyme Adduct in the Reaction Catalyzed by UDP-N-Acetylglucosamine Enolpyruvyl Transferase, MurZ; *Biochemistry* **1994**, *33*, 10638–10645.
- (197) A. M. Thomas, C. Ginj, I. Jelesarov, N. Amrhein, P. Macheroux; Role of K22 and R120 in the Covalent Binding of the Antibiotic Fosfomycin and the Substrate-Induced Conformational Change in UDP-N-Acetylglucosamine Enolpyruvyl Transferase; *Eur. J. Biochem.* **2004**, *271*, 2682–2690.
- (198) A. K. Samland, T. Etezady-Esfarjani, N. Amrhein, P. Macheroux; Asparagine 23 and Aspartate 305 Are Essential Residues in the Active Site of UDP-N-Acetylglucosamine Enolpyruvyl Transferase from *Enterobacter Cloacae*; *Biochemistry* **2001**, *40*, 1550–1559.
- (199) E. Schönbrunn, D. I. Svergun, N. Amrhein, M. H. J. Koch; Studies on the Conformational Changes in the Bacterial Cell Wall Biosynthetic Enzyme UDP-N-Acetylglucosamine Enolpyruvyltransferase (MurA); *Eur. J. Biochem.* **1998**, *253*, 406–412.
- (200) J. Y. Zhu, Y. Yang, H. Han, S. Betzi, S. H. Olesen, F. Marsilio, E. Schönbrunn; Functional Consequence of Covalent Reaction of Phosphoenolpyruvate with UDP-N-Acetylglucosamine 1-Carboxyvinyltransferase (MurA); *J. Biol. Chem.* **2012**, *287*, 12657–12667.

- (201) H. Han, Y. Yang, S. H. Olesen, A. Becker, S. Betzi, E. Schönbrunn; The Fungal Product Terreic Acid Is a Covalent Inhibitor of the Bacterial Cell Wall Biosynthetic Enzyme UDP-*N*-Acetylglucosamine 1-Carboxyvinyltransferase (MurA); *Biochemistry* **2010**, *49*, 4276–4282.
- (202) S. Eschenburg, M. Priestman, E. Schönbrunn; Evidence That the Fosfomycin Target Cys115 in UDP-*N*-Acetylglucosamine Enolpyruvyl Transferase (MurA) Is Essential for Product Release; *J. Biol. Chem.* **2005**, *280*, 3757–3763.
- (203) A. Steinbach, A. J. Scheidig, C. D. Klein; The Unusual Binding Mode of Cnicin to the Antibacterial Target Enzyme MurA Revealed by X-Ray Crystallography; *J. Med. Chem.* **2008**, *51*, 5143–5147.
- (204) E. Schönbrunn, S. Eschenburg, K. Luger, W. Kabsch, N. Amrhein; Structural Basis for the Interaction of the Fluorescence Probe 8-Anilino-1-Naphthalene Sulfonate (ANS) with the Antibiotic Target MurA; *Proc. Natl. Acad. Sci. U.S.A* **2000**, *97*, 6345–6349.
- (205) M. E. Falagas, K. P. Giannopoulou, G. N. Kokolakis, P. I. Rafailidis; Fosfomycin: Use beyond Urinary Tract and Gastrointestinal Infections; *Clin. Infect. Dis.* **2008**, *46*, 1069–1077.
- (206) D. Hendlin, E. O. Stapley, M. Jackson, H. Wallick, A. K. Miller, F. J. Wolf, T. W. Miller, L. Chaiet, F. M. Kahan, E. L. Foltz, H. B. Woodruff, J. M. Mata, S. Hernandez, S. Mochales; Phosphonomycin, a New Antibiotic Produced by Strains of *Streptomyces*; *Science* **1969**, *166*, 122–123.
- (207) M. E. Falagas, E. K. Vouloumanou, G. Samonis, K. Z. Vardakasa; Fosfomycin. *Clin. Microbiol. Rev.*; **2016**, *29*, 321–347.
- (208) T. Horii, T. Kimura, K. Sato, K. Shibayama, M. Ohta; Emergence of Fosfomycin-Resistant Isolates of Shiga-like Toxin-Producing *Escherichia Coli* O26; *Antimicrob. Agents Chemother.* **1999**, *43*, 789–793.
- (209) J. L. Marquardt, E. D. Brown, W. S. Lane, T. M. Haley, Y. Ichikawa, C. H. Wong, C. T. Walsh; Kinetics, Stoichiometry, and Identification of the Reactive Thiolate in the Inactivation of UDP-GlcNAc Enolpyruvyl Transferase by the Antibiotic Fosfomycin; *Biochemistry* **1994**, *33*, 10646–10651.
- (210) E. Z. Baum, D. A. Montenegro, L. Licata, I. Turchi, G. C. Webb, B. D. Foleno, K. Bush; Identification and Characterization of New Inhibitors of the *Escherichia Coli* MurA Enzyme; *Antimicrob. Agents Chemother.* **2001**, *45*, 3182–3188.

- (211) A. J. McCoy, R. C. Sandlin, A. T. Maurelli; In Vitro and in Vivo Functional Activity of *Chlamydia* MurA, a UDP-N-Acetylglucosamine Enolpyruvyl Transferase Involved in Peptidoglycan Synthesis and Fosfomycin Resistance; *J. Bacteriol.* **2003**, *185*, 1218–1228.
- (212) D. E. Karageorgopoulos, R. Wang, X. H. Yu, M. E. Falagas; Fosfomycin: Evaluation of the Published Evidence on the Emergence of Antimicrobial Resistance in Gram-Negative Pathogens; *J. Antimicrob. Chemother.* **2012**, *67*, 255–268.
- (213) P. S. Venkateswaran, H. C. Wu; Isolation and Characterization of a Phosphonomycin-Resistant Mutant of *Escherichia Coli* K-12; *J. Bacteriol.* **1972**, *110*, 935–944.
- (214) J. L. Marquardt, D. A. Siegele, R. Kolter, C. T. Walsh; Cloning and Sequencing of *Escherichia Coli* MurZ and Purification of Its Product, a UDP-N-Acetylglucosamine Enolpyruvyl Transferase; *J. Bacteriol.* **1992**, *174*, 5748–5752.
- (215) R. E. Rigsby, K. L. Fillgrove, L. A. Beihoffer, R. N. Armstrong; Fosfomycin Resistance Proteins: A Nexus of Glutathione Transferases and Epoxide Hydrolases in a Metalloenzyme Superfamily; *Methods Enzymol.* **2005**, *401*, 367–379.
- (216) I. Nikolaidis, S. Favini-Stabile, A. Dessen; Resistance to Antibiotics Targeted to the Bacterial Cell Wall; *Protein Sci.* **2014**, *23*, 243–259.
- (217) S. Kobayashi, T. Kuzuyama, H. Seto; Characterization of the FomA and FomB Gene Products from *Streptomyces Wedmorensis*, Which Confer Fosfomycin Resistance on *Escherichia Coli*; *Antimicrob. Agents Chemother.* **2000**, *44*, 647–650.
- (218) P. Garcia, P. Arca, J. E. Suarez; Product of FosC, a Gene from *Pseudomonas Syringae*, Mediates Fosfomycin Resistance by Using ATP as Cosubstrate; *Antimicrob. Agents Chemother.* **1995**, *39*, 1569–1573.
- (219) J. E. Suarez, M. C. Mendoza; Plasmid-Encoded Fosfomycin Resistance; *Antimicrob. Agents Chemother.* **1991**, *35*, 791–795.
- (220) Z. Fu, Y. Ma, C. Chen, Y. Guo, F. Hu, Y. Liu, X. Xu, M. Wang; Prevalence of Fosfomycin Resistance and Mutations in MurA, GlpT, and UhpT in Methicillin-Resistant *Staphylococcus Aureus* Strains Isolated from Blood and Cerebrospinal Fluid Samples; *Front. Microbiol.* **2016**, *6*, 1–6

- (221) Y. Utsui, S. Ohya, T. Magaribuchi, M. Tajima, T. Yokota; Antibacterial Activity of Cefmetazole Alone and in Combination with Fosfomycin against Methicillin- and Cephem-Resistant *Staphylococcus Aureus*; *Antimicrob. Agents Chemother.* **1986**, *30*, 917–922.
- (222) V. M. Figueredo, H. C. Neti; Synergy of Ciprofloxacin with Fosfomycin in Vitro against *Pseudomonas* Isolates from Patients with Cystic Fibrosis; *J. Antimicrob. Chemother.* **1988**, *22*, 41–50.
- (223) S. Gatermann, E. Schulz, R. Marre; The Microbiological Efficacy of the Combination of Fosfomycin and Vancomycin Against Clinically Relevant *Staphylococci*; *Infection* **1989**, *17*, 35–37.
- (224) K. Fujita; An Effect of Fosfomycin on the Pharmacokinetics of Amikacin; *J. Antibiot.* **1984**, *37*, 408–412.
- (225) M. D. F. S. Barbosa, G. Yang, J. Fang, M. G. Kurilla, D. L. Pompliano; Development of a Whole-Cell Assay for Peptidoglycan Biosynthesis Inhibitors; *Antimicrob. Agents Chemother.* **2002**, *46*, 943–946.
- (226) A. Bachelier, R. Mayer, C. D. Klein; Sesquiterpene Lactones Are Potent and Irreversible Inhibitors of the Antibacterial Target Enzyme MurA; *Bioorg. Med. Chem. Lett.* **2006**, *16*, 5605–5609.
- (227) A. Steinbach, A. J. Scheidig, C. D. Klein; The Unusual Binding Mode of Cnicin to the Antibacterial Target Enzyme MurA Revealed by X-Ray Crystallography; *J. Med. Chem.* **2008**, *51*, 5143–5147.
- (228) J. Molina-López, F. Sanschagrin, R. C. Levesque; A Peptide Inhibitor of MurA UDP-*N*-Acetylglucosamine Enolpyruvyl Transferase: The First Committed Step in Peptidoglycan Biosynthesis; *Peptides* **2006**, *27*, 3115–3121.
- (229) T. Schewe; Molecular Actions of Ebselen—an Antiinflammatory Antioxidant; *Gen. Pharmacol.* **1995**, *26*, 1153–1169.
- (230) B. S. Jin, S. G. Han, W. K. Lee, S. W. Ryoo, S. J. Lee, S. W. Suh, Y. G. Yu; Inhibitory Mechanism of Novel Inhibitors of UDP-*N*-Acetylglucosamine Enolpyruvyl Transferase from *Haemophilus Influenzae*; *J. Microbiol. Biotechnol.* **2009**, *19*, 1582–1589.
- (231) T. Mendgen, T. Scholz, C. D. Klein; Structure-Activity Relationships of Tulipalines, Tuliposides, and Related Compounds as Inhibitors of MurA; *Bioorg. Med. Chem. Lett.* **2010**, *20*, 5757–5762.

- (232) K., Shigetomi, K. Shoji, S. Mitsuhashi, M. Ubukata; The Antibacterial Properties of 6-Tuliposide B. Synthesis of 6-Tuliposide B Analogues and Structure-Activity Relationship; *Phytochemistry* **2010**, *71*, 312–324.
- (233) S. H. Olesen, D. J. Ingles, Y. Yang, E.; Schönbrunn; Differential Antibacterial Properties of the MurA Inhibitors Terreic Acid and Fosfomycin; *J. Basic Microbiol.* **2014**, *54*, 322–326.
- (234) S. G. Han, W. K. Lee, B. S. Jin, K. I. Lee, H. H. Lee, Y. G. Yu; Identification of Novel Irreversible Inhibitors of UDP-N-Acetylglucosamine Enolpyruvyl Transferase (MurA) from Haemophilus Influenzae; *J. Microbiol. Biotechnol.* **2013**, *23*, 329–334.
- (235) T. Scholz, C. L. Heyl, D. Bernardi, S. Zimmermann, L. Kattner, C. D. Klein; Chemical, Biochemical and Microbiological Properties of a Brominated Nitrovinylfuran with Broad-Spectrum Antibacterial Activity; *Bioorg. Med. Chem.* **2013**, *21*, 795–804.
- (236) C. M.; Chang, J.; Chern, M. Y.; Chen, K. F.; Huang, C. H.; Chen, Y. L.; Yang, S. H. Wu; Avenaciolides: Potential MurA-Targeted Inhibitors against Peptidoglycan Biosynthesis in Methicillin-Resistant *Staphylococcus Aureus* (MRSA); *J. Am. Chem. Soc.* **2015**, *137*, 267–275.
- (237) A. D. S. Magaton, M. M. M. Rubinger, F. C. de Macedo Junior, L. Zambolim; Synthesis and Antifungal Activity of New Bis- γ -Lactones Analogous to Avenaciolide; *J. Braz. Chem. Soc.* **2007**, *18*, 284–290.
- (238) J. D. McGivan, J. B. Chappell; Avenaciolide: A Specific Inhibitor of Glutamate Transport in Rat Liver Mitochondria; *Biochem. J.* **1970**, *116*, 37–38.
- (239) J. Varga, J. C. Frisvad, R. A. Samson; Two New Aflatoxin Producing Species, and an Overview of *Aspergillus* Section *Flavi*; *Stud. Mycol.* **2011**, *69*, 57–80.
- (240) J. C. Frisvad, L. L. H. Møller, T. O. Larsen, R. Kumar, J. Arnau; Safety of the Fungal Workhorses of Industrial Biotechnology: Update on the Mycotoxin and Secondary Metabolite Potential of *Aspergillus Niger*, *Aspergillus Oryzae*, and *Trichoderma Reesei*; *Appl. Microbiol. Biotechnol.* **2018**, *102*, 9481–9515.
- (241) K. Rožman, S. Lešnik, B. Brus, M. Hrast, M. Sova, D. Patin, H. Barreteau, J. Konc, D. Janežič, S. Gobec; Discovery of New MurA Inhibitors Using Induced-Fit Simulation and Docking; *Bioorg. Med. Chem. Lett.* **2017**, *27*, 944–949.

- (242) A. Kumar, R. Saranathan, K. Prashanth, B. K. Tiwary, R. Krishna; Inhibition of the MurA Enzyme in *Fusobacterium Nucleatum* by Potential Inhibitors Identified through Computational and *in Vitro* Approaches; *Mol. Biosyst.* **2017**, *13*, 939–954.
- (243) M. F. Chabán, M. Hrast, R. Frlan, D. G. Graikioti, C. M. Athanassopoulos, M. C. Carpinella; Inhibition of MurA Enzyme from *Escherichia Coli* and *Staphylococcus Aureus* by Diterpenes from *Lepechinia Meyenii* and Their Synthetic Analogs; *Antibiotics* **2021**, *10*, 1–15.
- (244) D. Raina, H. Tiwari, S. Sharma, Deepika, P. K. Chinthakindi, A. Nargotra, P. L. Sangwan, K. Eniyan, U. Bajpai, R. A. Vishwakarma, F. Gul Khan, S. Saran, I. A. Khan, F. G. Khan; Screening of Compound Library Identifies Novel Inhibitors against the MurA Enzyme of *Escherichia Coli*; *Appl. Microbiol. Biotechnol.* **2021**, *105*, 3611–3623.
- (245) N. Wang, E. B. Faber, G. I. Georg; Synthesis and Spectral Properties of 8-Anilino-naphthalene-1-Sulfonic Acid (ANS) Derivatives Prepared by Microwave-Assisted Copper(0)-Catalyzed Ullmann Reaction; *ACS Omega* **2019**, *4*, 18472–18477.
- (246) D. J. R. Laurence; Interactions of Calf-Thymus Histone Fractions in Aqueous Solution with 8-Anilino-naphthalene-1-Sulphonic Acid; *Biochem. J.* **1966**, *99*, 419–426.
- (247) X. C. Yu, H. W. Strobel; Interactions of 8-Anilino-1-Naphthalenesulfonic Acid (ANS) and Cytochrome P450 2B1: Role of ANS as an Effector as Well as a Reporter Group; *Mol. Cell. Biochem.* **1996**, *162*, 89–95.
- (248) O. K. Gasyimov, B. J. Glasgow; ANS Fluorescence: Potential to Augment the Identification of the External Binding Sites of Proteins; *Biochim. Biophys. Acta* **2007**, *1774*, 403–407.
- (249) D. Matulis, R. Lovrien; 1-Anilino-8-Naphthalene Sulfonate Anion-Protein Binding Depends Primarily on Ion Pair Formation; *Biophys. J.* **1998**, *74*, 422–429
- (250) L. Stryer; The Interaction of a Naphthalene Dye with Apomyoglobin and Apohemoglobin: A Fluorescent Probe of Non-Polar Binding Sites; *J. Mol. Biol.* **1965**, *13*, 482–495.

- (251) M. Cardamone, N. K. Puritt; Spectrofluorimetric Assessment of the Surface Hydrophobicity of Proteins; *Biochem. J.* **1992**, *282*, 589–593.
- (252) M. Ploug, J. Vincent Ellis; Ligand Interaction between Urokinase-Type Plasminogen Activator and Its Receptor Probed with 8-Anilino-1-Naphthalenesulfonate. Evidence for a Hydrophobic Binding Site Exposed Only on the Intact Receptor; *Biochemistry* **1994**, *33*, 8991–8997.
- (253) P. M. Horowitz, N. L. Criscimagna; Differential Binding of the Fluorescent Probe 8-Anilidonaphthalene-2-Sulfonic Acid to Rhodanese Catalytic Intermediates; *Biochemistry* **1985**, *24*, 2587–2593.
- (254) L. S. Itzhaki, P. A. Evans, C. M. Dobson, S. E. Radford; Tertiary Interactions in the Folding Pathway of Hen Lysozyme: Kinetic Studies Using Fluorescent Probes; *Biochemistry* **1994**; *33*, 5212–5220.
- (255) M. Ruoppolo, R. B. Freedman; Protein-S-S-Glutathione Mixed Disulfides as Models of Unfolded Proteins; *Biochemistry* **1994**; *33*, 7654–7662.
- (256) N. D. Younan, J. H. A Viles; Comparison of Three Fluorophores for the Detection of Amyloid Fibers and Prefibrillar Oligomeric Assemblies. ThT (Thioflavin T); ANS (1-Anilidonaphthalene-8-Sulfonic Acid); and BisANS (4,4'-Dianilino-1,1'-Binaphthyl-5,5'-Disulfonic Acid); *Biochemistry* **2015**, *54*, 4297–4306.
- (257) K. Kakuda, K. I. Yamaguchi, K. Kuwata, R. A. Honda; Valine-to-Lysine Substitution at Position 210 Induces Structural Conversion of Prion Protein into a β -Sheet Rich Oligomer; *Biochem. Biophys. Res. Commun.* **2018**, *506*, 81–86.
- (258) G. V. Semisotnov, N. A. Rodionova, O. I. Razgulyaev, V. N. Uversky, A. F. Gripas, R. I. Gilmanshin; Study of the “Molten Globule” Intermediate State in Protein Folding by a Hydrophobic Fluorescent Probe; *Biopolymers* **1991**, *31*, 119–128.
- (259) L. M. T. R. Lima, V. D. A. Silva, L. D. C. Palmieri, M. C. B. R. Oliveira, D. Foguel, I. Polikarpov; Identification of a Novel Ligand Binding Motif in the Transthyretin Channel; *Bioorg. Med. Chem.* **2010**, *18*, 100–110.
- (260) T. Yokoyama, Y. Kosaka, M. Mizuguchi; Structural Insight into the Interactions between Death-Associated Protein Kinase 1 and Natural Flavonoids; *J. Med. Chem.* **2015**, *58*, 7400–7408.
- (261) A. Lartigue, A. Gruez, S. Spinelli, S. Rivière, R. Brossut, M. Tegoni, C. Cambillau; The Crystal Structure of a Cockroach Pheromone-Binding Protein Suggests a

- New Ligand Binding and Release Mechanism; *J. Biol. Chem.* **2003**, *278*, 30213–30218.
- (262) S. Kofler, C. Asam, U. Eckhard, M. Wallner, F. Ferreira, H. Brandstetter; Crystallographically Mapped Ligand Binding Differs in High and Low IgE Binding Isoforms of Birch Pollen Allergen Bet v 1; *J. Mol. Biol.* **2012**, *422*, 109–123.
- (263) J. Smietanska, J. Sliwiak, M. Gilski, Z. Dauter, R. Strzalka, J. Wolny, M. A Jaskolski; New Modulated Crystal Structure of the ANS Complex of the St John's Wort Hyp-1 Protein with 36 Protein Molecules in the Asymmetric Unit of the Supercell; *Acta Crystallogr. D* **2020**, *76*, 653–667.
- (264) R. León, J. I. Murray, G. Cragg, B. Farnell, N. R. West, T. C. S. Pace, P. H. Watson, C. Bohne, M. J. Boulanger, F. Hof; Identification and Characterization of Binding Sites on S100A7, a Participant in Cancer and Inflammation Pathways; *Biochemistry* **2009**, *48*, 10591–10600.
- (265) M. Hirose, S. Sugiyama, H. Ishida, M. Niiyama, D. Matsuoka, T. Hara, E. Mizohata, S. Murakami, T. Inoue, S. Matsuoka, M. Murata; Structure of the Human-Heart Fatty-Acid-Binding Protein 3 in Complex with the Fluorescent Probe 1-Anilino-naphthalene-8-Sulphonic Acid; *J. Synchrotron Radiat.* **2013**, *20*, 923–928.
- (266) S. Betzi, R. Alam, M. Martin, D. J. Lubbers, H. Han, S. R. Jakkaraj, G. I. Georg, E. Schönbrunn; Discovery of a Potential Allosteric Ligand Binding Site in CDK2; *ACS Chem. Biol.* **2011**, *6*, 492–501.
- (267) M. R. Groves, I. B. Müller, X.; Kreplin, J. Müller-Dieckmann, A Method for the General Identification of Protein Crystals in Crystallization Experiments Using a Noncovalent Fluorescent Dye; *Acta Crystallogr. D* **2007**, *63*, 526–535.
- (268) A. M. Gilbert, A. Failli, J. Shumsky, Y. Yang, A. Severin, G. Singh, W. Hu, D. Keeney, P. J. Petersen, A. H. Katz; Pyrazolidine-3,5-Diones and 5-Hydroxy-1H-Pyrazol-3(2H)-Ones, Inhibitors of UDP-N-Acetylenolpyruvyl Glucosamine Reductases; *J. Med. Chem.* **2006**, *49*, 6027–6036.
- (269) J. M. Arencibia, W. Fröhner, M. Krupa, D. Pastor-Flores, P. Merker, T. Oellerich, S. Neimanis, C. Schmithals, V. Köberle, E. Süß, S. Zeuzem, H. Stark, A. Piiper, D. Odadzic, J. O. Schulze, R. M. Biondi; An Allosteric Inhibitor Scaffold Targeting

- the PIF-Pocket of Atypical Protein Kinase C Isoforms; *ACS Chem. Biol.* **2017**, *12*, 564–573.
- (270) R. Chollet, J. Chevalier, A. Bryskier, J. M. Pagès; The AcrAB-TolC Pump Is Involved in Macrolide Resistance but Not in Telithromycin Efflux in *Enterobacter Aerogenes* and *Escherichia Coli*; *Antimicrob. Agents Chemother.* **2004**, *48*, 3621–3624.
- (271) I. Ofek, S. Cohen, R. Rahmani, K. Kabha, D. Tamarkin, Y. Herzig, E. Rubinstein; Antibacterial Synergism of Polymyxin B Nonapeptide and Hydrophobic Antibiotics in Experimental Gram-Negative Infections in Mice; *Antimicrob. Agents Chemother.* **1994**, *38*, 374–377.
- (272) L. Wang, C. Hu, L. Shao; The Antimicrobial Activity of Nanoparticles: Present Situation and Prospects for the Future; *Int. J. Nanomed.* **2017**, *12*, 1227–1249.
- (273) A. Kumar, A. K. Pandey, S. S. Singh, R. Shanker, A. Dhawan; Cellular Uptake and Mutagenic Potential of Metal Oxide Nanoparticles in Bacterial Cells; *Chemosphere* **2011**, *83*, 1124–1132.
- (274) L. Shang, K. Nienhaus, G. U. Nienhaus; Engineered Nanoparticles Interacting with Cells: Size Matters; *J. Nanobiotechnology* **2014**, *12*, 5.
- (275) Z. Wang, Y. Ma, H. Khalil, R. Wang, T. Lu, W. Zhao, Y. Zhang, J. Chen, T. Chen; Fusion between Fluid Liposomes and Intact Bacteria: Study of Driving Parameters and in Vitro Bactericidal Efficacy; *Int. J. Nanomed.* **2016**, *11*, 4025–4036.
- (276) M. M. Kozlov, V. S. Markin; On the Theory of Membrane Fusion. The Adhesion-Condensation Mechanism; *Gen. Physiol. Biophys.* **1984**, *5*, 379–402.
- (277) P. W. Seo, S. Y. Park, A. Hofmann, J. S. Kim; Crystal Structures of UDP-N-Acetylmuramic Acid L-Alanine Ligase (MurC) from *Mycobacterium Bovis* with and without UDP-N-Acetylglucosamine; *Acta Crystallogr. D* **2021**, *77*, 618–627.
- (278) J. B. Raymond, N. P. Price, M. S. Pavelka; A Method for the Enzymatic Synthesis and HPLC Purification of the Peptidoglycan Precursor UDP-N-Acetylmuramic Acid; *FEMS Microbiol. Lett.* **2003**, *229*, 83–89.
- (279) W. T. Booth, C. R. Schlachter, S. Pote, N. Ussin, N. J. Mank, V. Klapper, L. R. Offermann, C. Tang, B. K. Hurlburt, M. Chruszcz; Impact of an N-terminal Polyhistidine Tag on Protein Thermal Stability; *ACS Omega* **2018**, *3*, 760–768.

7. Appendix

7.1 Fluorescence Binding Assays

Fluorescence binding is a widely used method to study the conformational changes of various proteins including MurA.^{192,199,204} This technique has been reported in chapter 3.4, where it has been used to study the binding of two ANS derivatives to MurA from *E. coli* and *E. cloacae*. Fluorescence binding assays were also utilized in this work to verify the binding of compound **46** to *E. coli* MurA in the presence of ANS.

7.1.1 Compound 46 Binding to MurA in the Fluorescence Binding Assay

The procedure followed for the fluorescence binding assay is detailed in 5.2.2.5. For the studying of the binding of compound **46**, increasing concentrations were added to the WT *E. coli* MurA-ANS complex and the samples were measured using a spectrofluorometer. The experiment was performed both in the presence and absence of UDP-GlcNAc. The results of these experiments are depicted in *Figure 7.1*. K_d values were calculated for compound **46** for both experiments in order to compare the binding of compound **46** to MurA both in the presence and absence of UDP-GlcNAc. The K_d value was calculated by plotting the hyperbole curve of the corrected fluorescence vs the conc of compound **46** (*Figure 7.2*). The corrected fluorescence is calculated as follows:

$$1 - \left[\frac{\text{Max Fluor of ligand} + \text{enz}}{\text{Fluor of enz} + \text{ANS alone}} \right]$$

The calculated K_d values were 14 μM for compound **46** in the presence of UDP-GlcNAc and 15 μM in its absence.

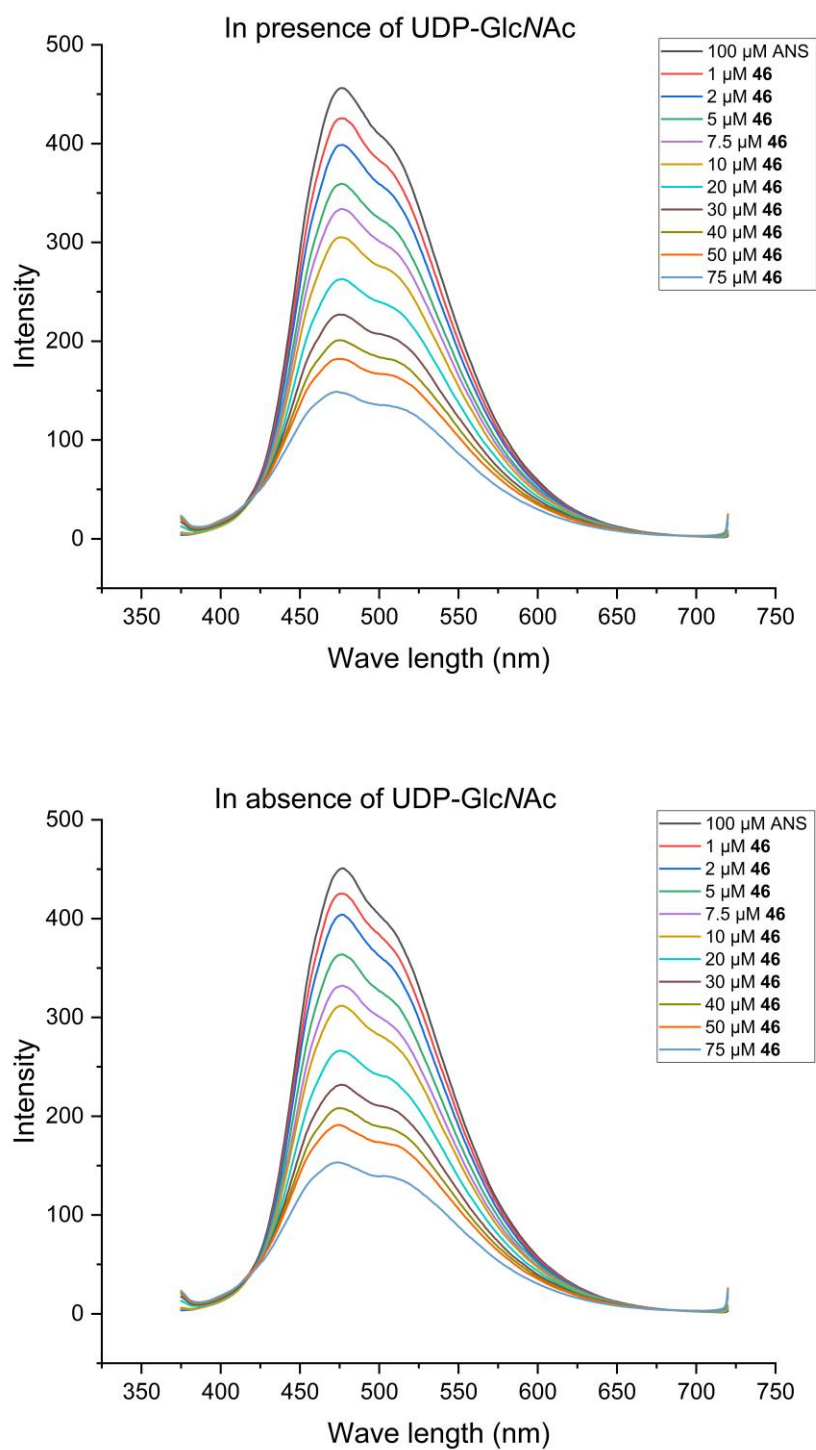


Figure 7.1. Fluorescence binding assay with compound **46** and WT MurA in presence and absence of UDP-GlcNAc

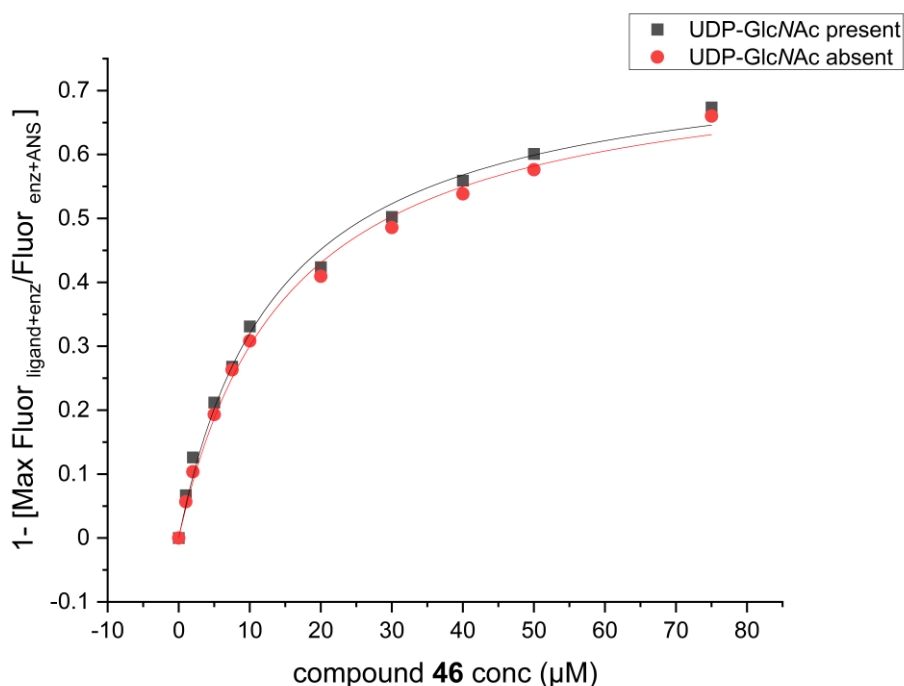


Figure 7.2. Curve of the corrected fluorescence vs concentration of compound **46**

From both *Figures 7.1* and *7.2* it is observed that while compound **46** is able to displace the ANS bound to MurA in a concentration-dependent manner, this ability is not dependent on the presence of the substrate UDP-GlcNAc. This conclusion seems at odds with our findings in section **3.3**, where the binding of compound **46** to the enzyme was not detected in the absence of UDP-GlcNAc as confirmed by native MS and protein NMR experiments. A suggested reason for the ability of compound **46** to bind to MurA and displace ANS in the absence of the substrate is that ANS preserves the enzyme in an open conformation, providing the opportunity for compound **46** to bind to MurA even in the absence of UDP-GlcNAc.

7.2 Design and Expression of MurA Mutants

Many MurA mutants have been discussed before, whether naturally occurring or synthetically made. The most relevant of these mutants is the widely discussed C115D mutant, which has been expressed and studied in sections **3.3** and **3.4**. Other mutants

that have been reported are N23A,¹⁹⁸ N23S,¹⁹⁸ C115S,^{192,202} C115A,¹⁷⁶ R120A,²⁰⁰ C251S,¹⁹³ C381S,¹⁹³ and D305A.^{181,198} Most of these mutants are catalytically inactive, particularly if the mutations occur near or at the active site.

Two novel MurA inhibitor classes were introduced in this work: pyrrolidinediones (such as compound **46**), and ANS and its derivatives as described in sections **3.3** and **3.4**, respectively. Prior to the protein NMR studies for MurA and **46**, an initial hypothesis for the binding of this compound was formed based on the fluorescence binding assays performed with ANS in addition to compound **46** (section **7.1**). Compound **46** was able to displace ANS from binding to MurA, and observing this interplay between the binding of compound **46** and ANS, we postulated that the binding sites for ANS and compound **46** would be close to each other. Due to the availability of an *E. cloacae* MurA-ANS co-crystal structure (PDB code 1EYN),²⁰⁴ the binding site of ANS is already known (section **1.7**). The protein surface was inspected for potential binding sites of **46** near the ANS binding pocket, leading to the identification of a shallow, hydrophobic groove encompassed by the side chains of Val109, Leu111, Pro121, Val122 and Ile94. No other region on the MurA protein surface, as displayed in the crystal structure, appeared suitable for the binding of small molecules. The hydrophobic groove offered a potential affinity gain through the hydrophobic effect upon binding of **46**. Concurrently, we attempted to co-crystallize MurA with several of our identified inhibitors. These co-crystallization attempts unfortunately failed, but while we did not isolate the MurA co-crystals with the inhibitors, we obtained crystals of a tetrameric form of the MurA apoprotein (section **3.3**). Consequently, we decided to perform site directed mutagenesis to MurA, to test whether compound **46** binds to the hydrophobic groove near the ANS binding site and to look further into the tetrameric protein structure.

To this end, three MurA mutants were designed. These mutants were V122D, L138D, and V143W MurA. These specific mutations were envisioned based on the following postulations:

- Mutation 1 (V122D): The valine at position 122 is located right at the end of the flexible catalytic loop containing the key Arg 120 residue. Replacing this valine with aspartate was postulated to furnish a salt bridge with Arg120, opening up the ANS binding pocket. This should also partially cover the hypothesized hydrophobic binding site of compound **46**, thus preventing its binding.
- Mutation 2 (L138D): The leucine is in the hydrophobic patch and is involved in an interaction to form the tetrameric protein form. MurA could only interact with **46** in the monomeric form as seen in the native MS data (chapter **3.3**). Therefore, it was hypothesized that changing this leucine to aspartate would repulse compound **46**.
- Mutation 3 (V143W): This valine is at the center of the hydrophobic surface that is postulated to be the binding site for compound **46**. The indole ring of the tryptophan would interact with the neighboring amino acids and seal the hydrophobic pocket, thus preventing the binding of compound **46**. Having this mutation would verify the binding site for compound **46**.

7.2.1 Expression of the MurA Mutants

7.2.1.1 Preparations for Site-directed Mutagenesis

QuikChange II XL Site-Directed Mutagenesis Kit™ and six custom oligonucleotide primers for the three mutants (forward and reverse sequences of the introduced mutation, *Table 7.1*) were purchased from Agilent Technologies, USA. NZY+ broth was

also prepared (*vide infra* for recipe). The PCR reactions were performed using a T100™ Thermal Cycler from Bio-Rad Laboratories, USA.

Table 7.1. Ordered oligonucleotide primers for site-directed mutagenesis.

No.	Oligo name	Sequence	OD	Weight (µg)	No. of Moles (nmol)	MW (g/mol)	GC amount (%)
1	V122D forward	GATTGGTGCACGT CCGGATGATCTAC ACATTTCTG (35)	28.82	828	77.0	10753	48.6%
2	V122D reverse	CAGAAATGTGTAG ATCATCCGGACGT GCACCAATC (35)	29.54	804	74.8	10749	48.6%
3	L138D forward	CGAACAATTAGGC GCGACCATCAAAG ATGAAGAAGGTTA CGTTAAAGC (48)	34.20	886	59.6	14876	43.8%
4	L138D reverse	GCTTTAACGTAAC CTTCTTCATCTTT GATGGTCGCGCCT AATTGTTTCG (48)	31.50	936	63.9	14656	43.8%
5	V143W forward	CATCAAACCTGGAA GAAGGTTACTGGA AAGCTTCCGTCGA TGGTCGTT (47)	38.48	1055	72.6	14542	46.8%
6	V143W reverse	AACGACCATCGAC GGAAGCTTTCCAG TAACCTTCTTCCA GTTTGATG (47)	33.15	939	65.4	14373	46.8%

Recipe for NZY⁺ broth:

10 g Bactocastone (pancreatic digest of casein)

5 g Yeast extract

5 g NaCl

ddH₂O to 1 L

Adjust to pH 7.5 using NaOH and autoclave. Then add the following filter-sterilized supplements:

12.5 mL 1 M MgCl₂

12.5 mL 1 M MgSO₄

20 mL 20% (w/v) glucose

7.2.1.2 Site-directed Mutagenesis

The primers were dissolved at a concentration of 100 ng/μL, and the WT MurA plasmid (*Figure 7.3*) was dissolved at a concentration of 25 ng/μL in ddH₂O.

```

ATGGATAAATTTTCGTGTTTCAGGGGCCAACGAAGCTCCAGGGCGAAGTCACAATTTCCGGCGCTAAAAATGCT
GCTCTGCCTATCCTTTTTGCCGCACTACTGGCGGAAGAACCGGTAGAGATCCAGAACGTCCCGAAACTAAAA
GACGTCGATACATCAATGAAGCTGCTAAGCCAGCTGGGTGCGAAAGTAGAACGTAATGGTTCTGTGCATATT
GATGCCCCGCGACGTTAATGTATTCTGCGCACCTTACGATCTGGTTAAAACCATGCGTGCTTCTATCTGGGCG
CTGGGGCCGCTGGTAGCGCGCTTTGGTCAGGGGCAAGTTTCACTGCCTGGCGGTTGTACGATTGGTGCACGT
CCGGTTGATCTACACATTTCTGGTCTCGAACAATTAGGCGCGACCATCAAACCTGGAAGAAGGTTACGTTAAA
GCTTCCGTCGATGGTCGTTTTGAAAGGCGCACATATCGTGATGGATAAAGTCAGCGTTGGCGCAACGGTGACC
ATCATGTGTGCTGCAACCCTGGCCGAAGGCACCACGATTATTGAAAACGCAGCGCGTGAACCGGAAATCGTC
GATACCGCGAACTTCTGATTACGCTGGGTGCGAAAATTAGCGGTCAGGGCACCGATCGTATCGTCATTGAA
GGTGTGGAACGTTTAGGCGGCGGTGTCTATCGCGTGCTGCCGGATCGTATCGAAACCGGTACTTTCTGGTG
GCGGCGGGGATCTCTCGCGGCAAATTATCTGCCGTAACGCGCAGCCAGATACTCTGGACGCCGTGCTGGCG
AAACTGCGTGACGCTGGAGCGGACATCGAAGTCGGCGAAGACTGGATTAGCCTGGATATGCATGGCAAACGT
CCGAAGGCTGTTAACGTACGTACCGCGCCGCATCCGGCATTCCCGACCGATATGCAGGCCAGTTCACGCTGT
TGAACCTGGTGGCAGAAGGGACCGGGTTCATCACCGAAACGGTCTTTGAAAACCGCTTTATGCATGTGCCAG
AGCTGAGCCGTATGGGCGCGCATGCCGAAATCGAAAGCAATACCGTTATTTGTCACGGTGTTGAAAACTTT
CTGGCGCACAGGTTATGGCAACCGATCTGCGTGCATCAGCAAGCCTGGTGCTGGCTGGCTGTATTGCGGAAG
GGACGACGGTAGTTGATCGTATTTATCACATCGATCGTGGCTACGAACGCATTGAAGACAAACTGCGCGCTT
TAGGTGCAAATATTGAGCGTGTGAAAGGCGAACTGGTGCCACGCGGTTCTAC

```

Figure 7.3. Sequence of the WT MurA plasmid

The mutation reactions were carried out as follows: in an Eppendorf Fast PCR tube, 5 μ L of the provided reaction buffer in the QuikChange II XL Site-Directed Mutagenesis Kit™ was mixed with 2 μ L of the MurA plasmid (50 ng), 1.25 μ L of the corresponding two oligonucleotide primers (forward and reverse) for each mutation (125 ng), 1 μ L of the provided dNTP mix, 3 μ L of the provided QuikSolution reagent, and 36.5 μ L of ddH₂O. Then, 1 μ L of the provided *PfuUltra* HF DNA polymerase was added and the tubes were cycled in the thermal cycler according to the parameters in *Table 7.2*.

Table 7.2. PCR reaction cycles.

Segment	Cycles	Temperature	Time
1	1	95 °C	1 min
2	18	95 °C	50 s
		60 °C	50 s
		68 °C	1 min
3	1	68 °C	7 min

After the thermal cycling, the tubes were taken out of the thermal cycler and cooled on ice for 2 min. After that, 1 μ L of the provided *Dpn* I restriction enzyme was added to the mix, gently mixed and spun down in a microcentrifuge for 1 min. Then the tubes were immediately incubated at 37 °C for 1 h to digest the parental super coiled dsDNA. This mix was then used to transform the provided XL10-Gold ultracompetent cells.

7.2.1.3 Transformation of XL10-Gold Ultracompetent Cells

To transform the XL10-Gold ultracompetent cells, for each mutant, a 14-ml BD Falcon polypropylene round-bottom tube was cooled on ice, and NZY⁺ broth was heated to 42 °C in a water bath. The cells were thawed on ice, and 45 μ L of the cells were added to each prechilled tube. 2 μ L of the provided β -ME mix was added to each aliquot of cells, and the tubes were gently swirled. The cells were rested on ice for 10 minutes, with gentle swirling every two minutes. 2 μ L of the *Dpn*I-treated mix was transferred to the ultracompetent cell tubes. The transformation reactions were gently swirled then incubated on ice for 30 min. The tubes were heat-pulsed in a 42 °C water bath for 30 s, then the cells were rested on ice for two minutes. 0.5 mL of the preheated NZY⁺ broth was added and the tubes were incubated at 37 °C for 1 h with shaking at 225-250 rpm. The contents of each tube were spread on two pre-warmed LB-Kanamycin (50 μ g/mL) agar plates, and incubated at 37 °C overnight.

The three mutant plasmids were extracted from overnight liquid cultures using the GenElute™ Plasmid Miniprep Kit from Sigma-Aldrich. The concentrations for each extracted mutant plasmid were 60.6 ng/μL for V122D, 53.4 ng/μL for L138D, and 61.9 ng/μL for V143W, as measured on a NanoDrop 2000 Microvolume Spectrophotometer from Thermo Fisher Scientific, USA. 15 μL of each of the extracted plasmids were sent for sequencing at Eurofins Genomics using their Mix2Seq kit, mixed with 10 μL of either T7 or T7 term primers. The results of the sequencing are shown in *Figure 7.4* and prove that the site-directed mutagenesis experiment was a success.

A

MDKFRVQGPTKLQGEVTISGAKNAALPILFAALLAEEPVEIQNVPKLDVDTSMKLLSQLGAKVERNGSVHID
 ARDVNVFCAPYDLVKTMRASIWALGPLVARFGQGQVSLPGGCTIGARP^VDLHISGLEQLGATIK^LEEGY^VCK
 ASVDGRLKGAHIVMDKVSVGATVTIMCAATLAEGTTIENAAREPEIVDTANFLITLGAKISGQGTDRIVIEGVE
 RLGGGVYRVLDPRIETGTFLVAAAISRGKIIICRNAQPDTLDAVLAKLRDAGADIEVGEDWISLDMHGKRPKAV
 NVRTAPHPAFPTDMQAQFTLLNLVAEGTGFITETVFENRFMHVPELSRMGAHAEIESNTVICHGVEKLSGAQ
 VMATDLRASASLVLAGCIAEGTTVVDRIYHIDRGYERIEDKLRALGANIERVKGELVPRGSTSSVDKLAALAEH
 HHHHH

B

MDKFRVQGPTKLQGEVTISGAKNAALPILFAALLAEEPVEIQNVPKLDVDTSMKLLSQLGAKVERNGSVHID
 ARDVNVFCAPYDLVKTMRASIWALGPLVARFGQGQVSLPGGCTIGARP^DDLHISGLEQLGATIKLEEGYVKAS
 VDGRLKGAHIVMDKVSVGATVTIMCAATLAEGTTIENAAREPEIVDTANFLITLGAKISGQGTDRIVIEGVERL
 GGGVYRVLDPRIETGTFLVAAAISRGKVICRNAQPDTLDAVLAKLRDAGADIEVGEDWISLDMHGKRPKAVN
 VRTAPHPAFPTDMQAQFTLLNLVAEGTGFITETVFENRFMHVPELSRMGAHAEIESNTVICHGVEKLSGAQV
 MATDLRASASLVLAGCIAEGTTVVDRIYHIDRGYERIEDKLRALGANIERVKGELVPRGSTSSVDKLAALAEHH
 HHHH

C

MDKFRVQGPTKLQGEVTISGAKNAALPILFAALLAEEPVEIQNVPKLKDVDTSMKLLSQLGAKVERNGSVHID
 ARDNNVFCAPYDLVKTMRASIWALGPLVARFGQGQVSLPGGCTIGARPVDLHISGLEQLGATIK^DEEGYVKAS
 VDGRLLKGAHIVMDKVSVGATVTIMCAATLAEGTTIENAAAREPEIVDTANFLITLGAKISGQGTDRIVIEGVERL
 GGGVYRVLPDRIETGTFLVAAAISRGKVICRNAQPDTLDAVLAKLRDAGADIEVGEDWISLDMHGKRPKAVN
 VRTAPHPAFPTDMQAQFTLLNLVAEGTGFITETVFENRFMHVPELSRMGAHAEIESNTVICHGVEKLSGAQV
 MATDLRASASLVLAGCIAEGTTVVDRIYHIDRGYERIEDKLRALGANIERVKGELVPRGSTSSVDKLAALAEHH
 HHHH

D

MDKFRVQGPTKLQGEVTISGAKNAALPILFAALLAEEPVEIQNVPKLKDVDTSMKLLSQLGAKVERNGSVHID
 ARDNNVFCAPYDLVKTMRASIWALGPLVARFGQGQVSLPGGCTIGARPVDLHISGLEQLGATIKLEEGY^WKAS
 VDGRLLKGAHIVMDKVSVGATVTIMCAATLAEGTTIENAAAREPEIVDTANFLITLGAKISGQGTDRIVIEGVERL
 GGGVYRVLPDRIETGTFLVAAAISRGKVICRNAQPDTLDAVLAKLRDAGADIEVGEDWISLDMHGKRPKAVN
 VRTAPHPAFPTDMQAQFTLLNLVAEGTGFITETVFENRFMHVPELSRMGAHAEIESNTVICHGVEKLSGAQV
 MATDLRASASLVLAGCIAEGTTVVDRIYHIDRGYERIEDKLRALGANIERVKGELVPRGSTSSVDKLAALAEHH
 HHHH

Figure 7.4. **A.** WT MurA amino acid sequence with the sites of three mutations marked as ^aV112D, ^bL138D, ^cV143W; **B.** V122D mutant amino acid sequence; **C.** L138D mutant amino acid sequence; **D.** V143W mutant amino acid sequence

7.2.1.4 Expression of the Mutant Proteins

The extracted plasmids were used to transform the competent *E. coli* Bl21 C41 cells according to the procedure in chapter 5.2.2.2. The three mutant proteins were then expressed and purified using the standard protein expression and purification procedure in chapters 5.1.4.1 and 5.2.2.3.

The concentrations for the mutant proteins were measured using the NanoDrop device and were: 1.7 µg/µL for the V122D mutant, 2.9 µg/µL for the L138D mutant, and 2.9 µg/µL for the V143W mutant. The protein stocks were flash frozen with liquid nitrogen and stored at -80 °C.

7.2.2 Activity and Inhibition of the Mutant Proteins

The activity of the three mutants was determined using the standard MurA assay discussed in chapter 5.1.4.2. The activities, in terms of absorbance measured, were compared to both WT and C115D MurA in *Figure 7.5*.

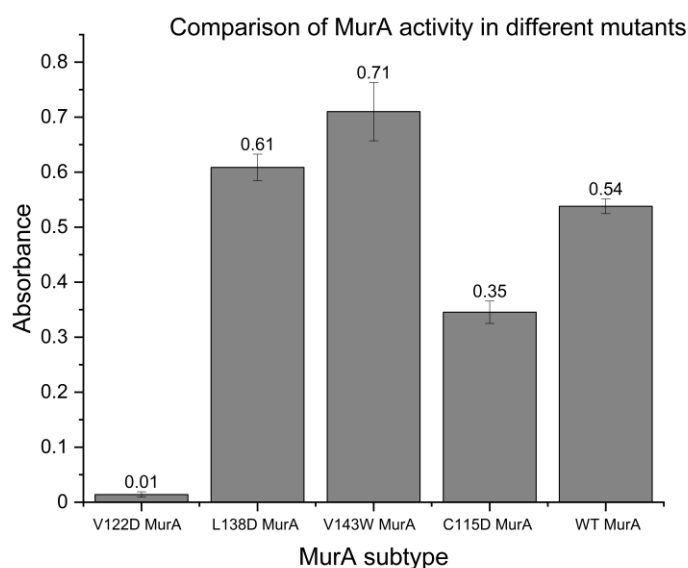


Figure 7.5. Activities of the different MurA mutants

Testing the activities of the different proteins revealed that the V122D mutant was catalytically inactive and that the other two mutants were slightly more active than the WT enzyme. The lowest activity found within this series of active mutants belonged to the C115D mutant.

Next, the inhibition of both compound **46** and ANS was tested on the two new active mutants, and again they were compared to the results obtained with the WT and C115D MurA (*Figure 7.6*).

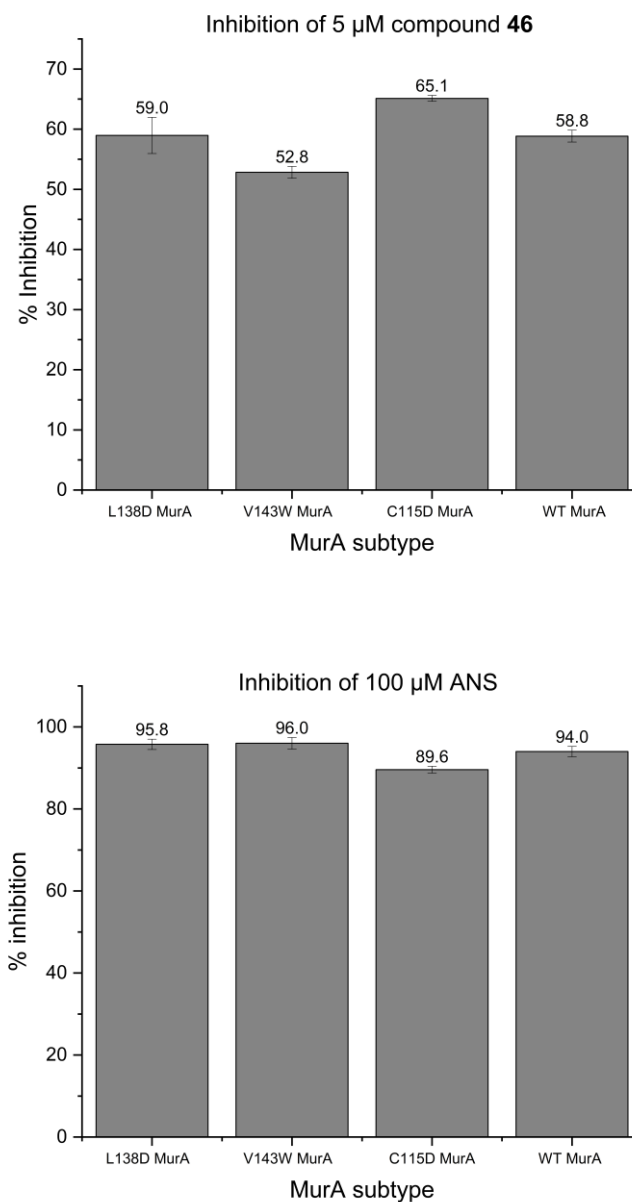


Figure 7.6. Inhibition by both compound **46** and ANS of the new mutants in comparison to WT MurA and C115D MurA

As seen in *Figure 7.6*, both compound **46** and ANS were almost equally as active on all the available MurA mutants as they were on WT MurA.

7.2.3 Native MS Analysis of the Mutant Proteins

To further study the structure of the mutant proteins, they were analyzed using non-native and native MS techniques discussed in sections **3.3** and **5.1.4.7**. The results of the MS analysis are summarized in *Table 7.3*.

Table 7.3. Non-native and native MS results.

Mutant	Non-native Mass (Da)	Calculated Mass by EXPASY (Da)	Native Mass (Da)	Suspected Species (suspected Mass in Da)	Difference (Da)
V122D	47569.8	47569.7	47736.4	Enzyme+PEP (47737.8)	1.4
L138D	47554.6	47555.6	47726.3	Enzyme+PEP (47722.6)	3.7
V143W	47640.8	47640.8	48510.2	Enzyme+UDP-MurNAc+PEP+Na (48511.3)	1.1

The MS analysis of the expressed mutants revealed that the masses of all three mutants lined up with the masses calculated from their amino acid sequence by EXPASY. It also showed that the native MS of the three proteins indicated binding to PEP whether alone or in combination with UDP-MurNAc and Na, a species often seen with WT MurA (section 3.3). Unfortunately, our native MS trials with the mutants in the presence of UDP-GlcNAc and compound **46** did not afford protein signals.

Thus, from the experiments performed with the newly expressed MurA mutants, we concluded that the presence of Val122 was essential for the enzymatic activity of MurA. However, replacing Leu138 and Val143 did not greatly affect the protein activity. It also had no impact on the binding ability of **46**, contrary to what was hypothesized. Instead, it was proven that both compound **46** and ANS were able to inhibit the active mutants, as well as WT and C115D MurA with almost the same efficiency. This led to the use of other techniques such as protein NMR (section 3.3) to gain more insight into the binding site of **46** to MurA.

7.3 Studies on 2-Phosphonopropionic acid, a PEP Analogue

PEP is the second substrate of MurA and it has been extensively discussed in section 1.6.1. An analogue of PEP that possesses a phosphonate group instead of a phosphate group is 2-phosphonopropionic acid (*Figure 7.7*)

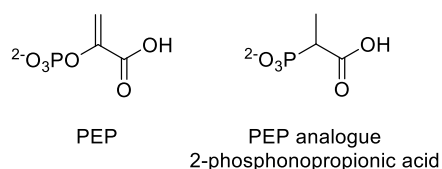


Figure 7.7. Structures of PEP and the PEP analogue

It was first tested in the standard MurA assay to see how it interacts with the enzyme. Various concentrations of the PEP analogue (dissolved in water) were tested ranging from 10 μM to 1 mM. The results of this test are shown in *Figure 7.8*.

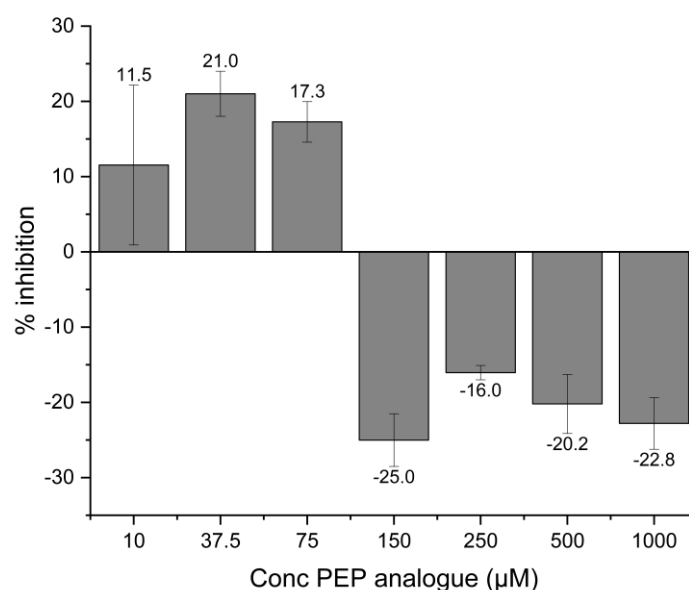


Figure 7.8. Effect of the PEP analogue on MurA

Based on these data, the PEP analogue appears to weakly inhibit MurA at lower concentrations up to 75 μM . Then the inhibition turns into activation of the enzymatic reaction. Another test done was to combine compound **46** (section 3.3) with the PEP analogue in the MurA assay to observe their interplay. To this end, 5 μM compound

46 was used in addition to increasing PEP analogue concentrations from 75 μM to 1 mM (Figure 7.9).

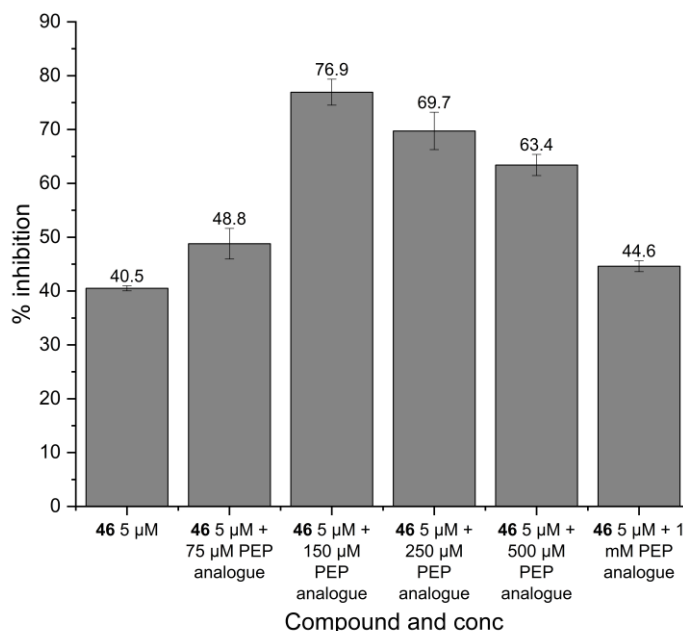


Figure 7.9. MurA inhibition using the PEP analogue in combination with compound **46**. The results show that the PEP analogue enhances the MurA inhibition when combined with compound **46**. This effect peaks at 150 μM PEP analogue but at higher concentrations of the PEP analogue, this effect decreases. The exact effect of the PEP analogue on both MurA on its own, and in combination with compound **46** could not be fully understood from the performed experiments. However, this analogue is important, as it can potentially be used instead of PEP in MurA X-ray co-crystallography experiments.

7.4 Enzymatic Synthesis of UDP-MurNAc

UDP-MurNAc is the product of MurB, the enzyme that follows MurA in the intracellular cell wall synthesis pathway. It is also one of the substrates of the subsequent enzyme, MurC.²⁷⁷ UDP-MurNAc is not commercially available, but its total

chemical synthesis has been previously reported, and also accomplished by our former group member Dr. Stefanie Wohnig in her PhD thesis (Synthese des dansylierten Park-Nucleotids und vereinfachter Analoga der Muraymycin-Antibiotika, section 4.2 page 65) in 7 steps with an overall yield of 16%. Total synthesis is a time-consuming and challenging process, so we looked into the enzymatic synthesis of UDP-MurNAc. As described in section 3.2, the enzymatic synthesis of the MurB substrate and MurA product EP-UDP-GlcNAc was successful and could be used to develop MurB assays using the crude product. Therefore, utilizing the available MurA and MurB enzymes in our lab, the synthesis of UDP-MurNAc was attempted.

7.4.1 Steps of the Enzymatic Synthesis of UDP-MurNAc

The enzymatic synthesis was performed according to Raymond *et al.* in a 50 mL falcon tube in which 1.4 mM of each of the three needed substrates (UDP-GlcNAc (1.8 mg), PEP (0.6 mg), and NADPH (2.3 mg)) was combined with 1 mM DTT, in addition to 125 µg MurA and 75 µg MurB, and 50 mM pH 8 Tris buffer with a final reaction volume of 2 mL.²⁷⁸ The reaction was gently shaken using a tabletop bench rocker 2D (Benchmark scientific) overnight at room temperature. Afterwards, the reaction was filtered through a vivaspin® 6, 10 kDa centrifugal filter from Sartorius Stedim Biotech, to remove the proteins. The filtrate was then analyzed by LC-MS where it showed a minor peak for UDP-GlcNAc (606.13 Da) and a major peak for UDP-MurNAc mass (678.17 Da) indicating its successful formation (*Figure 7.10*).

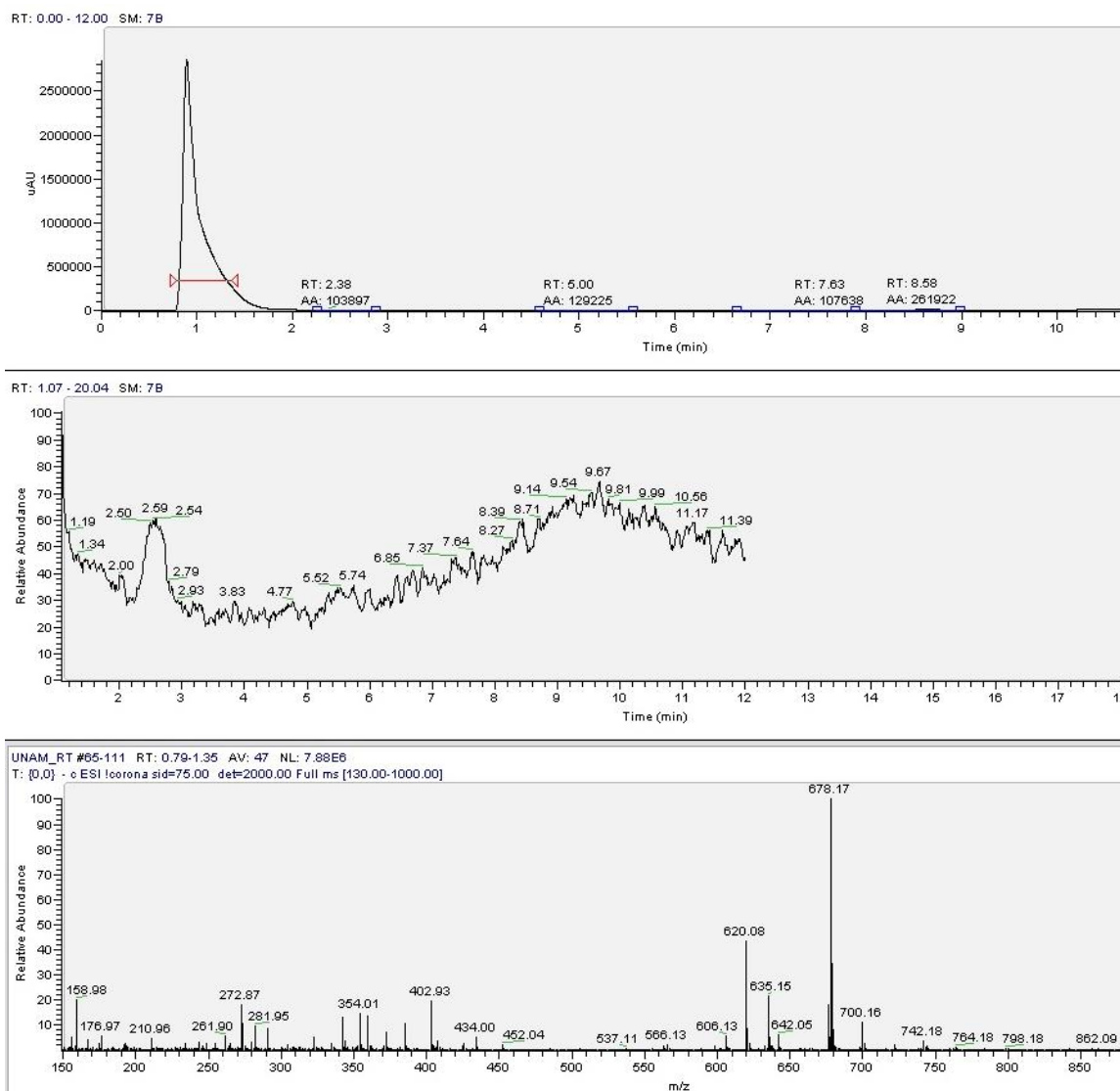


Figure 7.10. LC-MS chromatogram of the enzymatic synthesis of UDP-MurNAc

Purification of the produced UDP-MurNAc was attempted using the ÄKTA pure FPLC system (GE Healthcare), equipped with a Hitrap Q HP 1 mL anion exchange column (Sigma Aldrich), with running buffers A and B consisting of 0.02 M and 1 M ammonium acetate pH 5, respectively. The gradient used in the elution process (flow rate of 4 mL/min) is detailed in *Table 7.4*. The eluted fractions were collected, lyophilized, and weighed, however almost no product weight was detected. In conclusion, while the concept of enzymatic synthesis of the MurC substrate was a success, more optimization of the purification method is required.

Table 7.4. Gradient of buffers A and B used in the ÄKTA purification of UDP-MurNAc.

Type of Elution	% of running buffer B	Duration (min)
Isocratic	0%	5 min
Linear gradient	0-20%	20 min
Linear gradient	20-65%	15 min
Linear gradient	65-100%	5 min

7.5 Expression of MurC with a His-tag

The MurC plasmid was available and could be used to express MurC, but it suffered from a major shortcoming, which is that the expressed protein possessed no tag that could be used for its purification. It was therefore necessary to insert a specific tag to the protein that could be used to purify MurC. The chosen tag was His-tag, which is a sequence of six His amino acids. The His-tagged protein can be purified using the widely available Ni-agarose beads and an imidazole buffer.²⁷⁹ To this end we cloned a His-tag-containing MurC sequence into an expression plasmid.

7.5.1 Strategy for His-tag Insertion into MurC

A MurC insert with a His-tag-expressing sequence (*Figure 7.11*) was ordered from Eurofins Genomics arriving in a non-protein-expressing plasmid. The MurC insert was then subcloned into a protein-expressing pET-45b(+) plasmid already carrying a Dyrk1A insert. The subcloning was performed by cutting both plasmids using NcoI and NotI restriction enzymes (New England Biolabs, Inc) to obtain the free MurC insert and the pET-45b(+) vector without the Dyrk1A insert. This was followed by an agarose gel purification and extraction of the MurC insert and the vector. The two were then annealed together using T4 DNA ligase (New England Biolabs), and the MurC plasmid was then inserted into chemically competent *E. coli* BL21 C41 cells to express the His-tagged MurC protein.

CCATGGCGAATACACAACAATTGGCAAAACTGCGTTCATCGTGCCCGAAATGCGTTCGCGTTTCGGCACATAC
 ATTTTGTTCGGCATTGGTGGTGCCGGTATGGGCGGTATTGCCGAAGTCTGGCCAATGAAGGTTATCAGATCA
 GTGGTTCCGATTTAGCGCCAAATCCGGTCACGCAGCAGTTAATGAATCTGGGTGCGACGATTTATTTCAACC
 ATCGCCCGGAAAACGTACGTGATGCCAGCGTGGTTCGTTGTTTCCAGCGCGATTTCTGCCGATAACCCGGAAA
 TTGTCGCGGCTCATGAAGCGCGTATTCCGGTATCCGTCGTGCCGAAATGCTGGCTGAGTTAATGCGTTTTTC
 GTCATGGCATCGCCATTGCCGGAACGCACGGCAAAACGACAACCACCGCGATGGTTTTCCAGCATCTACGCAG
 AAGCGGGGCTCGACCCAACCTTCGTTAACGGCGGGCTGGTAAAAGCGGCGGGGGTTCATGCGCGTTTTGGGGC
 ATGGTCCGTACCTGATTGCCGAAGCAGATGAGAGTGATGCATCGTTCCTGCATCTGCAACCGATGGTGGCGA
 TTGTCACCAATATCGAAGCCGACCACATGGATACCTACCAGGGCGACTTTGAGAATTTAAAACAGACTTTTA
 TTAATTTTCTGCACAACCTGCCGTTTTACGGTCGTGCGGTGATGTGTGTTGATGATCCGGTGATCCGCGAAT
 TGTTACCGCGAGTGGGGCGTCAGACCACGACTTACGGCTTCAGCGAAGATGCCGACGTGCGTGTAGAAGATT
 ATCAGCAGATTGGCCCGCAGGGGCACTTTACGCTGCTGCGCCAGGACAAAGAGCCGATGCGCGTCACCCTGA
 ATGCGCCAGGTGCTCATAACGCGCTGAACGCCGAGCTGCGGTTGCGGTTGCTACGGAAGAGGGCATTGACG
 ACGAGGCTATTTTTCGCGGGCGCTTGAAAGCTTCCAGGGGACTGGTCGCGGTTTTGATTTCCCTCGGTGAATTCC
 CGCTGGAGCCAGTGAATGGTAAAAGCGGTACGGCAATGCTGGTTCGATGACTACGGCCACCACCCGACGGAAG
 TGGACGCCACCATTAAAGCGGCGCGCAGGCTGGCCGATAAAAACCTGGTAATGCTGTTTTACGCCGCACC
 GTTTTACCCGTACGCGCGACCTGTATGATGATTTTCGCCAATGTGCTGACGCAGGTTGATAACCCTGTTGATGC
 TGAAGTGTATCCGGTGGCGAAGCGCAATTCCGGGAGCGGACAGCCGTTTCGCTGTGTGCGACAATTCGTG
 GACGTGGGAAAATTGATCCCATTTCTGGTGCCGGATCCGGCGCGGGTAGCCGAGATGCTGGCACCGGTATTAA
 CCGGTAACGACCTGATTCTCGTTCAGGGGGCTGGTAATATTGGAAAAATTGCCGTTCTTTAGCTGAAATCA
 AACTGAAGCCGCAAACTCCGGAGGAAGAACAACATGACCACCATCACCATCACCATTGAGCGGCCGC

Figure 7.11. Sequence of the ordered His-tagged MurC insert

7.5.2 Procedure of the His-tagged MurC Subcloning

In an Eppendorf tube, 500 ng of the ordered MurC plasmid and 1 µg of the Dyrk1A pET-45b(+) plasmid were combined with 1 µL of each restriction enzyme (NcoI and NotI), 5 µL of NEBuffer 3.1 and water to a final volume of 50 µL. The mixtures were incubated for 2 h at 37 °C and were then purified using electrophoresis on an agarose gel and the Macherey Nagel NucleoSpin Gel and PCR Clean-up kit. The band size of the

MurC insert was 1500 bp and for the pET-45b(+) plasmid, it was 5200 bp (*Figure 7.12*). Details for the electrophoretic purification are found in chapter 5.2.2.1. The obtained amounts and concentrations were 20 μL of 11.2 $\text{ng}/\mu\text{L}$ of the MurC insert (224 ng) and 100 μL of 117 $\text{ng}/\mu\text{L}$ of the pET-45b(+) plasmid (11.7 μg). For the ligation step, 50 ng of the vector DNA was combined with 43 ng of the insert DNA. The insert and vector ligation steps are discussed in details in chapter 5.2.2.1, in addition to the transformation of the chemically competent C41 cells.

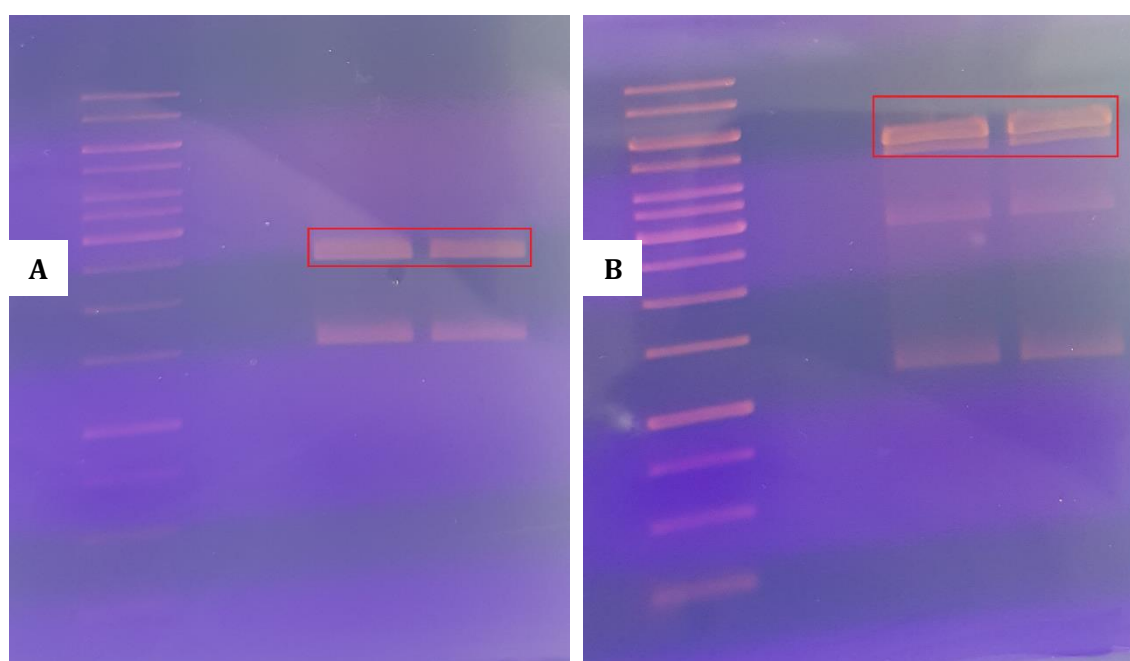


Figure 7.12. Gel electrophoresis on an agarose gel after double digestion of: **A.** ordered MurC plasmid; the red box denotes the band at 1500 bp corresponding to the MurC insert that was cut out and extracted. **B.** pET-45b(+) plasmid containing Dyr1A insert; the red box denotes the band at 5200 bp corresponding to the empty vector that was cut out and extracted

The successful uptake of the plasmid into the chemically competent C41 cells was verified by plasmid extraction from the transformed colonies, double digestion by *NcoI* and *NotI*, and then gel electrophoresis using the MurC insert and the pET-45b(+) plasmid as references. The details for these steps are provided in section 5.2.2.2. The

verification results are depicted in *Figure 7.13*. They clearly show that the test cultures do have the correct vector/insert combination.

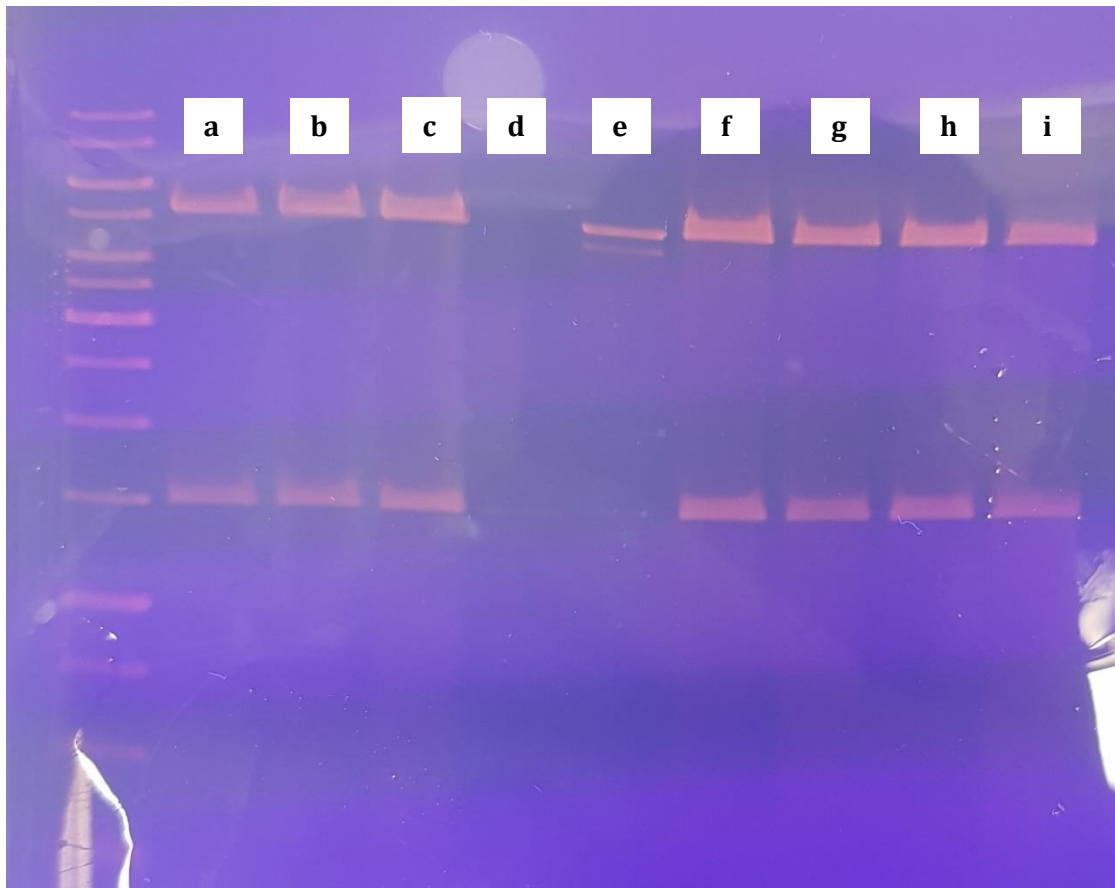


Figure 7.13. Electrophoresis on an agarose gel after extraction of plasmids from test cultures of transformed C41 cells. **a-c**, and **f-i** are the seven extracted plasmids from seven colonies double digested by *NcoI* and *NotI*; **d** is the purified MurC insert; **e** is the purified pET-45b(+) vector

7.5.3 Expression of His-tagged MurC

The protein expression of the His-tagged MurC followed the same standard procedure described in section 5.1.4.1. It was then followed by protein purification using Ni-agarose beads which again followed the standard procedure detailed in section 5.1.4.1. The obtained protein had a concentration of 1.1 $\mu\text{g}/\mu\text{L}$ and was aliquoted, flash frozen in liquid nitrogen, and stored at $-80\text{ }^{\circ}\text{C}$.

7.6 Supplementary Information for Chapter 3.3: Identification and Biochemical Characterization of Pyrrolidinediones as Novel Inhibitors of the Bacterial Enzyme MurA

Supplementary information for this article can be found under:

<https://doi.org/10.1021/acs.jmedchem.2c01275>

Additional Tables:

Table S1. Antibacterial activities: IC₉₀ values of the pyrrolidinedione derivatives against the growth of *E. coli* Δ tolC and *S. aureus* Newman strain.

Compd	IC ₉₀ <i>E. coli</i> Δ tolC (μ M) \pm SD (μ M) ^a	IC ₉₀ <i>S. aureus</i> Newman (μ M) \pm SD (μ M) ^a
1	>40	19 \pm 0
2	>40	>40
3	>40	>40
4	>40	>40
5	>40	>40
6	>40	>40
7	>40	>40
8	>40	40 \pm 0
9	>40	>40
10	>40	>40
11	>40	40 \pm 0
12	>40	40 \pm 0
13	>40	>40
14	>40	18 \pm 0
15	>40	>40
16	>40	>40
17	>40	>40
18	>40	>40
19	>40	>40
20	>40	>40
21	>40	>40
22	>40	>40

23	>40	>40
24	>40	>40
25	>40	>40
26	>40	>40
27	>40	>40
28	>40	>40
29	>40	>40
30	>40	>40
31	>40	>40
32	>40	>40
33	>40	>40
34	>40	>40
35	>40	>40
36	>40	>40
37	>40	20 ± 0
38	>40	>40
39	>40	>40
40	>40	>40
41	>40	>40
42	>40	>40
43	>40	>40
44	>40	>40
45	>40	13 ± 0
46	>40	38 ± 2
fosfomicin	89 ± 7	17 ± 2

^aResults are a mean of two experiments

Table S2. Antibacterial activities: IC₉₀ values of compound **46**, fosfomycin, and ampicillin against the growth of *E. coli* $\Delta tolC$ in the presence of PMBN.^a

Conc of PMBN ($\mu\text{g}/\text{mL}$)	0	3	4.5	6
IC₉₀ compound 46 (μM) \pm SD (μM)	>40	17 \pm 4	11 \pm 0	2.3 \pm 0.0
IC₉₀ fosfomycin (μM) \pm SD (μM)	89 \pm 7	74 \pm 3	87 \pm 0	86 \pm 0
IC₉₀ ampicillin (μM) \pm SD (μM)	7.3 \pm 0.0	6.9 \pm 0.0	7.8 \pm 0.0	6.8 \pm 0.0

^aResults are a mean of two experiments.

Table S3. Lipophilic properties and ligand efficiency of select compounds.

Compound	Ligand Efficiency	LogP	Lipophilic efficiency
7	0.22	5.3	0
38	0.19	5.9	-0.6
46	0.21	5	0.35

Additional Figures

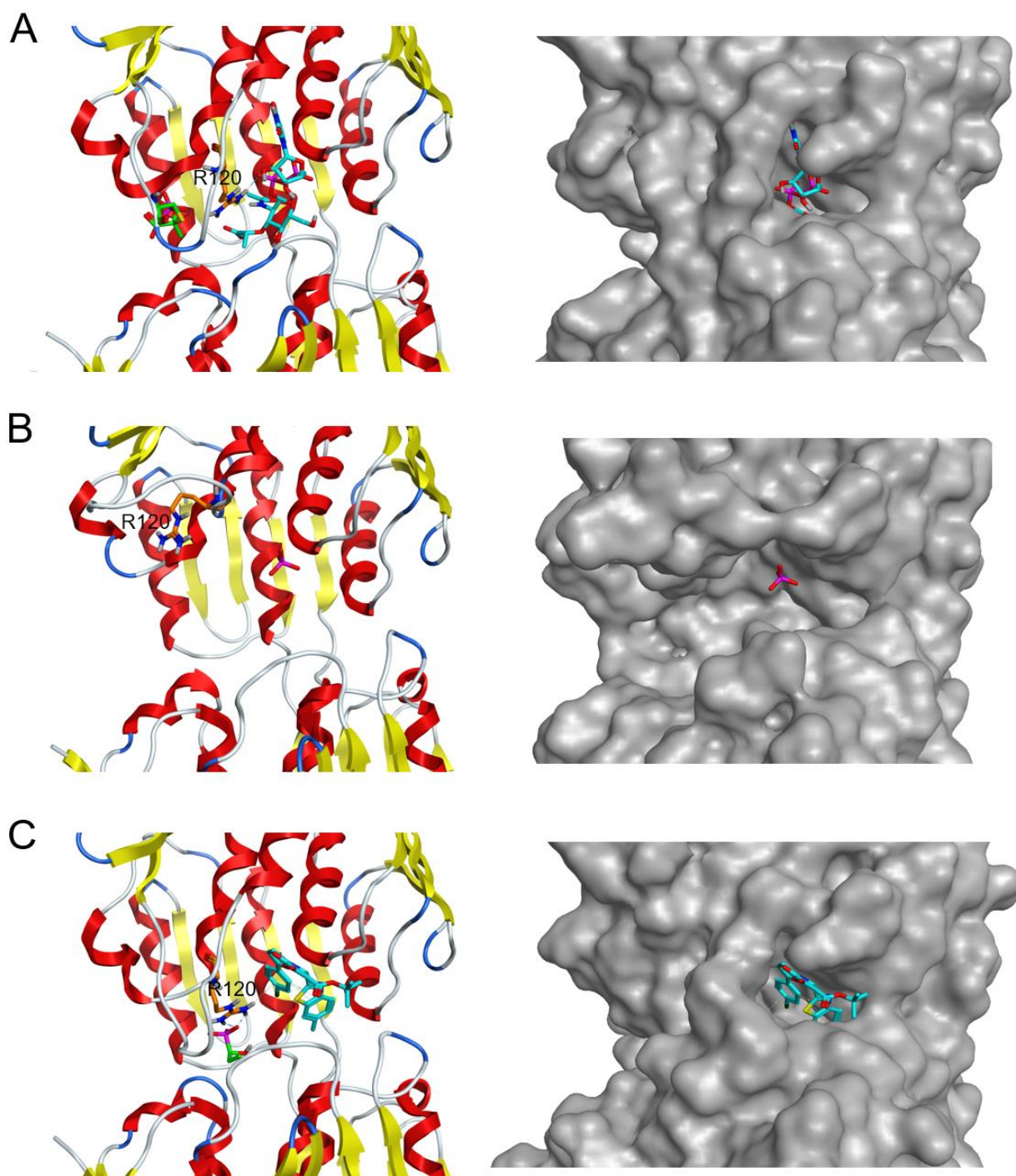
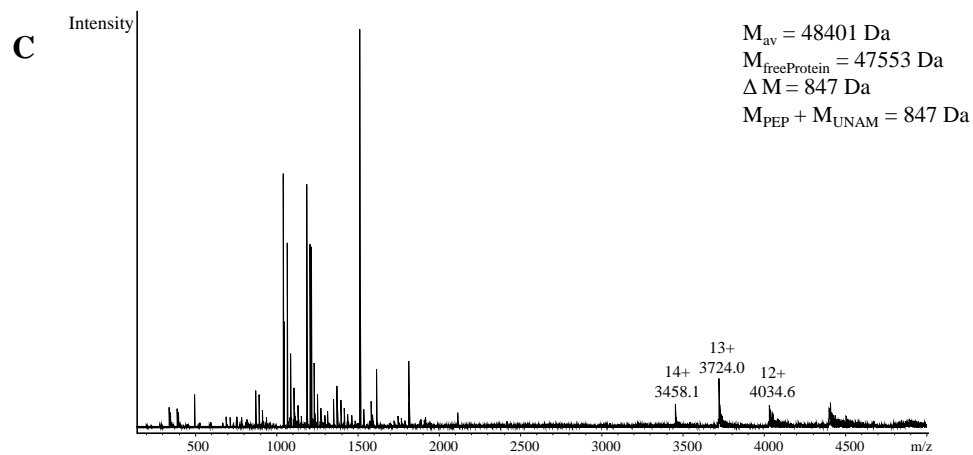
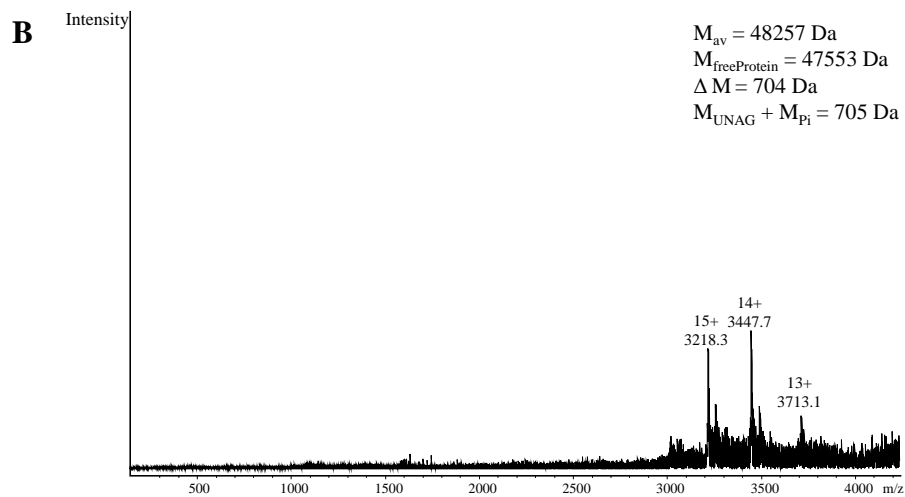
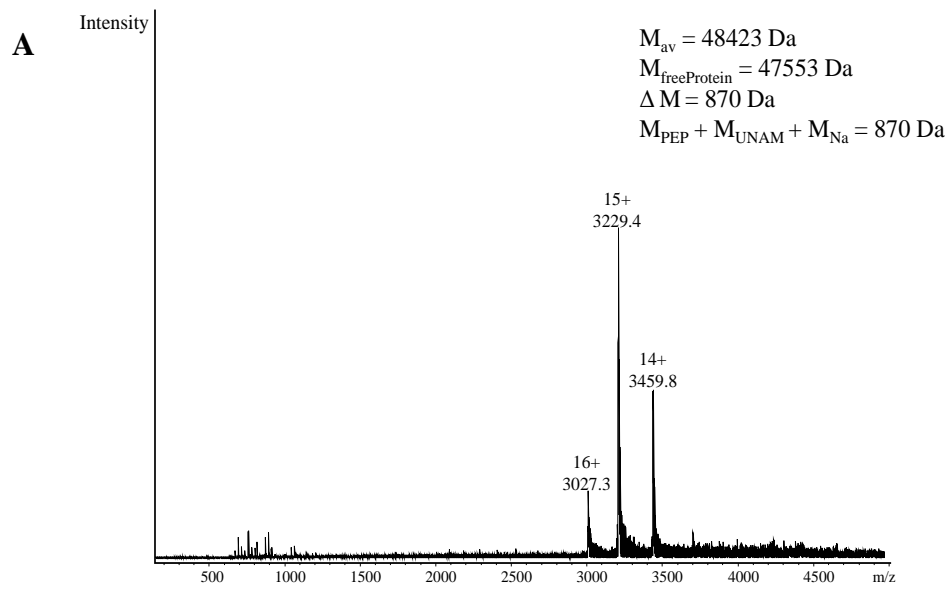


Figure S1. MurA in different ligand-dependent conformational states. **A.** Closed conformation with bound UNAM and PEP (PDB: 3SU9). **B.** Open conformation of the unliganded state (except one inorganic phosphate ion; PDB: 1EJD). **C.** Docking model of compound **46** (same model as in Figure 8, main part). Ligands are shown in cyan (UNAM and **46**), and the covalent phosphoenol pyruvate adduct on Cys115 is in green (not present in B). The essential active site loop residue Arg120 is colored in orange and labeled



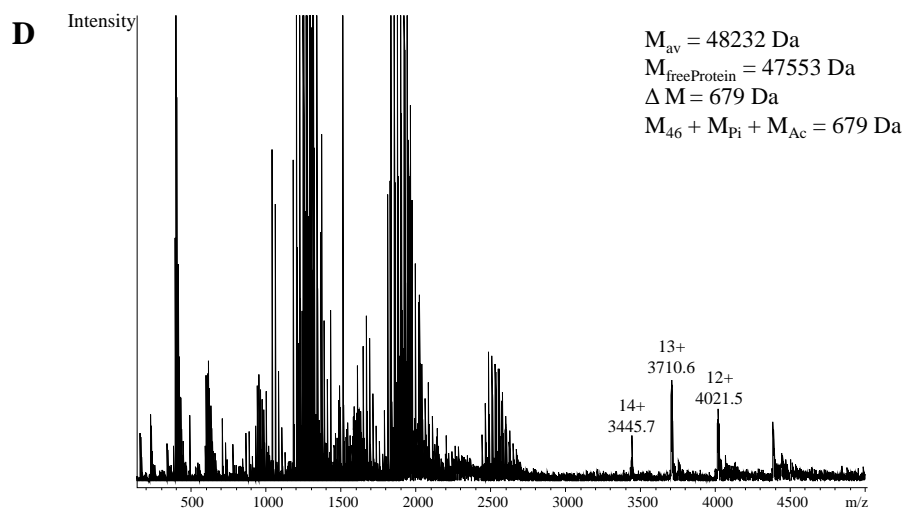


Figure S2. Native MS results of: **A.** MurA, **B.** MurA + UNAG, **C.** MurA + **46**, **D.** MurA + UNAG + **46**

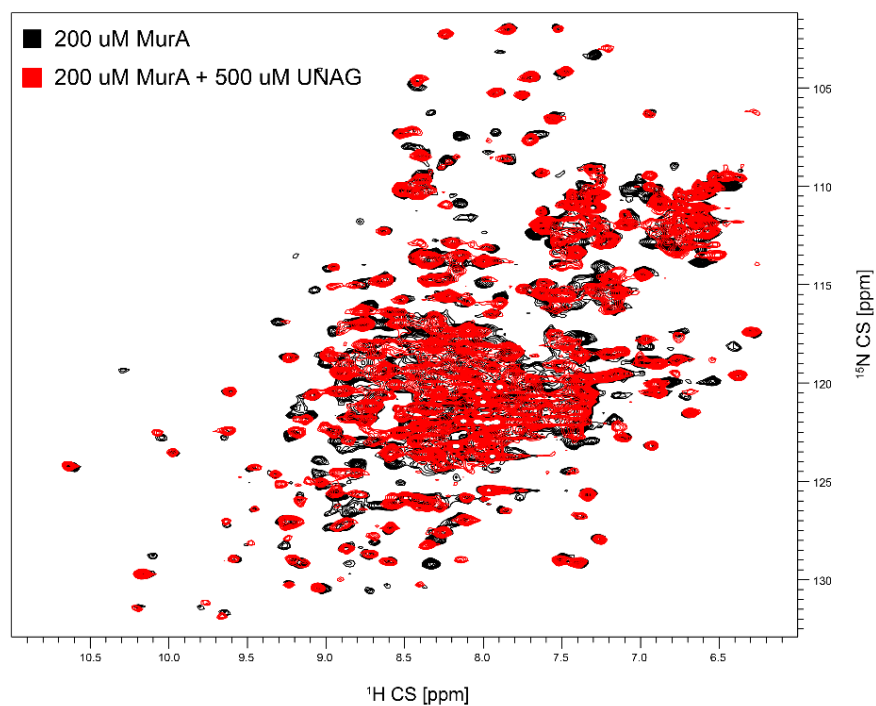


Figure S3. ^{15}N - ^1H TROSY HSQC spectra of wild-type (WT) MurA (black) overlaid with WT MurA in the presence of UNAG (red)

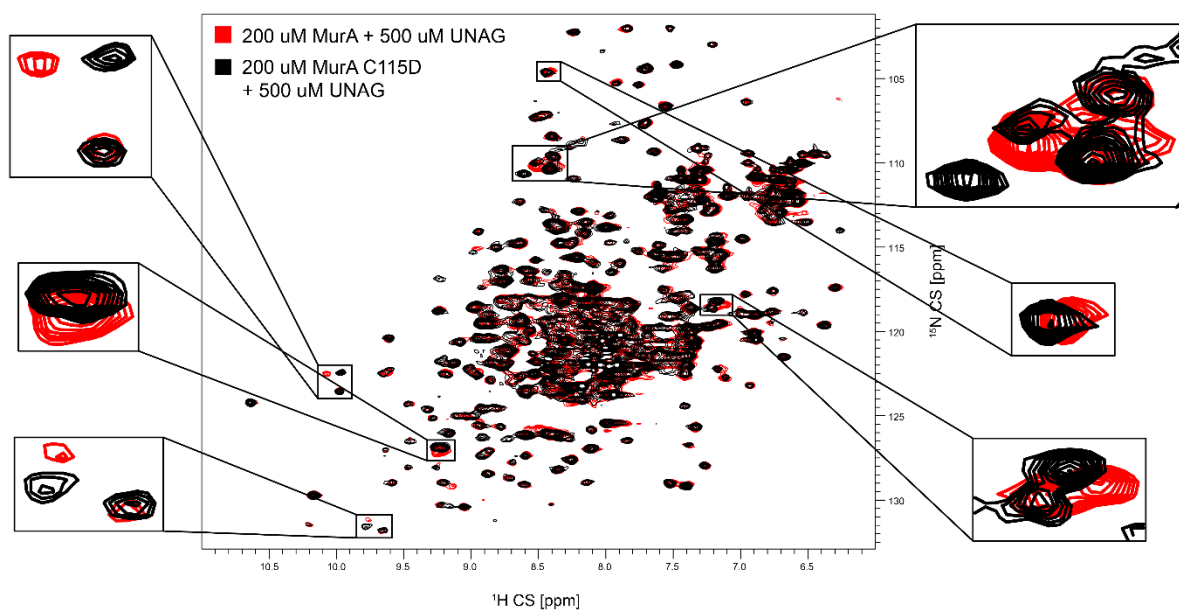


Figure S4. ^{15}N - ^1H TROSY HSQC spectra of WT MurA bound to UNAG (red) overlaid with C115D MurA bound to UNAG (black). Zoom in on selected regions highlights peaks that undergo chemical shift perturbations (CSPs)

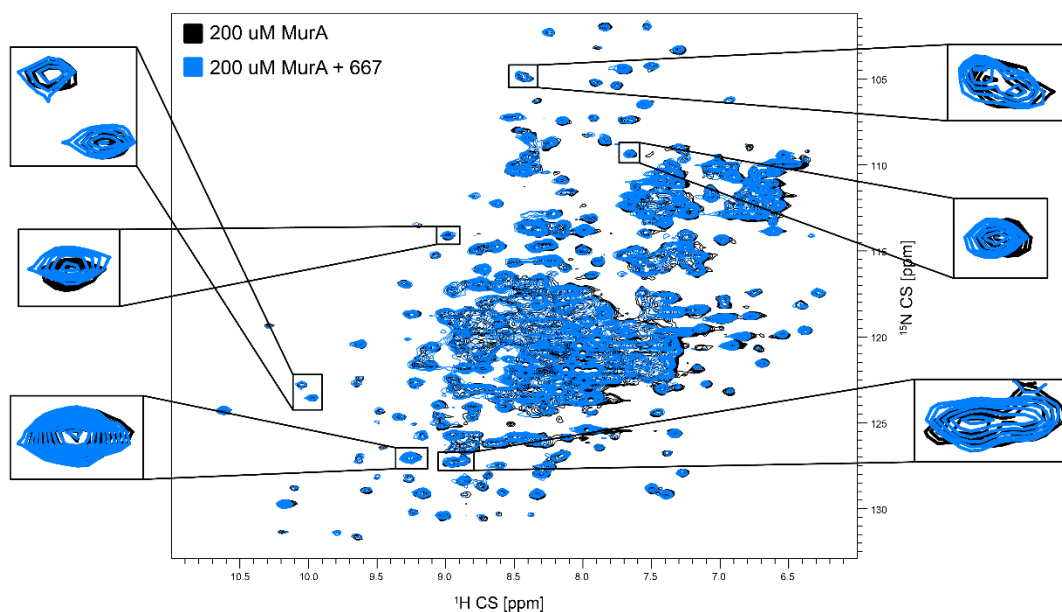


Figure S5. ^{15}N - ^1H TROSY HSQC spectra of WT MurA (black) overlaid with WT MurA in the presence of inhibitor **46** (blue). Zoom in on selected regions highlights key regions that show no chemical shift perturbations (CSPs)

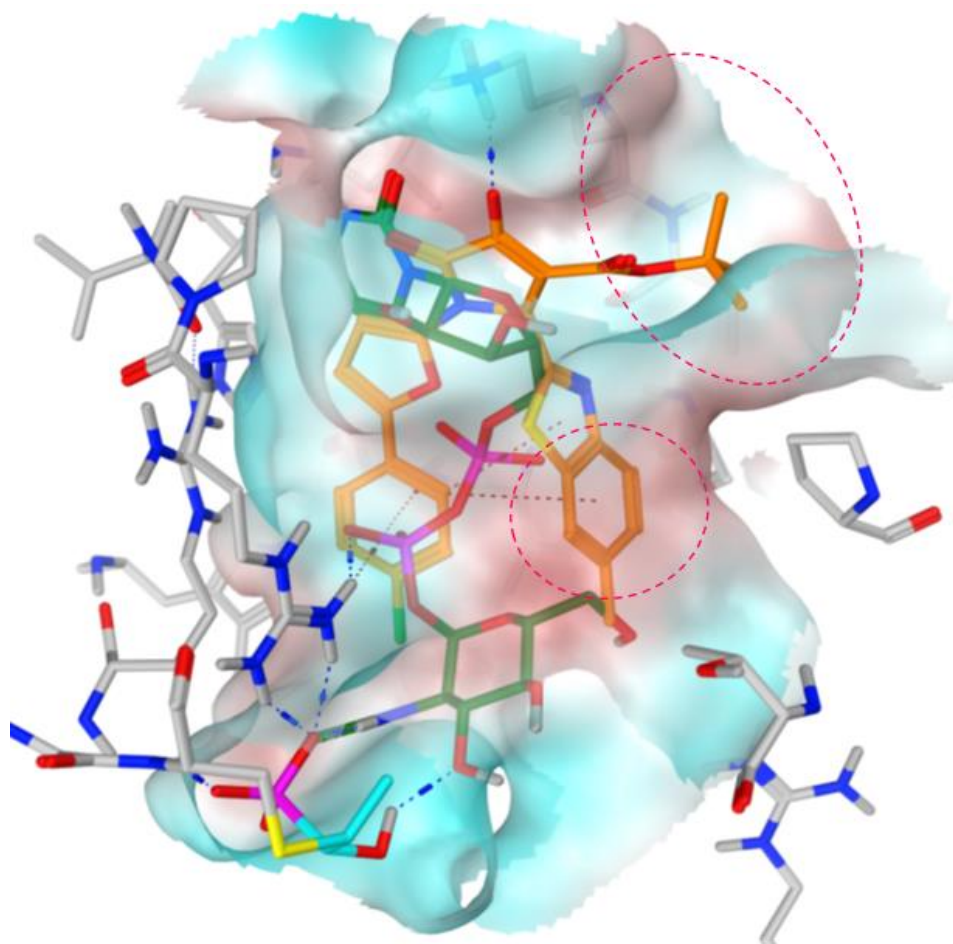


Figure S6. Superimposition of compound **46** in the predicted binding mode and UNAG in the X-ray co-crystal structure of UNAG and fosfomicin with MurA from *E. coli* (PDB code: 1UAE). The active site pocket is displayed as a transparent Connolly surface, with colors encoding hydrophilic (blue) and lipophilic (brown) areas. **46** and UNAG are shown in orange and dark green sticks for the hydrocarbon scaffold, respectively. The dashed pink ovals denote hydrophobic areas that are filled by the benzothiazole ring and the *tert*-butyl moiety, respectively, of compound **46**, but are occupied by water molecules in the complex with UNAG

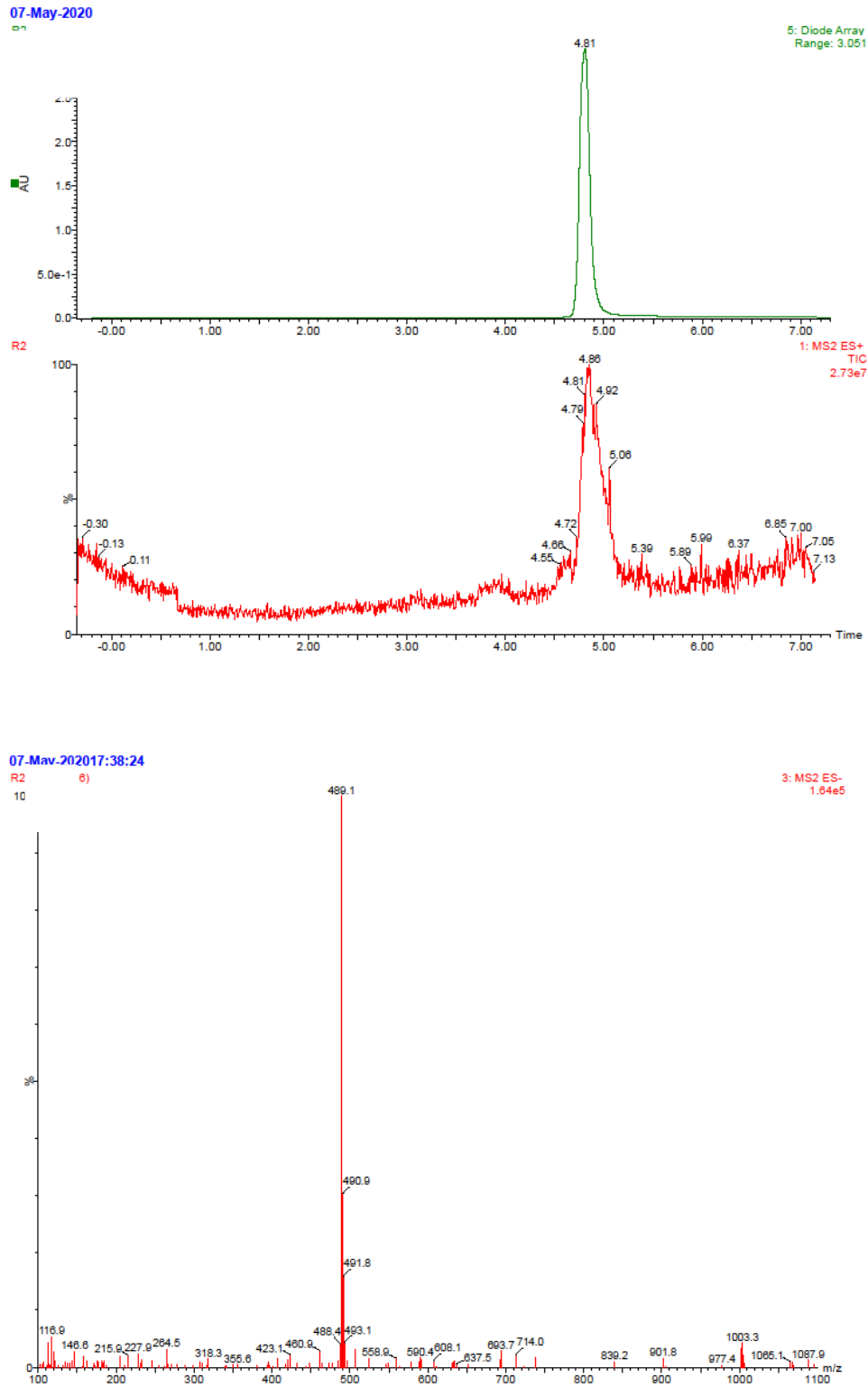


Figure S7. UPLC-MS chromatogram of 7

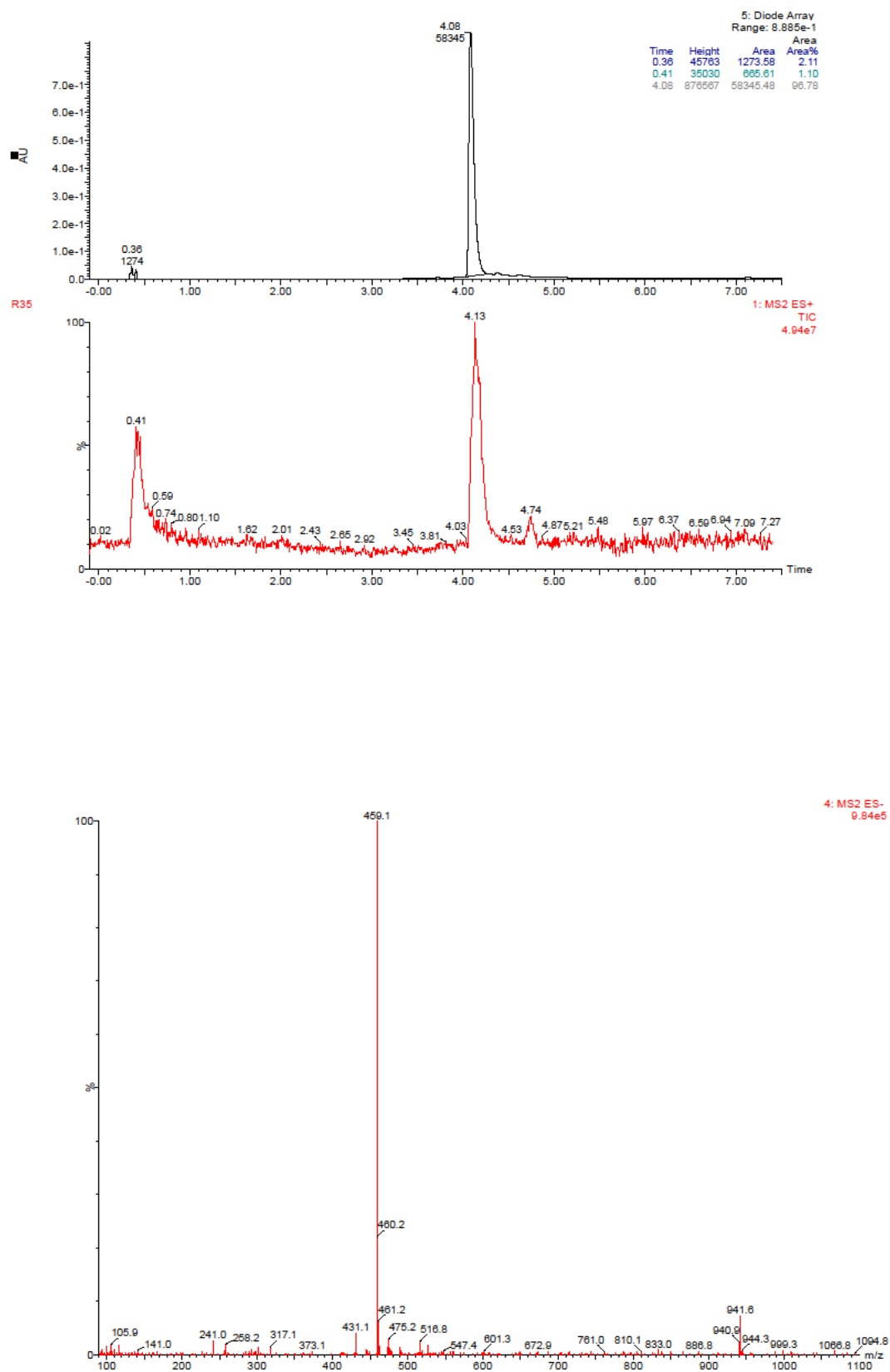
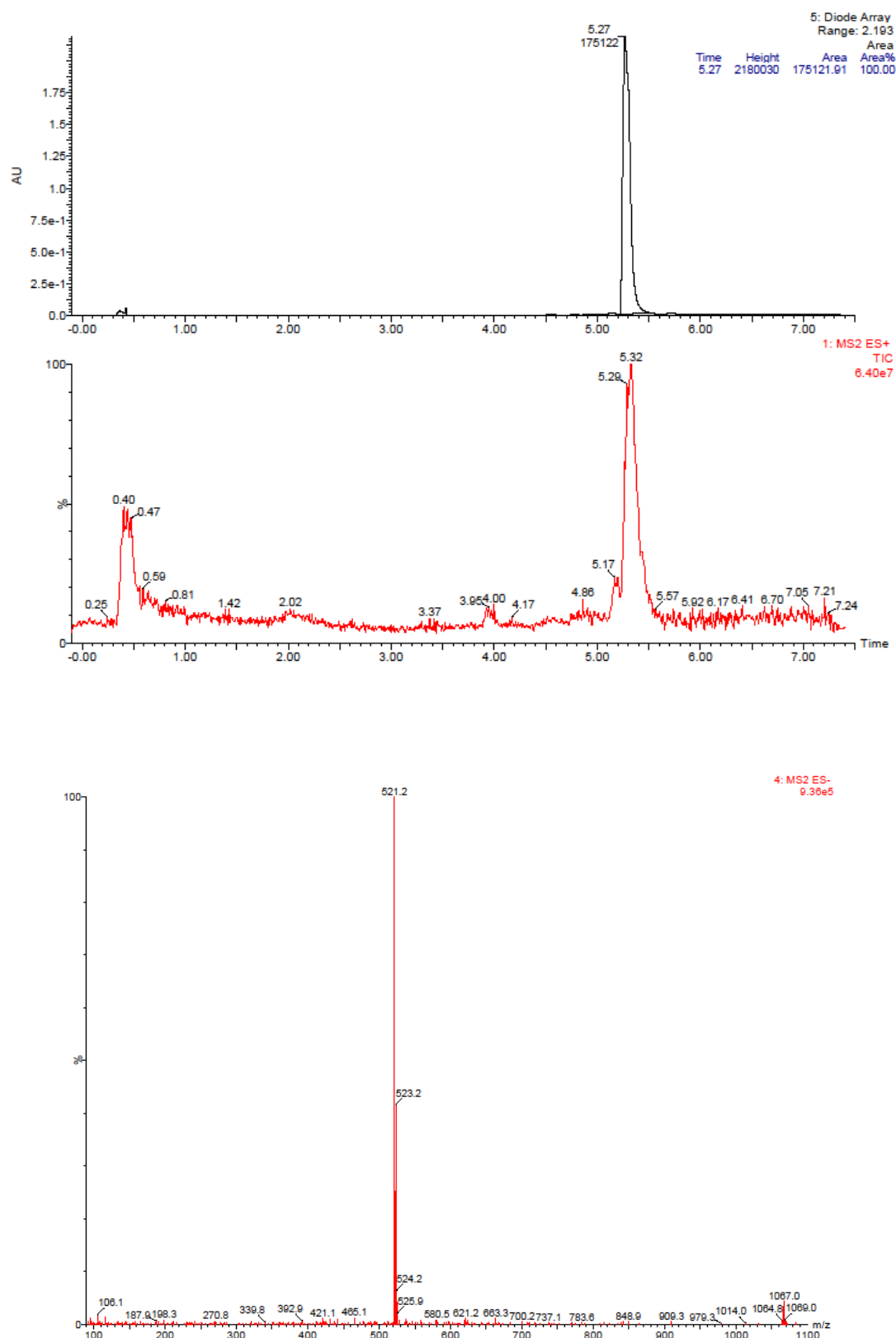
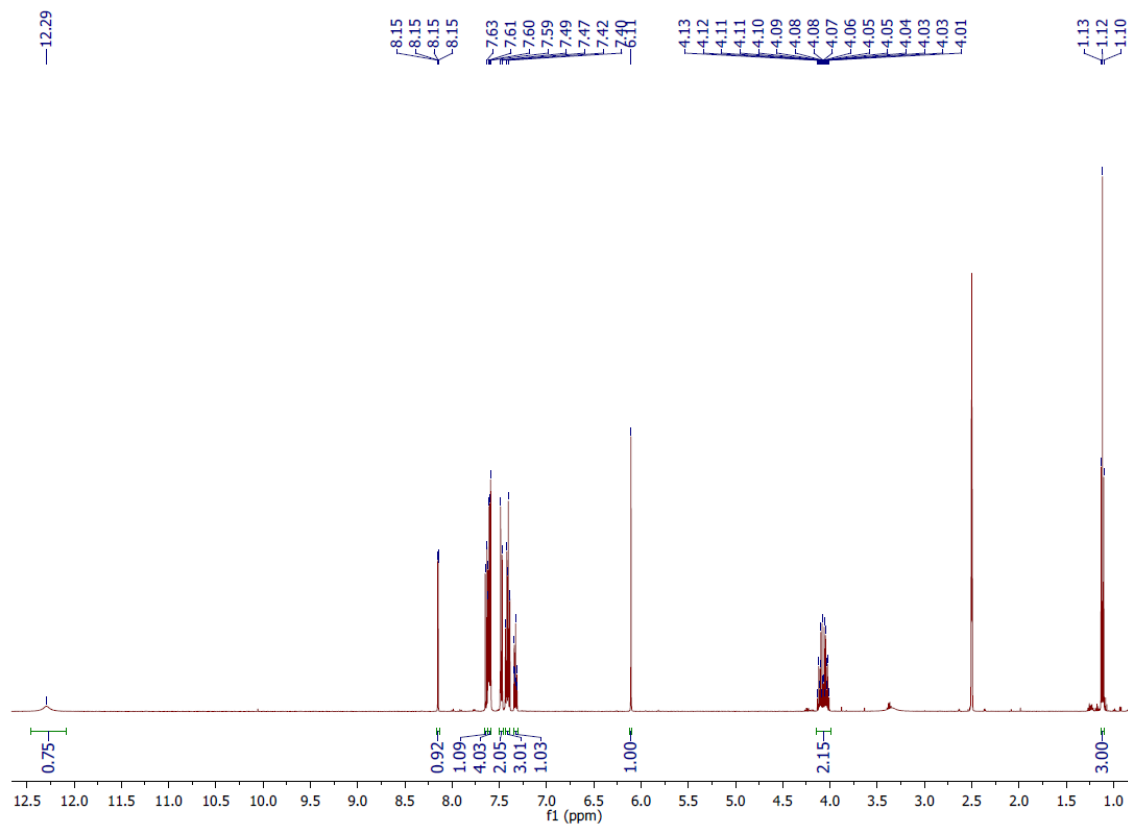
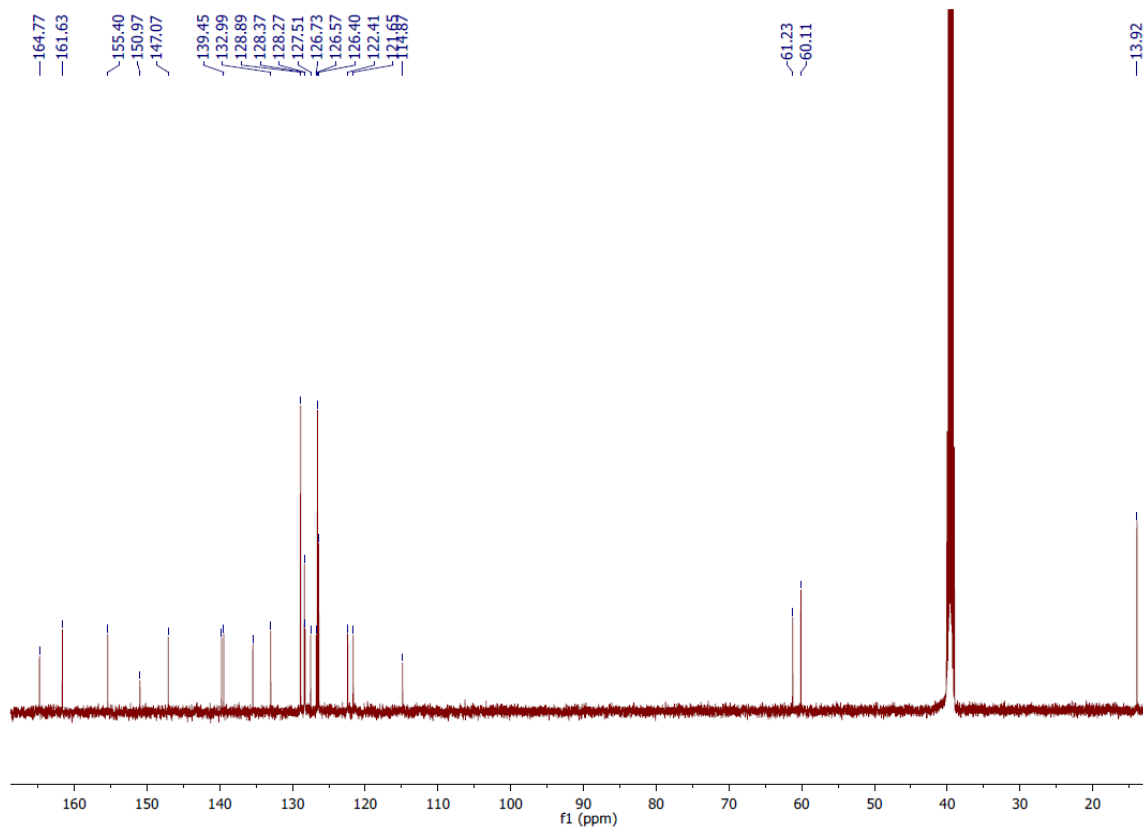
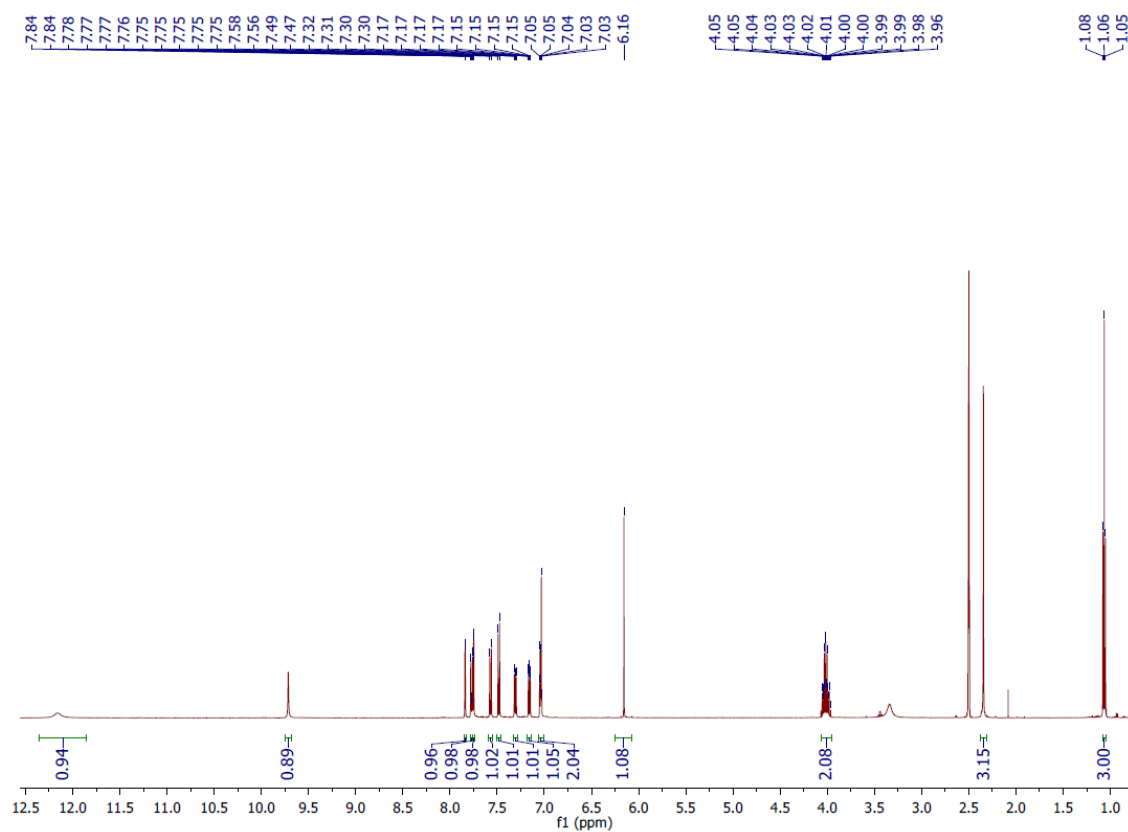
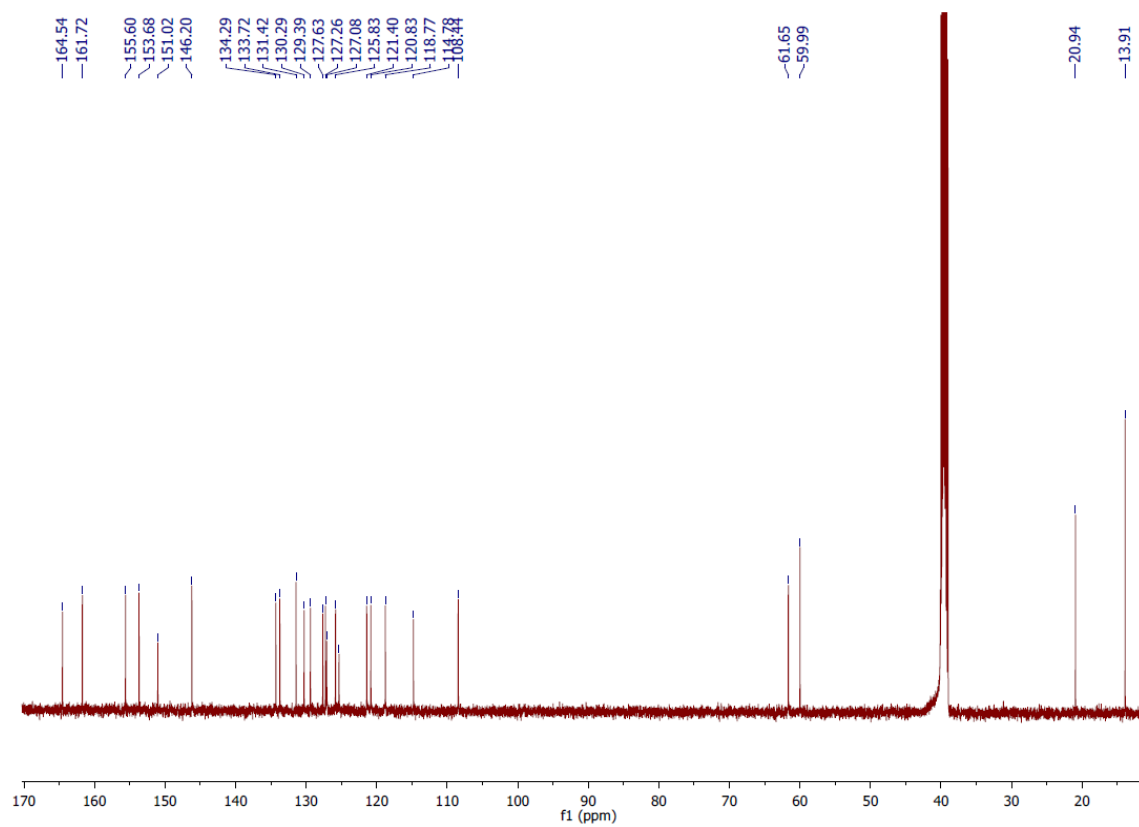


Figure S8. UPLC-MS chromatogram of 30

**Figure S9.** UPLC-MS chromatogram of 46

Figure S10. ^1H NMR spectrum of 7Figure S11. ^{13}C NMR spectrum of 7

**Figure S12.** ^1H NMR spectrum of **30****Figure S13.** ^{13}C NMR spectrum of **30**

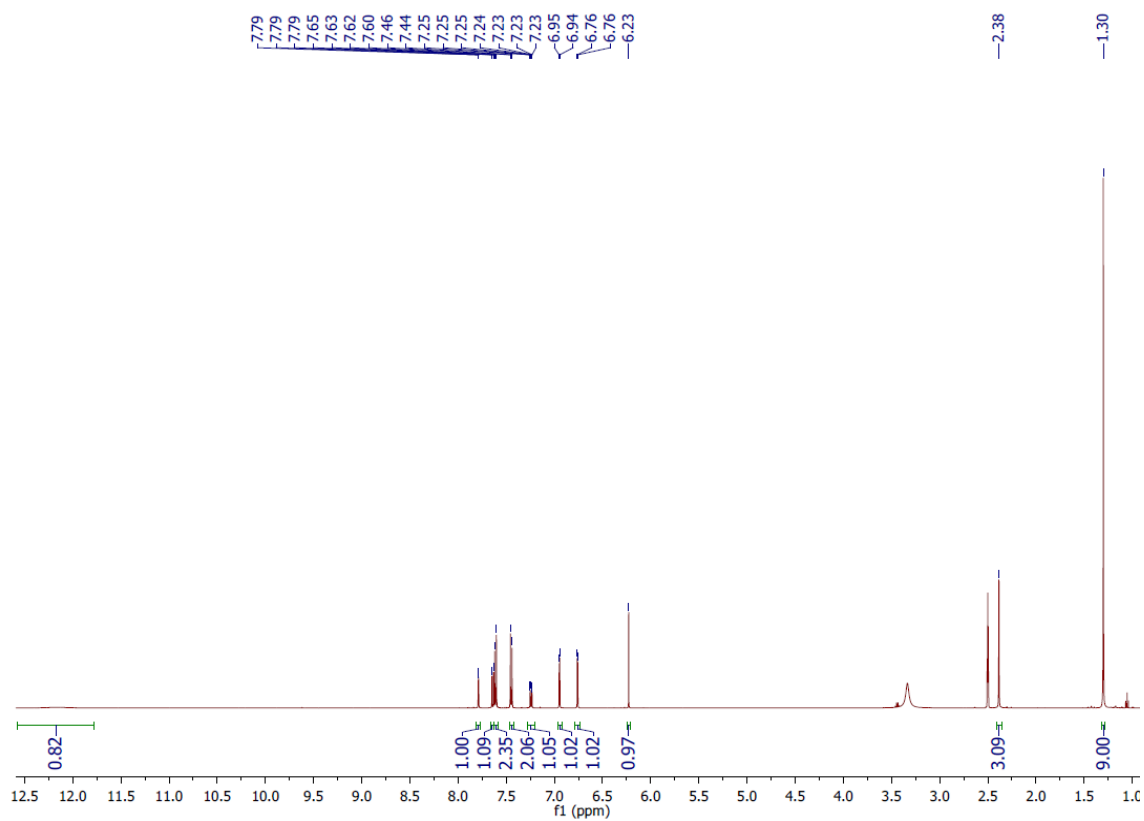


Figure S14. ¹H NMR spectrum of compound 46

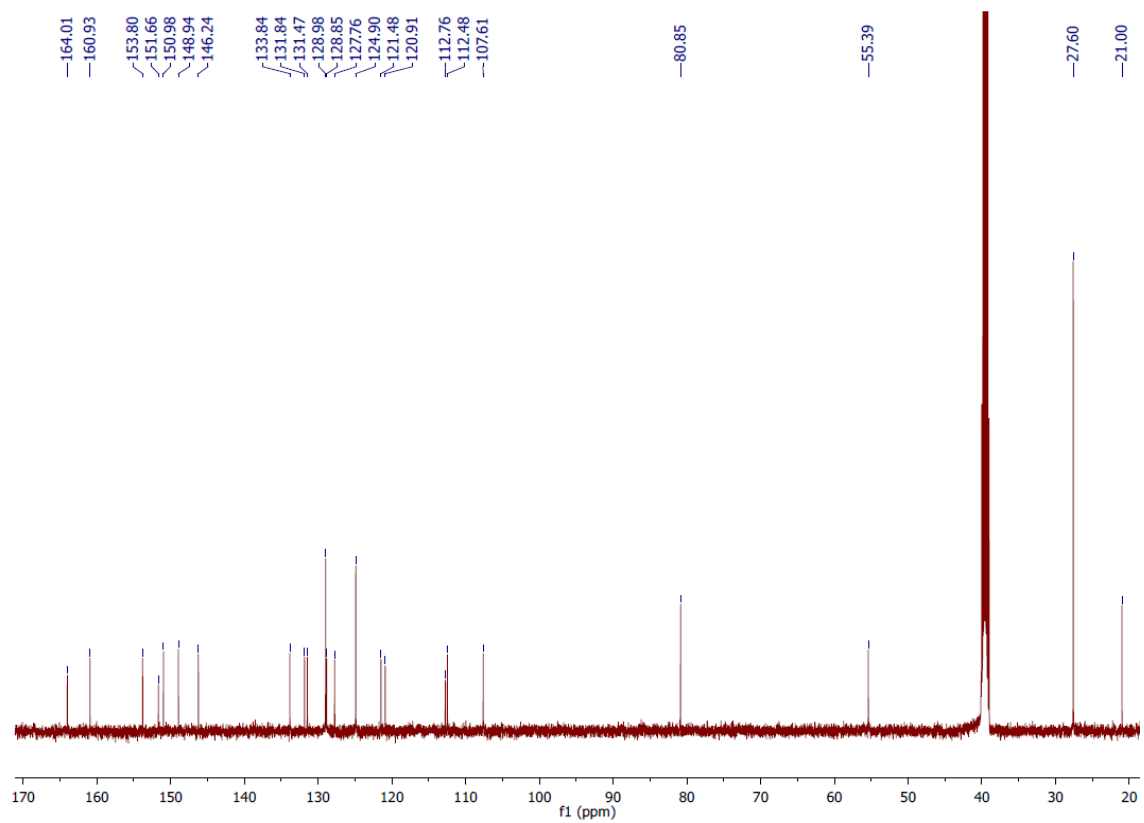


Figure S15. ¹³C NMR spectrum of compound 46

7.7 Supplementary Information for Chapter 3.4: Targeting the Binding Pocket of the Fluorescent Dye 8-Anilino-naphthalene-1-sulfonic acid (ANS) in MurA Holds Potential for the Development of Novel Antibacterial Agents

Additional Figures

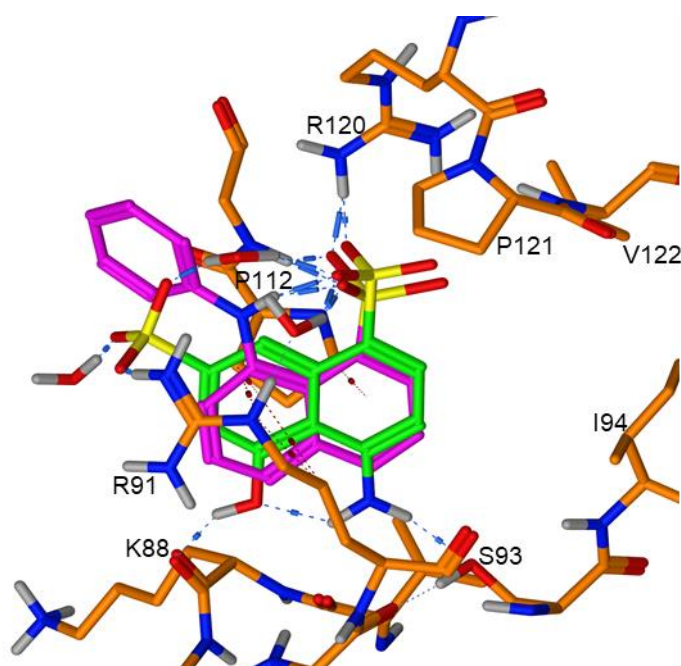
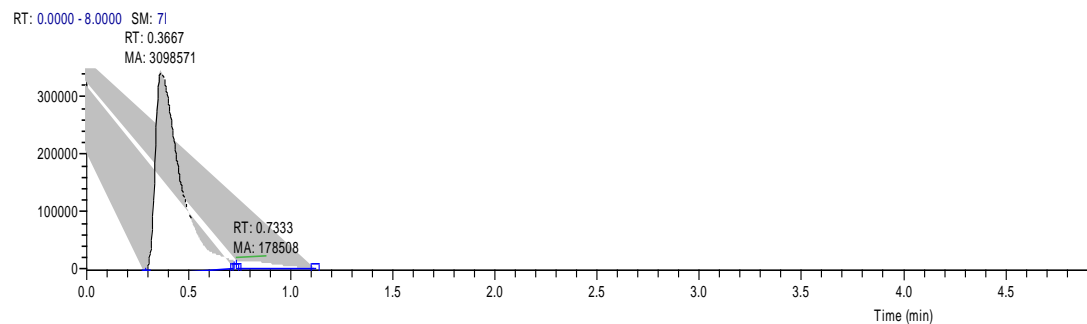


Figure S1. Predicted binding model of compound **26** (green sticks) in *E. cloacae* MurA, superimposed with the ANS molecule (magenta sticks) from the original cocrystal structure (PDB coordinates 1EYN). Residues of interacting side chains and of the adjacent hydrophobic cluster are labelled. Electrostatic interactions are indicated in blue and CH- π interactions in brown, the protein chain is coloured orange



RF_20220929_R_4iv #38-110 RT: 0.29-0.84 AV: 73 NL: 1.71E7
T: FTMS + c ESI Full ms [100.0000-1400.0000]

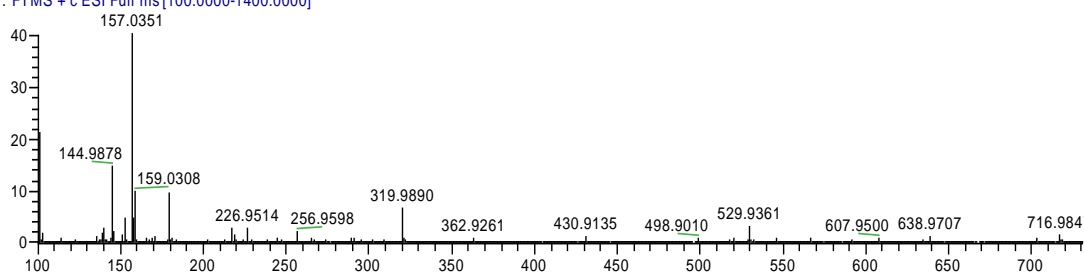
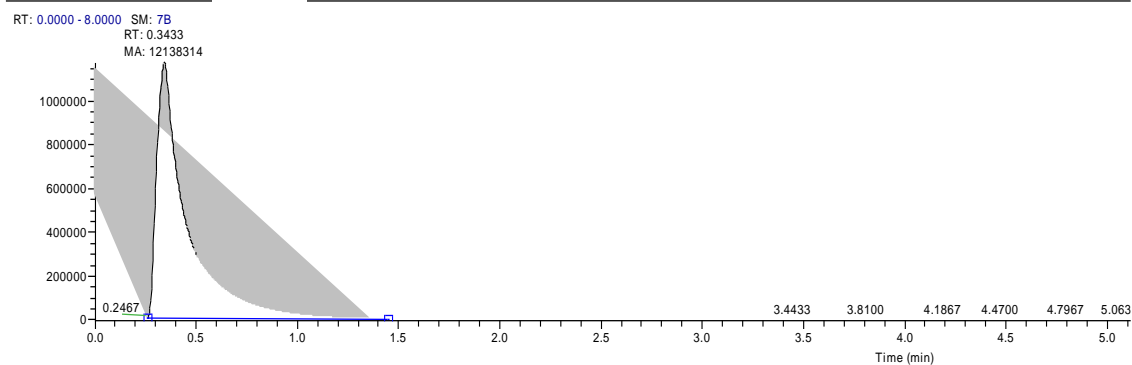


Fig. S2. LCMS analysis of compound **23**



RF_20220929_S #34-87 RT: 0.25-0.64 AV: 54 NL: 8.69E6
T: FTMS + c ESI Full ms [100.0000-1400.0000]

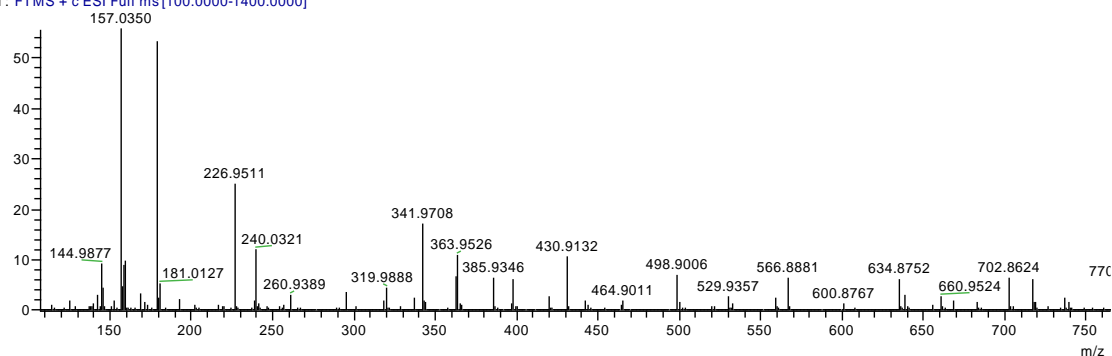
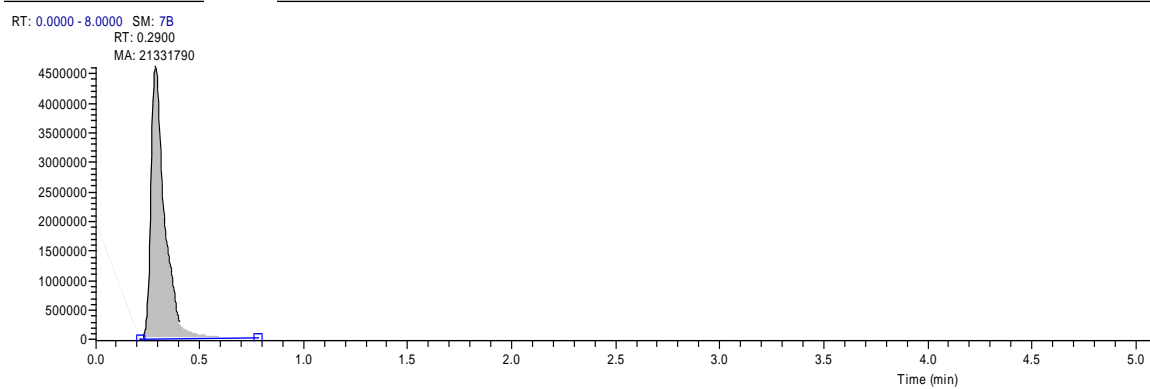


Fig. S3. LCMS analysis of compound **26**.



RF_20220929_V #51-184 RT: 0.24-0.84 AV: 134 NL: 2.63E7
T: FTMS - c ESI Full ms [133.4000-2000.0000]

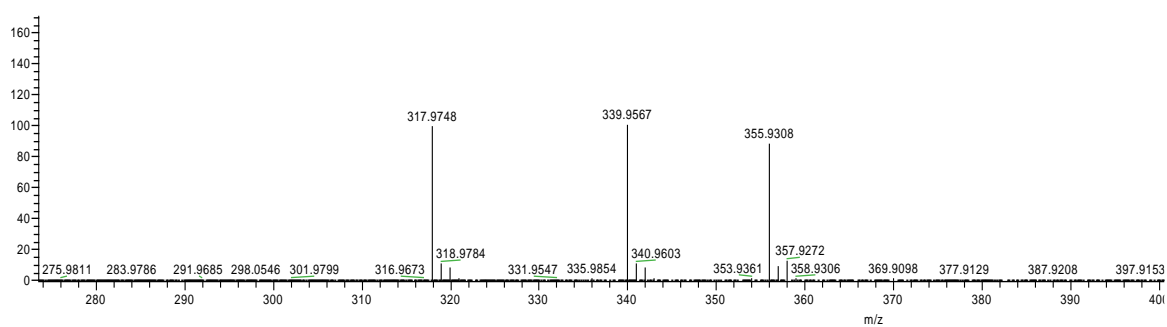


Fig. S4. LCMS analysis of compound **27**

CCATGGATAAAATTTTCGTGTGCAAGGCCCAACTCGTCTGCAGGGCGAAGTTACCAT
CTCTGGTGCGAAAACGCAGCACTGCCGATCCTGTTTCGCAGCACTGCTGGCTGAA
GAACCGGTGGAAATTCAGAACGTTCCGAAGCTGAAGGACATTGATACTACCATG
AAACTGCTGACCCAGCTGGGTACCAAAGTTGAACGTAACGGTTCGGTATGGATCG
ATGCTTCCAACGTTAACAACCTTCAGCGCGCCGTATGATCTGGTTAAAACGATGCG
TGCTTCTATTTGGGCGCTGGGTCCCTCTGGTTGCGCGTTCGGTCAGGGTCAAGTTA
GCCTGCCGGGTGGTTGTGCAATTGGTGC GCGTCCGGTAGATCTGCATATTTTCGG
CCTGGAAAACTGGGTGCGGAAATTAACCTGGAAGAGGGTTATGTAAAGGCCAG
CGTAAACGGTCGCCTGAAGGGTGCACATATCGTCATGGACAAAGTTTCTGTTGGT
GCAACTGTTACTATCATGTCCGCGGCTACCCTGGCAGAAGGCACCACTATCATCG
AAAACGCGGCGCGTGAACCGGAAATTGTGACACGGCCAACCTCCTGGTAGCGC
TGGGCGCAAAGATTAGCGGTCAAGGGTACTGATCGCATCACTATCGAAGGTGTTGA
ACGTCTGGGTGGCGGCGTTTACCGTGTACTGCCGGATCGTATTGAAACCGGTACT
TTCCTGGTTCGCGGCAGCGATCTCCGGTGGTAAGATTGTATGTCGTAACGCACAGC
CAGACACTCTGGATGCTGTTCTGGCAAACTGCGTGAAGCTGGTGCTGACATTGA
AACCGGTGAAGACTGGATTTCTCTGGATATGCACGGCAAACGCCCGAAAGCCGTT
ACCGTTCGTACTGCTCCGCATCCTGCTTCCCAACGGACATGCAGGCCCAATTTAC
CCTGCTGAACCTGGTCGCTGAAGGTACTGGTGTGATCACCGAAACCATCTTCGAA
AACCGTTTCATGCACGTCCCGGAACTGATCCGTATGGGTGCACACGCCGAAATCG
AAAGCAACACCGTGATCTGCCACGGTGTAGAAAACTGTCCGGTGCTCAGGTCAT
GGTACCGATCTGCGTGCGAGCGCTTCTCTGGTTCTGGCTGGTTGCATCGCGGAA
GGTACCACCGTTGTGATCGTATCTACCACATCGACCGCGGCTACGAACGCATCG
AAGACAACTGCGTGCTCTGGGTGCGAACATTGAACGTGTGAAAGGCGAAGGTC
ACCATCACCATCACCATTGAGCGGCCGC

Fig. S5. Sequence of the *E. cloacae* MurA insert in the ordered pEX-A258 vector. **NcoI** cutting site is in red and **NotI** cutting site is in blue

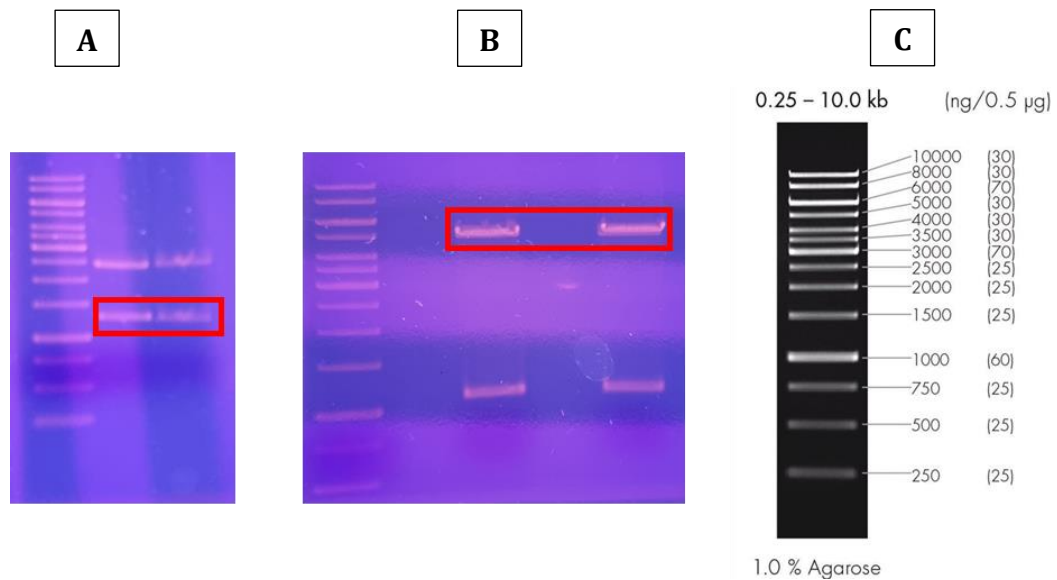


Fig. S6. A. agarose gel for the double digestion of the purchased pEX-A258 plasmid with the *E. cloacae* MurA insert (red box); B. agarose gel for the double digestion of the purchased pGEX-4T-1-3xMyc-ERK2-K52R containing the pGEX-4T-1 expression vector (in the red box); C. peqGOLD 1 kb DNA ladder

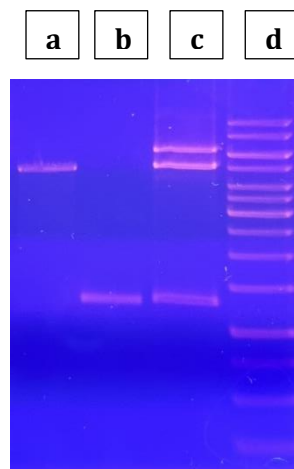


Fig. S7. Agarose gel with the bands from the left to right: a. pGEX-4T-1 expression vector (5050 bp); b. *E. cloacae* MurA insert (1291 bp), c. double digested plasmid from the transformed C41 cells containing the correct bands for both the insert and the vector (top band is the undigested plasmid); d. peqGOLD 1 kb DNA ladder

Additional Tables**Table S1.** CAS number of all the purchased compounds.

Compound	CAS number
ANS	82-76-8
1	98-11-3
2	120-18-3
3	86-87-3
4	86-87-3
5	90-15-3
6	135-19-3
7	575-44-0
8	575-38-2
9	582-17-2
10	81-16-3
11	84-89-9
12	81-05-0
13	82-75-7
14	119-79-9
15	117-59-9
16	117-22-6
17	116-63-2
18	52084-84-1
19	32018-88-5
20	6251-07-6
21	92-28-4
22	330581-20-9
23	90-20-0
24	7153-21-1
25	148-25-4
26	130-23-4
27	6535-70-2

Table S2: Ligand efficiency of some select compounds.

Compound	Ligand efficiency
ANS	0.32
11	0.5
23	0.36
26	0.39
27	0.35

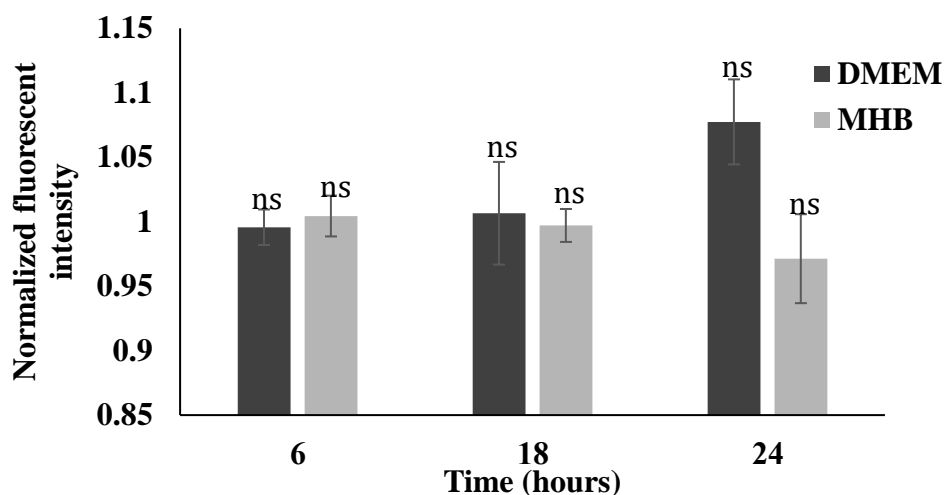
7.8 Supplementary information for Chapter 3.5: Nanoparticle Fraught Liposomes: A Platform for Increased Antibiotic Selectivity in Multidrug Resistant Bacteria

Supplementary information for this article can be found under:

<https://doi.org/10.1021/acs.molpharmaceut.2c00258>

Investigation of R123 release for 24 hours

To investigate the dye release, R123-NP-Lip were formulated and centrifuged at 10752 rcf at 10°C for 10 minutes to remove any unencapsulated dye or NPs. R123-NP-Lip were then either suspended in DMEM (Dulbecco's Modified Eagle Medium) or MHB (Müller-Hinton broth) (160 µg/ml final concentration in terms of PLGA) and incubated at 37 °C. At predetermined time points (0, 6, 18, and 24 hours) R123-NP-Lip were centrifuged and fluorescence intensity of supernatant was measured at 485/535 nm. The results were expressed as mean fluorescence intensity ± standard deviation (SD) recorded at each time point after normalization to fluorescence intensity recorded at 0 hours.



Supplementary Figure 1: Assessment of R123 release from NP-Lip in DMEM and MHB.

Results are expressed as mean fluorescence intensity relative to control (zero time).

Statistical analysis was performed by GraphPad-InStat software using one-way ANOVA, where $P > 0.05$ is considered not significant

Selection of Centrifugation Speed for Separation of NP-Lip

Regarding the incorporation of NPs in Lip, to validate that the centrifugation speed selected did not result in the precipitation of unencapsulated NPs and that centrifugation only resulted in the precipitation of the NPs encapsulated in liposomes. R123-NPs were centrifuged at 10752 rcf for 10 minutes. The concentration of NPs in the supernatant was determined by fluorometry at the excitation/emission wavelength λ at 485/535 nm and then compared to the concentration of the whole batch of the NPs before the centrifugation.

Supplementary Table 1 shows, there is no change in the readings pre- and post-centrifugation which means that NPs could not form a pellet under these conditions of centrifugation and that centrifugation at this speed and duration would only result in the precipitation of the NPs encapsulated in liposomes.

For calibration, serial dilution of R123-NPs (0.0004, 0.002, 0.004, and 0.04) mg/ml in terms of PLGA concentration were prepared.

Supplementary Table 1: Fluorescence intensity of R123-NPs pre- and post-centrifugation at 10752 rcf for 10 minutes.

Applied conditions	Formulation name	Fluorescence intensity \pm SD
Pre centrifugation	The whole batch of R123-NPs	51014 \pm 412
Post centrifugation	Supernatant of R123-NPs	51454 \pm 514

Quantification of Erythromycin (Er) and 3c by UPLC-MS/MS

A newly developed UPLC-MS/MS method was validated according to ICH guidelines in terms of; specificity, linearity, limit of detection (LOD), limit of quantification (LOQ), precision (inter- and intra-day) and accuracy. Limit of Detection (LOD) was determined as the concentration of the sample giving a response three times the baseline noise. Limit of Quantitation (LOQ) was calculated as the concentration of sample giving a signal ten times the baseline noise. The intra-day precision was determined within one day by analyzing triplicates of calibration curve samples. The inter-day precision was determined on three consecutive days at the same concentrations. Accuracy was determined by injecting four different concentrations from Er (0.05, 0.1, 0.5, and 2 $\mu\text{g/ml}$) and three different concentrations from **3c** (0.01, 0.04, and 0.4 $\mu\text{g/ml}$), the accuracy of the method was defined as the absolute value of the ratio of the mean found values of the measured samples to their theoretical values, expressed as percentages. The criteria for acceptability of the data included precision within $\pm 15\%$ (RSD) and accuracy within $\pm 15\%$ deviation (85–115 %) from the nominal. For Er loaded NPs, the calibration curve was constructed by primarily dissolving Er in DMSO (20 mg/ml). Serial dilutions of Er were prepared by diluting

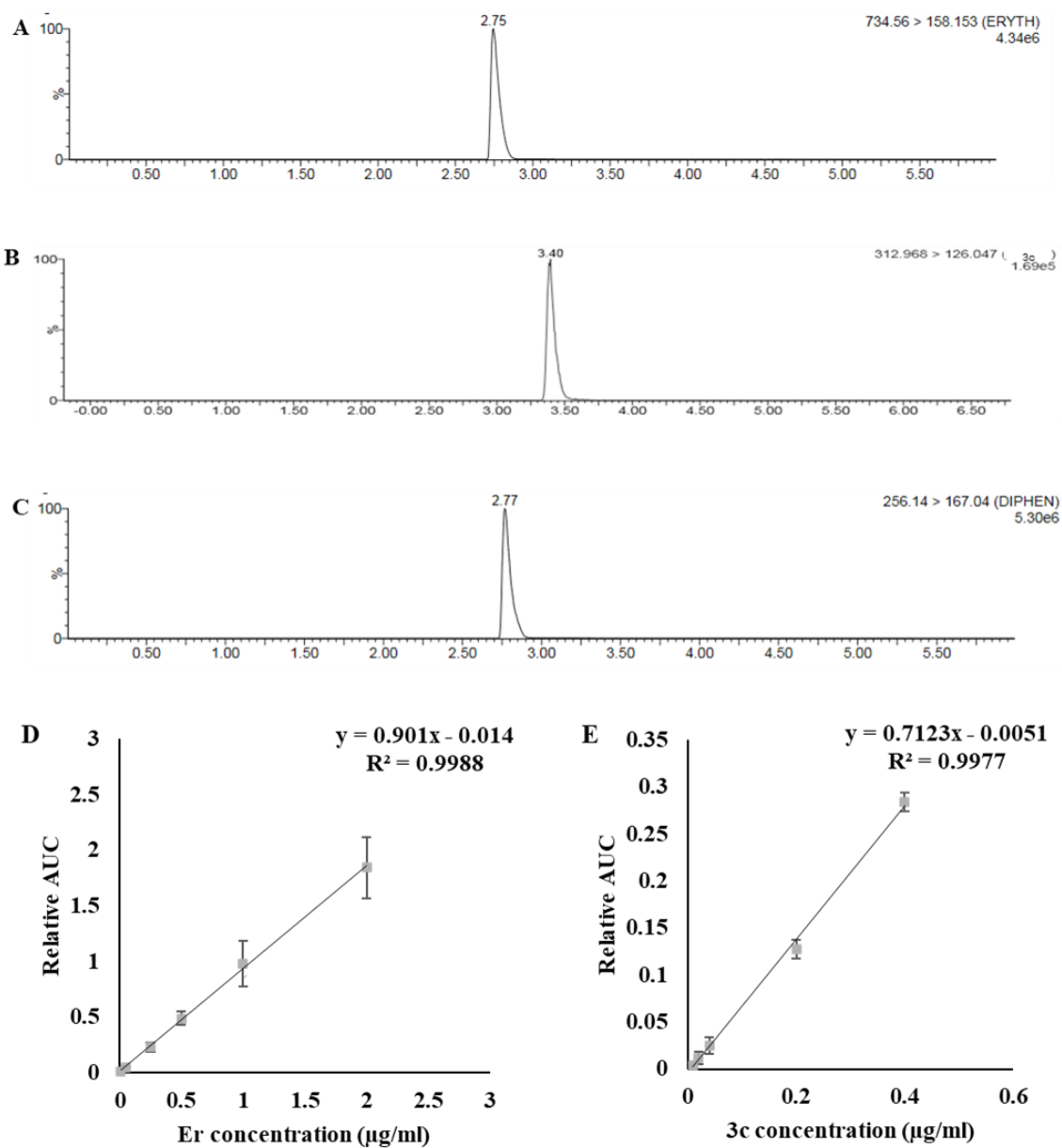
the Er stock solution with unloaded NPs flow-through obtained following NPs centrifugation in the 10 KD centricons to yield a final Er concentration of 0.01, 0.05, 0.1, 0.25, 0.5, 1, and 2 µg/ml. Similarly, a calibration curve of **3c** was also constructed. However, for **3c** the stock solution was prepared in a 50 % v/v ethanolic solution (2 mg/ml). The calibration curve concentrations were 0.01, 0.02, 0.04, 0.2, and 0.4 µg/ml. Three independent Er -NPs and **3c**-NPs batches were prepared. Final drug concentration per batch of NPs corresponded to 1 mg/ml for Er and 0.25 mg/ml for **3c**. NPs were centrifuged in centrifugal filter units as detailed in section 1 then the NPs flow-through was diluted to fit the range of the calibration curve and used to quantify the excess unencapsulated drug by LC-MS/MS. The concentration of unencapsulated drug was used to determine the encapsulated portion.

Quantification was conducted using multiple reaction monitoring (MRM) of the transitions of m/z 734.55>158.15 with collision energy of 32V for Er as shown in *Supplementary Supplementary Figure 2A*, 312.96>126.04 with collision energy of 18V for **3c** as shown *Supplementary Supplementary Figure 2B*, and m/z 256.14>167.04 with collision energy of 10V for diphenhydramine as shown in *Supplementary Supplementary Figure 2C*, respectively. The response of each calibration curve sample (y) was plotted against its concentration (x). All curves show linearity in the range of prepared concentrations. For Er-NPs, the linear correlation equation obtained was $y = 0.901x - 0.014$ with $R^2 = 0.9988$ while for **3c**-NPs, the linear correlation equation obtained was $y = 0.7123x - 0.0051$ with $R^2 = 0.9977$. The LOD was found to be 0.1 ng/ml and the LOQ was 0.33 ng/ml for Er. While for **3c** the LOD was found to be 2.2 ng/ml and the LOQ was 7.3 ng/ml. The intra-day repeatability evaluated as % RSD ranged from 2.6% to 6.9% for Er and from 1.1% to 5.1% for **3c**. The inter-day reproducibility, the % RSD ranged from 0.9% to 7.8% for Er and from 3.5% to 9.2%

for **3c**. For evaluation of the accuracy, four different samples were measured from Er and three different samples from **3c**, the % recovery ranged from 90.4% to 102.9% for Er and from 94.6% to 100.5% for **3c**. All calibration curves prepared for Er and **3c** were shown in *Supplementary Figure 2D and E*.

To confirm that there is no interaction between the drug and the filter membrane, 100 µg/ml of Er were dissolved in water then centrifuged at room temperature using 10 kDa Amicon® ultra-4 centrifugal filter units at 32928 rcf for 30 minutes followed by quantifying the flow-through using an in-house developed ultra-high performance liquid chromatography-tandem mass spectrometer (UHPLC-MS/MS) method using diphenhydramine as internal standard.

The results showed that the filtration step using the filter units did not affect the original concentration of Er. Concentration of Er in the flow-through was 101.12 ±2.58 µg/ml.



Supplementary Figure 2: UPLC-MS/MS chromatogram of (A) Er, (B) 3c, and (C) diphenhydramine in the MRM mode & calibration curve of (D) Er-NPs, and (E) 3c-NPs

Concentrations of Drugs, NPs and NP-Lip Used in Cytotoxicity Studies

Supplementary Table 2: Concentrations used in HEK293 viability studies

Formulation tested	Expression in terms of component concentration	Final concentration ($\mu\text{g/ml}$)								
Unloaded NPs	PLGA	10	50	100	300	700	1000	-	-	-
Unloaded NP-Lip	PLGA	10	50	100	300	700	1000	2000	4000	-
Er-NPs	PLGA	10	50	100	200	400	800	-	-	-
	Er	12.5	62.5	125	250	500	1000	-	-	-
3c-NPs	PLGA	50	250	500	-	-	-	-	-	-
	3c	12.5	62.5	125	-	-	-	-	-	-
Er- NP-Lip	PLGA	10	50	100	200	400	800	1200	1600	2400
	Er	12.5	62.5	125	250	500	1000	1500	2000	3000
3c-NP-Lip	PLGA	50	250	500	1000	2000	4000	-	-	-
	3c	12.5	62.5	125	250	500	1000	-	-	-
Free Er	Er	12.5	62.5	125	250	500	1000	1500	2000	-
Free Er + unloaded NP-Lip	PLGA	10	50	100	200	400	800	-	-	-
	Er	12.5	62.5	125	250	500	1000	-	-	-

Supplementary Table 3: Concentrations used in bacterial viability studies

Formulation tested	Expression in terms of component concentration	Final concentration ($\mu\text{g/ml}$)								
		2.5	5	10	20	40	200	400	800	2000
Unloaded NP-Lip	PLGA	2.5	5	10	20	40	200	400	800	2000
	Er	3.125	6.25	12.5	25	50	250	500	1000	2500
	3c	0.625	1.25	2.5	5	10	50	100	200	500
Er-NP-Lip	PLGA	2	4	8	40	80	160	400	-	-
	Er	2.5	5	10	50	100	200	500	-	-
3c-NP-Lip	PLGA	2.5	5	10	20	40	200	400	800	2000
	3c	0.625	1.25	2.5	5	10	50	100	200	500
Free Er	Er	2.5	5	10	50	100	200	500	-	-
Free 3c	3c	0.625	1.25	2.5	5	10	20	30	-	-

Formulation of Liposomes by Thin-film Hydration

Liposomes were initially formulated using thin film hydration method[1]. LEC and CHOL were dissolved in chloroform after which the chloroform was evaporated under vacuum at 40 °C for 20 minutes. The hydration of lipids was performed by adding 5 ml of ultra-pure water at 40 °C to the flask containing the lipid film. After hydration, the batch was sonicated for 10 minutes in a water bath sonicator. The obtained liposomes showed a HD of 201 \pm 10 nm and a ZP of -41 \pm 1 mV.

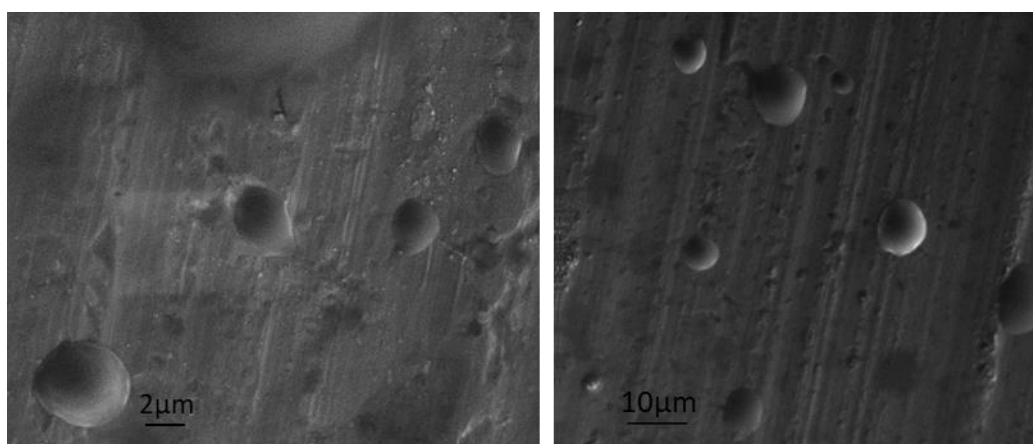
Formulation of NPs Loaded Liposomes

Supplementary Table 4: NPs incorporated into liposomes by thin-film hydration

NP type	NP size	Liposome size	References
Maghemite NPs	17 \pm 3 nm	100-250 nm	[2]
PLGA NPs	342.3 \pm 12.4 nm	363.6 \pm 4.5 nm	[3]
Alendronate-grafted maghemite nanocrystals	10 nm	139 nm	[4]

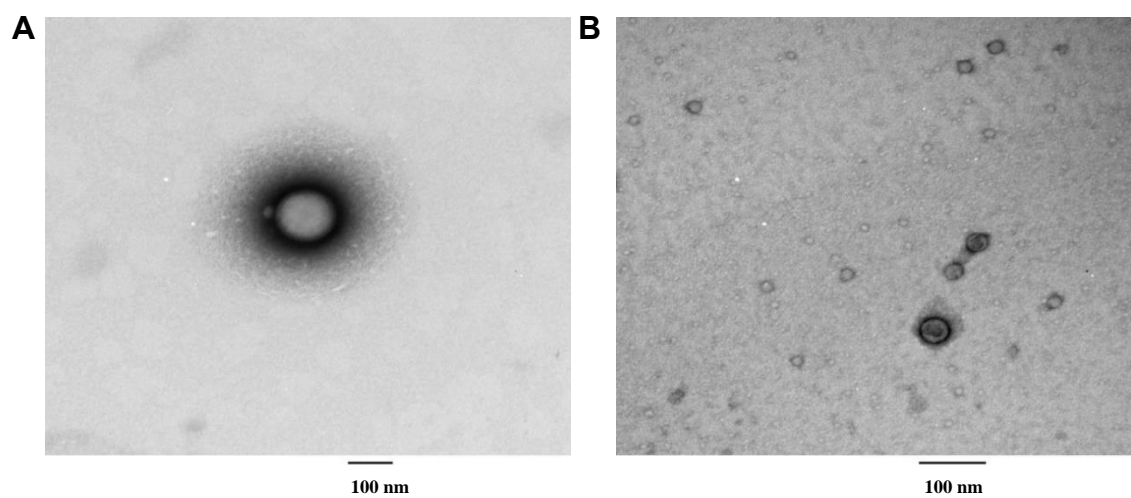
Polar surfactant-coated magnetite nanocrystals	10 nm	100-130 nm	[5]
Citrate-stabilized magnetite nanocrystals	12-15 nm	227 ± 75 nm	[6]
Phospholipid-stabilized magnetite nanocrystals	6-20 nm	100-400 nm	[7]

Investigation of NP-Lip Morphology by Scanning Electron Microscopy (SEM)



Supplementary Figure S3: SEM image of NP-Lip

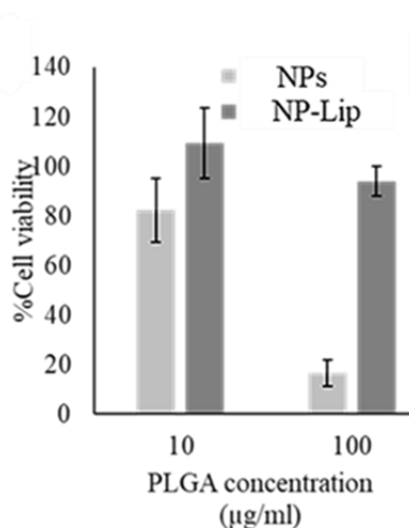
TEM Images of Drug Loaded NPs



Supplementary Figure S4: TEM images of (A) Er - NPs & (B) 3c-NPs

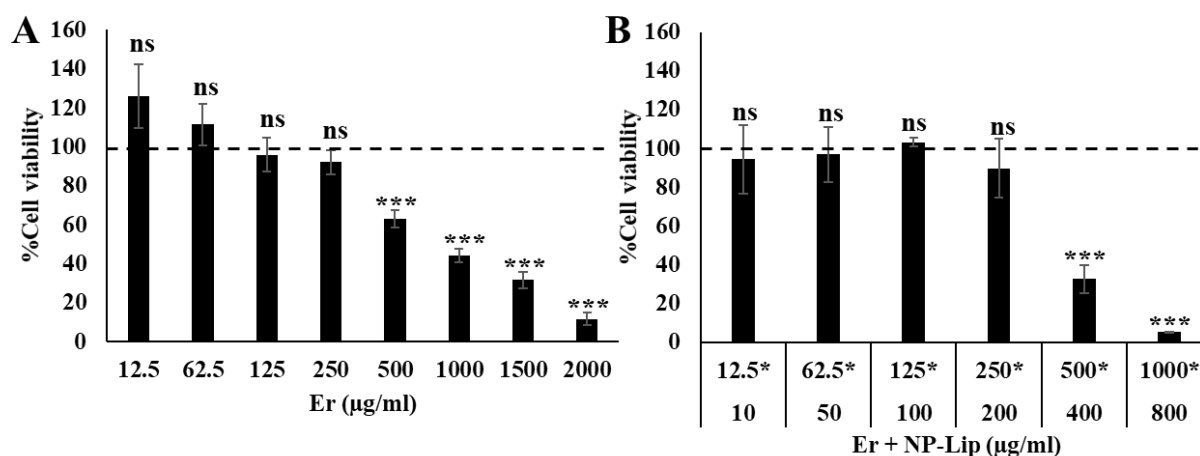
NP and NP-Lip Cell Viability After 2 Hours

Supplementary figure 5 shows that after 2 hours' treatment with 100 µg/ml, the blank NPs resulted in significant loss of viability in HEK293 cells. Therefore, the cellular association experiment was conducted using 10 µg/ml only.



Supplementary Figure 5: MTT cell viability assay on HEK293 cell line when treated with blank NPs and NP-Lip after 2 hours

In vitro Assessment of Free Er Toxicity

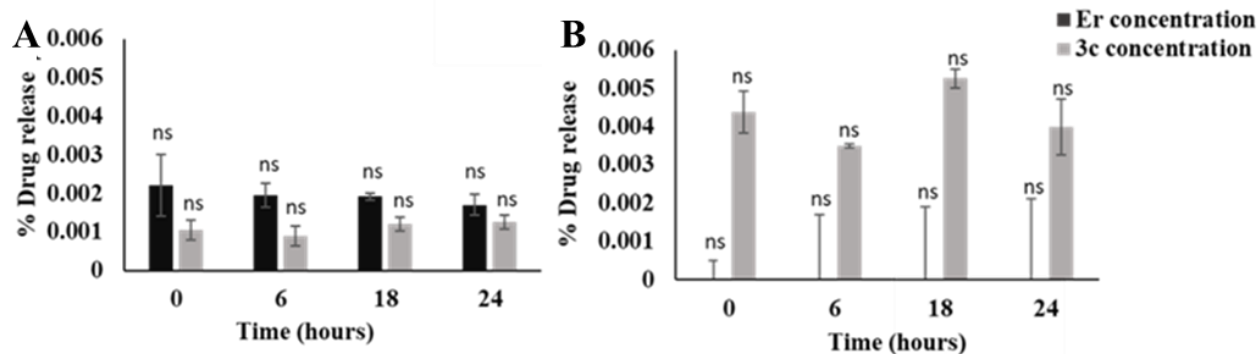


Supplementary Figure 6: Percentage of HEK293 cell viability when treated with (A) increasing concentrations of free Er and (B) increasing concentrations of Er + free unloaded NP-Lip in which concentrations in terms of Er are demonstrated with asterisks (*) while

concentrations in terms of PLGA are expressed without asterisks (*). Statistical analysis was performed by GraphPad InStat software using one-way ANOVA, where * $P < 0.05$, ** $P < 0.01$, and *** $P < 0.001$.

Assessment of Er and 3c Release from NP-Lip

To assess the drug release, Er-NP-Lip and 3c-NP-Lip were formulated and centrifuged at 10752 rcf, 10°C for 10 minutes. The drug loaded NP-Lip were resuspended in DMEM or MHB at a final concentration of 40 and 200 µg/ml for 3c-NP-Lip and Er-NP-Lip, respectively. At predetermined time intervals 6, 18 and 24 hours, NP-Lip were centrifuged and the concentration of the released drugs in the supernatant was then determined using UHPLC-MS/MS.



Supplementary Figure 7: Assessment of drug (Er and 3c) release from NP-Lip in (A) DMEM and (B) MHB. Results are expressed as % drug release from total drug amount encapsulated. Statistical analysis was performed by GraphPad-InStat software using one-way ANOVA, where $P > 0.05$ is considered not significant

Formulation of Er Loaded Liposomes and *in vitro* Assessment of Antibacterial Effects of Er-Lip against Gram-negative Bacteria

Er loaded liposomes were initially formulated using direct mixing of lipids in aqueous phase containing Er. Briefly, 16 mg soybean lecithin (LEC, Lipoid GmbH, Germany) and 2 mg cholesterol (CHOL, Sigma Aldrich, Germany) were dispersed directly in 5 ml of Er in ultra-pure water at final concentration of 2 mg/ml and subsequently mixed

using a vortex mixer for 2 minutes at 2500 rpm. Er-Lip were then collected by centrifugation in a cooling centrifuge adjusted to 10°C at 10752 rcf for 10 minutes.

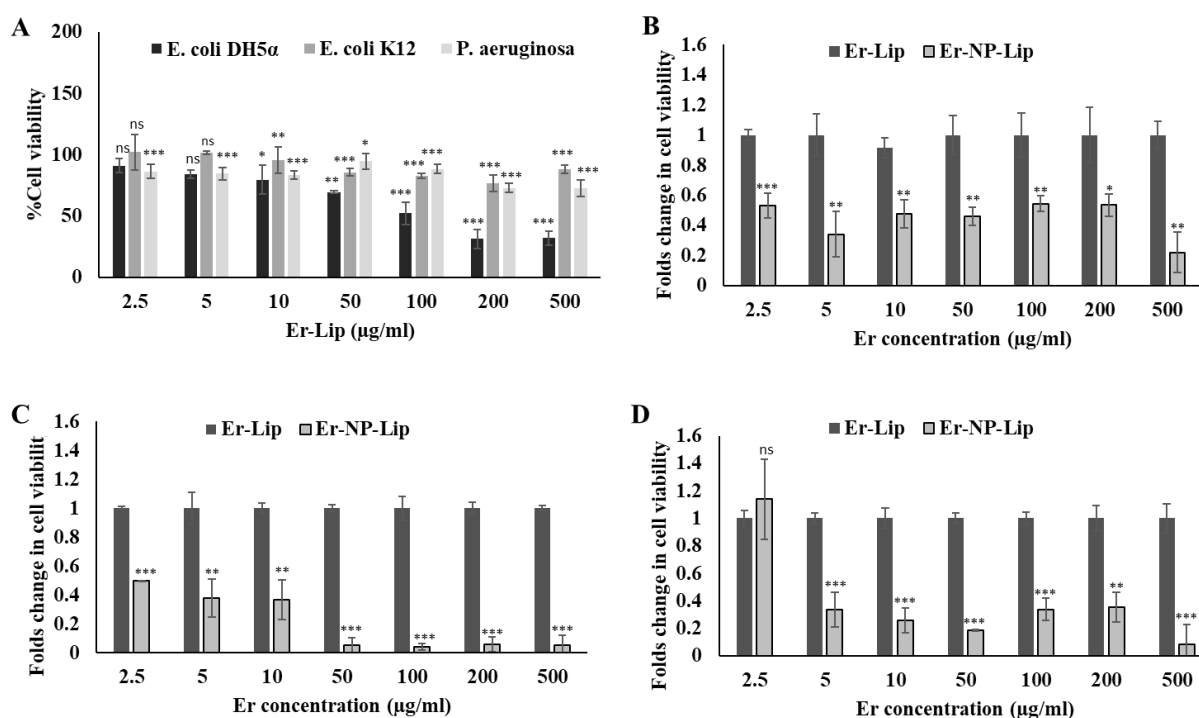
To quantify the un-encapsulated Er, Er-Lip were centrifuged at the previously mentioned conditions, the concentration of unencapsulated Er in the Lip supernatant was determined using an in-house developed ultra-high performance liquid chromatography-tandem mass spectrometer (UHPLC-MS/MS) method using diphenhydramine as internal standard. The concentration of the encapsulated was directly detected from the un-encapsulated one. Er-Lip showed EE of 233 µg/ml ± 0.0971.

To prove the effect of NP-Liposomal platform, MIC of Er-Lip was detected using MTT assay against *E. coli* DH5α, *E. coli* K12 and *P. aeruginosa* using similar concentration of Er-NP-Lip. Briefly, in a 96 well plate, 50 µl of Er-Lip were added, followed by the addition of 10×10⁵ CFU/ml bacterial cell suspensions (50 µl). The plates were incubated for 16-24 hours at 37 °C in aerobic conditions. Subsequently, (0.3 mg/ml) MTT solution was added to every single well and the 96-well plates were incubated for 2 hours at 37 °C. After 2 hours incubation with MTT solution, the produced formazan crystals were solubilized using DMSO. The absorbance values of the wells were determined using a Wallac plate reader at a wavelength of λ 595 nm. The results were reported as mean and SD calculated for each concentration. The % cell viability per well was calculated as follows:

$$\% \text{ Cell viability} = \frac{(\text{Absorbance of treated wells} - \text{Absorbance of -ve control wells})}{\text{Absorbance of growth control wells}} \times 100$$

The results are shown in the figure below and indicate that at the same concentrations tested with NP-Lip, drug loaded liposomes are less efficient. In fact, Er loaded liposomes showed cell viability reduction less than 50%. MIC₅₀ values could not be

computed at least for *E. coli* K12 and *P. aeruginosa*. It is worth noting that HD of Lip and NP-Lip platform are different, therefore the comparison between both formulations is invalid since the difference in the particles size may affect the interaction between the formulation and the bacterial membrane.



Supplementary Figure 8: (A) Percentage of bacterial cell viability when treated with increasing concentrations of Er-Lip. Folds change in cell viability in Er-NP-Lip compared to Er-Lip in (B) *E. coli* DH5α, (C) *E. coli* K12, and (D) *P. aeruginosa*. Statistical analysis was performed by GraphPad InStat software using one-way Anova in chart (A) and unpaired t-test in charts (B, C, D), where *P < 0.05, **P < 0.01, and ***P < 0.001 relative to untreated control cells in A and relative to Er-Lip in B, C, and D

Supplementary Table 5: Comparison between *in vitro* and *in vivo* results of Er and Er-NP-Lip

	Er	Er-NP-Lip	P-value
IC₅₀ on HEK293 cells	808 µg/ml ± 50.1681	1615.933 µg/ml ± 59.546	< 0.0001
MIC₅₀ on <i>E. coli</i> DH5α	8.67 µg/ml ± 2.14	4.18 µg/ml ± 0.084	0.0004
MIC₅₀ on <i>E. coli</i> K12	8.74 µg/ml ± 0.45	3.7 µg/ml ± 0.13	< 0.0001
MIC₅₀ on <i>P. aeruginosa</i>	11.9 µg/ml ± 0.64	3.26 µg/ml ± 0.29	< 0.0001

Log viability of <i>P. aeruginosa</i>	3.96 ± 0.126	4.205 ± 0.657	0.3202
--	--------------	---------------	--------

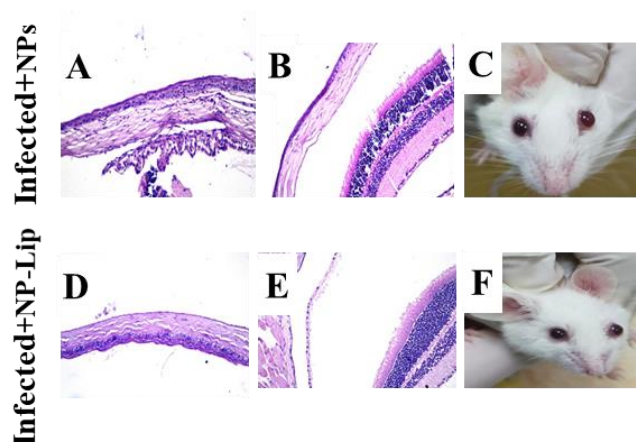
Keratitis Model Optimization and Validation



Supplementary Figure 9: Effect of topical administration of 10 μ l of 10^6 CFU/ml of *P. aeruginosa* at different time intervals. Clinical scores (0 \rightarrow +4) of corneal response assigned at each time point. Eyes received score between 0 to +4, where 0 indicated clear or slight corneal opacity, partially covering the pupil, +1 indicates slight opacity fully covering the anterior segment, +2 indicated dense opacity, partially or fully covering the pupil, +3 indicated dense opacity covering the entire anterior segment and finally +4 indicated corneal perforation or phthisis bulbi (i.e., shrunken eye)

At 24 hours post-infection, the culture of the infected mouse eye homogenate shows high levels of bacterial concentration compared to the initial applied one, since both left and right eyes yielded a bacterial concentration of 65600 and 67200 CFU/ml respectively. While the initial applied volume (10 μ l) contains 10000 CFU/ml.

Histopathological Investigation of Eyes following Treatment with NPs and NP-Lip



Supplementary Figure 10: Histological and clinical examination of mouse eyes from infected animals treated with NPs (A, B) and NP-Lip (D, E) showing (A, D) normal histological structure of the cornea (B, C) retina, choroid, and sclera and (C, F) normal appearance of eyes with no signs of inflammation nor corneal opacity

References

- (1) Ghanbarzadeh, S.; Valizadeh, H.; Zakeri-Milani, P. Application of response surface methodology in development of sirolimus liposomes prepared by thin film hydration technique. *Bioimpacts* **2013**, *3*, 75–81, doi:10.5681/bi.2013.016.
- (2) Martina, M.-S.; Fortin, J.-P.; Ménager, C.; Clément, O.; Barratt, G.; Grabielle-Madelmont, C.; Gazeau, F.; Cabuil, V.; Lesieur, S. Generation of Superparamagnetic Liposomes Revealed as Highly Efficient MRI Contrast Agents for in Vivo Imaging. *J. Am. Chem. Soc.* **2005**, *127*, 10676–10685, doi:10.1021/ja0516460.
- (3) Wang, H.; Zhao, P.; Su, W.; Wang, S.; Liao, Z.; Niu, R.; Chang, J. PLGA/polymeric liposome for targeted drug and gene co-delivery. *Biomaterials* **2010**, *31*, 8741–8748, doi:10.1016/j.biomaterials.2010.07.082.
- (4) Benyettou, F.; Chebbi, I.; Motte, L.; Seksek, O. Magnetoliposome for alendronate delivery. *J. Mater. Chem.* **2011**, *21*, 4813, doi:10.1039/c1jm00060h.
- (5) Prassl, R.; Frascione; Diwoy; Almer; Opriessnig; Vonach; Gradauer; Leitinger; Mangge; Stollberger Ultrasmall superparamagnetic iron oxide (USPIO)-based

- liposomes as magnetic resonance imaging probes. *Int. J. Nanomedicine* **2012**, 2349, doi:10.2147/IJN.S30617.
- (6) Kulshrestha, P.; Gogoi, M.; Bahadur, D.; Banerjee, R. In vitro application of paclitaxel loaded magnetoliposomes for combined chemotherapy and hyperthermia. *Colloids Surfaces B Biointerfaces* **2012**, 96, 1–7, doi:10.1016/j.colsurfb.2012.02.029.
- (7) Giri, J.; Guha Thakurta, S.; Bellare, J.; Kumar Nigam, A.; Bahadur, D. Preparation and characterization of phospholipid stabilized uniform sized magnetite nanoparticles. *J. Magn. Magn. Mater.* **2005**, 293, 62–68, doi:10.1016/j.jmmm.2005.01.044.